Radical-Driven Tandem Mass Spectrometry: Improved Analytical Strategies and Mechanistic Studies for Characterization of Labile Biomolecules

by

Nhat Hoang Van Le

A dissertation submitted in partial fulfillment
of the requirements for the degree of
Doctor of Philosophy
(Chemistry)
in the University of Michigan
2022

Doctoral Committee:

Professor Kristina I. Håkansson, Chair
Assistant Professor Aaron Frank
Professor Alexey Nesvizhskii
Professor Brandon T. Ruotolo

Nhat Hoang Van Le

nhle@umich.edu

ORCID iD: 0000-0002-6165-5073

Dedication

To my beloved parents and dear family, who supported and encouraged me throughout this difficult journey.

Acknowledgements

"At times, our own light goes out and is rekindled by a spark from another person. Each of us has cause to think with deep gratitude of those who have lighted the flame within us."

-Albert Schweitzer

Throughout my years at Michigan pursuing my doctoral degree, there were numerous difficult times and challenges that I needed to overcome. I would like to express my sincere appreciation to those who supported and helped me during this journey.

My first and utmost appreciation goes to my advisor, Dr. Kristina Håkansson, for her persistent and pertinent support and guidance in all stages of my thesis. I would like to thank her for all her contributions that made my Ph.D. experience more productive and rewarding. Because of her thoroughness aiding me in my work and her willingness to accept the flaws, I have grown as a better researcher and as a person. Her guidance and care have always been a source of strength for me to get through challenging times with my studies and my life. One simply could not wish for a better advisor.

I would also like to thank my dissertation committee members, Dr. Brandon Ruotolo, Dr. Alexey Neshviskii, and Dr. Aaron Frank for their insightful feedback, valuable recommendations,

and encouragement. I appreciate the time and efforts that my committee contributed to helping me fulfill the graduation requirements. I extend my gratitude to the Ruotolo lab for accepting me with open arms when I needed training for molecular dynamics simulations as well as helping me with numerous Python scripts to streamline my simulation data analysis. I would like to acknowledge Dr. Brandon Ruotolo and Dr. Aaron Frank for their mentorship and patience providing guidance for my computational work presented in this dissertation.

My special thanks go to all my former and current lab members: Dr. Hye Kyong Kweon, Dr. Isaac Agyekum, Dr. Nick Borotto, Dr. Qingyi (Emma) Wang Eunju Jang, Josh Salem, Carson Szot, James Brunemann, and LeeAnne Wang. It has been a pleasure to work with and learn from you all for the past 5 years. The Hakansson lab has provided me an environment to grow scientifically and holistically.

Last but not least, I want to thank my dearest friends and family around the world for their love, support and patience throughout these years. To my cherished love, Lizzy, you helped me through my ups and downs, with all your heart and soul—thank you so much for your love and support. For my parents, Lan Nguyen and Quan Le, whose unconditional love was my main driving force to make this possible. I cannot thank my parents enough for their great sacrifices throughout their lives that allowed me to be where I am today. I would not have made it this far without them.

Nhat Le
March 14th, 2022
Ann Arbor, Michigan

Table of Contents

List of Figures

List of Tables

List of Equations

List of Abbreviations

CEM ..... Chain Ejection Model

CID ..... Collision Induced Dissociation

CRM ..... Charge Residue Model

DMSO ..... Dimethyl Sulfoxide

ECD ..... Electron Capture Dissociation

EDD ..... Electron Detachment Dissociation

EID ..... Electron Induced Dissociation

ESI ..... Electrospray Ionization

ETD ..... Electron Transfer Dissociation

FA ..... Formic Acid

FT-ICR ..... Fourier Transform-Ion Cyclotron Resonance

HCD ..... High-Energy Collision Dissociation

IEM ..... Ion Ejection Model

IRMPD ..... Infrared Multiphoton Dissociation

LC ..... Liquid Chromatography

m-NBA ..... 3-nitrobenzyl alcohol

m/z ..... Mass-to-Charge Ratio

mAb ..... Monoclonal Antibody

MS ..... Mass Spectrometry

MS/MS or MS2 ..... Tandem Mass Spectrometry

nCID ..... Negative-Ion Collision Induced Dissociation

nESI ..... Nano electrospray ionization

niECD .....Negative-Ion Electron Capture Dissociation

PC ..... Propylene Carbonate

PTM ..... Posttranslational Modification

RP .....Reversed-Phase

S/N .....Signal-to-Noise Ratio

TCEP ..... Tris(2-carboxyethyl) phosphine

TFA .....Trifluoroacetic Acid

TIC .....Total Ion Chromatogram

TOF .....Time-of-Flight

Abstract

Posttranslational modifications (PTMs) have significant impacts on structure and function of proteins. Thus, characterization of PTMs is essential for understanding their roles in disease progression. Mass spectrometry is a powerful tool for PTM analysis. This research involves the development of novel approaches for structural characterization of labile biomolecules, including labile PTMs. Through innovation in radical-driven tandem mass spectrometry (MS/MS), analytical obstacles are resolved and ultimately allow the answering of long-standing questions surrounding protein modifications. Throughout this thesis, a variety of PTM-containing peptides with different chemical and physical properties, ranging from hydrophilic glycopeptides to hydrophobic palmitoylated peptides, are examined, including evaluation of appropriate separation techniques for liquid chromatography mass spectrometry (LC/MS) analysis.

Specifically, Chapter 2 discusses how post-column "supercharging" in nanoflow LC/MS improves glycopeptide analysis in several MS/MS techniques, including high energy collision dissociation (HCD), electron transfer dissociation (ETD), HCD product dependent ETD (HCDpdETD), and ETD followed by HCD (EThcD). Supercharging enhanced the average charge state of N-glycosylated peptides from 3.00 to 3.39 and resulted in a significant increase in fragmentation from 6.25% to 93.75%. Chapter 3 extends this work to lipid-containing peptides, including optimization of nanoflow C8 chromatography for such hydrophobic analytes. We also considered protocols for preparation of lipidated peptides with minimal sample loss for direct

detection of this PTM. For example, with supercharging, the N-Ras C-terminal peptide was directly detected due to an enhanced charge state from 1.59 to 2.31. This charge enhancement allowed ETD analysis of the triply protonated peptide, resulting in extensive fragmentation corresponding to ~95% sequence coverage without loss of farnesyl or the C-terminal *O*-methyl group.

Chapter 4 discusses the extension of collision induced unfolding (CIU) coupled with ion mobility spectrometry towards PTM-carrying peptides. This approach allows observation of gas-phase structural transitions and direct analysis of how such transitions affect electron capture dissociation (ECD) sequence coverage. Intriguingly, unfolding of such species proceed via minimum PTM loss and rich ECD fragmentation patterns (i.e., ~82% sequence coverage) are observed for the resulting extended conformations. Replica exchange molecular dynamics was performed to better understand this unfolding process for phosphorylated peptides. In Chapter 5, the CIU-ECD approach from Chapter 4 is extended towards monoclonal antibodies (mAbs) for middle-down analysis of their glycosylation. With CIU-ECD, sequence coverage for Fc dimer fragments were greatly improved from 14% to ≥30%. Through this work, we discovered that supercharging could stabilize protein structure prior to CIU for improved CIU fingerprints. An automated 2D-LC online digestion setup was developed for middle-down digestion of mAbs. Such automation improves digestion reproducibility and reduces human error.

Finally, Chapter 6 discusses the extension of negative ion ECD (niECD) to a new class of molecules, gangliosides. Such analytes are acidic and benefit from negative ion mode analysis. We found that niECD outperforms both collision induced dissociation (CID) and electron induced

dissociation (EID) for GM1, GM3, GD1a and GD1b. Furthermore, through unique radical ion chemistry, niECD allowed differentiation of isomeric gangliosides.

Overall, the research presented in this dissertation improves our understanding of radical-driven tandem mass spectrometry for improved analysis of labile biomolecules. This work enables new analytical tools for structural characterization of biological samples.

Chapter 1. Introduction

1.1. Mass Spectrometry-Based Protein Structural Analysis for Labile Post-Translational Modifications

1.1.1. Post-translationally Modified Proteins

With the advent of crucial breakthroughs in mass analyzer technologies, advanced bioinformatics analysis tools, and ionization modalities, mass spectrometry (MS) has become the mainstream technique for structural biology within the last few decades[1–5]. Proteins perform numerous biological functions within cells. These functions are modulated through protein structural changes and, thus, characterizing these structures is critical. Indeed, protein structure elucidation is of great importance to provide an insight into their roles in human health and disease. Within the last few decades, scientists have revealed a vastly multifaceted nature of the human proteome compared to our genome[6]. Beyond the genetic code, the human proteome complexity is further expanded via post-translational modifications (PTMs). After emerging from the translational process on the ribosomes, PTMs greatly increase the functional diversity of the proteome through covalent modifications on

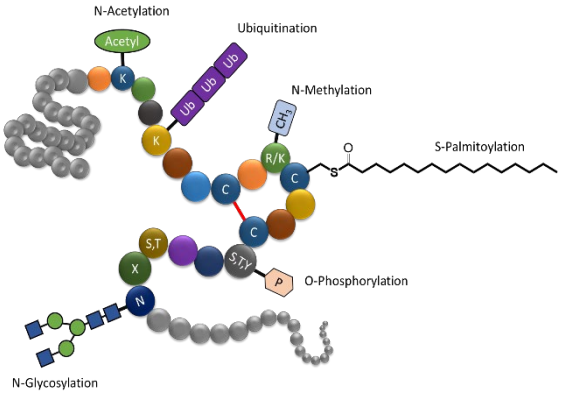

Figure 1.1. Posttranslational modifications on biological proteins

amino acid side chains (methylation, phosphorylation, lipidation, acetylation, ubiquitination, etc…), proteolytic cleavage, or via the addition of carbohydrate moieties (N-glycosylation and O-glycosylation)[7–10] (*Fig. 1.1*). These modifications allow proteins to gain essential functions for regulating biological activities, assisting cellular trafficking, and facilitating interactions with other macromolecules.

Labile PTMs, including lipidation and glycosylation, are ubiquitous in proteins. The attachment of lipids, e.g., palmitoylation, to proteins affects their localization, trafficking, and compartmentalization[11], whereas addition of carbohydrate moieties plays important roles in cell-cell recognition[12], immune response[13], and cellular signaling[14,15]. These two classes of modifications have nearly orthogonal properties with palmitoylation being non-polar and glycosylation being polar. However, both types of PTMs add a relatively large labile moiety to the corresponding proteolytic peptides, thus presenting challenges in their analysis.

1.1.2. Gangliosides

Gangliosides are composed of a glycan headgroup and a ceramide lipid tail. These glycoconjugates are classified as sialic acid-containing glycosphingolipids and are the main carriers of sialic acids on the surface of neuronal cells. Gangliosides often carry one or more sialic acids linked to the sugar moiety. These sialic acids are typically negatively charged at physiological pH[16] and assist in modulating cell signaling and cell-to-cell communication. Gangliosides also play a significant role in cellular dysfunction and disease progression such as in Alzheimer's disease, Parkinson's disease, and Huntington's disease[17–21]. However, it is difficult to study gangliosides due to their labile and acidic nature. Additionally, they show poor ionization

in positive ion mode. Furthermore, structural heterogeneity, resulting g from different glycan branching arrangements and fatty acyl chain length/saturation, also contributes to challenges in their analysis.

1.2. Strategies in Modern Proteomics for Post-Translational Modification Analysis

1.2.1. Bottom-up, Middle-Down and Top-down Proteomic Strategies

There are three main modes of proteomic methods, i.e., bottom-up, middle-down, and top-down analysis (*Fig. 2.1*)[22]. Bottom-up proteomics is the most popular strategy due to its robust nature, allowing for comprehensive peptide mass fingerprinting, quantitative information, and the characterization of protein-protein interactions[23,24]. In a bottom-up experiment, intact proteins are denatured, reduced, and alkylated to inhibit reformation of disulfide bridges before undergoing proteolytic digestion (e.g., trypsin, pepsin, chymotrypsin, etc.…). Such digestion typically generates peptide fragments of < 3 kDa that are readily analyzed by MS. However, there are a few shortcomings in bottom-up analysis: proteolytic cleavage adds another layer of

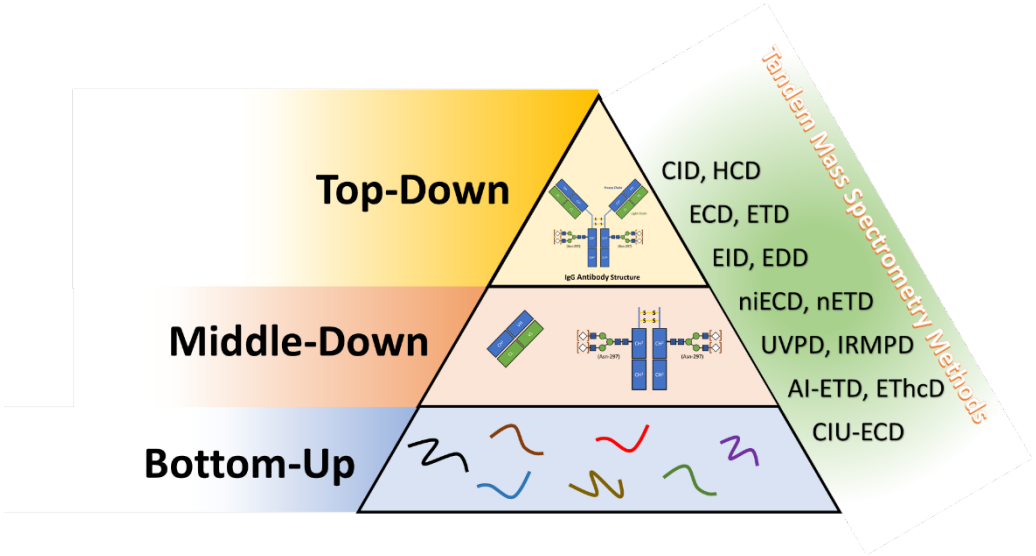

Figure 1.2. Mass Spectrometry Methods for Structural Biology

complexity with an increasing number of analytes, thus making it challenging to achieve complete protein sequence coverage as well as to achieve proper proteoform determination. Bottom-up approaches also heavily depend on the digestion efficiency of utilized proteases. Incomplete or improper digestion can lead to misidentifications. However, this issue can be remedied with multi-stage protease digestion protocols[25] to increase digestion effectiveness.

To resolve problems of bottom-up proteomics, a top-down strategy[26] which analyzes intact proteins directly without prior digestion was termed by McLafferty and coworkers[27–29]. In a typical top-down approach, proteins are often buffer-exchanged to remove detergent and salts, which can be detrimental to MS analysis. With the removal of such impurities, substantially higher protein signals can be obtained[30,31]. However, in top-down proteomics, it is also challenging to generate high sequence coverage, especially for larger proteins. Additionally, the requirements for high resolution instrumentation[32] and poor detection limits for large proteins are significant setbacks.

Although both top-down and bottom-up proteomics continue to improve, they each suffer shortcomings. To reduce the number of potential artifacts from lengthy sample preparation in bottom-up analysis[33] and overcome the technical challenges[34,35] in top-down anaysis, middle-down proteomics was introduced as a compromise with particular potential for characterization of large biomolecules such as antibodies and protein complexes[36–40]. Middle-down proteomics can be achieved by analyzing larger protein fragments from partial proteolysis. However, in such approaches, the cleavage sites may differ from experiment to experiment, greatly affecting reproducibility[41]. Thus, a protease cutting at well-defined sites is needed for successful middle-

down proteomics. Recently, Genovis developed an IgG-specific protease that cleaves at "LL***GG***PS" sites below the hinge region to produce F(ab')2 and Fc/2[42–44] fragments (*Fig. 1.3*).

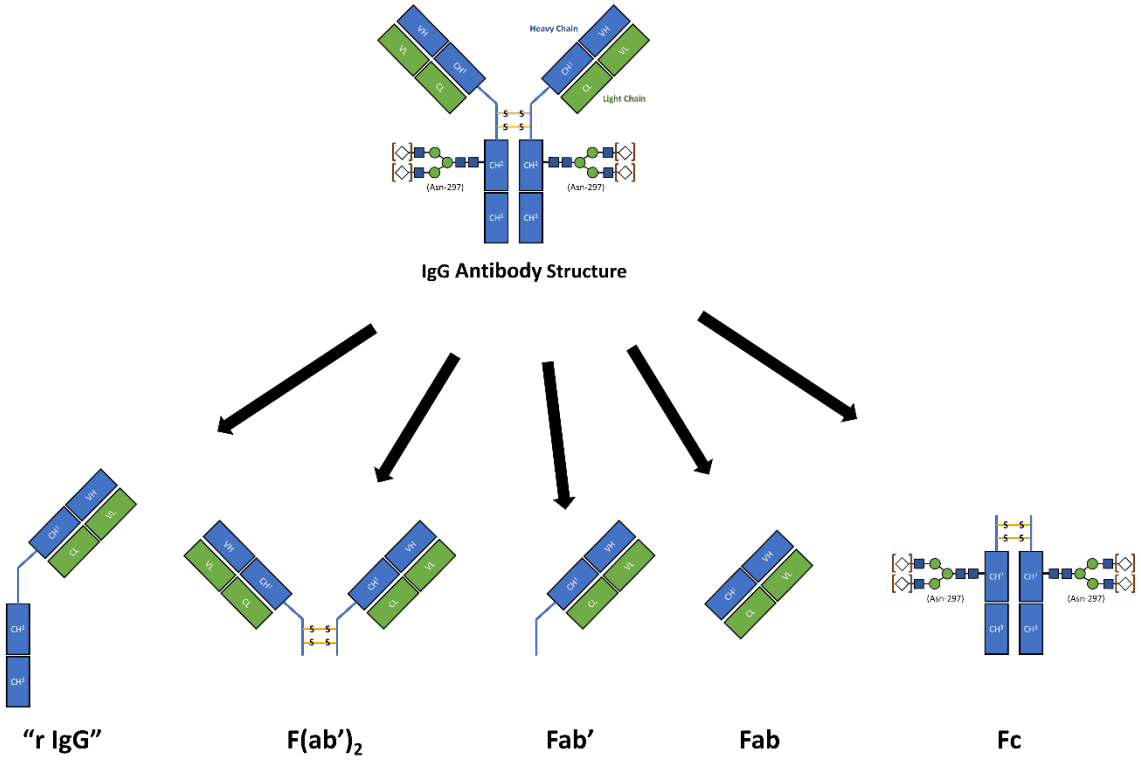

Figure 1.3. Type of antibody fragments from middle-down digestion.

1.2.2. Liquid Chromatography Mass Spectrometry (LC/MS)

For highly complex samples from, e.g., clinical, environmental, and pharmaceutical laboratories, MS alone suffers from dynamic range limitations. Liquid chromatography coupled to mass spectrometry (LC/MS) has emerged as a routine analytical platform to characterize and analyze such complex samples due to its robustness, sensitivity[45], specificity, and selectivity. For example, in a proteomics experiment involving hundreds of thousands of peptides, some type of separation is required to avoid ion suppression from co-ionization of competing species within a sample[46,47]. LC/MS offers an ideal solution because it inherits not only accuracy and sensitivity

from mass spectrometric measurements but also the selectivity and specificity from chromatographic separation.

In proteomics, nanoflow LC (i.e., flow rates from 300 to 500 nL/min) is the most popular tool for peptide separation prior to MS due to its enhanced sensitivity over conventional LC[48,49]. Peptide mixtures are typically separated over a fused-silica column (75-125 µm inner diameter) packed with reverse-phase (RP) silica stationary phase beads covalently bonded with octadecyl (C18) hydrocarbon chains. The principle of separation is based on hydrophobic interactions between analyte and stationary phase[50–52]. Upon gradient change (i.e., commencing at low organic composition to high organic concentration), the strongly interacting analytes are retained in the column longer while weakly interacting solutes elute first. On the other hand, for more hydrophilic samples such as saccharides[53], normal-phase separation (e.g., hydrophilic interaction liquid chromatography (HILIC)) may be required to effectively separate solutes in the order of their hydrophilicity[54]. In HILIC separations, polar stationary phases such as unmodified silica, amide, and diol, derivatives, etc., are used[55–57].

1.3. Charging and Supercharging of Analytes for Mass Spectrometry Analysis

1.3.1. Electrospray Ionization (ESI)

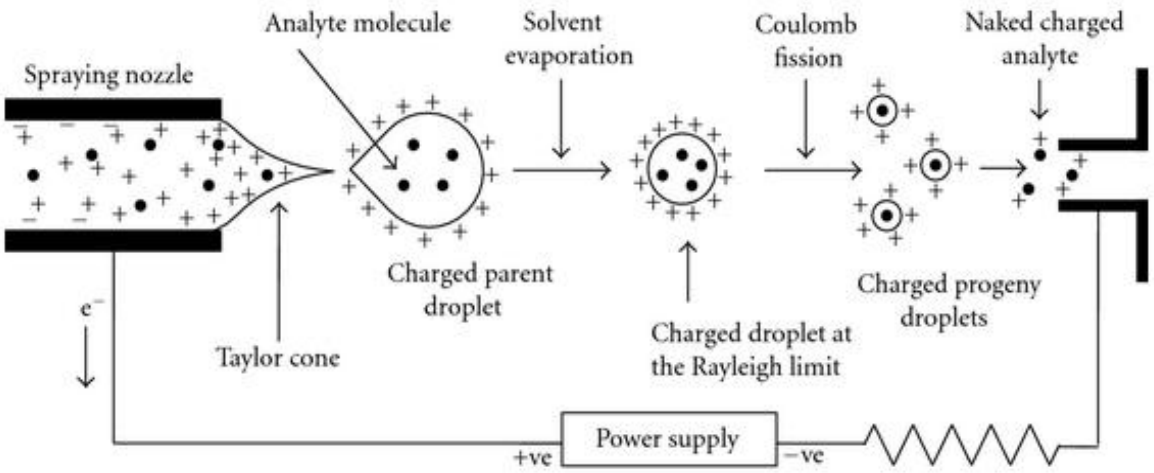

Figure 1.4. Mechanism of electrospray ionization.[61]

To detect analytes by mass spectrometry, they must first be converted into gaseous ions. Electrospray ionization (ESI) is a widespread method that generates multiply charged ions for larger analytes, such as peptides and proteins. Several models for the ESI mechanism have been proposed, including the ion evaporation model (IEM)[58], the charged residue model (CRM)[59], and the chain ejection model (CEM)[60]. Each model focuses on particular types of molecules, ranging from small analytes (e.g., amino acids) to large biomolecules (e.g., protein complexes). For all three mechanisms, analytes undergo three distinct stages to generate gas-phase ions from the solution phase. First, charged droplets are produced at the ESI capillary tip by a potential difference (*Fig. 1.4*)[61]. Second, solvent evaporation leads to droplet shrinkage and ultimately causes Coulomb fission events after the droplet size reaches the Rayleigh limit—the maximum number of charges on droplet surface before droplet degeneration[62]. Finally, gas-phase ions are formed from very small, highly charged droplets with the specific mechanisms depending on analyte properties.

For low molecular weight species, analytes are believed to be generated via the IEM. In this mechanism, ejection of relatively small ions from the droplet surface occurs due to the electric field of a Rayleigh-charged nanodroplet (*Fig. 1.5 (left)*)[63,64]. Large globular species (i.e., natively folded proteins and other biomolecules) are generally thought to be ionized into the gas phase via the CRM[59,63,65]. In this mechanism, analytes inside Rayleigh-charged nanodroplets evaporate to dryness via solvent shedding from the outermost to the innermost solvent shell (*Fig. 1.5 (middle)*)[59,66]. To enhance protonation in ESI, solvents are typically acidic and, thus, proteins are more commonly unfolded/denatured. Such unfolded proteins have been proposed to follow the CEM. In the latter mechanism, unfolded proteins, in contrast to the compact/hydrophilic nature of native proteins, have more extended configurations with exposed hydrophobic motifs[67,68]. Such hydrophobic regions are surface active and drift to the droplet surface. At the liquid-gas interphase, one of the charged protein termini is expelled into the vapor phase followed by the rest of the polypeptide chain (*Fig. 1.5 (right)*). The time scale for each model varies from nanoseconds (IEM) to microseconds (CRM).

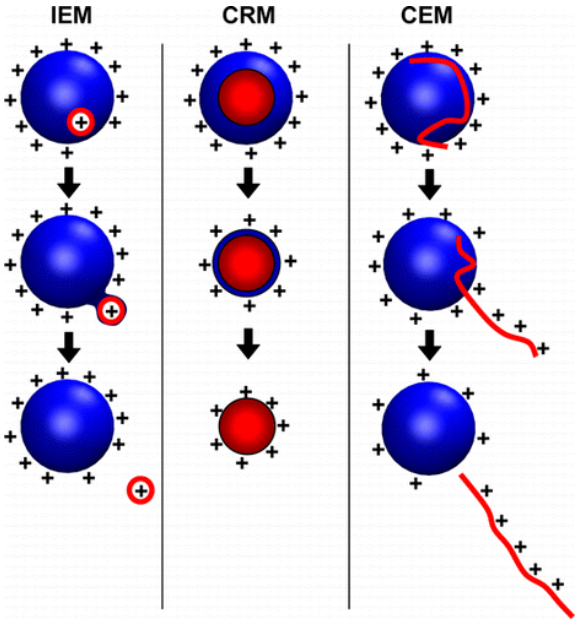

Figure 1.5. Different models of the ESI process: the ion evaporation model (IEM), the charged residue model (CRM), and the chain ejection model (CEM).[63,64]

1.3.2. Nanoscale electrospray ionization (nano-ESI or nESI)

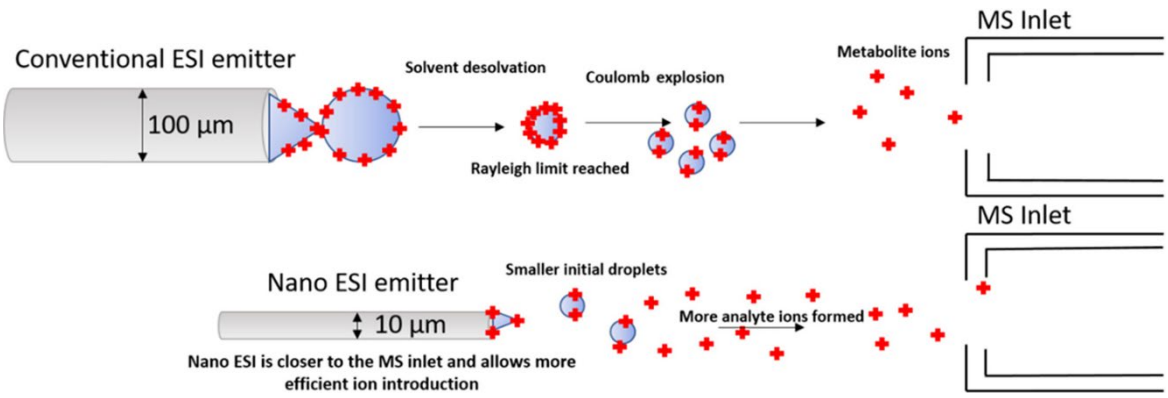

Figure 1.6. Conventional vs. nanoflow ESI.[72]

Nanoflow ESI was developed by Wilm and Mann in 1996 and has found a wide range of analysis applications such as metabolomics[69], lipidomics[70], glycomics[70], and proteomics[71]. In a standard ESI device, the ion source operates at flow rates ~1000 µL/min, often with the need for sheath flow or pneumatic assistance. The needle orifice is typically beyond 100 µm inner diameter, and thus, upon ESI, generates larger initial droplets[62]. With larger droplets, analytes must undergo a higher number of fission events before giving rise to observable ions and, as a result, the ionization process is less efficient (*Fig. 1.6)*[72]. For scarce samples in small volumes, conventional ESI is also not ideal. On the other hand, nano-ESI emitter orifices are around 1-10 µm and can sustain low flow rates ~20 nL/min[73] with no requirement for sheath gas. With the smaller orifice and lower flow rate, nano-ESI consumes much less sample and generates smaller initial droplets. The formation of smaller droplets can lower susceptibility to salt-based ion suppression and increase sensitivity for difficult analytes (i.e., glycoproteins and hydrophilic analytes like oligosaccharides)[74,75].

1.3.3. Supercharging Strategies

Multiple charging allows analysis of large biomolecules at lower m/z ratios, more compatible with many mass analyzers[76,77]. In addition, other advantages such as improved structural analysis can be achieved, i.e., maximizing analyte charge can be beneficial. Several methods have been developed to increase charging in ESI. One strategy is to chemically modify acidic functional groups with fixed positive charge derivatives[78]. While effective, chemical derivatization processes often result in sample loss and side reactions. Alternative approaches to derivatization are to introduce gaseous acid vapors[79] to the electrospray ionization cloud[80] and to change the composition of ESI solutions[81,82]. For the latter approach, Williams and co-workers showed that a small percentage of meta-nitro benzyl alcohol (m-NBA) results in "supercharging" of proteins[76]. Other supercharging reagents have since been introduced[76,83], including tetra-methylene sulfone (sulfolane)[84], dimethyl sulfoxide (DMSO)[85], propylene carbonate[86], and many others[87]. Novel supercharging reagents continue to be discovered[87,88] and some have been found to be effective for native protein analysis, including 2-thiophenone and 4-hydroxymethyl-1,3-dioxolan-2-one (HD)[89]. However, current work has mostly focused on intact proteins and other macromolecules[90]; thus, the influence of supercharging reagents on peptide gas-phase structures is not well understood, neither is the supercharging mechanism for peptide ions.

Charge enhancement depends on many factors, such as solvent composition[91–93], charge competition[94,95], and instrument parameters[96–98]. In positive ion mode, the presence of cations (e.g., H^+, NH_4^+, Na^+, and K^+) contribute to droplet charge. However, the main contributors to the net droplet charge are often protons due to the acidic nature of typical ESI solvents. In addition to supercharging via chemical addition, supercharging can also be achieved via changing the nESI spray potentials and temperature to denaturing conditions (i.e., increase spray voltage and 0.8

kV to 1.8 kV and temperature from 150°C to 300°C)[99]. Recently, large-area triboelectric nanogenerator (TENG)[100] and theta capillary nanoESI[101] have also been utilized to modulate supercharging effects.

Protein supercharging (native and unfolded proteins)

Surface tension plays an important role in the ESI process. The number of charges, z_R, that can be sustained by a spherical droplet of radius, R, and surface tension, γ, is given by Rayleigh's equation:

$$z_R e = 8\pi(\in_o \gamma R^3)^{1/2} \qquad \textit{(Equation 1)}$$

where e is the elementary charge, and $\in_o$ is the permittivity of the surrounding medium. The supercharging phenomenon of globular proteins can be explained by two leading ideas: according to Williams and coworkers, the analyte charge for protonated species follows the Rayleigh equation and depends on the surface tension of the electrospray droplets[102]. For droplets with higher surface tension (presumably those from solvents containing supercharging reagent), higher charge retention is achieved before reaching the Rayleigh limit, i.e., before droplet fission occurs. Thus, more charge is available in the final droplets in the CRM. On the other hand, Loo and coworkers proposed that Bronsted acid-base effects during droplet evaporation play a crucial role in adding more charges to the analytes[103]. The basicity of solvent molecules, i.e., supercharging additivities, thus determine the number of charges added to the gaseous analytes[103]. Later, Williams and coworkers proposed that the charge increase in supercharging is caused by unfolding and conformational changes of proteins with the increased concentration of supercharging reagents in the late-stage ESI droplets[77,104,105].

For CEM, three different scenarios can occur. In the first scenario, charged analyte species are ejected from the charged droplets by electrostatic repulsion. Proton migration from the droplet to the protruding protein chain is the main source of charge increase to minimize Coulomb repulsion (*Fig. 1.7a*). *Figure 1.7b*, shows an extension of the CEM where the protein droplet charge state is greater than its gas-phase charge state. In this case, reverse proton migration occurs from overcharged proteins to leave some charge behind on the droplet. In the case of CEM supercharging, unfolded proteins in acidified solutions containing a supercharging agent will be charged to the point where all basic sites (N-terminus, Arg, Lys, His) carry a proton[68,106–108]. Venter and coworkers suggested that the supercharging reagent sulfolane forms ion pairs with protonated sites via charge-dipole contacts for unfolded proteins[107]. In this scenario, CEM supercharging is caused by residual sulfolane molecules stabilizing protonated sites on the protruding protein (*Fig. 1.7c*)[108].

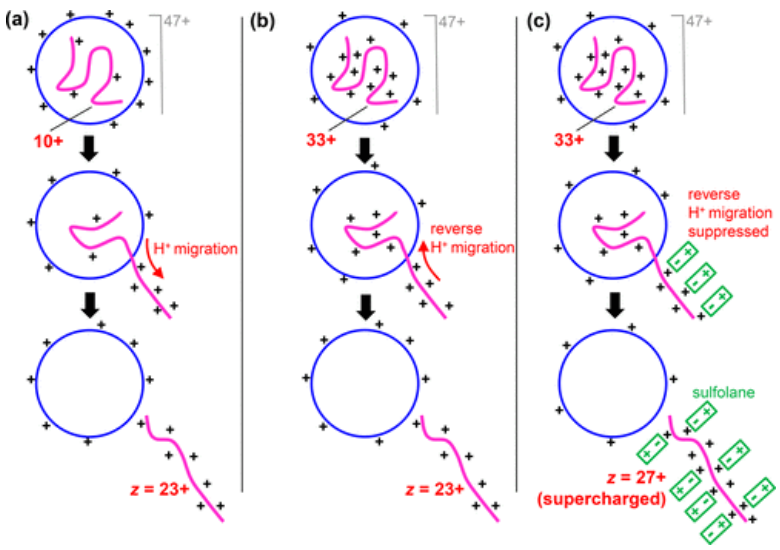

Figure 1.7. CEM of supercharged unfolded proteins.[106-108]

Peptide supercharging

Meta-nitrobenzyl alcohol (mNBA) has been shown to generate higher charge states upon electrospray ionization for both proteins and peptides[109,110] (*Fig. 1.8*) The alternative reagent sulfolane (SL) has been demonstrated to effectively supercharge proteins and tryptic peptides[84,111]. Our group also found that sulfolane generated higher charge states for peptic peptides[112]. In a typical supercharging experiment, a small percentage (0.1%—5%)[113,114] of supercharging agents (SCAs) is added to the ESI solution before analysis. With the decreasing nanodroplet size during the ESI process, saturation of SCA within the droplet can occur due to the volatile nature of SCA. SCA saturation may not occur in peptide supercharging since peptides undergo the IEM process. However, the mechanism may be similar to that of unfolded proteins with protonated sites being stabilized by the presence of SCAs; thus, promoting proton retention following ejection from droplets. However, more work is needed to understand the supercharging processes of peptides.

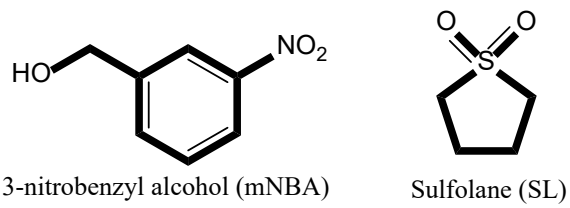

3-nitrobenzyl alcohol (mNBA) Sulfolane (SL)

Figure 1.8. Common Supercharging Reagents.

1.4. High Resolution Mass Spectrometry (HR-MS)

Once analyte ions have been formed, mass spectrometry measures the mass-to-charge ratio (m/z) of such charged molecules present in a sample [115]. A mass spectrometer comprises three basic components: an ion source, a mass analyzer, and a detector. While there is a broad variation in instrument components to obtain different resolution, mass range, and sensitivity, a mass spectrometer with superior selectivity and high mass resolution is highly desirable, especially for complex sample analysis. Here, three such high-resolution mass spectrometers are discussed,

including Fourier transform ion cyclotron resonance (FT-ICR), orbitraps, and high-resolution time-of-flight (TOF).

1.4.1. Fourier Transform Ion Cyclotron Resonance (FT-ICR) Mass Spectrometry

Fourier transform ion cyclotron resonance (FT-ICR) mass spectrometry was first introduced in 1974 by Comisarow and Marshall[116]. Since its introduction, the technology has grown immensely pushing the boundaries of high mass resolution and mass accuracy[117]. FT-ICR MS provides unprecedented resolution and mass accuracy compared with other mass analyzers such as TOF, quadrupole (Q), or ion trap (IT) mass analyzers. Unlike other mass analyzers, the detection of ions in FT-ICR is accomplished by measuring their cyclotron frequency in a homogenous magnetic field (*Fig. 1.9*). As the frequency can be measured accurately and precisely without the influence of ion kinetic energy spread, unsurpassed resolution and mass accuracy can be

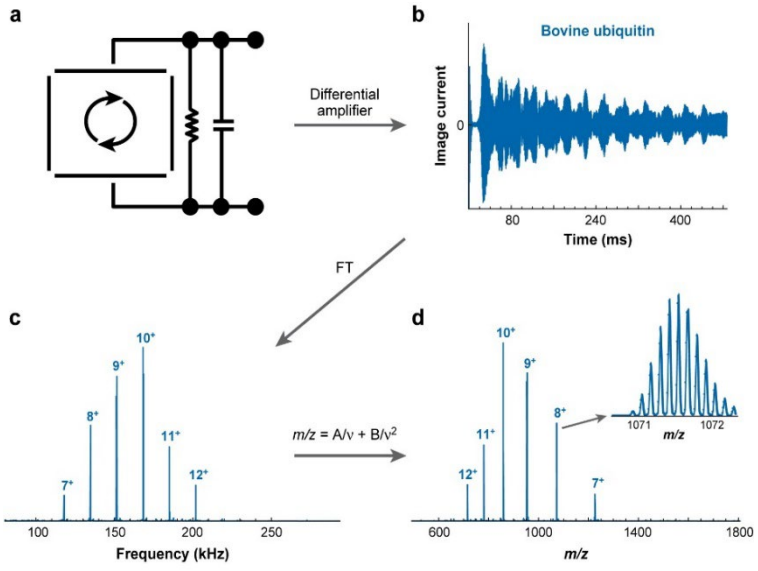

Marshall AG, Hendrickson CL. 2008. Annu. Rev. Anal. Chem. 1:579–99.

Figure 1.9. Principles of operation for an FT-ICR MS Instrument: (a) Ion excitation/detection, (b) Time-domain image-current signal, (c) Frequency-domain spectrum from fast Fourier transform, (d) MS spectrum obtained from frequency to m/z conversion.[116]

achieved[117–119]. For larger analytes (e.g., therapeutic antibodies), higher magnetic field strength (e.g., 21 Tesla available at the National Mag Lab[120]) is essential to achieve baseline isotopic resolution[121]. Another major benefit of FT-ICR MS is that it is compatible with various tandem MS activation techniques.

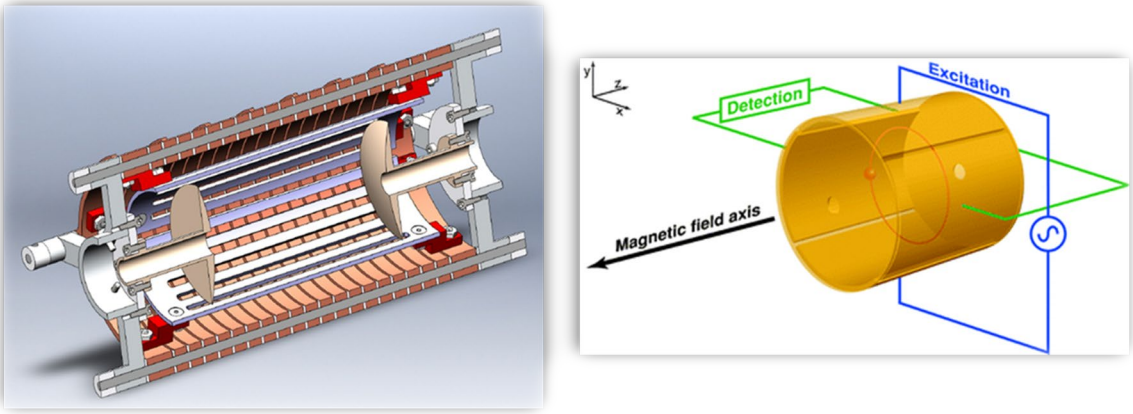

Figure 1.10. Schematic representation of a cylindrical FT-ICR analyzer cell.[125,126]

The theory of ion cyclotron resonance was developed by Lawrence[122]. In an ICR mass analyzer, the Lorentz force causes ions to travel in circular paths perpendicular to the magnetic field. They are also trapped in the axial direction with a low electric field[123,124]. To efficiently trap and detect ions in an ICR cell (*Fig. 1.10)*[125,126], ultra-high vacuum is required. Ion motion at a cyclotron frequency, f_c (in Hz), in a spatially uniform static magnetic field, B, is defined as:

$$\boldsymbol{f_c = \frac{zeB}{2\pi m}} \qquad \textbf{(Equation 2)}$$

where e is the elementary charge. Cyclotron frequency is therefore independent of ion velocity and kinetic energy, ultimately eliminating the prerequisite for ion focusing as encountered in other mass analyzers. To obtain a measurable signal, the ions must be excited coherently with an alternating electric field differentially applied to excitation plates (*Fig. 9*). Ions with an m/z ratio corresponding to the frequency of the applied electric field will absorb energy and thus increase

their cyclotron radius[127]. When orbiting closer to a pair of detection plates (*Fig. 9*), an image current is generated for a predetermined time (*Fig. 9*[128]). By applying a frequency sweep (or chirp), ions of a range of frequencies can be detected and the corresponding convoluted time-domain transients are fast Fourier transformed to generate a frequency-domain spectrum, and ultimately a mass spectrum via *equation (2)*.

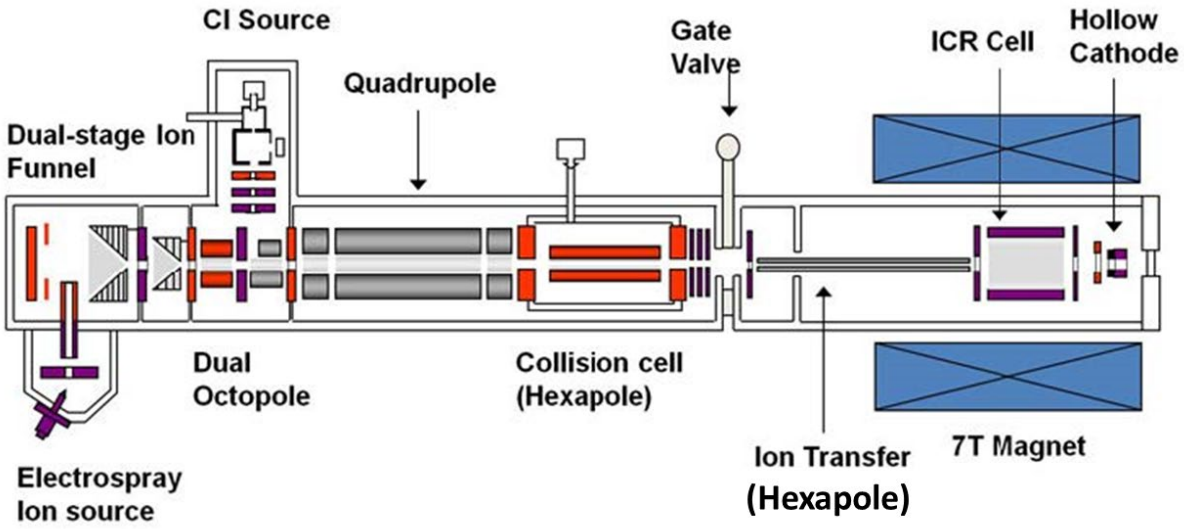

Figure 1.11. Schematic diagram of a 7T SolariX quadrupole-FT-ICR mass spectrometer (Bruker Daltonics).

A schematic diagram of an FT-ICR mass spectrometer from Bruker, available in our laboratory, is shown in *Fig. 1.11*. This instrument is equipped with an electrospray ion source, dual stage ion funnels, a mass-selective quadrupole, a chemical ionization (CI) source for electron transfer dissociation (ETD), a hexapole collision cell for collision induced dissociation, a transfer hexapole, a hollow dispenser cathode for ion-electron activation, a 10.6 μm Synrad CO_2 IR laser for infrared multiphoton dissociation (IRMPD), and an Infinity ICR cell. The dual stage ion funnels can serve several purposes: (1) Improving desolvation of analytes (2) ion focusing for improved transmission and sensitivity, and (3) in-source activation.

1.4.2. Orbitrap Fourier Transform Mass Spectrometers

In the early 2000s, a new type of FT mass analyzer "Orbitrap" with resolution rivaling FT-ICR was introduced by Makarov[129]. Orbitrap mass spectrometers operate based on the principle of image current detection from ions trapped in an electrostatic field generated from a geometrically well-defined electrode[130,131] rather than a magnetic field, thus eliminating the need for a superconducting magnet as in FT-ICR 104. Similar to FT-ICR, an ultrahigh vacuum is required to ensure sufficiently long mean free paths for the trapped ions and thus enable high resolution. Ion motion in the Orbitrap at axial frequency[130,131], ω (in rad/sec), is defined as:

$$\boldsymbol{\omega = \left(\frac{kq}{m}\right)^{1/2}} \qquad \textbf{(}\textbf{\textit{Equation 3}}\textbf{)}$$

where m and q are the mass and charge of the ion, respectively. To effectively detect ions in the Orbitrap, a curved RF-only quadrupole ion trap (C-trap) was designed for collisional cooling of ions[130]. This ultimately allows the uniform injection of large ion population with similar kinetic energy and prevents spatial/temporal spread of ion energy[131,133–135]. In a similar fashion to FT-ICR, the digitized image current time-domain signal is converted to a frequency-domain spectrum via Fourier transformation. However, due to a faster sampling rate per high resolution mass spectrum[130], Orbitraps can operate at higher throughput compared with FT-ICR, and therefore are more suitable for, e.g., complex bottom-up proteomics[132,136].

1.4.2.1. Orbitrap Fusion Lumos Tribrid Mass Spectrometer

Fig. 1.12 shows the Orbitrap Fusion Lumos Tribrid mass spectrometer - a state-of-the-art model. This instrument offers a tribrid architecture, including a front-end segmented quadrupole, a back-end dual-pressure ion trap, and an ultra-high field Orbitrap mass analyzer. The instrument available in our department is equipped with in-source EASY-ETD to generate radical anions for ETD. In addition, we have added a 60 W continuous wave (CW) CO_2 IR laser (Synrad, Mukilteo, WA) on the rear side of dual-pressure linear ion trap for (IRMPD)[137] and activated-ion electron transfer dissociation (AI-ETD)[138].

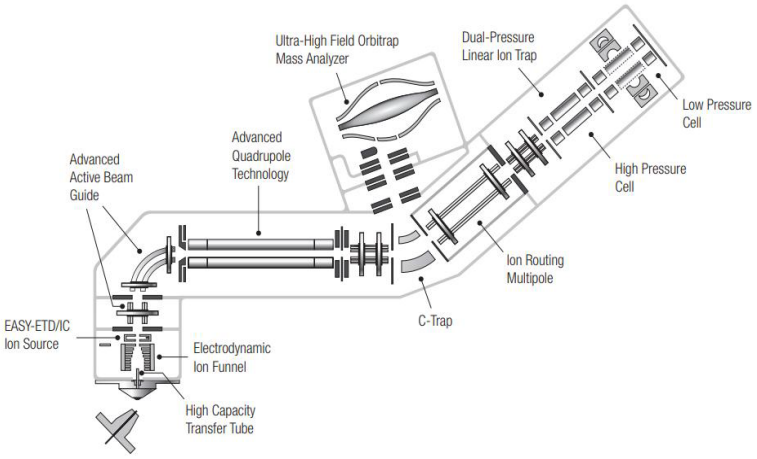

Figure 1.12. Schematic diagram of an Orbitrap Fusion Lumos mass spectrometer (Thermo Fisher Scientific)

1.4.2.2. Q Exactive UHMR Hybrid Quadrupole-Orbitrap Mass Spectrometer

Fig. 1.13 shows a schematic diagram of a Thermo Scientific Q Exactive UHMR hybrid quadrupole-Orbitrap mass spectrometer. This instrument comprises an in-source trapping (IST) region, a high-performance quadrupole, a higher-energy collision induced dissociation (HCD) cell, and a high-mass Orbitrap mass analyzer, with optimized RF voltages for improved high mass detection. Unlike a typical orbitrap (e.g., the Fusion Lumos (Fig. 5)) that suffers from low transmission efficiency, sensitivity, and resolution at high m/z values, the high-resolution, accurate-mass (HRAM) Orbitrap provides unrivaled sensitivity and resolution for identification and characterization of large proteins and protein complexes in native MS[133,139–142] via adjusting the voltage ramp rate on the central Orbitrap electrode to significantly improve transmission of

high m/z ions. Another significant upgrade is the clever design of in-source trapping to allow improved desolvation of large proteins. Within the in-source trapping region, an injection flatapole in the advanced active beam guide (AABG) section is pulsed with a negative voltage for enhanced desolvation. After in-source trapping, the restoration of voltage gradients in the bent flatapole of this ABBG region permits low-energy elution of ions to improve transmission for higher m/z ions. Lastly, for high mass ion transmission, RF frequencies are reduced for all ion routing multipoles in the AABG region, quadrupole, transport mutipole, C-trap as well as HCD cell.

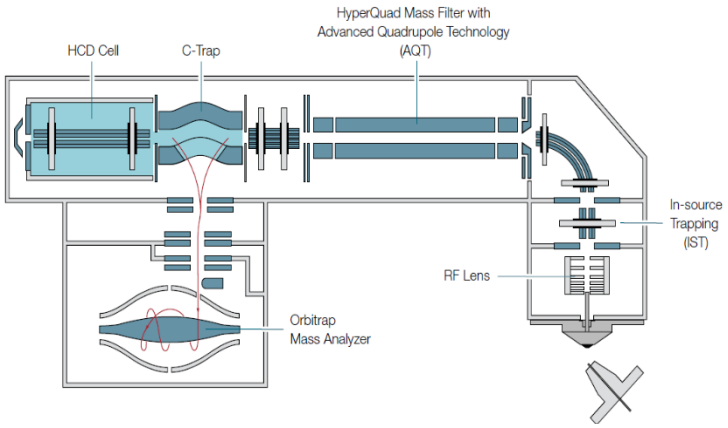

Figure 1.13. Schematic diagram of a QE-UHMR (Thermo Fisher Scientific).

1.4.2.3. A modified Agilent 6560 Drift Tube Ion Mobility-Quadrupole Time-of-Flight Mass Spectrometer (Agilent 6560C)

An Agilent 6560 drift tube ion mobility-quadrupole time-of-flight (IM-Q-TOF) mass spectrometer (*Fig. 1.14*) was retrofitted with advanced technologies such as a modified ion source for collision induced unfolding (CIU) and addition of an e-MSion ExD cell. In the modified CIU source, addition of a capillary exit (CE) lens immediately following the ion transfer capillary enables potential differences of ≥450 V between the CE and fragmentor,

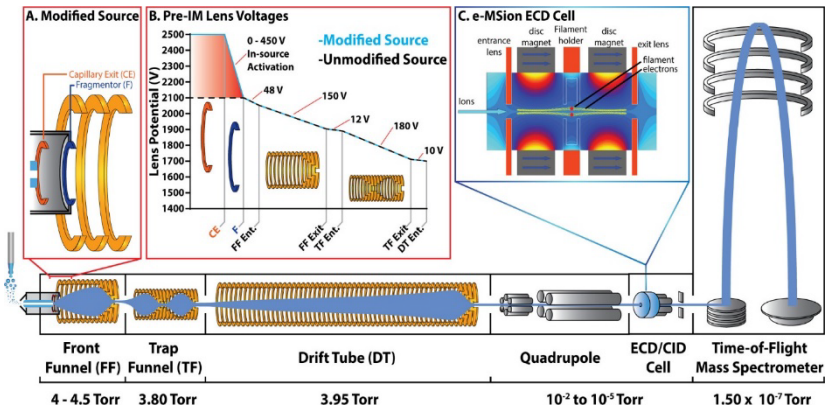

Figure 1.14. Schematic of an Agilent 6560 IM QTOF mass spectrometer.[143]

resulting in higher ion acceleration and ultimately higher energy collisions with the background gas (i.e., N_2 or SF_6 for $\Delta V > 350$ V). SF_6 serves dual purposes in this instrument; (1) acting as an electron scavenger for anti-arcing and (2) acting as a more massive buffer gas for improved internal energy conversion upon collision. An e-MSion electromagnetostatic linear ExD cell[143] was installed post the IM drift tube between the quadrupole and collision cell, to allow electron capture dissociation experiments of IM-separated ions. The pioneering designs from the electrodynamic ion funnel and the low field drift tube allows for direct collision cross section (CCS) measurements and retains the structure of labile samples[144–146].

1.5. Tandem Mass Spectrometry (MS/MS)

In a typical electrospray ionization MS1 spectrum, m/z ratios provide information on the overall mass of analytes but little structural information. Tandem MS (or MS/MS) is an analytical method that involves breaking chemical bonds in isolated precursor ions to form fragment (or product) ions. Fragment ion m/z information can provide detailed structural information for the precursor ions and MS/MS experiments also greatly improve the specificity of complex mixture analysis compared with single stage MS alone. In addition to its value for elucidation of biomolecular structures[147], MS/MS experiments are employed for determination of fragmentation mechanisms[148–150], observation of ion molecule reactions[151], and thermochemical data determination[152,153].

1.5.1. Vibrational Activation

Of all activation methods used for MS/MS, collision induced dissociation (CID) continues to be the most popular. In CID, precursor ions are accelerated into a neutral collision gas (i.e., N_2

or Ar) within a pressurized cell. As a result, a portion of the analyte ion kinetic energy is converted to internal energy followed by intramolecular vibrational energy redistribution (IVR) from inelastic collisions with the neutral gas[154]. Consequently, chemical bonds are vibrationally excited until their internal energy reach the dissociation thresholds. The weakest bonds (i.e., bond with lowest energy threshold) in a molecule thus are preferentially cleaved.

For peptides, *b*- and *y*-type ions are preferentially produced upon amide backbone cleavages[155,156] (*Fig. 1.15*). The "mobile proton model" is the generally accepted mechanism for dissociation of protonated peptides upon collisional activation. This model postulates that protons located at basic sites migrate to the less basic backbone amides upon collisional activation[157,158]. This rapid proton transfer process weakens the amide bonds and cause fragmentation.

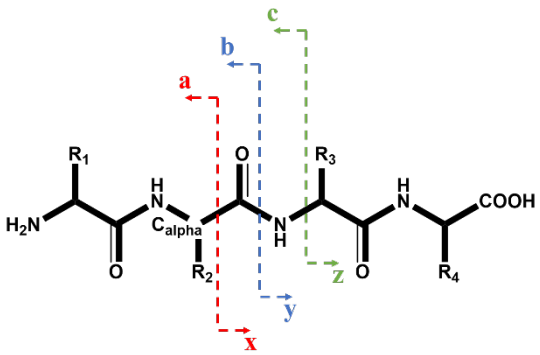

Figure 1.15. Peptide fragmentation nomenclature.

Even though CID is a quite efficient fragmentation method for peptides, lipids[159,160] and other small metabolites[161–163], the preferential loss of, e.g., labile post-translational modifications (e.g., phosphates, sulfates, and carbohydrates) can be a detriment[164,165].

1.5.2. Electron-Based Activation

Since its inception in the McLafferty laboratory, electron capture dissociation (ECD) and related radical-driven activation techniques have grown in popularity due to their ability to provide complementary fragmentation compared with CID. In particular, such approaches can retain labile chemical groups such as post-translational modifications and sulfate groups on carbohydrates.

❖ ***Electron Capture Dissociation (ECD) and Electron Transfer Dissociation (ETD)***

Electron capture dissociation was discovered by Zubarev et al. in 1998[166] and, since then, the McLafferty laboratory and many others have continued to develop, optimize, and upgrade the technique[164,166–168]. ECD (*eq. 4*) involves the interaction of free electrons with multiply protonated ions to form charge reduced radical cations, which, in turn, undergo radical-driven fragmentation. For peptides and protein, ECD induces N-C_α bond cleavages on the peptide backbone to primarily yield *c*- and *z*•-type fragment ions (*Fig. 14*). Due to the associated radical chemistry, ECD typically provides extensive fragmentation that can result in improved sequence coverage compared with CID. In addition, ECD often preserves labile chemical groups and thus is suitable for, e.g., PTM localization and identification.

$$(\boldsymbol{Equation\ 4})\ \mathbf{ECD}\text{: } [M+nH]^{n+} + e_{(<1\ eV)}{}^{-} \rightarrow [M+nH]^{(n-1)+\bullet} \rightarrow Fragments$$

Despite its success on FT-ICR instruments, ECD has proven difficult to implement on other instruments due to the low mass of free electrons and/or associated rapid RF heating in non-magnetic devices. To overcome these limitations, Syka, Coon and Hunt utilized gas-phase ion/ion chemistry to transfer electrons from radical anions to multiply-charged peptide cations, thus

inventing the electron transfer dissociation (ETD) technique[169]. The ETD principle is shown in *eq. 5*.

$$(\boldsymbol{Equation\ 5})\ \mathbf{ETD}\text{: } [M+nH]^{n+} + A^{-\bullet} \rightarrow [M+nH]^{(n-1)+\bullet} + A \rightarrow Fragments$$

This ion/ion strategy enables ECD-like fragmentation on a wider range of instrumentation, including less expensive and more common mass analyzers like ion traps. Similar to ECD, ETD induces N–C_α bond cleavages of peptide backbones with retention of labile PTMs (e.g., phosphorylation, glycosylation, etc.)[170,171]. ECD/ETD are well-suited for fragmenting highly charged precursor ions, but fragmentation efficiency suffers for low-charge density precursors[172,173]. Poor fragmentation efficiency can also occur due to noncovalent intramolecular interactions that prevent product ions from separating, particularly for precursors with low-charge density[174–176]that presumably have more compact gas-phase structures. For such precursor ions, product ions remain bound together by unbroken non-covalent bonds—even after successful backbone cleavage, resulting in non-dissociative electron capture/transfer events termed ECnoD or ETnoD. To overcome this issue additional ion activation may improve the quality of ECD/ETD spectra.

- ***Hybrid methods: Electron Transfer/Higher Energy Collision Induced Dissociation (EThcD) and Activated Ion-Electron Transfer Dissociation (AI-ETD)***

Hybrid fragmentation methods, achieved by applying sequential or simultaneous orthogonal activation strategies have been shown to greatly benefit the characterization of glyco- and phospho-peptides[177,178]. To mitigate the issue of ECnoD or ETnoD, pre-, concurrent, or post-activation strategies (e.g., gas collisions or IR photon irradiation) have been utilized to disrupt gas

phase secondary structures for more efficient ECD/ETD. Hybrid approaches like ETirD (i.e., IR irradiation following electron transfer)[179] or EThcD (i.e., collisional activation via HCD following electron transfer)[177] can greatly improve sequence coverage and PTM characterization via a combination of the unique advantages of each individual activation technique. In particular, EThcD is widely employed and commercially available to circumvent ETnoD[180,181]. For example, for *N*- and O-glycopeptides, EThcD generates both glycan and peptide backbone bond cleavages simultaneously in a single spectrum, thereby facilitating comprehensive characterization of such analytes (*Fig. 1.15*)[182]. Although EThcD is efficient for increasing peptide sequence coverage, spectral interpretation is complicated by the formation of odd electron $c^{\bullet}$- and even electron *z*′-type product ions through hydrogen atom migration, leading to ~ 1 Da shifts from theoretically calculated product ion m/z values[180,182].

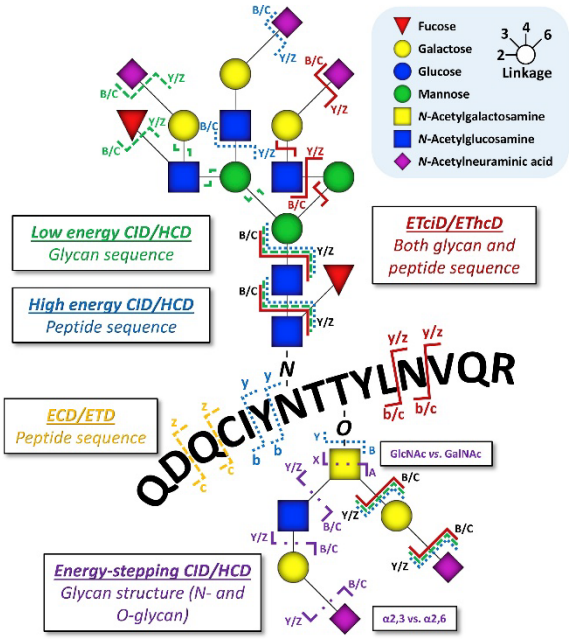

Figure 1.16. Glycan fragmentation from conventional and hybrid approaches.[182]

A solution to the latter problem[183] is the implementation of Activated Ion ETD (AI-ETD), in which ions are concomitantly activated with IR photons during the ETD event[183]. Not only does AI-ETD successfully increase sequence coverage for peptides/proteins (particularly for high m/z analytes)[179,184–186], but it also prevents hydrogen atom migration by more rapidly dissociating noncovalently bound product ion pairs, thereby generating predominantly even electron c' and odd electron *z*• fragment ions [187], corresponding to theoretically predicted m/z values. Thus, AI-

ETD improves the analysis of complex samples[188]. Furthermore, this technique is a promising tool for middle-down and top-down proteomics, as it displays improved fragmentation efficiency[185,189]. However, ECD/ETD require positive polarity mass spectrometry, which is less compatible with acidic analytes such as phosphorylated, sulfated, and sialyated analytes, as well as oligonucleotides. Such biomolecules are more readily deprotonated to form anions and thus can yield little to no signal in positive ion mode[190–193]. Additionally, labile PTMs (e.g., sulfation) are better retained in negative ion mode during both ionization and MS/MS activation[194,195]. Lastly, negative ion mode may increase sensitivity because many contaminants are more readily ionized in positive ion mode and thus exert a higher degree of ion suppression in positive polarity. For these reasons, negative-ion MS/MS activation techniques such as electron detachment dissociation (EDD) and negative ion ECD (niECD) are desirable.

- ***Electron detachment dissociation (EDD) and negative ion electron capture dissociation (niECD)***

Electron detachment dissociation, an electron-mediated method operating in negative analyte polarity, was first introduced by the Zubarev group[196]. In EDD, multiply deprotonated precursor ions are bombarded with high energy (>10 eV) electrons, resulting in electron detachment from the precursor ions and formation of charged-reduced, anionic radicals. For peptides, these electron deficient radicals then undergo C_α-C bond cleavages to yield mainly *a*•- and *x*-type ions. The EDD fragmentation scheme is shown in *eq. 6*.

$$(\boldsymbol{Equation\ 6})\ \mathbf{EDD}\text{: } [M-nH]^{n-} + e_{(>10\ eV)}{}^{-} \rightarrow [M+nH]^{(n-1)-\bullet} + 2e^{-} \rightarrow Fragments$$

However, as a result of the charge reduction process, it is only possible to detect EDD fragments if the precursors ions are at least doubly deprotonated. Another setback of EDD is that

structurally uninformative products, such as neutral, e.g., CO_2, and amino acid side-chain losses dominate[197].

Negative ion electron capture dissociation (niECD), a term coined for a unique MS/MS method in negative ion mode, was first discovered in the Håkansson laboratory. In niECD, electrons with a relatively narrow energy range (3.5–6.5 eV) can be captured by a negatively charged precursor ion to form a charge-*increased* radical that undergo ECD-type dissociation, producing c' and z• peptide fragments[194,198]. A gas-phase zwitterionic structure was proposed to explain the niECD mechanism with electron capture occurring at a positively charged site[198]. The overall scheme for niECD is shown below (*eq. 7*).

$$(\boldsymbol{Equation\ 7})\ \mathbf{niECD}\text{: } [M-nH]^{n-} + e^{-}(\sim 2.5-6.5\ eV) \rightarrow [M+nH]^{(n+1)-\bullet} \rightarrow Fragments$$

Over the last two and a half decades, electron-based methods have demonstrated utility for bottom-up, middle-down, and top-down proteomics. The increasing wealth of electron-based activation mechanisms has led to vibrant research on mechanisms and novel applications. However, much remains to be discovered in these areas.

1.6. Gas-phase Structures of PTM-containing Peptide Ions

For singly charged ions generated via matrix-assisted laser desorption/ionization (MALDI), it has been shown by ion mobility (IM) analysis and molecular dynamics (MD) calculations that phosphorylated and non-phosphorylated peptides have different gas-phase conformations[199]. The mobility for phosphorylated peptides is higher than their non-phosphorylated counterparts (*Fig. 1.17*)[199]. Evidence for intramolecular salt-bridging in multiply charged phosphopeptides,

generated with ESI, has been provided from the propensity to form abundant charge-reduced species in ECD,[200] and from the stability of phosphate-containing non-covalent complexes[201]. Further evidence for "folded" structures in multiply charged peptides was recently provided by Russell, Clemmer and co-workers who demonstrated that triply protonated substance P ions show four conformers following ESI[202]. Collisional activation of these gas-phase species revealed two types of conformers: kinetically trapped structures produced upon solvent evaporation, and extended structures formed upon annealing of the desolvated peptide ions. In another work, Cooper and co-workers have incorporated ion mobility and simulated annealing molecular dynamics simulation to explain that the phosphopeptides with "compact" states from a salt-bridge structure and ionic hydrogen bond exhibit poor ECD performance[203].

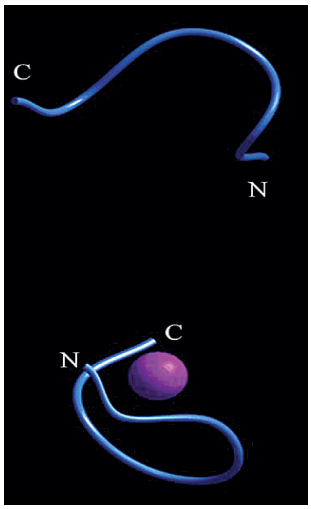

Figure 1.17. Computed gas-phase structures of a phosphorylated (phosphate in purple) and non-phosphorylated peptide.[199]

Electron-based tandem MS is a sensitive tool to probe subtle structural differences in gaseous peptides. For example, structural differences in melittin have been observed from different solvent compositions with ECD[204,205]. ECD of phosphorylated peptides was shown to provide less fragmentation compared with the corresponding modified peptides[174]. Cooper and coworkers proposed that intramolecular salt-bridge formation between deprotonated phosphate groups and protonated amino acid side chains[174] may explain this observed fragmentation pattern. Similar behavior has been observed for glycopeptides: while ECD of a 5 kDa glycopeptide produced only a charge-reduced radical species and a few side chain losses, extensive backbone dissociation into *c*- and *z*-type ions was observed following post-activation via IR irradiation, i.e.,

ECirD[137]. These data suggest glycopeptide structure compactness associated with the carbohydrate moeity[206,207]. Overall, both computational methods and electron-based MS/MS experiments lend indirect evidence that peptide modifications affect their gas-phase structures towards more compact states. However, direct measurements of such compact structures have been lacking.

1.7. Ion Mobility-Mass Spectrometry

Ion mobility-mass spectrometry can separate gas-phase analytes based on their collision cross sections (CCSs), a quality related to their charge and shape[208]. Analyte ions are typically produced by ESI and then introduced into an ion mobility cell.

1.8. Drift Tube Ion Mobility (DTIM)

In an IM drift tube, ions traverse the drift cell via an electrostatic field. As ions travel through the drift tube, collisions with a neutral gas such as nitrogen affect travelling time based on ion size, shape, and charge state (*Fig. 18*)[209]. The larger the ions, the slower is their velocity through the drift cell. The velocity of the ion, v, is a product of the electric field, E, and the mobility of the ion, K_0, or the inverse of the time required, t_D, to traverse a drift cell with known length, d [210].

$$\boldsymbol{v = K_0 E = \frac{d}{t_D}} \qquad \text{(Equation 8)}$$

The time t_D is used to determine the reduced mobility, K_0 at the standard temperature and pressure (STP):

$$\boldsymbol{K_0 = \frac{d}{E t_d} \cdot \frac{273}{T} \cdot \frac{P}{760}} \qquad \text{(Equation 9)}$$

in which P is the pressure and T is the temperature. The reduced mobility can also be expressed in terms of the characteristics of the ion and drift cell conditions [211] [i.e. the ion charge (ze), rotationally averaged cross section (Ω), number density of the collision gas (N), and the reduced mass of the ion and buffer gas (μ)]:

$$K_0 = \frac{3ze}{16N} \cdot \frac{1}{\Omega} \cdot \left(\frac{2\pi}{\mu k_B T}\right)^{\frac{1}{2}} \qquad \textit{(Equation 10)}$$

Based on the above equations, the mass, charge, and collision cross section of an ion determine its mobility under specific IM conditions. When coupling IM with mass spectrometry, the mass and charge are known, thus allowing Ω to be determined. Assuming hard sphere collisions, the rotationally averaged collision cross section of an ion can be derived from equation 3 as follows:

$$\Omega = \frac{(18\pi)^{\frac{1}{2}}}{16} \frac{ze}{(k_B T)^{\frac{1}{2}}} \left[\frac{1}{m_i} + \frac{1}{m_n}\right]^{\frac{1}{2}} \frac{t_d E}{d} \frac{760}{P} \frac{T}{273.15} \frac{1}{N} \qquad \textit{(Equation 11)}$$

in which z is the charge state of the ion, e is the elementary charge, and m_i and m_n are the masses of the ion and the neutral drift gas, respectively. *Eq. 1.11* is known as the Mason-Schamp equation. Following the drift cell, ions are typically directed into a time-of-flight (TOF) mass spectrometer.

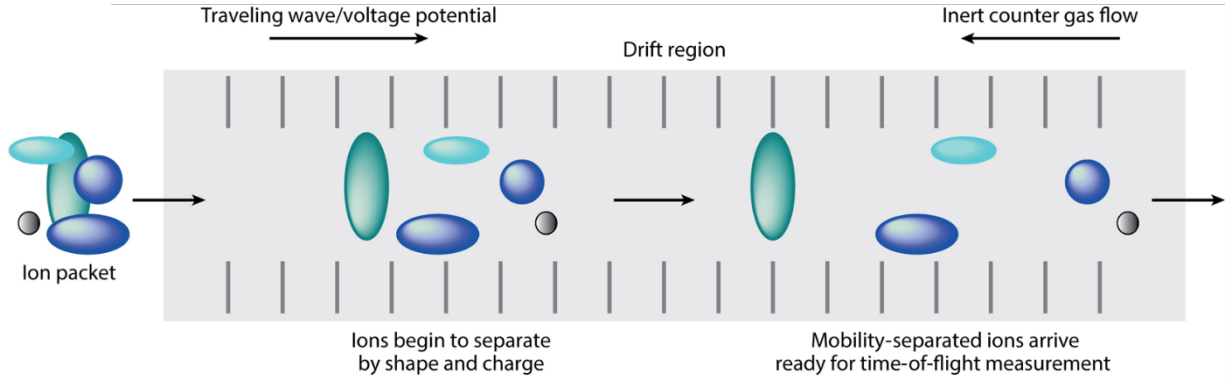

Figure 1.18. Ion mobility separation of ions with different sizes.[209]

The coupling of IM to MS has allowed new approaches to structural biology of macromolecules [209,212,213], including determination of stoichiometry and topology for complex biological assemblies[209,212–215]. Despite significant advances of IM-MS technology, separation and characterization of isomeric glycoconjugates remain challenging due to their extraordinary structural diversity. Sobott and coworkers used travelling wave ion mobility spectrometry (TWIMS) for separation of isomeric glycoconjungates but clear separation of isomeric tryptic glycopeptides was unsuccessful [216].

1.9. Collision Induced Unfolding (CIU)

Within the past decades, the use of collisional activation to study structure and stability of gas phase protein ions has become widespread[217,218]. Collision induced unfolding (CIU) is an extension of this work where isolated biomolecular ions are activated via energetic collisions with a background gas (e.g., argon) in order to increase the internal energy of a molecule and cause them to unfold without fragmentation[219] (*Fig. 19a*). The combination of CIU with ion mobility-mass spectrometry (IM-MS) can generate fingerprints related to the stability of proteins and protein complexes (*Figs. 1.19b and 1.19c*)[217,220]. In combination with CIU fingerprints, MD simulations provide greater insights into the dynamic nature of proteins, protein-protein complexes, and protein-ligand interactions[221]. CIU has been mostly used for proteins, e.g., to rapidly distinguish subtle

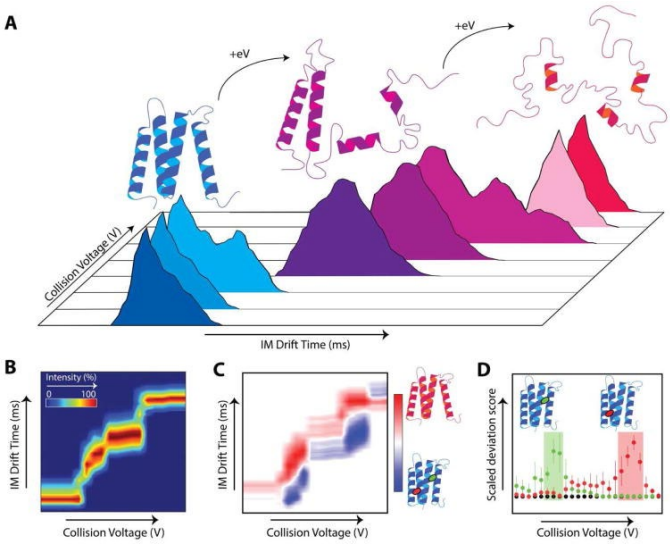

Figure 1.19. Principles of collision induced unfolding.[219]

differences in large therapeutic monoclonal antibodies with different disulfide bonding patterns[222], with limited work focusing on peptides[223]. CIU of PTM-modified peptides has, to our knowledge, not been studied to date.

1.10. Molecular Dynamics (MD) Simulations for Peptide Gas-Phase Structure Elucidation

Molecular dynamics (MD) is a computational approach for examining the atom location and movement in space[224]. The simulation of motion is accomplished by solving the numerical solution of the classical Newtonian laws of motion for the system, producing a set of conformational profiles. By exploring this energy surface, thermodynamic properties of proteins can be obtained to predict shape and refine structures from X-Ray crystallography[225]. MD can be performed using several popular program packages such as AMBER, CHARMM, GROMACS, NAMD, and Desmond[226].

While MD simulations provide unrivaled details of spatial arrangement of selected states, it suffers a limited scope to explore full conformational space relevant for chosen systems[227,228]. To study biomolecular systems more effectively, incorporation of complementary MS technology to MD simulations have offered unprecedented insights into protein dynamics, assemblies, and interactions[203,229–232]. MS strategies (e.g., IM, hydrogen/deuterium exchange (HDX), crosslinking, oxidative foot printing, etc...) provide composition, size, and overall shape of biological ensembles, so that experimentally derived constraints can be refined in order to sample only specific regions of interest, reducing computational power needed for a given simulation. One prime example is the combination of MD with cryogenic IM-MS to reveal stepwise dehydration and kinetic trapping of hydrated substance P ions during the evaporative ESI process[233]. Another

example of such an integrative approach is the use of combinatorial MS techniques (IM, label-free quantitative bottom-up and top-down MS) with steered MD and several variants of meta-dynamics simulations to provide an insight into conformational distributions of intrinsically disordered proteins upon transition-metal binding [231]. While most current MD work focuses on large biological systems such as proteins and protein complexes, peptide structure dynamics is often overlooked.

1.11. Dissertation Overview

This dissertation presents efforts to improve radical driven tandem mass spectrometry methods for studying biomolecular structure. Specifically, Chapters 2 and 3 explore post-separation supercharging in nanoHPLC along with open data-base searching for improved electron transfer dissociation of labile glycosylated and lipid-containing peptides, respectively. The latter work also involved implementation of C8 RPLC chromatography higher temperature (i.e., 50^{o}C) for optimum retention of lipidated peptides. Chapters 4 and 5 present the first applications of collision induced unfolding coupled with ion mobility analysis to directly observe structural changes in PTM-containing peptides and how such changes affect their electron capture dissociation behavior in both bottom up and middle down implementations, respectively. Molecular dynamics simulations were also employed to further illuminate the associated structural transitions. Overall, this CIU-ECD approach results in greatly improved analysis of large PTM-containing peptides, including therapeutic monoclonal antibody fragments. Chapter 6 explores a new analytical target as well as the mechanism of negative ion electron capture dissociation. Specifically, the utility of niECD for ganglioside analysis is discussed. Overall,

my research work will enrich our understanding of improved approaches for labile PTM analysis as well as provide insights into novel methods such CIU-ECD.

1.12. References

(1) Walzthoeni, T.; Leitner, A.; Stengel, F.; Aebersold, R. Mass Spectrometry Supported Determination of Protein Complex Structure. *Current Opinion in Structural Biology* **2013**, *23* (2), 252–260. https://doi.org/10.1016/J.SBI.2013.02.008.

(2) Kong, A. T.; Leprevost, F. V; Avtonomov, D. M.; Mellacheruvu, D.; Nesvizhskii, A. I. MsFragger: Ultrafast and Comprehensive Peptide Identification in Mass Spectrometry-Based Proteomics. **2017**, *14* (5), 513. https://doi.org/10.1038/nmeth.4256.

(3) Harris, G. A.; Nyadong, L.; Fernandez, F. M. Recent Developments in Ambient Ionization Techniques for Analytical Mass Spectrometry. **2008**. https://doi.org/10.1039/b806810k.

(4) Benesch, J. L. P.; Ruotolo, B. T. Mass Spectrometry: Come of Age for Structural and Dynamical Biology. *Current Opinion in Structural Biology* **2011**, *21* (5), 641–649. https://doi.org/10.1016/J.SBI.2011.08.002.

(5) Van Den Heuvel, R. H. H.; Heck, A. J. R. Native Protein Mass Spectrometry: From Intact Oligomers to Functional Machineries. *Current opinion in chemical biology* **2004**, *8* (5), 519–526. https://doi.org/10.1016/J.CBPA.2004.08.006.

(6) O'Reilly, F. J.; Rappsilber, J. Cross-Linking Mass Spectrometry: Methods and Applications in Structural, Molecular and Systems Biology. *Nature Structural & Molecular Biology 2018 25:11* **2018**, *25* (11), 1000–1008. https://doi.org/10.1038/s41594-018-0147-0.

(7) Cohen, P. The Origins of Protein Phosphorylation. *Nature Cell Biology 2002 4:5* **2002**, *4* (5), E127–E130. https://doi.org/10.1038/ncb0502-e127.

(8) LIS, H.; SHARON, N. Protein Glycosylation. *European Journal of Biochemistry* **1993**, *218* (1), 1–27. https://doi.org/10.1111/J.1432-1033.1993.TB18347.X.

(9) McLachlin, D. T.; Chait, B. T. Analysis of Phosphorylated Proteins and Peptides by Mass Spectrometry. *Current Opinion in Chemical Biology* **2001**, *5* (5), 591–602. https://doi.org/10.1016/S1367-5931(00)00250-7.

(10) Boyer, R. Posttranslational Modification of Proteins: Expanding Nature's Inventory. Christopher T. Walsh, Roberts & Company Publishers, Greenwood Village, CO, 2005, 576 Pp., ISBN 0-9747077-3-2, $98.00. *Biochemistry and Molecular Biology Education* **2006**, *34* (6), 461–462. https://doi.org/10.1002/BMB.2006.494034069996.

(11) Tom, C. T. M. B. M. B.; Martin, B. R. Fat Chance! Getting a Grip on a Slippery Modification. *ACS Chemical Biology* **2013**, *8* (1), 46–57. https://doi.org/10.1021/cb300607e.

(12) Campbell, C. T.; Yarema, K. J. Large-Scale Approaches for Glycobiology. *Genome Biology* **2005**, *6* (11), 236. https://doi.org/10.1186/gb-2005-6-11-236.

(13) Bertozzi, C. R.; Kiessling, and L. L. Chemical Glycobiology. *Science* **2001**, *291* (5512), 2357–2364. https://doi.org/10.1126/SCIENCE.1059820.

(14) Helenius, A.; Aebi, M. Intracellular Functions of N-Linked Glycans. *Science (New York, N.Y.)* **2001**, *291* (5512), 2364–2369. https://doi.org/10.1126/SCIENCE.291.5512.2364.

(15) Varki, A. Biological Roles of Oligosaccharides: All of the Theories Are Correct. *Glycobiology* **1993**, *3* (2), 97–130. https://doi.org/10.1093/glycob/3.2.97.

(16) Kolter, T. Ganglioside Biochemistry. *Article ID* **2012**, *2012*, 36. https://doi.org/10.5402/2012/506160.

(17) Wu, G.; Lu, Z. H.; Kulkarni, N.; Ledeen, R. W. Deficiency of Ganglioside GM1 Correlates with Parkinson's Disease in Mice and Humans. *Journal of neuroscience research* **2012**, *90* (10), 1997–2008. https://doi.org/10.1002/JNR.23090.

(18) Maglione, V.; Marchi, P.; di Pardo, A.; Lingrell, S.; Horkey, M.; Tidmarsh, E.; Sipione, S. Impaired Ganglioside Metabolism in Huntington's Disease and Neuroprotective Role of GM1. *Journal of Neuroscience* **2010**, *30* (11), 4072–4080. https://doi.org/10.1523/JNEUROSCI.6348-09.2010.

(19) Desplats, P. A.; Denny, C. A.; Kass, K. E.; Gilmartin, T.; Head, S. R.; Sutcliffe, J. G.; Seyfried, T. N.; Thomas, E. A. Glycolipid and Ganglioside Metabolism Imbalances In Huntington's Disease. *Neurobiology of disease* **2007**, *27* (3), 265. https://doi.org/10.1016/J.NBD.2007.05.003.

(20) Davidsson, P.; Wallin, A.; Fredman, P.; Gottfries, C. G.; Karlsson, I.; Månsson, J. E.; Svennerholm, L.; Blennow, K. Gangliosides in Cerebrospinal Fluid in "Probable Alzheimer's Disease." *Archives of neurology* **1991**, *48* (10), 1032–1035. https://doi.org/10.1001/ARCHNEUR.1991.00530220048018.

(21) Sipione, S.; Monyror, J.; Galleguillos, D.; Steinberg, N.; Kadam, V. Gangliosides in the Brain: Physiology, Pathophysiology and Therapeutic Applications. *Frontiers in Neuroscience* **2020**, *14*, 1004. https://doi.org/10.3389/FNINS.2020.572965/BIBTEX.

(22) Hyung, S. J.; Ruotolo, B. T. Integrating Mass Spectrometry of Intact Protein Complexes into Structural Proteomics. *Proteomics* **2012**, *12* (10), 1547. https://doi.org/10.1002/PMIC.201100520.

(23) Zhang, Y.; Fonslow, B. R.; Shan, B.; Baek, M.-C.; Yates, J. R. Protein Analysis by Shotgun/Bottom-up Proteomics. **2013**. https://doi.org/10.1021/cr3003533.

(24) Gillet, L. C.; Leitner, A.; Aebersold, R. Mass Spectrometry Applied to Bottom-Up Proteomics: Entering the High-Throughput Era for Hypothesis Testing. *Annual Review of Analytical Chemistry* **2016**, *9*, 449–472. https://doi.org/10.1146/ANNUREV-ANCHEM-071015-041535.

(25) Switzar, L.; Giera, M.; Niessen, W. M. A. Protein Digestion: An Overview of the Available Techniques and Recent Developments. *Journal of Proteome Research* **2013**, *12* (3), 1067–1077. https://doi.org/10.1021/PR301201X.

(26) Breuker, K.; Jin, M.; Han, X.; Jiang, H.; McLafferty, F. W. Top-Down Identification and Characterization of Biomolecules by Mass Spectrometry. *Journal of the American Society for Mass Spectrometry* **2008**, *19* (8), 1045. https://doi.org/10.1016/J.JASMS.2008.05.013.

(27) McLafferty, F. W.; Proc Natl, D. F.; Biol, C. C. Ion Processes. *Int. J. Mass Spectrom. Ion Processes* **1994**, *27* (2), 24.

(28) Kelleher, N. L. Peer Reviewed: Top-Down Proteomics. *Analytical Chemistry* **2004**, *76* (11), 196 A-203 A. https://doi.org/10.1021/AC0415657.

(29) McLafferty, F. W. A Century of Progress in Molecular Mass Spectrometry. *The Annual Review of Analytical Chemistry is online Annual Rev. Anal. Chem* **2011**, *4*, 1–22. https://doi.org/10.1146/annurev-anchem-061010-114018.

(30) Catherman, A. D.; Skinner, O. S.; Kelleher, N. L. Top Down Proteomics: Facts and Perspectives. *Biochemical and Biophysical Research Communications* **2014**, *445* (4), 683–693. https://doi.org/10.1016/J.BBRC.2014.02.041.

(31) Chen, B.; Brown, K. A.; Lin, Z.; Ge, Y. Top-Down Proteomics: Ready for Prime Time? *Analytical Chemistry* **2017**, *90* (1), 110–127. https://doi.org/10.1021/ACS.ANALCHEM.7B04747.

(32) Tsybin, Y. O. From High- to Super-Resolution Mass Spectrometry. *Chimia* **2014**, *68* (3), 168–174. https://doi.org/10.2533/CHIMIA.2014.168.

(33) Du, Y.; Wang, F.; May, K.; Xu, W.; Liu, H. Determination of Deamidation Artifacts Introduced by Sample Preparation Using 18O-Labeling and Tandem Mass Spectrometry Analysis. *Analytical Chemistry* **2012**, *84* (15), 6355–6360. https://doi.org/10.1021/AC3013362/SUPPL_FILE/AC3013362_SI_001.PDF.

(34) Mao, Y.; Valeja, S. G.; Rouse, J. C.; Hendrickson, C. L.; Marshall, A. G. Top-down Structural Analysis of an Intact Monoclonal Antibody by Electron Capture Dissociation-Fourier Transform Ion Cyclotron Resonance-Mass Spectrometry. *Analytical Chemistry* **2013**, *85* (9), 4239–4246. https://doi.org/10.1021/AC303525N/SUPPL_FILE/AC303525N_SI_002.PDF.

(35) Fornelli, L.; Damoc, E.; Thomas, P. M.; Kelleher, N. L.; Aizikov, K.; Denisov, E.; Makarov, A.; Tsybin, Y. O. Analysis of Intact Monoclonal Antibody IgG1 by Electron Transfer Dissociation Orbitrap FTMS. *Molecular and Cellular Proteomics* **2012**, *11* (12), 1758–1767. https://doi.org/10.1074/MCP.M112.019620/ATTACHMENT/7EAED268-329B-40C5-8879-35F77B1440DD/MMC1.PDF.

(36) Sidoli, S.; Lin, S.; Karch, K. R.; Garcia, B. A. Bottom-Up and Middle-Down Proteomics Have Comparable Accuracies in Defining Histone Post-Translational Modification Relative Abundance and Stoichiometry. *Analytical Chemistry* **2015**, *87* (6), 3129–3133. https://doi.org/10.1021/ACS.ANALCHEM.5B00072/SUPPL_FILE/AC5B00072_SI_001.PDF.

(37) Sidoli, S.; Schwämmle, V.; Ruminowicz, C.; Hansen, T. A.; Wu, X.; Helin, K.; Jensen, O. N. Middle-down Hybrid Chromatography/Tandem Mass Spectrometry Workflow for Characterization of Combinatorial Post-Translational Modifications in Histones. *PROTEOMICS* **2014**, *14* (19), 2200–2211. https://doi.org/10.1002/PMIC.201400084.

(38) Wu, C.; Tran, J. C.; Zamdborg, L.; Durbin, K. R.; Li, M.; Ahlf, D. R.; Early, B. P.; Thomas, P. M.; Sweedler, J. v.; Kelleher, N. L. A Protease for "middle-down" Proteomics. *Nature Methods 2012 9:8* **2012**, *9* (8), 822–824. https://doi.org/10.1038/nmeth.2074.

(39) Cristobal, A.; Marino, F.; Post, H.; van den Toorn, H. W. P.; Mohammed, S.; Heck, A. J. R. Toward an Optimized Workflow for Middle-Down Proteomics. *Analytical Chemistry* **2017**, *89* (6), 3318–3325. https://doi.org/10.1021/ACS.ANALCHEM.6B03756/SUPPL_FILE/AC6B03756_SI_001.PDF.

(40) Fornelli, L.; Ayoub, D.; Aizikov, K.; Beck, A.; Tsybin, Y. O. Middle-down Analysis of Monoclonal Antibodies with Electron Transfer Dissociation Orbitrap Fourier Transform Mass Spectrometry. *Analytical Chemistry* **2014**, *86* (6), 3005–3012. https://doi.org/10.1021/AC4036857/SUPPL_FILE/AC4036857_SI_001.PDF.

(41) Tsiatsiani, L.; Heck, A. J. R.; Heck, A. J. R.; Bijvoet, P. Proteomics beyond Trypsin. *The FEBS Journal* **2015**, *282* (14), 2612–2626. https://doi.org/10.1111/FEBS.13287.

(42) Sjögren, J.; Olsson, F.; Beck, A. Rapid and Improved Characterization of Therapeutic Antibodies and Antibody Related Products Using IdeS Digestion and Subunit Analysis. *Analyst* **2016**, *141* (11), 3114–3125. https://doi.org/10.1039/C6AN00071A.

(43) Chevreux, G.; Tilly, N.; Bihoreau, N. Fast Analysis of Recombinant Monoclonal Antibodies Using IdeS Proteolytic Digestion and Electrospray Mass Spectrometry. *Analytical Biochemistry* **2011**, *415* (2), 212–214. https://doi.org/10.1016/J.AB.2011.04.030.

(44) An, Y.; Zhang, Y.; Mueller, H. M.; Shameem, M.; Chen, X. A New Tool for Monoclonal Antibody Analysis. *https://doi.org/10.4161/mabs.28762* **2014**, *6* (4), 879–893. https://doi.org/10.4161/MABS.28762.

(45) Tautenhahn, R.; Bottcher, C.; Neumann, S. Highly Sensitive Feature Detection for High Resolution LC/MS. *BMC Bioinformatics* **2008**, *9* (1), 1–16. https://doi.org/10.1186/1471-2105-9-504/FIGURES/10.

(46) Volmer, D. L. Ion Suppression: A Major Concern in Mass Spectrometry. 2006.

(47) Annesley, T. M. Ion Suppression in Mass Spectrometry. *Clinical Chemistry* **2003**, *49* (7), 1041–1044. https://doi.org/10.1373/49.7.1041.

(48) Toms, S. A.; Weil, R. J.; Gaspari, M.; Cuda, G. Nano LC-MS/MS: A Robust Setup for Proteomic Analysis. *Methods in Molecular Biology 790*. https://doi.org/10.1007/978-1-61779-319-6_9.

(49) Wilson, S. R.; Vehus, T.; Berg, H. S.; Lundanes, E. Nano-LC in Proteomics: Recent Advances and Approaches. *Bioanalysis* **2015**, *7* (14), 1799–1815. https://doi.org/10.4155/BIO.15.92/ASSET/IMAGES/LARGE/FIGURE3.JPEG.

(50) Dorsey, J. G.; Dill, K. A. The Molecular Mechanism of Retention in Reversed-Phase Liquid Chromatography.

(51) Karlsson, K. -E; Novotny, M. A Miniature Gradient Elution System for Liquid Chromatography with Packed Capillary Columns. *Journal of High Resolution Chromatography* **1984**, *7* (7), 411–413. https://doi.org/10.1002/JHRC.1240070712.

(52) Davis, M. T.; Beierle, J.; Bures, E. T.; McGinley, M. D.; Mort, J.; Robinson, J. H.; Spahr, C. S.; Yu, W.; Luethy, R.; Patterson, S. D. Automated LC-LC-MS-MS Platform Using Binary Ion-Exchange and Gradient Reversed-Phase Chromatography for Improved Proteomic Analyses. *Journal of*

chromatography. B, Biomedical sciences and applications **2001**, *752* (2), 281–291. https://doi.org/10.1016/S0378-4347(00)00547-8.

(53) Wuhrer, M.; de Boer, A. R.; Deelder, A. M. Structural Glycomics Using Hydrophilic Interaction Chromatography (HILIC) with Mass Spectrometry. *Mass Spectrometry Reviews* **2009**, *28* (2), 192–206. https://doi.org/10.1002/MAS.20195.

(54) Buszewski, B.; Noga, S. Hydrophilic Interaction Liquid Chromatography (HILIC)—a Powerful Separation Technique. *Analytical and Bioanalytical Chemistry* **2012**, *402* (1), 231. https://doi.org/10.1007/S00216-011-5308-5.

(55) Chauve, B.; Guillarme, D.; Cléon, P.; Veuthey, J. L. Evaluation of Various HILIC Materials for the Fast Separation of Polar Compounds. *Journal of Separation Science* **2010**, *33* (6–7), 752–764. https://doi.org/10.1002/JSSC.200900749.

(56) Kawachi, Y.; Ikegami, T.; Takubo, H.; Ikegami, Y.; Miyamoto, M.; Tanaka, N. Chromatographic Characterization of Hydrophilic Interaction Liquid Chromatography Stationary Phases: Hydrophilicity, Charge Effects, Structural Selectivity, and Separation Efficiency. *Journal of Chromatography A* **2011**, *1218* (35), 5903–5919. https://doi.org/10.1016/J.CHROMA.2011.06.048.

(57) Ikegami, T.; Tomomatsu, K.; Takubo, H.; Horie, K.; Tanaka, N. Separation Efficiencies in Hydrophilic Interaction Chromatography. *Journal of Chromatography A* **2008**, *1184* (1–2), 474–503. https://doi.org/10.1016/J.CHROMA.2008.01.075.

(58) Iribarne, J. v.; Thomson, B. A. On the Evaporation of Small Ions from Charged Droplets. *The Journal of Chemical Physics* **2008**, *64* (6), 2287. https://doi.org/10.1063/1.432536.

(59) Dole, M.; Mack, L. L.; Hines, R. L.; Mobley, R. C.; Ferguson, L. D.; Alice, M. B. Molecular Beams of Macroions. *II The Journal of Chemical Physics* **1968**, *49*, 4977. https://doi.org/10.1063/1.1670391.

(60) Konermann, L.; Ahadi, E.; Rodriguez, A. D.; Vahidi, S. Unraveling the Mechanism of Electrospray Ionization. *Analytical Chemistry* **2013**, *85* (1), 2–9. https://doi.org/10.1021/ac302789c.

(61) Banerjee, S.; Mazumdar, S. Electrospray Ionization Mass Spectrometry: A Technique to Access the Information beyond the Molecular Weight of the Analyte. *International Journal of Analytical Chemistry* **2012**, *2012*, 1–40. https://doi.org/10.1155/2012/282574.

(62) Wilm, M. Principles of Electrospray Ionization. *Molecular & Cellular Proteomics : MCP* **2011**, *10* (7). https://doi.org/10.1074/MCP.M111.009407.

(63) Kebarle, P.; Verkcerk, U. H. Electrospray: From Ions in Solution to Ions in the Gas Phase, What We Know Now. *Mass Spectrometry Reviews* **2009**, *28* (6), 898–917. https://doi.org/10.1002/mas.20247.

(64) Ahadi, E.; Konermann, L. Ejection of Solvated Ions from Electrosprayed Methanol/Water Nanodroplets Studied by Molecular Dynamics Simulations. *J. Am. Chem. Soc* **2011**, *133*, 9354–9363. https://doi.org/10.1021/ja111492s.

(65) Ahadi, E.; Konermann, L. Modeling the Behavior of Coarse-Grained Polymer Chains in Charged Water Droplets: Implications for the Mechanism of Electrospray Ionization. *Journal of Physical Chemistry B* **2012**, *116* (1), 104–112. https://doi.org/10.1021/jp209344z.

(66) Fenn, J. B. Ion Formation from Charged Droplets: Roles of Geometry, Energy, and Time. *Journal of the American Society for Mass Spectrometry* **1993**, *4* (7), 524–535. https://doi.org/10.1016/1044-0305(93)85014-O.

(67) Ahadi, E.; Konermann, L. Ejection of Solvated Ions from Electrosprayed Methanol/Water Nanodroplets Studied by Molecular Dynamics Simulations. *Journal of the American Chemical Society* **2011**, *133* (24), 9354–9363. https://doi.org/10.1021/ja111492s.

(68) Konermann, L.; Rodriguez, A. D.; Liu, J. On the Formation of Highly Charged Gaseous Ions from Unfolded Proteins by Electrospray Ionization. *Analytical Chemistry* **2012**, *84* (15), 6798–6804. https://doi.org/10.1021/ac301298g.

(69) Wickremsinhe, E.; Singh, G.; Ackermann, B.; Gillespie, T.; Chaudhary, A. A Review of Nanoelectrospray Ionization Applications for Drug Metabolism and Pharmacokinetics. *Current drug metabolism* **2006**, *7* (8), 913–928. https://doi.org/10.2174/138920006779010610.

(70) Tousi, F.; Bones, J.; Hancock, W. S.; Hincapie, M. Differential Chemical Derivatization Integrated with Chromatographic Separation for Analysis of Isomeric Sialylated N -Glycans: A Nano-Hydrophilic Interaction Liquid Chromatography-MS Platform. *Analytical Chemistry* **2013**, *85* (17), 8421–8428. https://doi.org/10.1021/AC4018007/SUPPL_FILE/AC4018007_SI_001.PDF.

(71) Martin, S. E.; Shabanowitz, J.; Hunt, D. F.; Marto, J. A. Subfemtomole MS and MS/MS Peptide Sequence Analysis Using Nano-HPLC Micro-ESI Fourier Transform Ion Cyclotron Resonance Mass Spectrometry. *Analytical Chemistry* **2000**, *72* (18), 4266–4274. https://doi.org/10.1021/AC000497V.

(72) Chetwynd, A. J.; David, A. A Review of Nanoscale LC-ESI for Metabolomics and Its Potential to Enhance the Metabolome Coverage. *Talanta* **2018**, *182*, 380–390. https://doi.org/10.1016/J.TALANTA.2018.01.084.

(73) Yamashita, M.; Fenn, J. B.; Meng, C. K.; Mann, M.; Wilm, M.; Wilm, M. S. Analytical Properties of the Nanoelectrospray Ion Source. *Analytical Chemistry* **1996**, *68* (1), 1–8. https://doi.org/10.1021/AC9509519.

(74) Juraschek, R.; Dü, T.; Karas, M. Nanoelectrospray-More Than Just a Minimized-Flow Electrospray Ionization Source. **1998**.

(75) Karas, M.; Bahr, U.; Dülcks, T. Nano-Electrospray Ionization Mass Spectrometry: Addressing Analytical Problems beyond Routine. *Fresenius' Journal of Analytical Chemistry* **2000**, *366* (6–7), 669–676. https://doi.org/10.1007/s002160051561.

(76) Iavarone, A. T.; Jurchen, J. C.; Williams, E. R. Supercharged Protein and Peptide Ions Formed by Electrospray Ionization. *Analytical Chemistry* **2001**, *73* (7), 1455–1460. https://doi.org/10.1021/ac001251t.

(77) Sterling, H. J.; Williams, E. R. Origin of Supercharging in Electrospray Ionization of Noncovalent Complexes from Aqueous Solution. *Journal of the American Society for Mass Spectrometry* **2009**, *20* (10), 1933–1943. https://doi.org/10.1016/j.jasms.2009.06.012.

(78) Krusemark, C. J.; Frey, B. L.; Belshaw, P. J.; Smith, L. M. Modifying the Charge State Distribution of Proteins in Electrospray Ionization Mass Spectrometry by Chemical Derivatization. *Journal of the American Society for Mass Spectrometry* **2009**, *20* (9), 1617–1625. https://doi.org/10.1016/j.jasms.2009.04.017.

(79) Kharlamova, A.; Prentice, B. M.; Huang, T.-Y.; McLuckey, S. A. Electrospray Droplet Exposure to Gaseous Acids for the Manipulation of Protein Charge State Distributions. *Analytical Chemistry* **2010**, *82* (17), 7422–7429. https://doi.org/10.1021/ac101578q.

(80) Fenn, J. B.; Mann, M.; Meng, C. K.; Wong, S. F.; Whitehouse, C. M. Electrospray Ionization–Principles and Practice. *Mass Spectrometry Reviews* **1990**, *9* (1), 37–70. https://doi.org/10.1002/mas.1280090103.

(81) Flick, T. G.; Williams, E. R. Supercharging with Trivalent Metal Ions in Native Mass Spectrometry. *Journal of the American Society for Mass Spectrometry* **2012**, *23* (11), 1885–1895. https://doi.org/10.1007/s13361-012-0463-2.

(82) Iavarone, A. T.; Jurchen, J. C.; Williams, E. R. Effects of Solvent on the Maximum Charge State and Charge State Distribution of Protein Ions Produced by Electrospray Ionization. *Journal of the American Society for Mass Spectrometry* **2000**, *11* (11), 976–985. https://doi.org/10.1016/S1044-0305(00)00169-0.

(83) Iavarone, A. T.; Williams, E. R. Supercharging in Electrospray Ionization: Effects on Signal and Charge. *International Journal of Mass Spectrometry* **2002**, *219* (1), 63–72. https://doi.org/10.1016/S1387-3806(02)00587-0.

(84) Lomeli, S. H.; Peng, I. X.; Yin, S.; Ogorzalek Loo, R. R.; Loo, J. A. New Reagents for Increasing ESI Multiple Charging of Proteins and Protein Complexes. *Journal of the American Society for Mass Spectrometry* **2010**, *21* (1), 127–131. https://doi.org/10.1016/j.jasms.2009.09.014.

(85) Sterling, H. J.; Prell, J. S.; Cassou, C. A.; Williams, E. R. Protein Conformation and Supercharging with DMSO from Aqueous Solution. *Journal of the American Society for Mass Spectrometry* **2011**, *22* (7), 1178–1186. https://doi.org/10.1007/S13361-011-0116-X.

(86) Teo, C. A.; Donald, W. A. Solution Additives for Supercharging Proteins beyond the Theoretical Maximum Proton-Transfer Limit in Electrospray Ionization Mass Spectrometry. *Analytical chemistry* **2014**, *86* (9), 4455–4462. https://doi.org/10.1021/AC500304R.

(87) Abaye, D. A.; Agbo, I. A.; Nielsen, B. v. Current Perspectives on Supercharging Reagents in Electrospray Ionization Mass Spectrometry. *RSC Advances* **2021**, *11* (33), 20355–20369. https://doi.org/10.1039/D1RA00745A.

(88) Feng, C.; Commodore, J. J.; Cassady, C. J. The Use of Chromium(III) to Supercharge Peptides by Protonation at Low Basicity Sites. *Journal of the American Society for Mass Spectrometry* **2015**, *26* (2), 347–358. https://doi.org/10.1007/S13361-014-1020-Y/FIGURES/3.

(89) Going, C. C.; Xia, Z.; Williams, E. R. New Supercharging Reagents Produce Highly Charged Protein Ions in Native Mass Spectrometry. *Analyst* **2015**, *140* (21), 7184–7194. https://doi.org/10.1039/C5AN01710F.

(90) Brahim, B.; Alves, S.; Cole, R. B.; Tabet, J. C. Charge Enhancement of Single-Stranded DNA in Negative Electrospray Ionization Using the Supercharging Reagent Meta-Nitrobenzyl Alcohol. *Journal of the American Society for Mass Spectrometry* **2013**, *24* (12), 1988–1996. https://doi.org/10.1007/s13361-013-0732-8.

(91) Konermann, L.; Douglas, D. J. Acid-Induced Unfolding of Cytochrome c at Different Methanol Concentrations: Electrospray Ionization Mass Spectrometry Specifically Monitors Changes in the Tertiary Structure. *Biochemistry* **1997**, *36* (40), 12296–12302. https://doi.org/10.1021/bi971266u.

(92) Babu, K. R.; Douglas, D. J. Methanol-Induced Conformations of Myoglobin at PH 4.0. *Biochemistry* **2000**, *39* (47), 14702–14710. https://doi.org/10.1021/bi001265t.

(93) Le Blanc, J. C. Y.; Wang, J.; Guevremont, R.; Siu, K. W. M. Electrospray Mass Spectra of Protein Cations Formed in Basic Solutions. *Organic Mass Spectrometry* **1994**, *29* (11), 587–593. https://doi.org/10.1002/oms.1210291103.

(94) Loo, R. R. O.; Smith, R. D. Proton Transfer Reactions of Multiply Charged Peptide and Protein Cations and Anions. *Journal of Mass Spectrometry* **1995**, *30* (2), 339–347. https://doi.org/10.1002/jms.1190300217.

(95) Iavarone, A. T.; Jurchen, J. C.; Williams, E. R. Effects of Solvent on the Maximum Charge State and Charge State Distribution of Protein Ions Produced by Electrospray Ionization. *Journal of the American Society for Mass Spectrometry* **2000**, *11* (11), 976–985. https://doi.org/10.1016/S1044-0305(00)00169-0.

(96) Yang, P.; Cooks, R. G.; Ouyang, Z.; Hawkridge, A. M.; Muddiman, D. C. Gentle Protein Ionization Assisted by High-Velocity Gas Flow. *Analytical chemistry* **2005**, *77* (19), 6174–6183. https://doi.org/10.1021/ac050711l.

(97) Page, J. S.; Kelly, R. T.; Tang, K.; Smith, R. D. Ionization and Transmission Efficiency in an Electrospray Ionization-Mass Spectrometry Interface. *Journal of the American Society for Mass Spectrometry* **2007**, *18* (9), 1582–1590. https://doi.org/10.1016/j.jasms.2007.05.018.

(98) Benkestock, K.; Sundqvist, G.; Edlund, P.-O.; Roeraade, J. Influence of Droplet Size, Capillary-Cone Distance and Selected Instrumental Parameters for the Analysis of Noncovalent Protein-Ligand Complexes by Nano-Electrospray Ionization Mass Spectrometry. *Journal of mass spectrometry : JMS* **2004**, *39* (9), 1059–1067. https://doi.org/10.1002/jms.685.

(99) Sterling, H. J.; Cassou, C. A.; Susa, A. C.; Williams, E. R. Electrothermal Supercharging of Proteins in Native Electrospray Ionization. *Analytical Chemistry* **2012**, *84* (8), 3795–3801. https://doi.org/10.1021/AC300468A/SUPPL_FILE/AC300468A_SI_001.PDF.

(100) Bouza, M.; Li, Y.; Wu, C.; Guo, H.; Wang, Z. L.; Fernández, F. M. Large-Area Triboelectric Nanogenerator Mass Spectrometry: Expanded Coverage, Double-Bond Pinpointing, and

Supercharging. *Journal of the American Society for Mass Spectrometry* **2020**, *31* (3), 727–734. https://doi.org/10.1021/JASMS.0C00002/SUPPL_FILE/JS0C00002_SI_001.PDF.

(101) Wang, H.; Yong, G.; Brown, S. L.; Lee, H. E.; Zenaidee, M. A.; Supuran, C. T.; Donald, W. A. Supercharging Protein Ions in Native Mass Spectrometry Using Theta Capillary Nanoelectrospray Ionization Mass Spectrometry and Cyclic Alkylcarbonates. *Analytica Chimica Acta* **2018**, *1003*, 1–9. https://doi.org/10.1016/J.ACA.2017.11.075.

(102) Iavarone, A. T.; Williams, E. R. Mechanism of Charging and Supercharging Molecules in Electrospray Ionization. *Journal of the American Chemical Society* **2003**, *125* (8), 2319–2327. https://doi.org/10.1021/ja021202t.

(103) Ogorzalek Loo, R. R.; Lakshmanan, R.; Loo, J. A. What Protein Charging (and Supercharging) Reveal about the Mechanism of Electrospray Ionization. *Journal of the American Society for Mass Spectrometry* **2014**, *25* (10), 1675–1693. https://doi.org/10.1007/s13361-014-0965-1.

(104) Sterling, H. J.; Kintzer, A. F.; Feld, G. K.; Cassou, C. A.; Krantz, B. A.; Williams, E. R. Supercharging Protein Complexes from Aqueous Solution Disrupts Their Native Conformations. *Journal of the American Society for Mass Spectrometry* **2012**, *23* (2), 191–200. https://doi.org/10.1007/s13361-011-0301-y.

(105) Sterling, H. J.; Prell, J. S.; Cassou, C. A.; Williams, E. R. Protein Conformation and Supercharging with DMSO from Aqueous Solution. *Journal of the American Society for Mass Spectrometry* **2011**, *22* (7), 1178–1186. https://doi.org/10.1007/s13361-011-0116-x.

(106) Compton, P. D.; Zamdborg, L.; Thomas, P. M.; Kelleher, N. L. On the Scalability and Requirements of Whole Protein Mass Spectrometry. *Analytical Chemistry* **2011**, *83* (17), 6868–6874. https://doi.org/10.1021/ac2010795.

(107) Douglass, K. A.; Venter, A. R. Investigating the Role of Adducts in Protein Supercharging with Sulfolane. *Journal of the American Society for Mass Spectrometry* **2012**, *23* (3), 489–497. https://doi.org/10.1007/s13361-011-0319-1.

(108) Peters, I.; Metwally, H.; Konermann, L. Mechanism of Electrospray Supercharging for Unfolded Proteins: Solvent-Mediated Stabilization of Protonated Sites during Chain Ejection. *Analytical Chemistry* **2019**. https://doi.org/10.1021/acs.analchem.9b01470.

(109) Thingholm, T. E.; Palmisano, G.; Kjeldsen, F.; Larsen, M. R. Undesirable Charge-Enhancement of Isobaric Tagged Phosphopeptides Leads to Reduced Identification Efficiency. *Journal of Proteome Research* **2010**, *9* (8), 4045–4052. https://doi.org/10.1021/pr100230q.

(110) Iavarone, A. T.; Jurchen, J. C.; Williams, E. R. Supercharged Protein and Peptide Ions Formed by Electrospray Ionization. *Analytical Chemistry* **2001**, *73* (7), 1455–1460. https://doi.org/10.1021/ac001251t.

(111) Nshanian, M.; Lakshmanan, R.; Chen, H.; Loo, R. R. O.; Loo, J. A. Enhancing Sensitivity of Liquid Chromatography–Mass Spectrometry of Peptides and Proteins Using Supercharging Agents. *International Journal of Mass Spectrometry* **2018**, *427*, 157–164. https://doi.org/10.1016/j.ijms.2017.12.006.

(112) Wang, Q. Protein-Protein Interaction Analysis: Expanded Hydrogen/Deuterium Exchange Tandem Mass Spectrometry and Host Cell Protein Characterization, University of Michigan, 2019.

(113) Going, C. C.; Xia, Z.; Williams, E. R. New Supercharging Reagents Produce Highly Charged Protein Ions in Native Mass Spectrometry. *Analyst* **2015**, *140* (21), 7184–7194. https://doi.org/10.1039/c5an01710f.

(114) Lomeli, S. H.; Peng, I. X.; Yin, S.; Ogorzalek Loo, R. R.; Loo, J. A. New Reagents for Increasing ESI Multiple Charging of Proteins and Protein Complexes. *Journal of the American Society for Mass Spectrometry* **2010**, *21* (1), 127–131. https://doi.org/10.1016/j.jasms.2009.09.014.

(115) Gross, J. H. Mass Spectrometry : A Textbook. **2004**.

(116) Comisarow, M. B.; Marshall, A. G. Fourier Transform Ion Cyclotron Resonance Spectroscopy. *Chemical Physics Letters* **1974**, *25* (2), 282–283. https://doi.org/10.1016/0009-2614(74)89137-2.

(117) Nikolaev, E. N.; Kostyukevich, Y. I.; Vladimirov, G. N. Fourier Transform Ion Cyclotron Resonance (FT ICR) Mass Spectrometry: Theory and Simulations. *Mass Spectrometry Reviews* **2016**, *35* (2), 219–258. https://doi.org/10.1002/MAS.21422.

(118) Marshall, A. G.; Grosshans, P. B. Fourier Transform Ion Cyclotron Resonance Mass Spectrometry: The Teenage Years. *Analytical Chemistry* **2008**, *63* (4), 215–229. https://doi.org/10.1021/AC00004A001.

(119) Comisarow, M. B.; Marshall, A. G. The Early Development of Fourier Transform Ion Cyclotron Resonance (FT-ICR) Spectroscopy. *JOURNAL OF MASS SPECTROMETRY* **1996**, *31*, 581–585.

(120) Hendrickson, C. L.; Quinn, J. P.; Kaiser, N. K.; Smith, D. F.; Blakney, G. T.; Chen, T.; Marshall, A. G.; Weisbrod, C. R.; Beu, S. C. 21 Tesla Fourier Transform Ion Cyclotron Resonance Mass Spectrometer: A National Resource for Ultrahigh Resolution Mass Analysis. *Journal of The American Society for Mass Spectrometry* **2015**, *26* (9), 1626–1632. https://doi.org/10.1007/S13361-015-1182-2.

(121) Hendrickson, C. L.; Quinn, J. P.; Kaiser, N. K.; Smith, D. F.; Blakney, G. T.; Chen, T.; Marshall, A. G.; Weisbrod, C. R.; Beu, S. C. 21 Tesla Fourier Transform Ion Cyclotron Resonance Mass Spectrometer: A National Resource for Ultrahigh Resolution Mass Analysis. *Journal of The*

American Society for Mass Spectrometry **2015**, *26* (9), 1626–1632. https://doi.org/10.1007/S13361-015-1182-2.

(122) Lawrence, E. O.; Livingston, M. S. The Production of High Speed Light Ions without the Use of High Voltages. *Physical Review* **1932**, *40* (1), 19–35. https://doi.org/10.1103/PHYSREV.40.19/FIGURE/1/THUMB.

(123) Beu, S. C.; Laude, D. A. Open Trapped Ion Cell Geometries for Fourier Transform Ion Cyclotron Resonance Mass Spectrometry. *International Journal of Mass Spectrometry and Ion Processes* **1992**, *112* (2–3), 215–230. https://doi.org/10.1016/0168-1176(92)80006-M.

(124) Marshall, A. G. Milestones in Fourier Transform Ion Cyclotron Resonance Mass Spectrometry Technique Development. *International Journal of Mass Spectrometry* **2000**, *200* (1–3), 331–356. https://doi.org/10.1016/S1387-3806(00)00324-9.

(125) Barrow, M. P.; Burkitt, W. I.; Derrick, P. J. Principles of Fourier Transform Ion Cyclotron Resonance Mass Spectrometry and Its Application in Structural Biology. *Analyst* **2005**, *130* (1), 18–28. https://doi.org/10.1039/B403880K.

(126) Tolmachev, A. v.; Robinson, E. W.; Smith, R. D.; Leach, F. E.; Futrell, J. H.; Paa-Tolić, L. A Conceptual Approach for FT-ICR Cell Harmonization Utilizing External Shim Electrodes. *International Journal of Mass Spectrometry* **2012**, *325–327*, 45–50. https://doi.org/10.1016/J.IJMS.2012.06.027.

(127) Marshall, A. G.; Hendrickson, C. L.; Jackson, G. S. FOURIER TRANSFORM ION CYCLOTRON RESONANCE MASS SPECTROMETRY: A PRIMER. https://doi.org/10.1002/(SICI)1098-2787(1998)17:1.

(128) Marshall, A. G.; Hendrickson, C. L. High-Resolution Mass Spectrometers. *Annual review of analytical chemistry (Palo Alto, Calif.)* **2008**, *1* (1), 579–599. https://doi.org/10.1146/ANNUREV.ANCHEM.1.031207.112945.

(129) Piyadasa, C. K.; Hakansson, P.; Ariyarathe, T. R.; Benner, H. W.; Bryant, P.; Johnsen, K.; Sakurai, T.; Nakabushi, H.; Hiasa, T.; Okanishi K ; Kingdon, K. H.; Mcilraith, A. H.; Knight, R. D.; Lewis, R. R.; Yang, L.; Church, D. A.; Sekioka, T.; Terasama, M.; Awaya, Y.; Rad ; Gillig, K. J.; Bluhm, B. K.; Russell, D. H. Electrostatic Axially Harmonic Orbital Trapping: A High-Performance Technique of Mass Analysis. *Analytical Chemistry* **2000**, *72* (6), 1156–1162. https://doi.org/10.1021/AC991131P.

(130) Perry, R. H.; Cooks, R. G.; Noll, R. J. Orbitrap Mass Spectrometry: Instrumentation, Ion Motion and Applications. *Mass Spectrometry Reviews* **2008**, *27* (6), 661–699. https://doi.org/10.1002/MAS.20186.

(131) Hu, Q.; Noll, R. J.; Li, H.; Makarov, A.; Hardman, M.; Cooks, R. G. The Orbitrap: A New Mass Spectrometer. *Journal of Mass Spectrometry* **2005**, *40* (4), 430–443. https://doi.org/10.1002/JMS.856.

(132) Michalski, A.; Damoc, E.; Hauschild, J. P.; Lange, O.; Wieghaus, A.; Makarov, A.; Nagaraj, N.; Cox, J.; Mann, M.; Horning, S. Mass Spectrometry-Based Proteomics Using Q Exactive, a High-Performance Benchtop Quadrupole Orbitrap Mass Spectrometer. *Molecular & Cellular Proteomics : MCP* **2011**, *10* (9). https://doi.org/10.1074/MCP.M111.011015.

(133) Fort, K. L.; van de Waterbeemd, M.; Boll, D.; Reinhardt-Szyba, M.; Belov, M. E.; Sasaki, E.; Zschoche, R.; Hilvert, D.; Makarov, A. A.; Heck, A. J. R. Expanding the Structural Analysis Capabilities on an Orbitrap-Based Mass Spectrometer for Large Macromolecular Complexes. *Analyst* **2017**, *143* (1), 100–105. https://doi.org/10.1039/C7AN01629H.

(134) Makarov, A.; Denisov, E.; Lange, O.; Horning, S. Dynamic Range of Mass Accuracy in LTQ Orbitrap Hybrid Mass Spectrometer. *Journal of The American Society for Mass Spectrometry 2006 17:7* **2006**, *17* (7), 977–982. https://doi.org/10.1016/J.JASMS.2006.03.006.

(135) Makarov, A.; Denisov, E.; Kholomeev, A.; Balschun, W.; Lange, O.; Strupat, K.; Horning, S. Performance Evaluation of a Hybrid Linear Ion Trap/Orbitrap Mass Spectrometer. *Analytical Chemistry* **2006**, *78* (7), 2113–2120. https://doi.org/10.1021/AC0518811.

(136) Dupree, E. J.; Jayathirtha, M.; Yorkey, H.; Mihasan, M.; Petre, B. A.; Darie, C. C. A Critical Review of Bottom-Up Proteomics: The Good, the Bad, and the Future of This Field. *Proteomes 2020, Vol. 8, Page 14* **2020**, *8* (3), 14. https://doi.org/10.3390/PROTEOMES8030014.

(137) Håkansson, K.; Chalmers, M. J.; Quinn, J. P.; McFarland, M. A.; Hendrickson, C. L.; Marshall, A. G. Combined Electron Capture and Infrared Multiphoton Dissociation for Multistage MS/MS in a Fourier Transform Ion Cyclotron Resonance Mass Spectrometer. *Analytical Chemistry* **2003**, *75* (13), 3256–3262. https://doi.org/10.1021/AC030015Q.

(138) Riley, N. M.; Westphall, M. S.; Coon, J. J. Activated Ion Electron Transfer Dissociation for Improved Fragmentation of Intact Proteins. *Analytical Chemistry* **2015**, *87* (14), 7109–7116. https://doi.org/10.1021/ACS.ANALCHEM.5B00881.

(139) Belov, M. E.; Damoc, E.; Denisov, E.; Compton, P. D.; Horning, S.; Makarov, A. A.; Kelleher, N. L. From Protein Complexes to Subunit Backbone Fragments: A Multi-Stage Approach to Native Mass Spectrometry. *Analytical chemistry* **2013**, *85* (23), 11163–11173. https://doi.org/10.1021/AC4029328.

(140) Ben-Nissan, G.; Belov, M. E.; Morgenstern, D.; Levin, Y.; Dym, O.; Arkind, G.; Lipson, C.; Makarov, A. A.; Sharon, M. Triple-Stage Mass Spectrometry Unravels the Heterogeneity of an Endogenous

Protein Complex. *Analytical chemistry* **2017**, *89* (8), 4708. https://doi.org/10.1021/ACS.ANALCHEM.7B00518.

(141) van de Waterbeemd, M.; Fort, K. L.; Boll, D.; Reinhardt-Szyba, M.; Routh, A.; Makarov, A.; Heck, A. J. R. High-Fidelity Mass Analysis Unveils Heterogeneity in Intact Ribosomal Particles. *Nature methods* **2017**, *14* (3), 283–286. https://doi.org/10.1038/NMETH.4147.

(142) Fedorova, O. A.; Moiseeva, T. N.; Nikiforov, A. A.; Tsimokha, A. S.; Livinskaya, V. A.; Hodson, M.; Bottrill, A.; Evteeva, I. N.; Ermolayeva, J. B.; Kuznetzova, I. M.; Turoverov, K. K.; Eperon, I.; Barlev, N. A. Proteomic Analysis of the 20S Proteasome (PSMA3)-Interacting Proteins Reveals a Functional Link between the Proteasome and MRNA Metabolism. *Biochemical and Biophysical Research Communications* **2011**, *416* (3–4), 258–265. https://doi.org/10.1016/J.BBRC.2011.10.126.

(143) Voinov, V. G.; Deinzer, M. L.; Barofsky, D. F. Electron Capture Dissociation in a Linear Radiofrequency-Free Magnetic Cell. *Rapid communications in mass spectrometry : RCM* **2008**, *22* (19), 3087. https://doi.org/10.1002/RCM.3709.

(144) Abi-Ghanem, J.; Rabin, C.; Porrini, M.; Rosu, F.; Gabelica, V. Compaction of RNA Hairpins and Their Kissing Complexes in Native Electrospray Mass Spectrometry. *Journal of the American Society for Mass Spectrometry* **2020**, *31* (10), 2035–2043. https://doi.org/10.1021/JASMS.0C00060/SUPPL_FILE/JS0C00060_SI_001.PDF.

(145) Abi-Ghanem, J.; Rabin, C.; Porrini, M.; Rosu, F.; Gabelica, V. Compaction of RNA Hairpins and Their Kissing Complexes in Native Electrospray Mass Spectrometry. *Journal of the American Society for Mass Spectrometry* **2020**, *31* (10), 2035–2043. https://doi.org/10.1021/JASMS.0C00060/SUPPL_FILE/JS0C00060_SI_001.PDF.

(146) D'Atri, V.; Gabelica, V. DNA and RNA Telomeric G-Quadruplexes: What Topology Features Can Be Inferred from Ion Mobility Mass Spectrometry? *Analyst* **2019**, *144* (20), 6074–6088. https://doi.org/10.1039/C9AN01216H.

(147) de Hoffmann, E. Tandem Mass Spectrometry: A Primer. *JOURNAL OF MASS SPECTROMETRY* **1996**, *31*, 129–137. https://doi.org/10.1002/(SICI)1096-9888(199602)31:2.

(148) Syrstad, E. A.; Tureček, F. Toward a General Mechanism of Electron Capture Dissociation. *Journal of the American Society for Mass Spectrometry 2004 16:2* **2005**, *16* (2), 208–224. https://doi.org/10.1016/J.JASMS.2004.11.001.

(149) Zubarev, R. A.; Haselmann, K. F.; Budnik, B.; Kjeldsen, F.; Jensen, F. Towards An Understanding of the Mechanism of Electron-Capture Dissociation: A Historical Perspective and Modern Ideas: *http://dx.doi.org/10.1255/ejms.517* **2017**, *8* (5), 337–349. https://doi.org/10.1255/EJMS.517.

(150) Leymarie, N.; Costello, C. E.; O'Connor, P. B. Electron Capture Dissociation Initiates a Free Radical Reaction Cascade. *Journal of the American Chemical Society* **2003**, *125* (29), 8949–8958. https://doi.org/10.1021/JA028831N.

(151) McLuckey, S. A.; Huang, T. Y. Ion/Ion Reactions: New Chemistry for Analytical MS. *Analytical Chemistry* **2009**, *81* (21), 8669–8676. https://doi.org/10.1021/AC9014935.

(152) Armentrout, P. B. Mass Spectrometry—Not Just a Structural Tool: The Use of Guided Ion Beam Tandem Mass Spectrometry to Determine Thermochemistry. *Journal of the American Society for Mass Spectrometry 2002 13:5* **2002**, *13* (5), 419–434. https://doi.org/10.1016/S1044-0305(02)00347-1.

(153) Graham Cooks, R.; Patrick, J. S.; Kotiaho, T.; McLuckey, S. A. Thermochemical Determinations by the Kinetic Method. *Mass Spectrometry Reviews* **1994**, *13* (4), 287–339. https://doi.org/10.1002/MAS.1280130402.

(154) Stannard, P. R.; Gelbart, W. M. Intramolecular Vibrational Energy Redistribution. *Journal of Physical Chemistry* **2002**, *85* (24), 3592–3599. https://doi.org/10.1021/J150624A015.

(155) Roepstorff, P.; Fohlman, J. Proposal for a Common Nomenclature for Sequence Ions in Mass Spectra of Peptides. *Biomedical mass spectrometry* **1984**, *11* (11), 601–601. https://doi.org/10.1002/BMS.1200111109.

(156) Mitchell Wells, J.; McLuckey, S. A. Collision-Induced Dissociation (CID) of Peptides and Proteins. *Methods in Enzymology* **2005**, *402*, 148–185. https://doi.org/10.1016/S0076-6879(05)02005-7.

(157) Wysocki, V. H.; Tsaprailis, G.; Smith, L. L.; Breci, L. A. Mobile and Localized Protons: A Framework for Understanding Peptide Dissociation. *JOURNAL OF MASS SPECTROMETRY J. Mass Spectrom* **2000**, *35*, 1399–1406. https://doi.org/10.1002/1096-9888.

(158) Dongré, A. R.; Jones, J. L.; Somogyi, Á.; Wysocki, V. H. Influence of Peptide Composition, Gas-Phase Basicity, and Chemical Modification on Fragmentation Efficiency: Evidence for the Mobile Proton Model. *Journal of the American Chemical Society* **1996**, *118* (35), 8365–8374. https://doi.org/10.1021/JA9542193.

(159) Schuhmann, K.; Herzog, R.; Schwudke, D.; Metelmann-Strupat, W.; Bornstein, S. R.; Shevchenko, A. Bottom-up Shotgun Lipidomics by Higher Energy Collisional Dissociation on LTQ Orbitrap Mass Spectrometers. *Analytical Chemistry* **2011**, *83* (14), 5480–5487. https://doi.org/10.1021/AC102505F/SUPPL_FILE/AC102505F_SI_001.PDF.

(160) Murphy, R. C.; Axelsen, P. H. Mass Spectrometric Analysis of Long-Chain Lipids. *Mass Spectrometry Reviews* **2011**, *30* (4), 579–599. https://doi.org/10.1002/MAS.20284.

(161) Zhu, X.; Kalyanaraman, N.; Subramanian, R. Enhanced Screening of Glutathione-Trapped Reactive Metabolites by in-Source Collision-Induced Dissociation and Extraction of Product Ion Using UHPLC-High Resolution Mass Spectrometry. *Analytical Chemistry* **2011**, *83* (24), 9516–9523. https://doi.org/10.1021/AC202280F/SUPPL_FILE/AC202280F_SI_001.PDF.

(162) Bijlsma, L.; Sancho, J. v.; Hernández, F.; Niessen, W. M. A. Fragmentation Pathways of Drugs of Abuse and Their Metabolites Based on QTOF MS/MS and MS E Accurate-Mass Spectra. *Journal of Mass Spectrometry* **2011**, *46* (9), 865–875. https://doi.org/10.1002/JMS.1963.

(163) Wang, P.; Bartlett, M. G. Collision-Induced Dissociation Mass Spectra of Cocaine, and Its Metabolites and Pyrolysis Products. *JOURNAL OF MASS SPECTROMETRY J. Mass Spectrom* **1998**, *33*, 961–967. https://doi.org/10.1002/(SICI)1096-9888(1998100)33:10.

(164) Zubarev, R. A. Electron-Capture Dissociation Tandem Mass Spectrometry. *Current Opinion in Biotechnology* **2004**, *15* (1), 12–16. https://doi.org/10.1016/J.COPBIO.2003.12.002.

(165) Mikesh, L. M.; Ueberheide, B.; Chi, A.; Coon, J. J.; Syka, J. E. P.; Shabanowitz, J.; Hunt, D. F. The Utility of ETD Mass Spectrometry in Proteomic Analysis. *Biochimica et Biophysica Acta (BBA) - Proteins and Proteomics* **2006**, *1764* (12), 1811–1822. https://doi.org/10.1016/J.BBAPAP.2006.10.003.

(166) Zubarev, R. A.; Kelleher, N. L.; McLafferty, F. W. Electron Capture Dissociation of Multiply Charged Protein Cations. A Nonergodic Process. *Journal of the American Chemical Society* **1998**, *120* (13), 3265–3266. https://doi.org/10.1021/JA973478K.

(167) Tsybin, Y. O.; Witt, M.; Baykut, G.; Kjeldsen, F.; Håkansson, P. Combined Infrared Multiphoton Dissociation and Electron Capture Dissociation with a Hollow Electron Beam in Fourier Transform Ion Cyclotron Resonance Mass Spectrometry. *Rapid Communications in Mass Spectrometry* **2003**, *17* (15), 1759–1768. https://doi.org/10.1002/RCM.1118.

(168) Pan, J.; Borchers, C. H. Top-down Structural Analysis of Posttranslationally Modified Proteins by Fourier Transform Ion Cyclotron Resonance-MS with Hydrogen/Deuterium Exchange and Electron Capture Dissociation. *PROTEOMICS* **2013**, *13* (6), 974–981. https://doi.org/10.1002/PMIC.201200246.

(169) Syka, J. E. P.; Coon, J. J.; Schroeder, M. J.; Shabanowitz, J.; Hunt, D. F. Peptide and Protein Sequence Analysis by Electron Transfer Dissociation Mass Spectrometry. *Proceedings of the National Academy of Sciences* **2004**, *101* (26), 9528–9533. https://doi.org/10.1073/PNAS.0402700101.

(170) Zhurov, K. O.; Fornelli, L.; Wodrich, M. D.; Laskay, Ü. A.; Tsybin, Y. O. Principles of Electron Capture and Transfer Dissociation Mass Spectrometry Applied to Peptide and Protein Structure Analysis. *Chemical Society Reviews* **2013**, *42* (12), 5014–5030. https://doi.org/10.1039/C3CS35477F.

(171) Coon, J. J. Collisions or Electrons? Protein Sequence Analysis in the 21st Century. *Analytical Chemistry* **2009**, *81* (9), 3208–3215. https://doi.org/10.1021/AC802330B.

(172) Kalli, A.; Håkansson, K. Comparison of the Electron Capture Dissociation Fragmentation Behavior of Doubly and Triply Protonated Peptides from Trypsin, Glu-C, and Chymotrypsin Digestion. *Journal of Proteome Research* **2008**, *7* (7), 2834–2844. https://doi.org/10.1021/PR800038Y/SUPPL_FILE/PR800038Y-FILE001.PDF.

(173) Good, D. M.; Wirtala, M.; McAlister, G. C.; Coon, J. J. Performance Characteristics of Electron Transfer Dissociation Mass Spectrometry. *Molecular and Cellular Proteomics* **2007**, *6* (11), 1942–1951. https://doi.org/10.1074/MCP.M700073-MCP200/ATTACHMENT/69C18BFB-489A-43F1-87C2-A330601D7797/MMC1.ZIP.

(174) Creese, A. J.; Cooper, H. J. The Effect of Phosphorylation on the Electron Capture Dissociation of Peptide Ions. *Journal of the American Society for Mass Spectrometry* **2008**, *19* (9), 1263–1274. https://doi.org/10.1016/J.JASMS.2008.05.015.

(175) Laszlo, K. J.; Munger, E. B.; Bush, M. F. Folding of Protein Ions in the Gas Phase after Cation-to-Anion Proton-Transfer Reactions. *Journal of the American Chemical Society* **2016**, *138* (30), 9581–9588. https://doi.org/10.1021/JACS.6B04282/SUPPL_FILE/JA6B04282_SI_001.PDF.

(176) Breuker, K.; Oh, H. bin; Horn, D. M.; Cerda, B. A.; McLafferty, F. W. Detailed Unfolding and Folding of Gaseous Ubiquitin Ions Characterized by Electron Capture Dissociation. *Journal of the American Chemical Society* **2002**, *124* (22), 6407–6420. https://doi.org/10.1021/JA012267J.

(177) Yu, Q.; Wang, B.; Chen, Z.; Urabe, G.; Glover, M. S.; Shi, X.; Guo, L. W.; Kent, K. C.; Li, L. Electron-Transfer/Higher-Energy Collision Dissociation (EThcD)-Enabled Intact Glycopeptide/Glycoproteome Characterization. *Journal of the American Society for Mass Spectrometry* **2017**, *28* (9), 1751. https://doi.org/10.1007/S13361-017-1701-4.

(178) Riley, N. M.; Hebert, A. S.; Dürnberger, G.; Stanek, F.; Mechtler, K.; Westphall, M. S.; Coon, J. J. Phosphoproteomics with Activated Ion Electron Transfer Dissociation. *Analytical Chemistry* **2017**, *89* (12), 6367–6376. https://doi.org/10.1021/ACS.ANALCHEM.7B00212.

(179) Ledvina, A. R.; Mcalister, G. C.; Gardner, M. W.; Smith, S. I.; Madsen, J. A.; Schwartz, J. C.; Stafford, G. C.; Syka, J. E. P.; Brodbelt, J. S.; Coon, J. J.; Ledvina,] A R; Mcalister, G. C.; Coon, J. J.;

Gardner, M. W.; Smith, S. I.; Madsen, J. A.; Brodbelt, J. S.; Schwartz, J. C.; Stafford, G. C.; Syka, J. E. P. Infrared Photoactivation Reduces Peptide Folding and Hydrogen-Atom Migration Following ETD Tandem Mass Spectrometry. *Angewandte Chemie International Edition* **2009**, *48* (45), 8526–8528. https://doi.org/10.1002/ANIE.200903557.

(180) Swaney, D. L.; McAlister, G. C.; Wirtala, M.; Schwartz, J. C.; Syka, J. E. P.; Coon, J. J. Supplemental Activation Method for High-Efficiency Electron-Transfer Dissociation of Doubly Protonated Peptide Precursors. *Analytical chemistry* **2007**, *79* (2), 477–485. https://doi.org/10.1021/AC061457F.

(181) Xia, Y.; Han, H.; McLuckey, S. A. Activation of Intact Electron-Transfer Products of Polypeptides and Proteins in Cation Transmission Mode Ion/Ion Reactions. *Analytical chemistry* **2008**, *80* (4), 1111–1117. https://doi.org/10.1021/AC702188Q.

(182) Reiding, K. R.; Bondt, A.; Franc, V.; Heck, A. J. R. The Benefits of Hybrid Fragmentation Methods for Glycoproteomics. *TrAC Trends in Analytical Chemistry* **2018**, *108*, 260–268. https://doi.org/10.1016/J.TRAC.2018.09.007.

(183) Ledvina, A. R.; McAlister, G. C.; Gardner, M. W.; Smith, S. I.; Madsen, J. A.; Schwartz, J. C.; Stafford, G. C.; Syka, J. E. P.; Brodbelt, J. S.; Coon, J. J. Infrared Photoactivation Reduces Peptide Folding and Hydrogenatom Migration Following ETD Tandem Mass Spectrometry. *Angewandte Chemie - International Edition* **2009**, *48* (45), 8526–8528. https://doi.org/10.1002/anie.200903557.

(184) Riley, N. M.; Westphall, M. S.; Coon, J. J. Activated Ion Electron Transfer Dissociation for Improved Fragmentation of Intact Proteins. *Analytical Chemistry* **2015**, *87* (14), 7109–7116. https://doi.org/10.1021/ACS.ANALCHEM.5B00881.

(185) Riley, N. M.; Westphall, M. S.; Coon, J. J. Activated Ion-Electron Transfer Dissociation Enables Comprehensive Top-Down Protein Fragmentation. *Journal of Proteome Research* **2017**, *16* (7), 2653–2659. https://doi.org/10.1021/ACS.JPROTEOME.7B00249/SUPPL_FILE/PR7B00249_SI_001.PDF.

(186) Ledvina, A. R.; Beauchene, N. A.; McAlister, G. C.; Syka, J. E. P.; Schwartz, J. C.; Griep-Raming, J.; Westphall, M. S.; Coon, J. J. Activated-Ion Electron Transfer Dissociation Improves the Ability of Electron Transfer Dissociation to Identify Peptides in a Complex Mixture. *Analytical Chemistry* **2010**, *82* (24), 10068–10074. https://doi.org/10.1021/AC1020358.

(187) Ledvina, A. R.; McAlister, G. C.; Gardner, M. W.; Smith, S. I.; Madsen, J. A.; Schwartz, J. C.; Stafford, G. C.; Syka, J. E. P.; Brodbelt, J. S.; Coon, J. J. Infrared Photoactivation Reduces Peptide Folding and Hydrogen-Atom Migration Following ETD Tandem Mass Spectrometry. *Angewandte Chemie (International ed. in English)* **2009**, *48* (45), 8526–8528. https://doi.org/10.1002/ANIE.200903557.

(188) Ledvina, A. R.; Beauchene, N. A.; McAlister, G. C.; Syka, J. E. P.; Schwartz, J. C.; Griep-Raming, J.; Westphall, M. S.; Coon, J. J. Activated-Ion ETD (AI-ETD) Improves the Ability of ETD to Identify Peptides in a Complex Mixture. *Analytical chemistry* **2010**, *82* (24), 10068. https://doi.org/10.1021/AC1020358.

(189) Lodge, J. M.; Schauer, K. L.; Brademan, D. R.; Riley, N. M.; Shishkova, E.; Westphall, M. S.; Coon, J. J. Top-Down Characterization of an Intact Monoclonal Antibody Using Activated Ion Electron Transfer Dissociation. *Analytical Chemistry* **2020**, *92* (15), 10246–10251. https://doi.org/10.1021/ACS.ANALCHEM.0C00705/SUPPL_FILE/AC0C00705_SI_001.PDF.

(190) Khoury, S.; el Banna, N.; Tfaili, S.; Chaminade, P. A Study of Inter-Species Ion Suppression in Electrospray Ionization-Mass Spectrometry of Some Phospholipid Classes. https://doi.org/10.1007/s00216-015-9245-6.

(191) Clifford, M. N.; Lopez, V.; Poquet, L.; Williamson, G.; Kuhnert, N. A Systematic Study of Carboxylic Acids in Negative Ion Mode Electrospray Ionisation Mass Spectrometry Providing a Structural Model for Ion Suppression. *Rapid Communications in Mass Spectrometry* **2007**, *21* (13), 2014–2018. https://doi.org/10.1002/RCM.3038.

(192) Antignac, J. P.; de Wasch, K.; Monteau, F.; de Brabander, H.; Andre, F.; le Bizec, B. The Ion Suppression Phenomenon in Liquid Chromatography–Mass Spectrometry and Its Consequences in the Field of Residue Analysis. *Analytica Chimica Acta* **2005**, *529* (1–2), 129–136. https://doi.org/10.1016/J.ACA.2004.08.055.

(193) Furey, A.; Moriarty, M.; Bane, V.; Kinsella, B.; Lehane, M. Ion Suppression; A Critical Review on Causes, Evaluation, Prevention and Applications. *Talanta* **2013**, *115*, 104–122. https://doi.org/10.1016/J.TALANTA.2013.03.048.

(194) Medzihradszky, K. F.; Guan, S.; Maltby, D. A.; Burlingame, A. L. Sulfopeptide Fragmentation in Electron-Capture and Electron-Transfer Dissociation. *Journal of the American Society for Mass Spectrometry 2007 18:9* **2007**, *18* (9), 1617–1624. https://doi.org/10.1016/J.JASMS.2007.06.002.

(195) Liu, H.; Håkansson, K. Electron Capture Dissociation of Tyrosine O-Sulfated Peptides Complexed with Divalent Metal Cations. *Analytical chemistry* **2006**, *78* (21), 7570–7576. https://doi.org/10.1021/AC061352C.

(196) Budnik, B. A.; Haselmann, K. F.; Zubarev, R. A. Electron Detachment Dissociation of Peptide Di-Anions: An Electron–Hole Recombination Phenomenon. *Chemical Physics Letters* **2001**, *342* (3–4), 299–302. https://doi.org/10.1016/S0009-2614(01)00501-2.

(197) Budnik, B. A.; Haselmann, K. F.; Zubarev, R. A. Electron Detachment Dissociation of Peptide Di-Anions: An Electron-Hole Recombination Phenomenon. *Chemical Physics Letters* **2001**, *342* (3–4), 299–302. https://doi.org/10.1016/S0009-2614(01)00501-2.

(198) Yoo, H. J.; Wang, N.; Zhuang, S.; Song, H.; Håkansson, K. Negative-Ion Electron Capture Dissociation: Radical-Driven Fragmentation of Charge-Increased Gaseous Peptide Anions. *Journal of the American Chemical Society* **2011**, *133* (42), 16790–16793. https://doi.org/10.1021/JA207736Y.

(199) Ruotolo, B. T.; Verbeck IV, G. F.; Thomson, L. M.; Woods, A. S.; Gillig, K. J.; Russell, D. H. Distinguishing between Phosphorylated and Nonphosphorylated Peptides with Ion Mobility-Mass Spectrometry. *Journal of Proteome Research* **2002**, *1* (4), 303–306. https://doi.org/10.1021/pr025516r.

(200) Chalmers, M. J.; Håkansson, K.; Johnson, R.; Smith, R.; Shen, J.; Emmett, M. R.; Marshall, A. G. Protein Kinase A Phosphorylation Characterized by Tandem Fourier Transform Ion Cyclotron Resonance Mass Spectrometry. *Proteomics* **2004**, *4* (4), 970–981. https://doi.org/10.1002/pmic.200300650.

(201) Woods, A. S.; Moyer, S. C.; Jackson, S. N. Amazing Stability of Phosphate-Quaternary Amine Interactions. *Journal of Proteome Research* **2008**, *7* (8), 3423–3427. https://doi.org/10.1021/pr8001595.

(202) Conant, C. R.; Fuller, D. R.; Zhang, Z.; Woodall, D. W.; Russell, D. H.; Clemmer, D. E. Substance P in the Gas Phase: Conformational Changes and Dissociations Induced by Collisional Activation in a Drift Tube. *Journal of the American Society for Mass Spectrometry* **2019**, *30* (6), 932–945. https://doi.org/10.1007/s13361-019-02160-3.

(203) Kim, D.; Pai, P.-J.; Creese, A. J.; Jones, A. W.; Russell, D. H.; Cooper, H. J. Probing the Electron Capture Dissociation Mass Spectrometry of Phosphopeptides with Traveling Wave Ion Mobility Spectrometry and Molecular Dynamics Simulations. *Journal of The American Society for Mass Spectrometry 2015 26:6* **2015**, *26* (6), 1004–1013. https://doi.org/10.1007/S13361-015-1094-1.

(204) Straus, R. N.; Jockusch, R. A. Hydrogen-Deuterium Exchange and Electron Capture Dissociation to Interrogate the Conformation of Gaseous Melittin Ions. *Journal of the American Society for Mass Spectrometry* **2019**, *30* (5), 864–875. https://doi.org/10.1007/S13361-019-02150-5/SUPPL_FILE/JS8B05998_SI_001.PDF.

(205) Yu, S.; Jang, H.-Y.; Oh, H. bin. Electron Capture Dissociation Mass Spectrometry for Gaseous Protonated Melittin Ions and Its Single Amino Acid Substituted Variants. **2019**, *10* (4). https://doi.org/10.5478/MSL.2019.10.4.117.

(206) Håkansson, K.; Cooper, H. J.; Emmett, M. R.; Costello, C. E.; Marshall, A. G.; Nilsson, C. L. Electron Capture Dissociation and Infrared Multiphoton Dissociation MS/MS of an N-Glycosylated Tryptic Peptide to Yield Complementary Sequence Information. *Analytical Chemistry* **2001**, *73* (18), 4530–4536. https://doi.org/10.1021/ac0103470.

(207) Håkansson, K.; Chalmers, M. J.; Quinn, J. P.; McFarland, M. A.; Hendrickson, C. L.; Marshall, A. G. Combined Electron Capture and Infrared Multiphoton Dissociation for Multistage MS/MS in a Fourier Transform Ion Cyclotron Resonance Mass Spectrometer. *Analytical Chemistry* **2003**, *75* (13), 3256–3262. https://doi.org/10.1021/ac030015q.

(208) Cumeras, R.; Figueras, E.; Davis, C. E.; Baumbach, J. I.; Gràcia, I. Review on Ion Mobility Spectrometry. Part 1: Current Instrumentation. *The Analyst* **2015**, *140* (5), 1376–1390. https://doi.org/10.1039/C4AN01100G.

(209) Mehmood, S.; Allison, T. M.; Robinson, C. V. Mass Spectrometry of Protein Complexes: From Origins to Applications. *Annu. Rev. Phys. Chem* **2015**, *66* (1), 453–474. https://doi.org/10.1146/annurev-physchem-040214-121732.

(210) M. F. Mesleh; J. M. Hunter, †; A. A. Shvartsburg; G. C. Schatz, * and; Jarrold*, M. F.; Mesleh, M. F.; Hunter, J. M.; Shvartsburg, A. A.; Schatz, G. C.; Jarrold, M. F. *Structural Information from Ion Mobility Measurements: Effects of Long-Rnage Potentials*; American Chemical Society, 1996. https://doi.org/10.1021/JP961623V.

(211) Uetrecht, C.; Rose, R. J.; Van Duijn, E.; Lorenzen, K.; Heck, A. J. R. Ion Mobility Mass Spectrometry of Proteins and Protein Assemblies. *Chemical Society Reviews* **2009**. https://doi.org/10.1039/b914002f.

(212) Ruotolo, B. T.; Benesch, J. L. P.; Sandercock, A. M.; Hyung, S.-J.; Robinson, C. V. Ion Mobility–Mass Spectrometry Analysis of Large Protein Complexes. *Nature Protocols* **2008**, *3* (7), 1139–1152. https://doi.org/10.1038/nprot.2008.78.

(213) Fenn, L. S.; Kliman, M.; Mahsut, A.; Zhao, S. R.; Mclean, J. A. Characterizing Ion Mobility-Mass Spectrometry Conformation Space for the Analysis of Complex Biological Samples. *Analytical and Bioanalytical Chemistry* **2009**, *394* (1), 235–244. https://doi.org/10.1007/s00216-009-2666-3.

(214) Gray, C. J.; Thomas, B.; Upton, R.; Migas, L. G.; Eyers, C. E.; Barran, P. E.; Flitsch, S. L. Applications of Ion Mobility Mass Spectrometry for High Throughput, High Resolution Glycan Analysis ☆. **2016**. https://doi.org/10.1016/j.bbagen.2016.02.003.

(215) Lanucara, F.; Holman, S. W.; Gray, C. J.; Eyers, C. E. The Power of Ion Mobility-Mass Spectrometry for Structural Characterization and the Study of Conformational Dynamics. *Nature Chemistry* **2014**, *6* (4), 281–294. https://doi.org/10.1038/nchem.1889.

(216) Barroso, A.; Giménez, E.; Konijnenberg, A.; Sancho, J.; Sanz-Nebot, V.; Sobott, F. Evaluation of Ion Mobility for the Separation of Glycoconjugate Isomers Due to Different Types of Sialic Acid Linkage, at the Intact Glycoprotein, Glycopeptide and Glycan Level. *Journal of Proteomics* **2018**, *173*, 22–31. https://doi.org/10.1016/j.jprot.2017.11.020.

(217) Hyung, S. J.; Robinson, C. V.; Ruotolo, B. T. Gas-Phase Unfolding and Disassembly Reveals Stability Differences in Ligand-Bound Multiprotein Complexes. *Chemistry and Biology* **2009**, *16* (4), 382–390. https://doi.org/10.1016/j.chembiol.2009.02.008.

(218) Benesch, J. L. P.; Aquilina, J. A.; Ruotolo, B. T.; Sobott, F.; Robinson, C. V. Tandem Mass Spectrometry Reveals the Quaternary Organization of Macromolecular Assemblies. *Chemistry & biology* **2006**, *13* (6), 597–605. https://doi.org/10.1016/j.chembiol.2006.04.006.

(219) Dixit, S. M.; Polasky, D. A.; Ruotolo, B. T. Collision Induced Unfolding of Isolated Proteins in the Gas Phase: Past, Present, and Future. *Current Opinion in Chemical Biology*. Elsevier Ltd February 1, 2018, pp 93–100. https://doi.org/10.1016/j.cbpa.2017.11.010.

(220) Shelimov, K. B.; Clemmer, D. E.; Hudgins, R. R.; Jarrold, M. F. Protein Structure in Vacuo: Gas-Phase Conformations of BPTI and Cytochrome c. *Journal of the American Chemical Society* **1997**, *119* (9), 2240–2248. https://doi.org/10.1021/ja9619059.

(221) Popa, V.; Trecroce, D. A.; McAllister, R. G.; Konermann, L. Collision-Induced Dissociation of Electrosprayed Protein Complexes: An All-Atom Molecular Dynamics Model with Mobile Protons. *Journal of Physical Chemistry B* **2016**, *120* (23), 5114–5124. https://doi.org/10.1021/acs.jpcb.6b03035.

(222) Tian, Y.; Han, L.; Buckner, A. C.; Ruotolo, B. T. Collision Induced Unfolding of Intact Antibodies: Rapid Characterization of Disulfide Bonding Patterns, Glycosylation, and Structures. *Analytical Chemistry* **2015**, *87* (22), 11509–11515. https://doi.org/10.1021/acs.analchem.5b03291.

(223) Conant, C. R.; Fuller, D. R.; Zhang, Z.; Woodall, D. W.; Russell, D. H.; Clemmer, D. E. Substance P in the Gas Phase: Conformational Changes and Dissociations Induced by Collisional Activation in a Drift Tube. *Journal of the American Society for Mass Spectrometry* **2019**, *30* (6), 932–945. https://doi.org/10.1007/s13361-019-02160-3.

(224) Leach, A. R. Ligand-Based Approaches: Core Molecular Modeling. *Comprehensive Medicinal Chemistry II* **2007**, *4*, 87–118. https://doi.org/10.1016/B0-08-045044-X/00246-7.

(225) Roy, K.; Kar, S.; Das, R. N. Computational Chemistry. *Understanding the Basics of QSAR for Applications in Pharmaceutical Sciences and Risk Assessment* **2015**, 151–189. https://doi.org/10.1016/B978-0-12-801505-6.00005-3.

(226) Han, X.; Shin, W. H.; Christoffer, C. W.; Terashi, G.; Monroe, L.; Kihara, D. Study of the Variability of the Native Protein Structure. *Encyclopedia of Bioinformatics and Computational Biology: ABC of Bioinformatics* **2019**, *1–3*, 606–619. https://doi.org/10.1016/B978-0-12-809633-8.20148-9.

(227) van den Bedem, H.; Fraser, J. S. Integrative, Dynamic Structural Biology at Atomic Resolution—It's about Time. *Nature Methods 2015 12:4* **2015**, *12* (4), 307–318. https://doi.org/10.1038/nmeth.3324.

(228) Bottaro, S.; Lindorff-Larsen, K. Biophysical Experiments and Biomolecular Simulations: A Perfect Match? *Science* **2018**, *361* (6400), 355–360. https://doi.org/10.1126/SCIENCE.AAT4010/ASSET/47B2CA07-355F-4A48-9FCE-8D9A46A17F68/ASSETS/GRAPHIC/361_355_F3.JPEG.

(229) Beveridge, R.; Migas, L. G.; Das, R. K.; Pappu, R. v.; Kriwacki, R. W.; Barran, P. E. Ion Mobility Mass Spectrometry Uncovers the Impact of the Patterning of Oppositely Charged Residues on the Conformational Distributions of Intrinsically Disordered Proteins. *Journal of the American Chemical Society* **2019**, *141* (12), 4908–4918. https://doi.org/10.1021/JACS.8B13483/SUPPL_FILE/JA8B13483_SI_001.PDF.

(230) Marklund, E. G.; Benesch, J. L. Weighing-up Protein Dynamics: The Combination of Native Mass Spectrometry and Molecular Dynamics Simulations. *Current Opinion in Structural Biology* **2019**, *54*, 50–58. https://doi.org/10.1016/J.SBI.2018.12.011.

(231) Peris-Díaz, M. D.; Guran, R.; Domene, C.; de Los Rios, V.; Zitka, O.; Adam, V.; Krężel, A. An Integrated Mass Spectrometry and Molecular Dynamics Simulations Approach Reveals the Spatial Organization Impact of Metal-Binding Sites on the Stability of Metal-Depleted Metallothionein-2 Species. *Journal of the American Chemical Society* **2021**, *143* (40), 16486–16501. https://doi.org/10.1021/JACS.1C05495/SUPPL_FILE/JA1C05495_SI_001.PDF.

(232) Brandon T. Ruotolo, †; Guido F. Verbeck IV, †; Lisa M. Thomson, ‡; Amina S. Woods, §; Kent J. Gillig, † and; David H. Russell*, †. Distinguishing between Phosphorylated and Nonphosphorylated Peptides with Ion Mobility−Mass Spectrometry. *Journal of Proteome Research* **2002**, *1* (4), 303–306. https://doi.org/10.1021/PR025516R.

(233) Silveira, J. A.; Fort, K. L.; Kim, D.; Servage, K. A.; Pierson, N. A.; Clemmer, D. E.; Russell, D. H. From Solution to the Gas Phase: Stepwise Dehydration and Kinetic Trapping of Substance p

Reveals the Origin of Peptide Conformations. *Journal of the American Chemical Society* **2013**, *135* (51), 19147–19153. https://doi.org/10.1021/JA4114193/SUPPL_FILE/JA4114193_SI_001.PDF.

Chapter 2. Post-Separation Supercharging in nanoHPLC for Improved Electron-Based Fragmentation of Glycopeptides

2.1. Introduction:

The cell surface is heavily modified by a range of posttranslational modifications (PTMs) with specialized biological roles. Among those modifications, glycosylation is highly common and occurss in more than 50% of eukaryotic proteins.,[1] Protein glycosylation is classified as either N-linked or O-linked with the former typically being more complex, including a higher degree of branching.[2] In contrast to other biomacromolecules (e.g., proteins and nucleic acids), glycan biosynthesis is not template-driven and straightforward[3–5] but rather highly heterogeneous and complex.[3] Unlike the polymerase chain reaction for nucleic acids and overexpression for proteins, an amplification technique for carbohydrates, available for a variety of samples, is lacking.[5] As a result, glycan studies often involve an enrichment step for improved detection.[6] Classical methods for analysis of protein glycosylation include gas chromatography/mass spectrometry (GC/MS) in conjunction with chemical derivatization approaches (e.g., per-methylation, hydrolysis, or acetylation)[7,8] and direct examination via nuclear magnetic resonance (NMR) spectroscopy[8,9]. However, GC/MS is not compatible with larger molecules and NMR spectroscopy is not sufficiently sensitive for analyzing low abundance glycosylation.

With a shifting paradigm to higher throughput global analysis, mass spectrometry has become a workhorse tool in structural glycobiology due to its resolution, sensitivity, scan speed, and mass range.[10–12] Nanoflow liquid chromatography tandem mass spectrometry (nanoLC/MS/MS) of proteolytically generated glycopeptides is one of the most powerful tools available to sequence glycoproteins and determine the compositions/structures of glycan attachments. Collision induced dissociation or higher-energy collision dissociation (CID/HCD) are the most popular and widely available activation techniques for MS/MS. However, CID/HCD are not ideal for analyzing labile PTMs (e.g. sulfation, phosphorylation, and glycosylation).[13,14] Upon CID/HCD, glycopeptides yield complex mass spectra dominated by fragments from glycosidic bond cleavages, thus often providing little peptide sequence information and, for *O*-glycopeptides, often precluding determination of the glycosylation site(s).[14] Alternative, electron-based activation methods (i.e., electron capture dissociation and electron transfer dissociation) are known for their ability to retain labile PTMs while cleaving peptide backbone bonds to yield extensive peptide sequence information and allowing determination of PTM sites.[15–22] However, ECD/ETD require multiply charged analyte cations for effective dissociation.[19,23] Also, ETD is ineffective at m/z ratios larger than ~1,000[24]. Carbohydrate moieties have low ionization efficiency and, thus, glycopeptide ions generated with electrospray ionization (ESI) tend to have lower charge than similarly sized unmodified peptides, consequently appearing at higher m/z ratios at which electron-based MS/MS methods are ineffective.[23,25] Furthermore, high-resolution (HR) mass spectrometers (i.e., Orbitrap and ion cyclotron resonance (ICR)) have a limited m/z range.[26,27] Thus, improvements in MS/MS methods for analyzing glycoproteins are still needed.

Supplemental collisional activation combined with ETD (i.e., EThCD) and activated ion ETD (AI-ETD) via infrared photon irradiation have been reported to improve the sequence coverage of glycopeptides and glycoproteins.[28–30] However, such methods are not ideal for labile glycopeptides as significant glycosidic bond cleavage can occur on top of peptide backbone cleavage, rendering spectra complex and more challenging to annotate, and glycan site information can be lost, particularly for *O*-glycopeptides. In another alternative approach, "supercharging" or charge state enhancement, was applied to increase the charge state of glycopeptides for improved detection of glycopeptides with HR-MS[31]. Such supercharging can be achieved via addition of various chemicals (e.g., m-nitrobenzyl alcohol (*m*NBA)[32], sulfolane[33], dimethyl sulfoxide (DMSO)[34], etc..) to the electrospray ionization solvents. Lin et al. combined mNBA-based supercharging with HCD for analysis of acidic, high molecular weight[31]. With the implementation of supercharging, these authors were able to detect high molecular weight glycopeptides in the lower m/z region to validate the presence of glycosylation in singly glycosylated peptides from diagnostic HCD glycan fragments. However, this approach suffers from the HCD shortcomings described above.

Cooper and coworkers combined HCD with ETD for targeted analysis of glycopeptides in an approach termed HCD product dependent ETD (HCDpdETD). This approach employs the detection of diagnostic oxonium ions from HCD (e.g., m/z 163 for hexose (Hex), m/z 204 for *N*-acetyl hexosamine (HexNAc), and m/z 366 for a HexHexNAc disaccharide)[35] to trigger a subsequent ETD event only for peptides yielding such ions upon HCD.[36] HCDpdETD maximizes the number of MS/MS spectra that can be collected in a single glycoproteomic LC/MS/MS run as each ETD event (which primarily benefits glycosylated peptides) involves a reaction time with electron-

donating anions. However, one pitfall of this approach is the aforementioned issue of poor ETD performance for high m/z glycopeptides. Here, we explore post-column addition of supercharging reagent in nanoLC/MS/MS on an Orbitrap Fusion Lumos mass spectrometer for improved ETD and HCDpdETD of N- and O-linkedglycopeptides from a lectin and transferrin. A post-column approach was chosen to avoid column contamination and previously observed retention time shifts when supercharging reagent was present in the LC mobile phase[37]. Three different bioinfomatics tools (i.e., Proteome Discoverer, MSFragger-Glyco, and p-Glyco) are also evaluated for their efficacy in identifying these glycopeptides following ETD/HCDpdETD.

2.2. Experimental:

2.2.1. Preparation and Digestion of Glycoproteins:

Lectin from *Erythrina cristagalli* and transferrin from human plasma were purchased from Sigma-Aldrich (St. Louis, MO, USA). Trypsin digestion was performed based on Thermo protocols with modifications: briefly, glycoproteins were reduced with 5 mM Tris(2-carboxyethyl)-phosphine hydrochloride (TCEP) in 50 mM ammonium bicarbonate (NH_4HCO_3) buffer, pH 8.5, at 37℃ for 1 hour. Subsequent alkylation was peformed with 20 mM iodoacetamide (Sigma-Aldrich) at room temperature for another hour. Proteins were then incubated with Promega (Madison, WI) sequencing-grade modified trypsin at an enzyme:protein ratio of 1:50 at 37 ^{o}C overnight. Samples were desalted with C-18 Zip-Tips from Sigma-Aldrich. The desalted digests were dried in a SpeedVac (Company, City, State) and stored at -80℃ until analysis. Water with 0.1% formic acid (FA) was added to the dried sample prior to nanoLC-MS/MS analysis.

2.2.2. NanoLC/MS/MS with Post-column Addition of Supercharging Reagent:

All experiments were performed on an Orbitrap Fusion Lumos tribrid mass spectrometer (Thermo Fisher, Waltham, MA) coupled with a Dionex (Part of Thermo Fisher, Sunnyvale, CA) ultrahigh pressure LC (UPLC) system and equipped with ETD. Proteolytic peptides were separated on a 75 µm×50 cm, 2 µm, 100 Å, C18 column (Thermo Fisher) at a flow rate of 250 nL/min. Mobile phase solvent A was 0.1% FA in H_2O and mobile phase solvent B was 80% acetonitrile (ACN)/20% H_2O/0.1% FA. For lectin analysis, a 60 min gradient was ramped from 2% to 50% solvent B over 35 mins, ramped up again to 95% solvent B over 10 mins, and held at 95% solvent B for 5 mins before returning to 2% solvent B for 5 mins. An extended 90 min gradient was used to separate the other glycoproteins. The gradient started at 2% for 5 mins, then was ramped to 35 in 40 mins, ramped up again to 95% over 25 mins, and held at 95% solvent B for 5 mins before returning to 2% solvent B for 5 mins

*m*NBA supercharging reagent, delivered by an Agilent (Santa Clara, CA) 1290 Infinity II HPLC system, was introduced at a flow rate between 50-70 nL/min through a post-column nanoTee (Figure 1). This flow rate was achieved via an Agilent Infinity UHPLC Nanodapter, which reduces a microflow between 10-20 µL/min in a 1:100 ratio split via a tee and a resistor capillary. The nanoflow was controlled with an Agilent electronic flow sensor and attenuator system. With a mixing ratio of 1:7 in our added nanotee (*Fig. 2.1*), the output flow rate, wich entered the mass spectrometer, after fusion of the two liquid streams was 300 nL/min. The supercharging solution was 1% *m*NBA in 80% ACN/20% H_2O/0.1% FA. The instrument was operated in data-dependent mode. Product ions were detected in the Orbitrap.

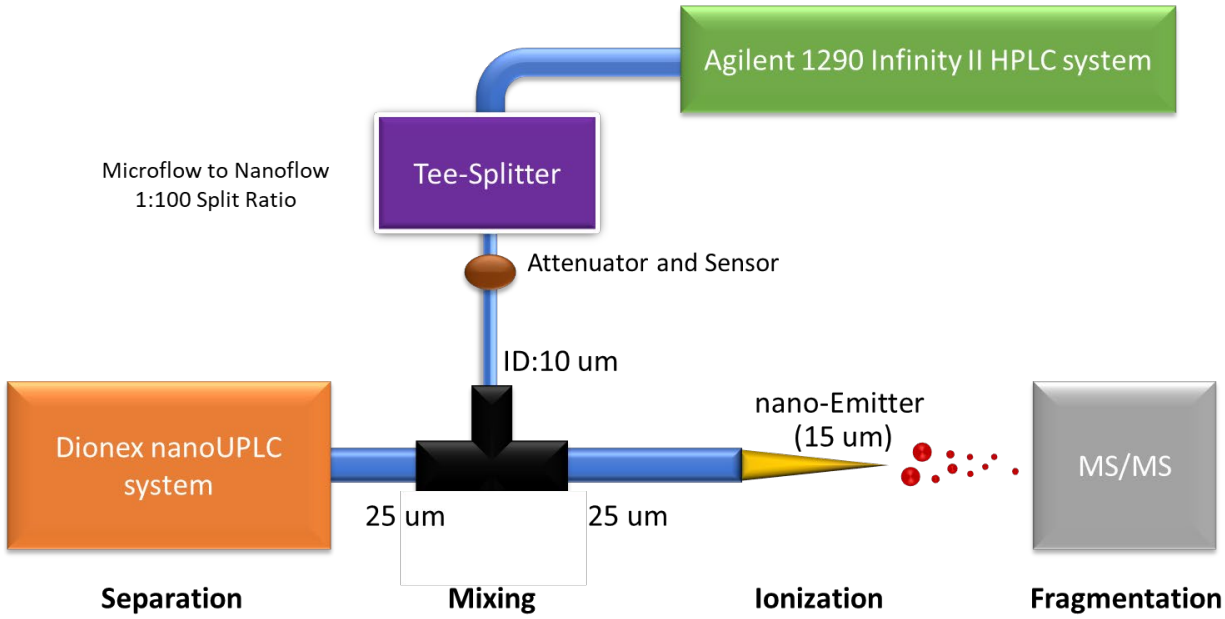

Figure 2.1. Post-column nanoLC supercharging via nano-tee mixing.

The MS1 scans (300mz-2000mz) were acquired in the Orbitrap (120K resolution and 4e5 AGC) followed by one of the following tandem activation methods: HCD, ETD, EThCD, or HCD product ion-triggered ETD (HCDptETD). The detection for MS2 events with mass range between 150mz-2000mz occurred in the Orbitrap with 60K resolution and 4e5 AGC. Dynamic exclusion was enabled with an exclusion duration of 15s and both mass tolerances of low and high as 10 ppm. HCD was performed with stepped collisional activation energy at 20%, 25% and 30%. ETD was performed based on calibrated charge-dependent reaction times. EThcD was operated with ETD reaction time of 50ms with supplemental energy of 20% HCD activation. For HCDptETD experiments. Subsequent ETD events occurred if one of the oxonium ions were identified (i.e., 204.09 m/z 366.14 m/z for HexHexNAc fragments) within the top 20 peak intensities. ETD reactions for HCDptETD was executed based on calibrated charge-dependent reaction times.

2.2.3. Data Analysis:

All raw MS/MS spectra were searched with Proteome Discoverer, MSFragger-Glyco1, and p-Glyco2. The search parameters were as follows: (1) up to two missed cleavages; (2) fixed modification: carbamidomethyl (C); (3) variable modifications: oxidation (M), deamidation (N,Q), user-defined N-glycan and O-glycan modifications; and (4) mass tolerance: 20 ppm for MS1 scans and 20 ppm for MS2 scans. The results were filtered with both strict false discovery rate (FDR) < 0.05 and relaxed FDR < 0.1. XCaliber 3.0 was used for manual data processing. To monitor and validate the presence of glycans in HCD, EThCD, and HCDpdETD experiments, all MS/MS spectra were examined manually for the signature oxonium ions m/z 163.06z for Hex, m/z 168.06 for HexNAc - $2H_2O$, m/z 186.07 for HexNAc - H_2O, m/z 204.08 for HexNAc, m/z 274.09 for *N*-acetylneuraminic acid (Neu5Ac) - H_2O, m/z 292.10 for NeuAc, m/z 366.14 for HexHexNAc, m/z 512.19 for the fucose (Fuc)-containing trisaccharide HexHexNAcFuc, and m/z 657.2354 for HexHexNAcNeuAc. Our overall workflow is shown in *Figure 2.2*.

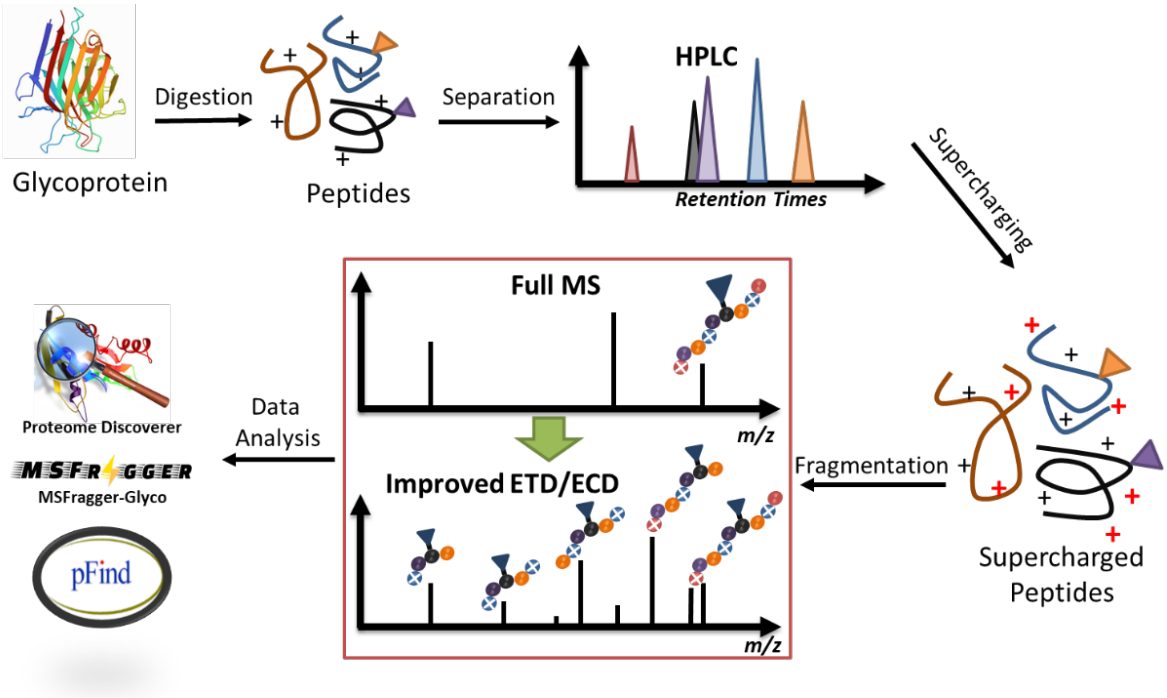

Figure 2.2. Supercharging workflow.

2.3. Results and Discussion

2.3.1. Optimization of Post-column Supercharging

Peak broadening was a major concern for any type of post-separation flow manipulation. Initially, we introduced to the nano Tee-setup with the syringe pump. However, the syringe was not able to withstand the high backpressure of the nano-Tee and would break often. Additionally, syringe pump mechanics was not able to maintain a consistent nanoflow and ultimately led to significant diffusion and peak broadening (*Fig. 2.3, top, right*). One remedy for this issue was to utilize a nano HPLC pump. With new setup, we were able to introduce a more consistent flow and reduce the effect of peak broadening (*Fig. 2.3, bottom, left*). To further reduce peak broadening issue, a smaller 10 µm ID silica capillary tubing was used. With all of the mentioned modifications, a significant improvement in reduction of peak broadening issue was observed (*Fig. 3, bottom, right*).

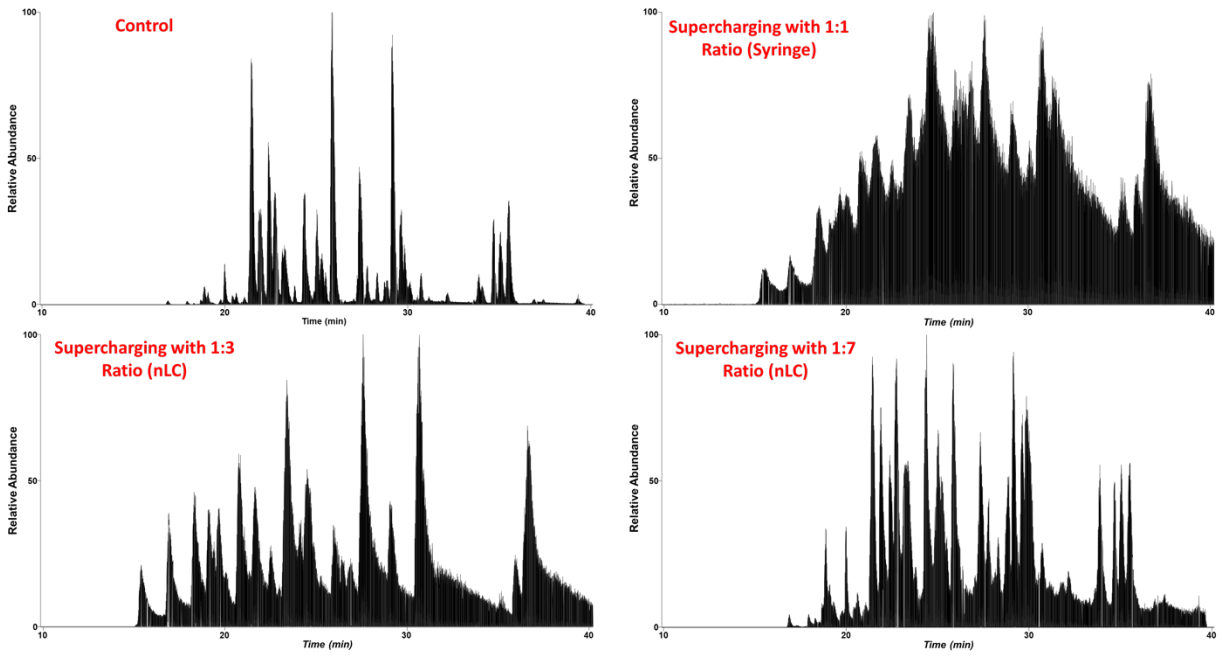

Figure 2.3 Nano-Tee optimization for improved peak shapes.

Another potential concern for the addition of supercharging reagent is an increase in chemical noise. Thus, we carefully examined the noise level in LC/MS experiments at various *m*NBA concentrations. At our chosen concentration (1%), diluted to 0.15% via the post-column tee (*Fig. 2.3*), only a minor noise level increase was noted (Fig. 2.4). In the absence of supercharging reagent, the LC/MS baseline was at ~1% (*Fig. 2.4, bottom*) whereas the addition of mNBA raised this baseline to ~4% (*Fig. 2.4, top*).

2.3.2. Effects of Post-column Supercharging in Lectin N-glycosylation Analysis

While our main goal with adding supercharging reagent was to improve the quality of glycopeptide ETD MS/MS spectra, we found that the number of ETD events triggered in data-dependent LC-ETD MS/MS experiments in the presence of supercharging reagent was significantly higher (~20% increase) compared with a control experiment lacking supercharging reagent (*Figure 2.5*). However, when looking at eluting gradient from 17 min to 35 min, a significant increase in ETD (~50%) scans was observed. We hypothesize that this increase in ETD scans is due to the higher Orbitrap signal with increased peptide charge. Interestingly, supercharging improved the ionization of tryptic peptides for ETD events. For non-supercharging experiments, most of the ETD events are mostly resulted from lower charge state ions (i.e., doubly protonated species) (*Fig. 2.5, bottom*).

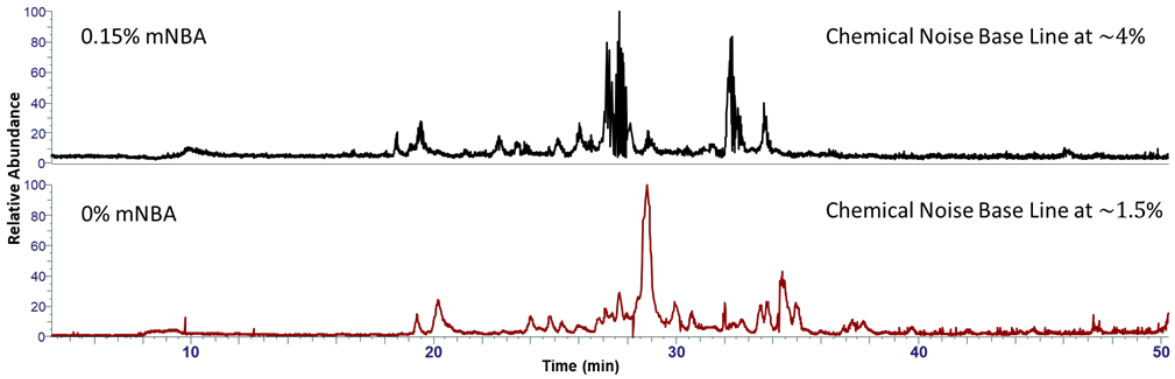

Figure 2.4. Chemical noise level in non-supercharging and supercharging experiments.

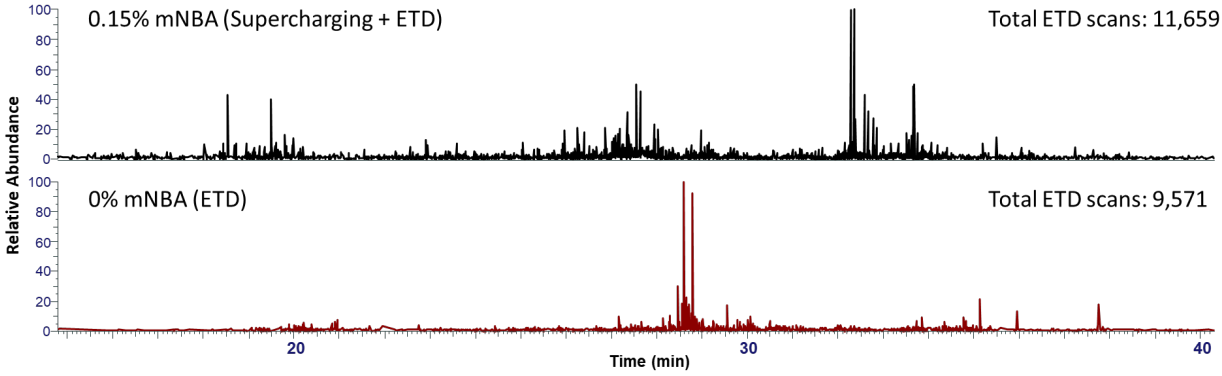

Figure 2.5. Comparison of the number of ETD events triggered in data-dependent LC/MS/MS experiments in the presence (Top) and absence (Bottom) of supercharging reagent for a lectin tryptic digest.

With post-column supercharging, a lectin *N*-glycopeptide showed an average charge state increase from 3.00 to 3.59 (*Fig. 2.6, Left Panel*), including a previously unobserved 5+ ion and an abundant 4+ ion in nanoLC/MS. In the absence of supercharging, ETD of the dominant triply protonated peptide only yielded two product ions, c_{16}^{+} and z_{16}^{+} (*Fig. 2.6, Right Panel, Top*). This peptide has previously been shown to yield higher sequence coverage in its triply protonated form in ECD[38] and ETD[39] with different reagent anions, sulfur dioxide and nitrobenzene, respectively. In our experiments with fluoranthene ETD reagent, the increase in charge accomplished via supercharging has profound consequences for ETD sequence coverage: ETD of the quadruply protonated precursor ions provides extensive backbone fragmentation, including a variety of *c* and *z*-type ions, with complete retention of the glycan (*Fig. 6, Right Panel, Bottom*).

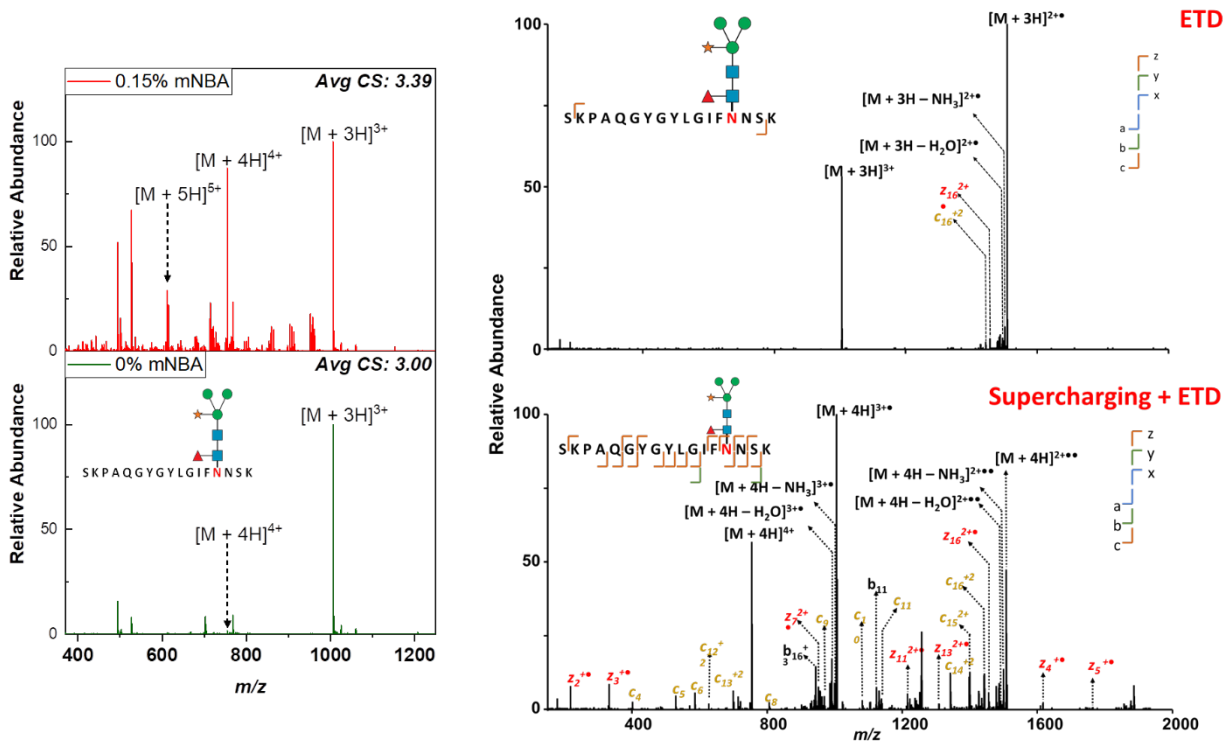

Figure 2.6. Lectin tryptic N-glycopeptide mass spectra from nanoLC-MS in the presence (Top Left) and absence (Bottom Left) of supercharging reagent. ETD MS/MS spectra of the triply protonated N-glycopeptide (Top Right) and the quadruply protonated tryptic N-glycopetides.

In addition, for the previously unobserved quintuply protonated precursor ions, ETD not only provides extensive backbone fragmentation via both c/z and *b*/*y*-type fragment ions but also results in significant glycan fragmentation (*Fig. 2.7, Bottom*). Thus, glycan composition information is also provided for this glycopeptide charge state, similar to EThcD experiments of the triply protonated precursor ion (*Fig. 2.7, Top, Right*). HCD alone also provides a mixture of peptide backbone and glycan fragmentation for the 3+ charge state (*Fig. 2.7, Top Left*). However, the peptide sequence coverage is higher in EThcD for this charge state. Interestingly, previous ion trap CID only reported glycan fragmentation for the 3+ charge state[39]. The occurrence of backbone *b*-type ions has previously been reported in ECD of peptides with charge states higher than their number of basic sites[37].

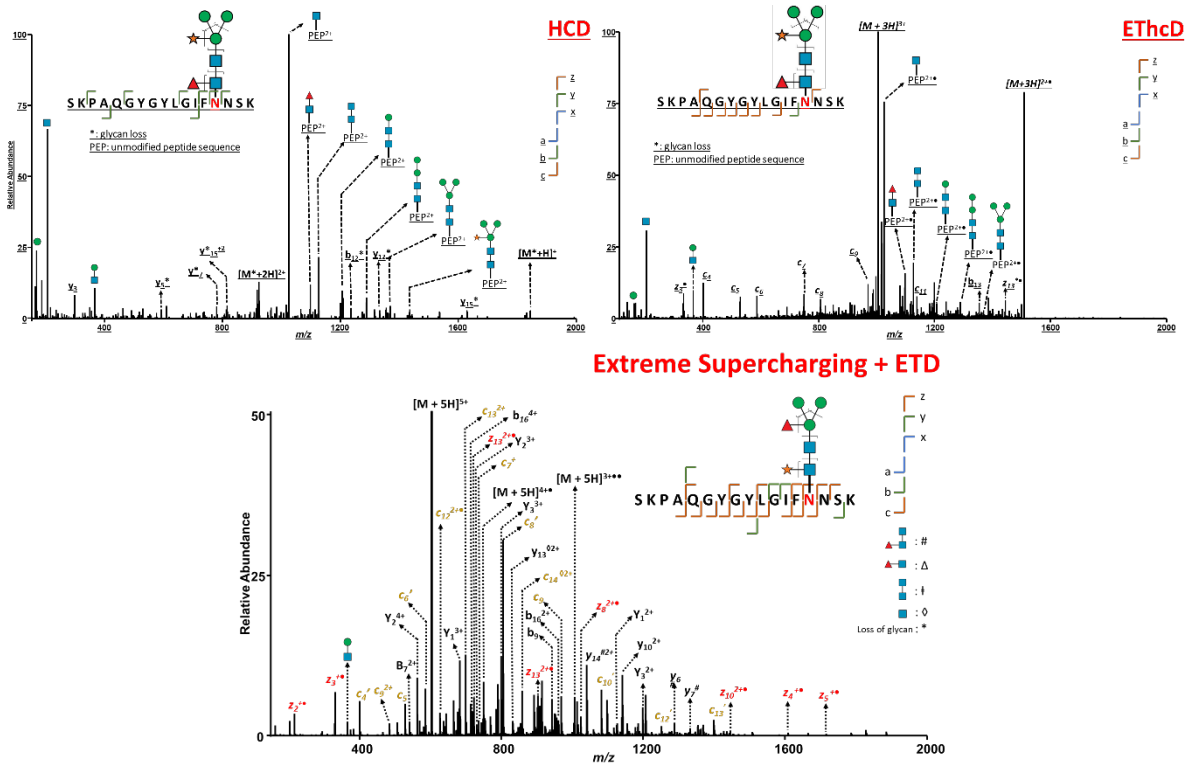

Figure 2.7. ETD of a highly supercharged (5+) lectin tryptic N-glycopeptide (Bottom) compared with more conventional approaches for the 3+ charge state, dominant in the absence of supercharging: HCD (Top Left) and EThcD (Top Right).

Without any pre-enrichment before nLC-MS/MS, we were able to detect a secondlarger *N*-glycopeptide, VNSVETISFSFSEFEPGNDN$_{Hex(3)HexNAc(2)Pent(1)dHex(1)}$LTLQGAALITQSGVLQLTK, presumably with the same glycan structure as the shorter glycopeptide discussed above (*Fig. 2.6 and 2.7*), in the lectin tryptic digest. This relatively large (~5.2 kDa), lower abundance, *N*-glycopeptide was only detected following supercharging. Previous direct infusion experiments were able to observe this peptide in its triply protonated form at m/z of 1731. However, ECD of that charge state did not yield any backbone fragment ions. Similarly, as expected, ETD of the 4^+ charge state (m/z of 1299), observed following supercharging, also did not produce any backbone fragmentation (*Fig. 2.8, Top*). However, ETD of the 5^+ charge state at an even lower m/z value of 1039 yielded a number of backbone fragment ions (*Fig. 2.8, bottom).*

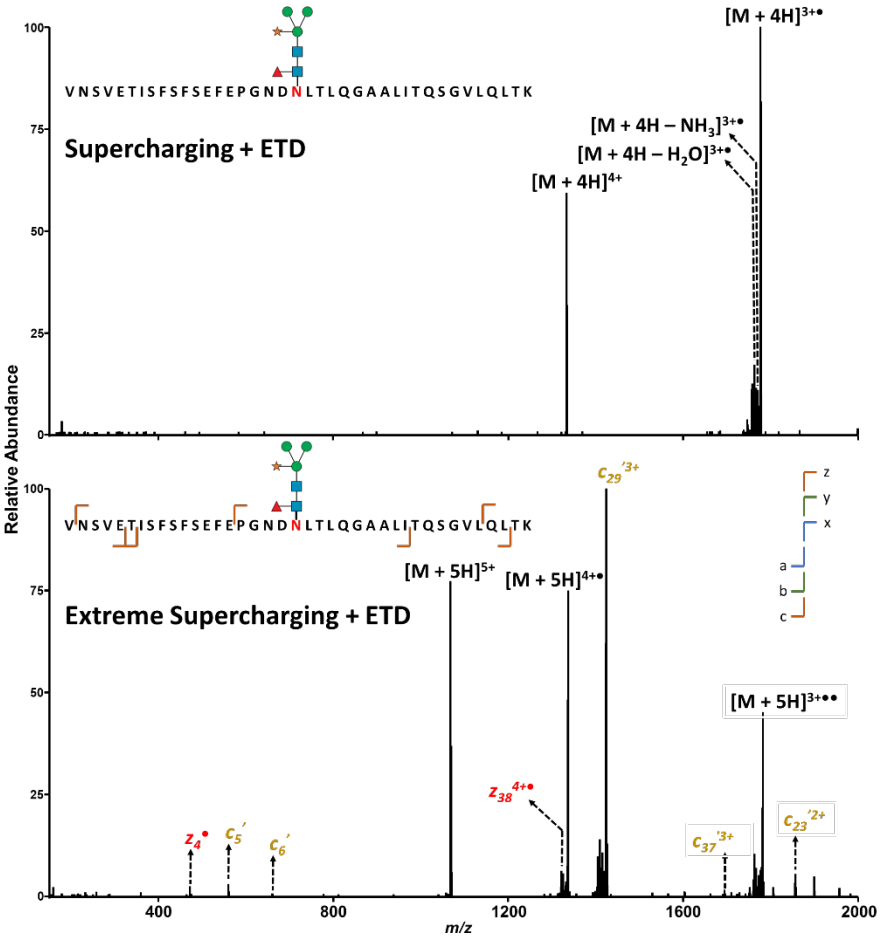

Figure 2.8. ETD of a supercharged low abundance N-glycopeptide (Lectin). (Top) ETD of 4+precursor ions. (Bottom) ETD of 5+ precursor ions.

We also explored HCDpdETD for the lectin tryptic digest with and without supercharging. In such experiments, the presence of diagnostic oxonium ions from HCD of glycopeptides is key to triggering subsequent ETD events. While HCD of doubly charged precursor ions generated oxonium ion signals (*Fig, 2.9, Top*), HCD of triply charged precursors resulted in significantly higher oxonium ion signals (*Fig. 2.8, bottom*). As the result, there would be more ETD events from the supercharged HCDpdETD experiments due to the increased numbers of higher charged state precursor.

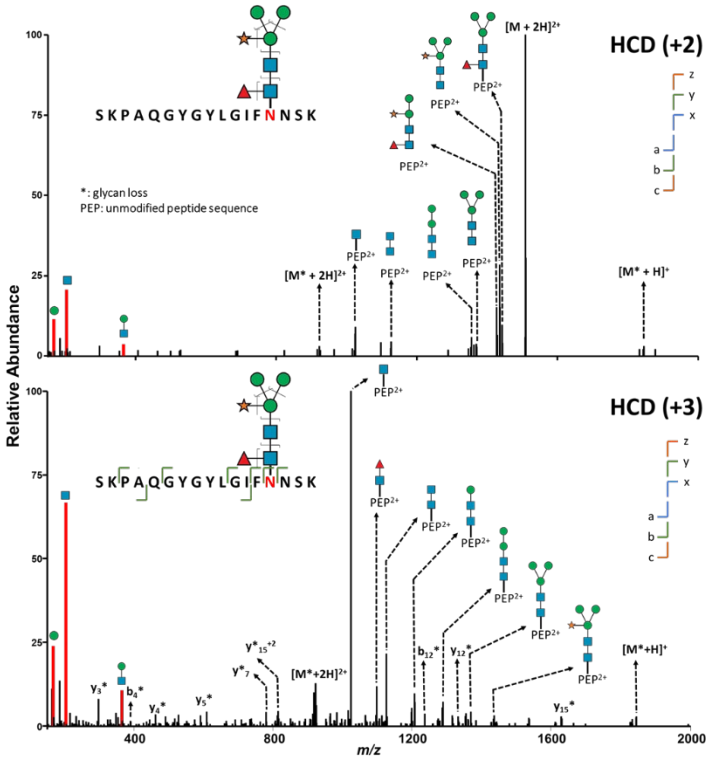

Figure 2.9. HCD MS/MS of a lectin tryptic N-glycopeptide. (Top) HCD of 2+ ions. (Bottom) HCD of 3+ ions.

2.3.3. Effects of Post-column Supercharging in Transferrin N- and O-glycosylation Analysis:

2.3.3.1. N-glycopeptide detection with supercharging

With supercharging, we detected all 10 glycoforms of transferrin *N*-glycopeptides, corresponding to ~300% performance improvement compared with other methods, including conventional HCD/CID), EThcD, HCDpdETD, and ETD without supercharging. All the latter approaches resulted in observation of only 3-4 of these glycoforms (*Table 2.1*). For the observed transferrin *N*-glycopeptides, supercharging increased the average charge state from 3.38 to 3.82 for mono-sialylated peptides and from 3.75 to 4.40 for di-sialylated peptides (*Fig. 2.10*).

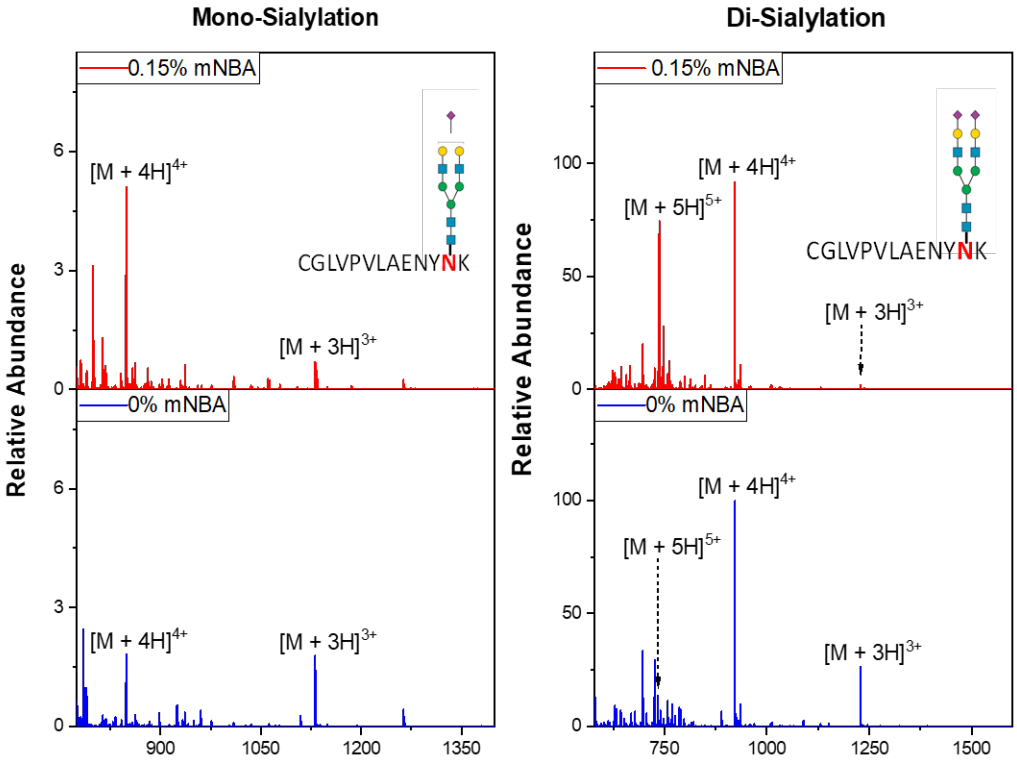

Figure 2.10. Supercharging of N-glycoeptide from transferrin with mono- and di-sialylation.

Siaylated glycan is widely acknowledged for low ionization efficiency in positive mode and thus it is challenging to detect sialyalted glycopeptides, especially with such low abundance. With supercharging, we were able to boost and detect sialylated glycans with relatively high m/z (*Fig. 13*) from human transferrin. One glycopeptide was detected with 4+ and 5+ charge states. With 4+ charge state, ETD shows great fragmentation pattern. However, with 5+ ions, there are a variety of c/z and y ions. Additionally, we can see the similar effect of supercharged ETD. With 5+, various glycan fragments from glycosidic cleavages, b-and y- type ions, were observed (*Fig. 2.11*).

In the presence of m-NBA, we detected the *N*-glycopeptide, I**N**HCR, featuring an uncommon glycosylation motif with a cysteine rather than serine or threonine in the (N-X-S/T) typical motif. Within transferrin, supercharging allows us to detect low abundance species of atypical N-Glycan. This glycan contains N-glycan that does not follow the usual motif N-X-T/S40. ETD confirms the presence of the glycans on the peptide and successfully sequence this glycopeptide with high confidence (*Fig. 2.12*). This

peptide was relatively short and has high content of acidic glycan. Thus, the glycopeptide is not easily ionized. With supercharging, ionization of this glycopeptide was greatly enhanced and ultimately allowed the detection of this glycopeptide. Additionally, with higher charge state, HCD fragment types were observed, and the glycan structure can be characterized with those fragments. This glycopeptide was not detected in the MSFragger-Glyco since MSFragger-Glyco only counts the glycopeptides with N-glycan motif (N-X-S/T), which X can be any amino acids.

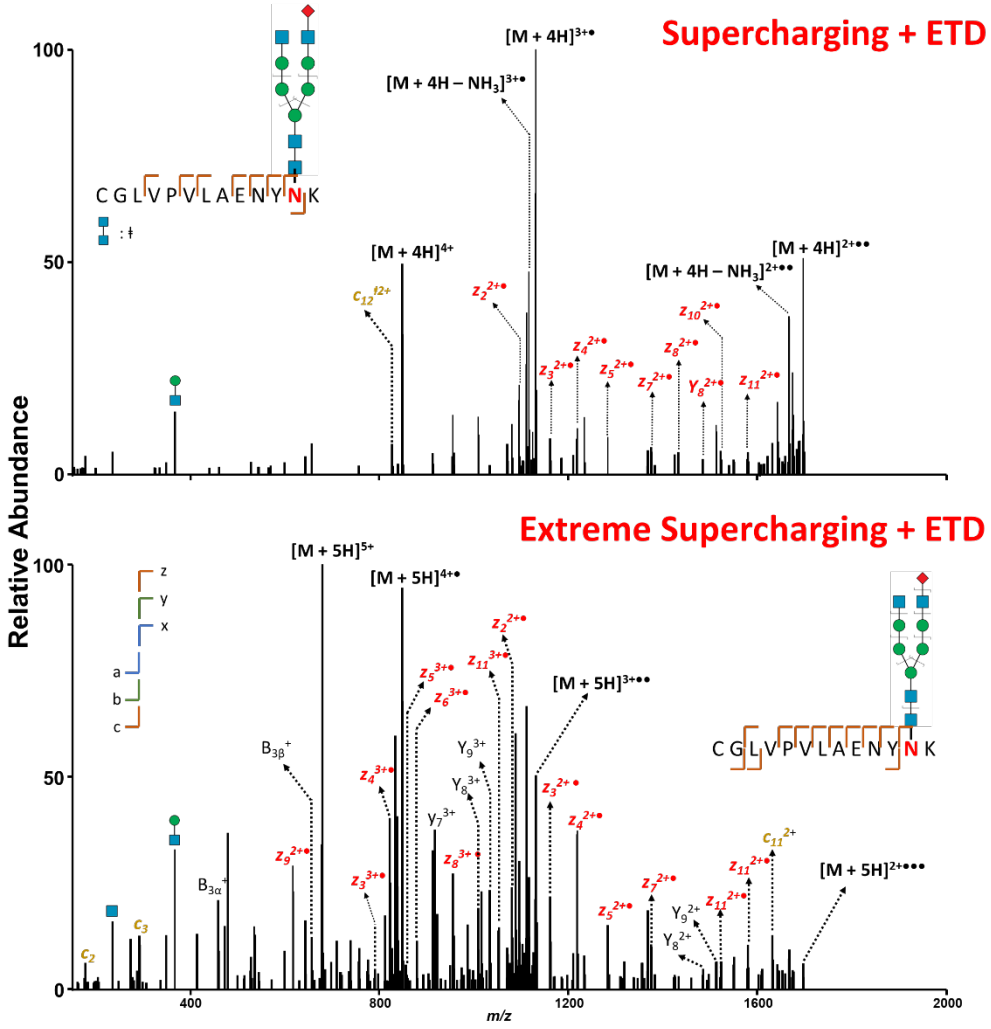

Figure 2.11. Improved analysis of ETD with supercharging.

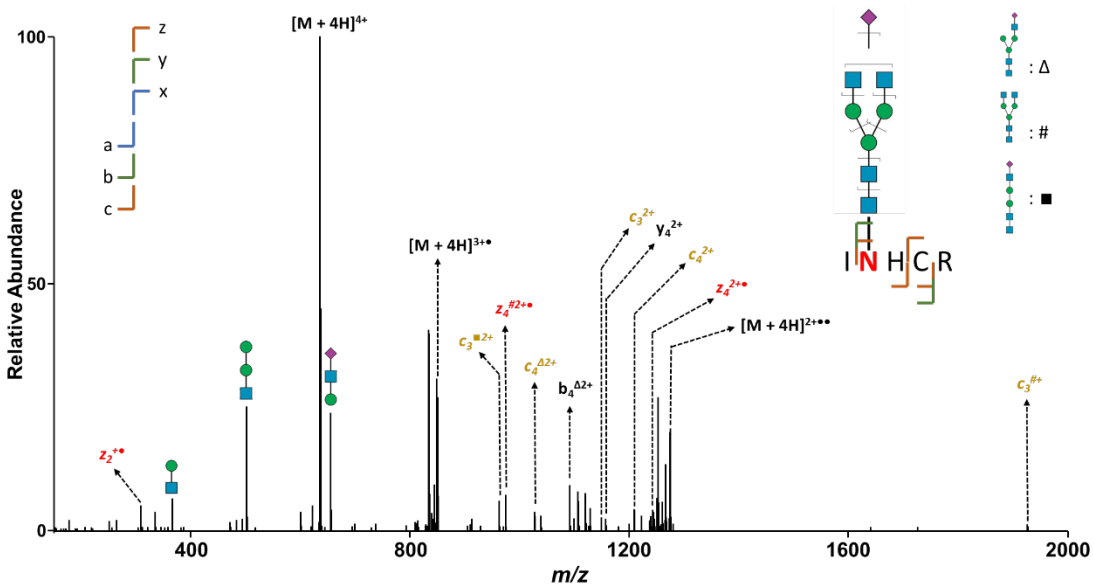

Figure 2.12. Supercharging for improved detection of atypical N-glycopeptide from transferrin.

When compared substitution of sialyation on the same glycopeptide, we can see that sialylation does affect the charge state distribution of the glycopeptides (*Fig. 2.13*). With mono-substituted sialyation site, we can see that the glycopeptide only exists in 3+ and 4+ in non-supercharged experiments. The presence of 4+ is especially low for ETD to occur and thus signal boost from supercharging is needed. For mono-sialyated glycan, 5+ ions only exist in the supercharging experiment. Interestingly, the glycopeptide exists at 3+, 4+, and 5+ for di-substituted sialylation. However, presence of 5+ is relatively low in non-supercharging experiment. Due to the low abundance of tri-sialyated N-glycans and ion suppression, there is no presence of tri-sialyated glycans with control experiment. However, the presence of tri-sialylated *N*-glycopeptides from tryptic transferrin digest was observed in the presence of m-NBA (*Fig. 2.13*).

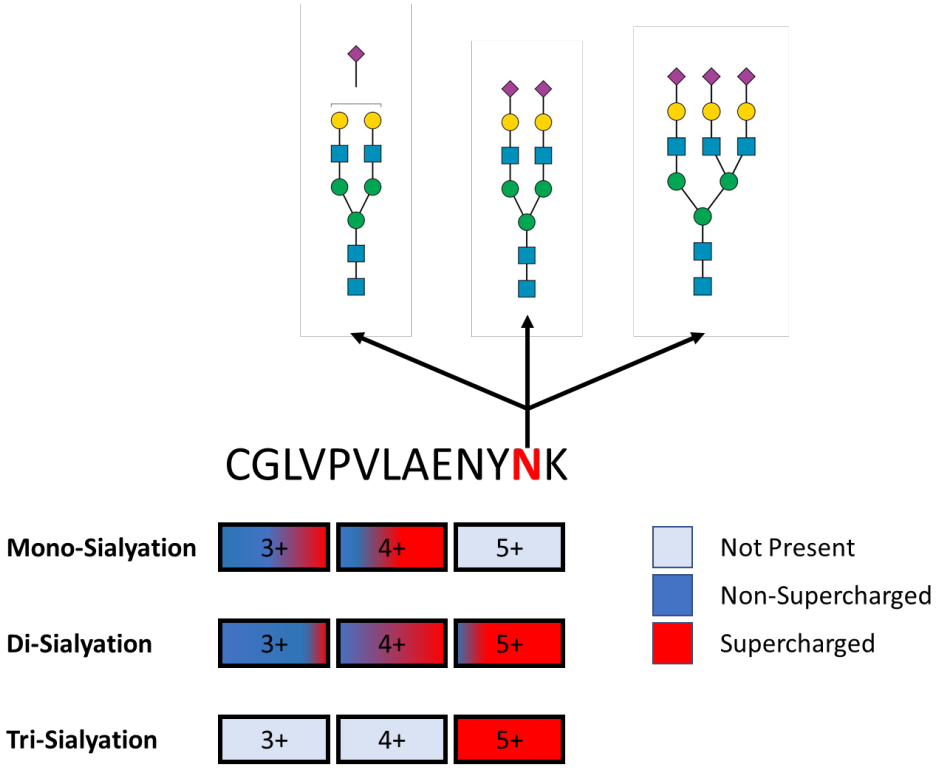

Figure 2.13. Detected O-glycopeptides from supercharging experiments.

For N-glycopeptide, we can clearly see the effect of supercharging for both mono- and di-substituted glycopeptide. With mono-substituted glycans, the ionization is harder and the glycans exists in the 3+ and 4+ with very low abundance. However, with the addition of m-NBA, the signal for 4+ is boosted by 3 times. For di-substituted N-glycans, the signals for 5+ is strongly enhanced. Overall, we can conclude that supercharging does work very well for sialylated N-glycopeptide. It enables higher charge state ions which do not exist in non-supercharging experiment.

ETD of supercharged peptides resulted in extensive peptide backbone fragmentation whereas ETD of highly supercharged *N*- and *O*-glycopeptides also yielded glycan fragmentation, i.e., B and Y type ions, similar to EThcD or activated ion-ETD but with the added benefit of higher experimental throughput as ETD reaction times can be greatly shortened (from 150 ms for doubly/triply-charged ions to 25-45 ms for higher charge states). The number of ETD events following post-column supercharging increased ~50%

compared with conventional nanoHPLC ETD MS/MS. Abundances of glycopeptide-specific oxonium fragment ions from HCD also increased in the presence of *m*NBA. Supercharging therefore also appears beneficial for targeted glycopeptide analysis, i.e., HCDpdETD. With supercharging, 40% more glycopeptides were detected from lectin and transferrin tryptic digests in HCDpdETD experiments (*Fig. 2. 14, bottom panel*) compared with conventional HCD/CID, EThcD, and HCDpdETD without supercharging.

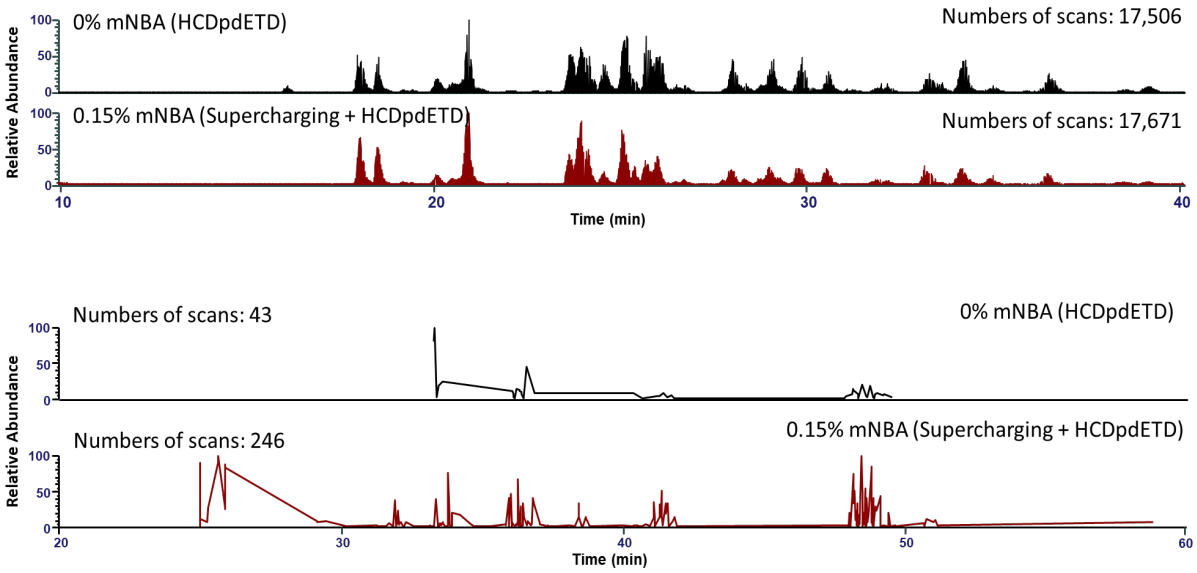

Figure 2.14. Supercharging in combination with hydrid MS/MS techniques, HCDpdETD, (Top Panel) Numbers of HCD scans in HCDpdETD (Bottom Panel) Numbers of Triggered ETD Events in HCDpdETD for Tryptic Digest of Transferrin.

2.3.3.2. O-glycopeptide detection with supercharging

With supercharging, we were able to detect 7 glycoforms for the glycopeptide, SVIPS^{51}DGPSVACVKK, indicating the highly distinct heterogeneity (*Fig. 2.15*). We were able to detect de-sialyated and sialyated O-glycans. A few rare glycoforms with low abundance, $HexNAc_{(2)}Hex_{(2)}$ and $HexNAc_{(2)}Hex_{(2)}NeuAc_{(2)}$, were identified within the supercharged ETD and HCDpdETD experiments. The charge state of de-sialyated glycans were generally lower than the sialyated ones. Only one de-sialyated O-glycan was detected in our control experiment whereas

total of three were detected within the supercharging experiment. For sialyated glycans, additional two rarer O-glycans were identified in the presence of m-NBA.

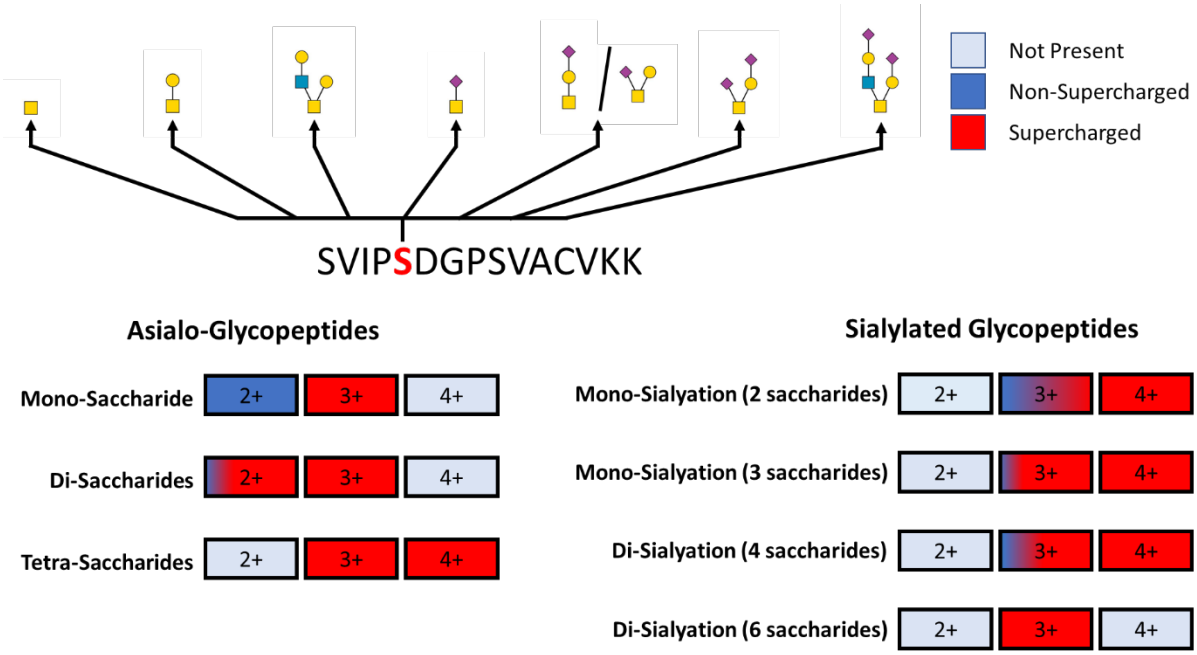

Figure 2.15. Detected O-glycopeptides from supercharging experiments.

O-glycopeptides are typically more labile than N-glycopeptides, thus precluding their detection with HCD or EThcD. Also, HCDpdETD yields poor ETD due to their low charge states (*Fig. 2.15, top*). With supercharging, ETD produces extensive backbone fragmentation without the glycan loss (*Fig. 2.15, bottom*). However, with supercharging, we identified all 7 glycoforms for the transferrin O-glycopeptide, SVIPSDGPSVACVKK, without enrichment.

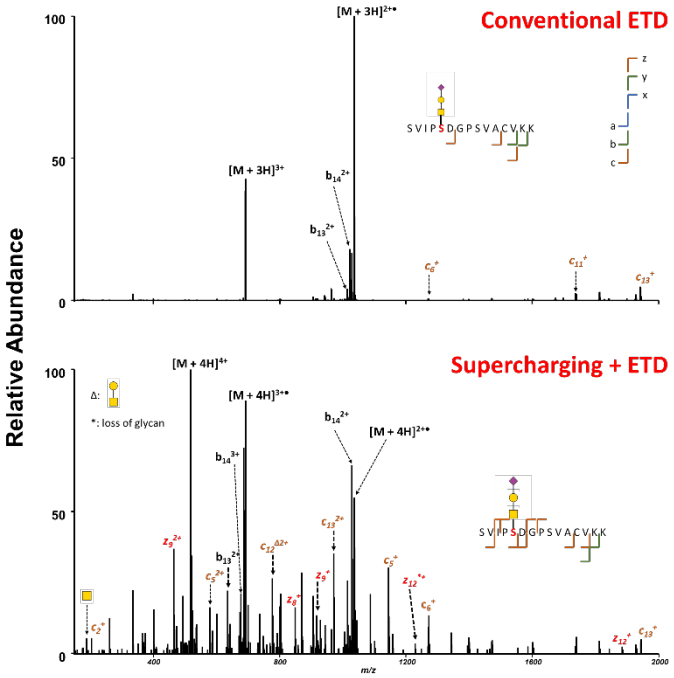

Figure 2.16. ETD for O-glycopeptides with and without m-NBA.

Different bioinformatics tools were used to identify the glycopeptides presented in my samples (i.e. Proteome Discoverer, p-Glyco, and MSFragger-Glyco). Search parameters are applied in the same manner while performing identification with all three tools. p-Glyco, however, is only comparable with HCD and only have the human and mouse glycan database for searching. For HCD, MSFragger-Glyco outperformed p-Glyco and Proteome Discoverer. The numbers of detected glycoforms were low with HCD. For SETD, MSFragger-Glyco outperformed ProteomeDiscoverer. MsFragger-Glyco were able to detect 16/17 glycopeptides from Lectin and Transferrin digests with SETD.

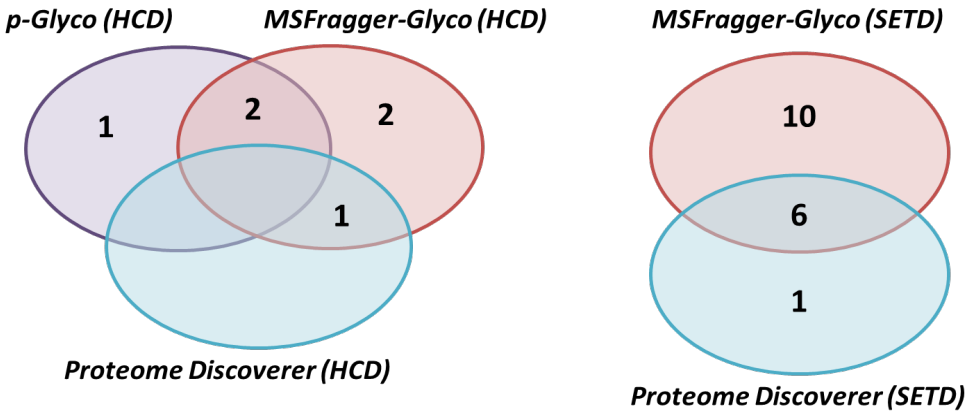

Figure 2.17. Bioinformatics tools used for glycopeptide Identifications from lectin and transferrin (Left) Comparison of HCD with all three bioinformatics tools (Right) Comparison of ETD with all MS-Fragger Glyco and Proteome Discoverer bioinformatics tools.

Different activation methods were also compared in this study with MSFragger-Glyco. Overall, SETD and SHCDpdETD outperform HCD, EThcD and HCDpdETD. With SHCDpdETD, higher data collection throughput could be achieved due to the HCD nature. At the same time, supercharging allowed higher triggering ability of HCD to the complementary ETD to map N-glycopeptides. Supercharging greatly enhances the detection of N-Glycopeptides for more targeted approach like HCDpdETD. SETD and SHCDpdETD increase the numbers of unique glycopeptide detection compared the traditional HCD, EThcD and HCDpdETD. Table 1 is the summary for all glycopeptides detected from all approaches.

Glycopeptide Sequence with Glycan Composition	**HCD**	**ETD**	**EThcD**	**HCDpdETD**	**Supercharged ETD**	**Supercharged HCDpdETD**
Lectin, Erythrina Corallodendron						
N-glycans						
SKPAQGYGYLGIFN#NSK	Position: 139					
Hex(3)HexNAc(2)Pent(1)dHex(1)	*PD, MSF*	*PD, MSF*	*PD, MSF*	*PD, MSF*	*PD, MSF*	*PD, MSF*
VNSVETISFSFSEFEPGNDN#LTLQGAALITQSGVLQLTK	Position: 43					
Hex(3)HexNAc(2)Pent(1)dHex(1)	*N/A*	*N/A*	*N/A*	*MSF*	*MSF*	*MSF*
Transferrin, human						
N-glycans						
C*GLVPVLAENYN#K	Position: 432					
Hex(5)HexNAc(4)NeuAc(1)	*N/A*	*PD, MSF*	*N/A*	*N/A*	*PD*	*MSF*

Hex(5)HexNAc(4)NeuAc(2)	*MSF*	*N/A*	*PD, MSF*	*MSF*	*PD, MSF*	*MSF*
IN[#]HC*R	Position: 491					
Hex(5)HexNAc(4)NeuAc(1)	*PG*	*N/A*	*N/A*	*N/A*	*PD, MSF*	*PD, MSF*
HexNAc(4)Hex(5)NeuAc(2) dHex(1)	*MSF*	*N/A*	*N/A*	*N/A*	*MSF*	*MSF*
Hex(6)HexNAc(5)NeuAc(3)	*N/A*	*N/A*	*PD, MSF*	*PD, MSF*	*MSF*	*PD, MSF*
Hex(5)HexNAc(4)NeuAc(1)	*N/A*	*N/A*	*MSF*	*N/A*	*MSF*	*MSF*
QQQHLFGSN[#]VTDC*SGNFC *LFR	Position: 630					
Hex(5)HexNAc(4)NeuAc(2)	*PD, MSF*	*N/A*	*PD*	*N/A*	*PD, MSF*	*PD, MSF*
Hex(5)HexNAc(4)NeuAc(1)	*N/A*	*N/A*	*N/A*	*MSF*	*MSF*	*MSF*
O-glycans						
SVIPS[Δ]DGPSVAC*VK	Position: 51					
HexNAc(1)NeuAc(1)	*N/A*	*N/A*	*N/A*	*N/A*	*MSF*	*PD*
HexNAc(1)Hex(1)NeuAc(1)	*N/A*	*PD, MSF*	*MSF*	*N/A*	*PD, MSF*	*PD, MSF*
HexNAc(1)Hex(1)NeuAc(2)	*N/A*	*N/A*	*PD, MSF*	*MSF*	*MSF*	*PD, MSF*
HexNAc(2)Hex(2)NeuAc(2)	*N/A*	*N/A*	*N/A*	*N/A*	*MSF*	*MSF*
HexNAc(1)	*N/A*	*N/A*	*N/A*	*N/A*	*MSF*	*MSF*
HexNAc(1)Hex(1)	*N/A*	*N/A*	*MSF*	*MSF*	*PD, MSF*	*MSF*
HexNAc(2)Hex(2)	*N/A*	*N/A*	*N/A*	*N/A*	*MSF*	*MSF*
	*Cysteine carbamidomethylation. [#]N-glycosylation site. [Δ]O-glycosylation site. ***PD***: SequestHT Node on Proteome Discoverer. ***PG***: p-Glyco (Note: only work for HCD). ***MSF***: MSFragger-Glyco					

Table 2.1 Detection of N- and O- glycopeptides from different bioinformatics tools.

2.4. Conclusion

The presented study provides a novel method for structural characterization of N- and O-glycopeptides by implementing post-column supercharging to ETD (i.e. SETD) and HCDpdETD (i.e. SHCDpdETD) in the nanoLC regime. N- and O-linked glycopeptides were significantly supercharged with the introduction of mNBA via a post-column nano-flow tee. The number of ETD events following post-column supercharging increased ~50% compared with conventional nanoHPLC ETD MS/MS. In this study, we were able to obtain quality ETD spectra from both SETD and SHCDpdETD via supercharging. Beside the extensive backbone fragmentation with supercharging, we also discovered that ETD of highly supercharged glycopeptides produced additional glycan fragmentations. ETD of highly supercharged N- and O-glycopeptides also yielded glycan fragmentation, i.e., B and Y type ions, like EThcD or activated ion-ETD. This proves to be very advantageous because supercharging would allow us to obtain both backbone sequence structure as well as the glycan composition, which is only observed with EThcD or AI-ETD. With

this approach, we would not need the implementation of complex laser system such as AI-ETD. Another benefit is that the throughput of ETD would greatly improve because higher charge state ions would need much less reaction time to efficiently fragment. Another interesting discovery is that abundances of glycopeptide-specific oxonium fragment ions from HCD also increased in the presence of mNBA and ultimately lead to higher triggering rate of HCDpdETD. Supercharging therefore also appears beneficial for targeted glycopeptide analysis, i.e., HCDpdETD. O-glycopeptides are known to be more labile and do not contain sequence motif like N-glycopeptide, so the detection of O-glycopeptides is not easy with HCD, EThcD or HCDpdETD. However, with supercharging, we successfully identified unprecedented numbers of glycoforms from human transferrin without any pre-enrichment. With supercharging, ETD reaction times can be greatly shortened (from 150 ms for doubly/triply charged ions to 25-45 ms for higher charge states). With supercharging, 40% more glycopeptides were detected from lectin and transferrin tryptic digests in HCDpdETD experiments compared with conventional HCD/CID, EThcD, and HCDpdETD without supercharging.

2.5. References

(1) Apweiler, R.; Hermjakob, H.; Sharon, N. On the Frequency of Protein Glycosylation, as Deduced from Analysis of the SWISS-PROT Database. *Biochimica et Biophysica Acta - General Subjects* **1999**, *1473* (1), 4–8. https://doi.org/10.1016/S0304-4165(99)00165-8.

(2) Spiro, R. G. Protein Glycosylation: Nature, Distribution, Enzymatic Formation, and Disease Implications of Glycopeptide Bonds. *Glycobiology* **2002**, *12* (4). https://doi.org/10.1093/glycob/12.4.43R.

(3) Yarema, K. J.; Bertozzi, C. R. Characterizing Glycosylation Pathways. *Genome Biology* **2001**, *2* (5), 1–10. https://doi.org/10.1186/gb-2001-2-5-reviews0004.

(4) Dennis, J. W.; Granovsky, M.; Warren, C. E. Protein Glycosylation in Development and Disease. *BioEssays* **1999**, *21* (5), 412–421. https://doi.org/10.1002/(SICI)1521-1878(199905)21:5<412::AID-BIES8>3.0.CO;2-5.

(5) Krasnova, L.; Wong, C. H. *Understanding the Chemistry and Biology of Glycosylation with Glycan Synthesis*; 2016; Vol. 85. https://doi.org/10.1146/annurev-biochem-060614-034420.

(6) Nilsson, J.; Rüetschi, U.; Halim, A.; Hesse, C.; Carlsohn, E.; Brinkmalm, G.; Larson, G. Enrichment of Glycopeptides for Glycan Structure and Attachment Site Identification. *Nature Methods* **2009**, *6* (11), 809–811. https://doi.org/10.1038/nmeth.1392.

(7) Hellerqvist, C. G. Linkage Analysis Using Lindberg Method. *Methods in Enzymology* **1990**, *193* (C), 554–573. https://doi.org/10.1016/0076-6879(90)93438-Q.

(8) Han, E. S.; Goleman, Daniel; Boyatzis, Richard; Mckee, A. *Glycoanalysis Protocols*, 2nd ed.; Houndsell, E., Ed.; Methods in Molecular Biology, Humana Press Inc., 1998; Vol. 76.

(9) Fu, D.; van Halbeek, H. N-Glycosylation Site Mapping of Human Serotransferrinby Serial Lectin Affinity Chromatography, Fast Atom Bombardment-Mass Spectrometry, and 1H Nuclear Magnetic Resonance Spectroscopy. *Analytical Biochemistry* **1992**, *206* (1), 53–63. https://doi.org/10.1016/S0003-2697(05)80010-7.

(10) Dominguez-Medina, S.; Fostner, S.; Defoort, M.; Sansa, M.; Stark, A. K.; Halim, M. A.; Vernhes, E.; Gely, M.; Jourdan, G.; Alava, T.; Boulanger, P.; Masselon, C.; Hentz, S. Neutral Mass Spectrometry of Virus Capsids above 100 Megadaltons with Nanomechanical Resonators. *Science* **2018**, *362* (6417), 918–922. https://doi.org/10.1126/science.aat6457.

(11) Iwamoto, N.; Shimada, T. Recent Advances in Mass Spectrometry-Based Approaches for Proteomics and Biologics: Great Contribution for Developing Therapeutic Antibodies.

Pharmacology and Therapeutics **2018**, *185* (December 2017), 147–154. https://doi.org/10.1016/j.pharmthera.2017.12.007.

(12) Babu, P.; North, S. J.; Jang-Lee, J.; Chalabi, S.; MacKerness, K.; Stowell, S. R.; Cummings, R. D.; Rankin, S.; Dell, A.; Haslam, S. M. Structural Characterisation of Neutrophil Glycans by Ultra Sensitive Mass Spectrometric Glycomics Methodology. *Glycoconjugate Journal* **2009**, *26* (8), 975–986. https://doi.org/10.1007/s10719-008-9146-4.

(13) Kelleher, N. L.; Zubarev, R. A.; Bush, K.; Furie, B.; Furie, B. C.; McLafferty, F. W.; Walsh, C. T. Localization of Labile Posttranslational Modifications by Electron Capture Dissociation: The Case of γ-Carboxyglutamic Acid. *Analytical Chemistry* **1999**, *71* (19), 4250–4253. https://doi.org/10.1021/ac990684x.

(14) Dalpathado, D. S.; Desaire, H. Glycopeptide Analysis by Mass Spectrometry. *Analyst* **2008**, *133* (6), 731–738. https://doi.org/10.1039/b713816d.

(15) Thaysen-Andersen, M.; Packer, N. H. Advances in LC-MS/MS-Based Glycoproteomics: Getting Closer to System-Wide Site-Specific Mapping of the N- and O-Glycoproteome. *Biochimica et Biophysica Acta - Proteins and Proteomics* **2014**, *1844* (9), 1437–1452. https://doi.org/10.1016/j.bbapap.2014.05.002.

(16) Thaysen-Andersen, M.; Packer, N. H.; Schulz, B. L. Maturing Glycoproteomics Technologies Provide Unique Structural Insights into the N-Glycoproteome and Its Regulation in Health and Disease. *Molecular and Cellular Proteomics* **2016**, *15* (6), 1773–1790. https://doi.org/10.1074/mcp.O115.057638.

(17) Zhu, Z.; Desaire, H. Carbohydrates on Proteins: Site-Specific Glycosylation Analysis by Mass Spectrometry. *Annual Review of Analytical Chemistry* **2015**, *8*, 463–483. https://doi.org/10.1146/annurev-anchem-071114-040240.

(18) Leymarie, N.; Zaia, J. Effective Use of Mass Spectrometry for Glycan and Glycopeptide Structural Analysis. *Analytical Chemistry* **2012**, *84* (7), 3040–3048. https://doi.org/10.1021/ac3000573.

(19) Bakhtiar, R.; Guan, Z. Electron Capture Dissociation Mass Spectrometry in Characterization of Peptides and Proteins. *Biotechnology Letters* **2006**, *28* (14), 1047–1059. https://doi.org/10.1007/s10529-006-9065-z.

(20) Breuker, K.; Oh, H.; Lin, C.; Carpenter, B. K.; McLafferty, F. W. Nonergodic and Conformational Control of the Electron Capture Dissociation of Protein Cations. *Proceedings of the National Academy of Sciences of the United States of America* **2004**, *101* (39), 14011–14016. https://doi.org/10.1073/pnas.0406095101.

(21) Molina, H.; Horn, D. M.; Tang, N.; Mathivanan, S.; Pandey, A. Global Proteomic Profiling of Phosphopeptides Using Electron Transfer Dissociation Tandem Mass Spectrometry. *Proceedings of the National Academy of Sciences of the United States of America* **2007**, *104* (7), 2199–2204. https://doi.org/10.1073/pnas.0611217104.

(22) Chi, A.; Huttenhower, C.; Geer, L. Y.; Coon, J. J.; Syka, J. E. P.; Bai, D. L.; Shabanowitz, J.; Burke, D. J.; Troyanskaya, O. G.; Hunt, D. F. Analysis of Phosphorylation Sites on Proteins from Saccharomyces Cerevisiae by Electron Transfer Dissociation (ETD) Mass Spectrometry. *Proceedings of the National Academy of Sciences of the United States of America* **2007**, *104* (7), 2193–2198. https://doi.org/10.1073/pnas.0607084104.

(23) Zubarev, R. A.; Horn, D. M.; Fridriksson, E. K.; Kelleher, N. L.; Kruger, N. A.; Lewis, M. A.; Carpenter, B. K.; McLafferty, F. W. Electron Capture Dissociation for Structural Characterization of Multiply Charged Protein Cations. *Analytical Chemistry* **2000**, *72* (3), 563–573. https://doi.org/10.1021/ac990811p.

(24) Good, D. M.; Wirtala, M.; McAlister, G. C.; Coon, J. J. Performance Characteristics of Electron Transfer Dissociation Mass Spectrometry. *Molecular & cellular proteomics : MCP* **2007**, *6* (11), 1942–1951. https://doi.org/10.1074/MCP.M700073-MCP200.

(25) Kalli, A.; Håkansson, K. Comparison of the Electron Capture Dissociation Fragmentation Behavior of Doubly and Triply Protonated Peptides from Trypsin, Glu-C, and Chymotrypsin Digestion. *Journal of Proteome Research* **2008**, *7* (7), 2834–2844. https://doi.org/10.1021/pr800038y.

(26) Karas, M.; Bahr, U.; Dülcks, T. Nano-Electrospray Ionization Mass Spectrometry: Addressing Analytical Problems beyond Routine. *Fresenius' Journal of Analytical Chemistry* **2000**, *366* (6–7), 669–676. https://doi.org/10.1007/s002160051561.

(27) Xian, F.; Hendrickson, C. L.; Marshall, A. G. High Resolution Mass Spectrometry. *Analytical Chemistry* **2012**, *84* (2), 708–719. https://doi.org/10.1021/ac203191t.

(28) Lodge, J. M.; Schauer, K. L.; Brademan, D. R.; Riley, N. M.; Shishkova, E.; Westphall, M. S.; Coon, J. J. Top-Down Characterization of an Intact Monoclonal Antibody Using Activated Ion Electron Transfer Dissociation. *Analytical Chemistry* **2020**, *92* (15), 10246–10251. https://doi.org/10.1021/acs.analchem.0c00705.

(29) Zhu, J.; Huang, J.; Zhang, J.; Chen, Z.; Lin, Y.; Grigorean, G.; Li, L.; Liu, S.; Singal, A. G.; Parikh, N. D.; Lubman, D. M. Glycopeptide Biomarkers in Serum Haptoglobin for Hepatocellular Carcinoma

Detection in Patients with Nonalcoholic Steatohepatitis. *Journal of Proteome Research* **2020**, *19* (8), 3452–3466. https://doi.org/10.1021/acs.jproteome.0c00270.

(30) Yu, Q.; Wang, B.; Chen, Z.; Urabe, G.; Glover, M. S.; Shi, X.; Guo, L.; Kent, K. C.; Li, L. Electron-Transfer/Higher-Engery Collision Dissociation (EThcD)-Enabled Intact Glycopeptide/Glycoproteome Characterization. **2017**, 1751–1764. https://doi.org/10.1021/jasms.8b05640.

(31) Lin, C. W.; Haeuptle, M. A.; Aebi, M. Supercharging Reagent for Enhanced Liquid Chromatographic Separation and Charging of Sialylated and High-Molecular-Weight Glycopeptides for NanoHPLC-ESI-MS/MS Analysis. *Analytical Chemistry*. 2016, pp 8484–8494. https://doi.org/10.1021/acs.analchem.6b00938.

(32) Iavarone, A. T.; Jurchen, J. C.; Williams, E. R. Supercharged Protein and Peptide Ions Formed by Electrospray Ionization. *Analytical Chemistry* **2001**, *73* (7), 1455–1460. https://doi.org/10.1021/ac001251t.

(33) Lomeli, S. H.; Yin, S.; Ogorzalek Loo, R. R.; Loo, J. A. SHORT COMMUNICATION Increasing Charge While Preserving Noncovalent Protein Complexes for ESI-MS. *JAM* **2008**, *20*, 593–596. https://doi.org/10.1016/j.jasms.2008.11.013.

(34) Grandori, R. Origin of the Conformation Dependence of Protein Charge-State Distributions in Electrospray Ionization Mass Spectrometry. *Journal of Mass Spectrometry* **2003**, *38* (1), 11–15. https://doi.org/10.1002/jms.390.

(35) Carr, S. A.; Huddleston, M. J.; Bean, M. F. Selective Identification and Differentiation of N-and O-linked Oligosaccharides in Glycoproteins by Liquid Chromatography-mass Spectrometry. *Protein Science* **1993**, *2* (2), 183–196. https://doi.org/10.1002/pro.5560020207.

(36) Singh, C.; Zampronio, C. G.; Creese, A. J.; Cooper, H. J. Higher Energy Collision Dissociation (HCD) Product Ion-Triggered Electron Transfer Dissociation (ETD) Mass Spectrometry for the Analysis of N-Linked Glycoproteins. *Journal of Proteome Research* **2012**, *11* (9), 4517–4525. https://doi.org/10.1021/pr300257c.

(37) Wang, Q. Protein-Protein Interaction Analysis: Expanded Hydrogen/Deuterium Exchange Tandem Mass Spectrometry and Host Cell Protein Characterization, Ann Arbor, 2019.

(38) Adamson, J. T.; Håkansson, K. Infrared Multiphoton Dissociation and Electron Capture Dissociation of High-Mannose Type Glycopeptides. *Journal of Proteome Research* **2006**, *5* (3), 493–501. https://doi.org/10.1021/pr0504081.

(39) Hogan, J. M.; Pitteri, S. J.; Chrisman, P. A.; McLuckey, S. A. Complementary Structural Information from a Tryptic N-Linked Glycopeptide via Electron Transfer Ion/Ion Reactions and Collision-Induced Dissociation. *Journal of Proteome Research* **2005**, *4* (2), 628–632. https://doi.org/10.1021/pr049770q.

(40) Satomi, Y.; Shimonishi, Y.; Hase, T.; Takao, T. Site-Specific Carbohydrate Profiling of Human Transferrin by Nano-Flow Liquid Chromatography/Electrospray Ionization Mass Spectrometry. *Rapid Communications in Mass Spectrometry* **2004**, *18* (24), 2983–2988. https://doi.org/10.1002/rcm.1718.

(41) Håkansson, K.; Chalmers, M. J.; Quinn, J. P.; McFarland, M. A.; Hendrickson, C. L.; Marshall, A. G. Combined Electron Capture and Infrared Multiphoton Dissociation for Multistage MS/MS in a Fourier Transform Ion Cyclotron Resonance Mass Spectrometer. *Analytical Chemistry* **2003**, *75* (13), 3256–3262. https://doi.org/10.1021/ac030015q.

(42) Good, D. M.; Wirtala, M.; McAlister, G. C.; Coon, J. J. Performance Characteristics of Electron Transfer Dissociation Mass Spectrometry. *Molecular and Cellular Proteomics* **2007**, *6* (11), 1942–1951. https://doi.org/10.1074/mcp.M700073-MCP200.

Chapter 3. Post-Separation Supercharging in nanoHPLC for Improved Electron Transfer Dissociation of Lipidated Peptides

3.1. Introduction

Protein *S*-palmitoylation results from the attachment of palmitate, a saturated sixteen-carbon fatty acid, to a cysteine residue through a thioester linkage. This reversible and dynamic modification (*Figure 3.1*) is essential for intracellular regulation, such as AMPA receptor trafficking[1], NO-related signaling pathway in endothelial cells [2], and signaling of Ras family proteins [3–5]. However, direct detection of cysteine palmitoylation remains elusive[6]. In order to develop new effective therapeutic approaches targeting protein palmitoylation, studying the dynamics of palmitoylation is essential and thus improved analytical methods that can successfully localize palmitoylation sites are needed.

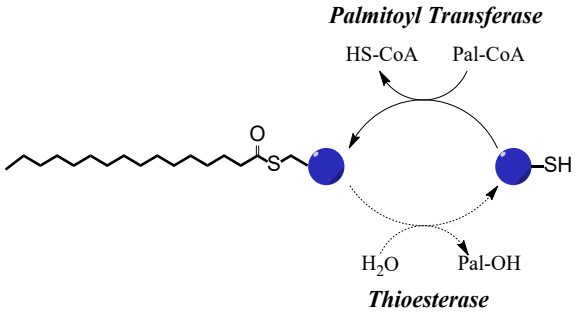

Figure 3.1 Protein palmitoylation and depalmitoylation in biological systems.

Mass spectrometry (MS) methods have revealed the importance of S-palmitoylation in relation to the progression of diabetes, Alzheimer's disease, schizophrenia, and cancer, highlighting the key role of MS-centered methods for studying protein function.[7–11] One MS-compatible method for *S*-acylation analysis involves acyl-biotinyl exchange (ABE) chemistry to

replace thioester-linked palmitoyl groups with biotin labels [12]. In this method, termed acyl-resin assisted capture (acyl-RAC), all cysteine residues are reduced and capped with N-ethylmaleimide (NEM) followed by chemolytic cleavage of Cys-thioester linkages with hydroxylamine. Released cysteine sulfhydryl groups, which are assumed to have been palmitoylated, are then labeled with biotin-HPDP. The corresponding biotinylated proteins are affinity-purified/enriched by streptavidin-agarose beads and released enzymatically for MS analysis. Despite some promise, the ABE method suffers from incomplete blockage of all non-palmitoylated cysteines and may not account for non-stoichiometric palmitoylation at a particular cysteine residue, i.e., ABE can result in false positives. Additionally, inaccurate palmitoylation assignments can arise from inefficient thioester hydrolysis or inadequate biotin labeling. As a result of these factors, nearly one-third of identified S-palmitoylation sites have been proposed to be false assignments [13]. An alternative approach involves metabolic labeling with alkynyl analogues of palmitic acid, 17-octadecynoic acid (17-ODYA). “Click chemistry” can then be used to attach either azide-linked fluorescent labels[14–16] or biorthogonal affinity[17,18] probes to the palmitoyl mimic, allowing enrichment and indirect detection of palmitate moeities[19,20]. However, this approach is tedious and costly to extend towards large scale palmitoylation analysis. Additionally, multiple-step and lengthy sample preparation/cleanup can result in significant loss of palmitoyl groups.

Despite >5,000 S-palmitoylation sites being predicted with existing liquid chromatography/tandem MS (LC/MS/MS) methods, only a small percentage has been experimentally validated. In addition to the aforementioned issues with the acyl-RAC and 17-ODYA methods [21] there is a lack of alternative affinity enrichment strategies targeting lipidated peptides. Palmitoyl groups lack functional moieties for immunocapture methods, thus, such

enrichment strategies for low abundance S-palmitoylated proteins are not available[22]. Additionally, care must be taken to avoid palmitoyl loss during alkylation reactions and sample processing [23–26].

The nature of S-acylated peptides presents numerous challenges for direct LC/MS/MS detection, including strong retention within reverse phase (RP)-LC columns, insolubility issues in typical buffer solutions, and abundant palmitate loss during collision induced dissociation (CID) MS^2 analysis. Palmitoylated proteins can also show resistance to digestion in the absence of surfactant (which are often not MS-compatible), and palmitoylated peptide have low ionization efficiency due to the long, neutral fatty acyl chain.

Ji et al. reported that electron transfer dissociation (ETD) MS/MS outperforms both electron capture dissociation (ECD) and CID in terms of palmitate retention in MS/MS[26]. However, ETD requires at least triply charged precursor ions for effective fragmentation312. Supplemental higher energy collision dissociation (EThcD[28]) or infrared activation during ETD (activated ion (AI) ETD [29]) have been shown to enhance ETD of doubly charged peptides. However, such approaches are not well suited for peptides with labile posttranslational modifications (PTMs), such as palmitoylation. For example, extensive phosphoric acid neutral loss was observed in AI-ETD[29]. Supercharging has been shown to improve ETD MS/MS of phosphopeptides, which also suffer from low charging in conventional electrospray ionization (ESI). This improvement was demonstrated by directly adding supercharging reagent to the LC solvents344. We also showed that improved ECD/ETD of peptic peptides could be achieved with supercharging345; however, even minute amounts of supercharging reagent can significantly alter retention times and remain

in the column, causing problems in a multiuser environment. Thus, a post-column Tee-junction was devised for introducing supercharging reagent post-column in capillary flow LC/MS. Here, I extend, the application of the T-junction introduced in Chapter 2 for nanoflow LC/MS/MS towards palmitoylated peptide analysis. A novel workflow for direct detection and efficient annotation of S-palmitoylated peptides in complex mixtures is presented involving nanoflow post-column supercharging reagent addition, optimized sample preparation, and C8 chromatography.

3.2. Experimental

3.2.1. Chemical S-Palmitoylation and MS/MS of Synthetic Peptides:

The synthetic peptides PDFRIAFQELLCLR, MGCVQCKDKEA, and ARAWCQVAQKF were purchased from GenScript. Thioacylation reactions were performed by dissolving ~100 µg of peptide standards in 10 µL of 100% TFA. Palmitoyl chloride (1 µL) was added to the mixture and allowed to react for 10 min under ambient conditions. The general scheme of this S-palmitoylation reaction is shown in *Scheme 3.1*.

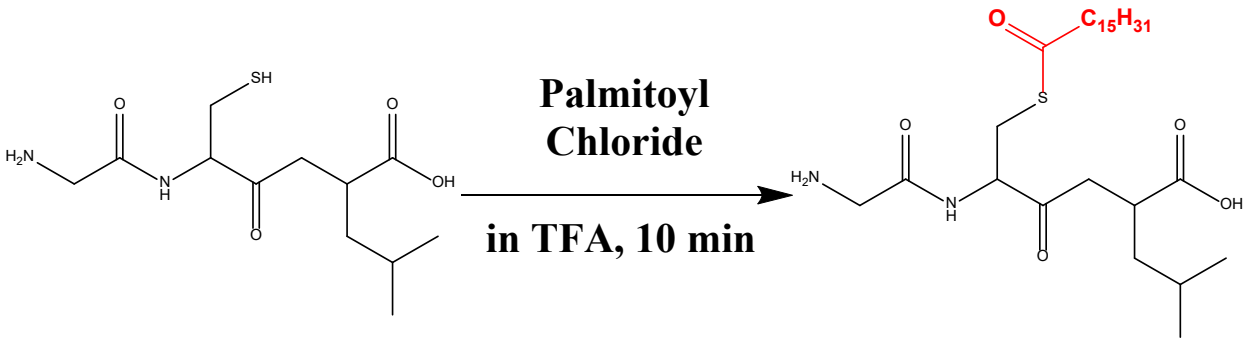

Scheme 1. Chemical reaction for cysteine S-palmitoylation.

The product mixture was dried under nitrogen and purified by reverse phase HPLC. This purification was performed on an Agilent Infinity II HPLC system using a Thermo Scientific™

Hypersil GOLD™ C4 HPLC Column (5 µm, 250 Å, 2.1 mm i.d. × 150 mm). Mobile phase A consisted of 95:5 water/acetonitrile (ACN) with 0.1% TFA, and mobile phase B consisted of 90:5:5 ACN/isopropanol(IPA)/water with 0.1% TFA. A linear gradient of 30−100% B (for singly palmitoylated peptides) or 40−100% B (for doubly palmitoylated peptides) over 20 min was employed with a flow rate of 0.3 mL/min. UV detection was performed at 210 nm. Palmitoylated peptide fractions were collected, aliquoted, and dried. Dried peptides were prepared in a solution of 40:10:50:0.1 ACN:IPA:water:formic acid (FA). Sulfolane at 0.2% or meta-nitrobenzyl alcohol (m-NBA) at 0.1% was added to the final spray solution for direct infusion experiments. Samples were infused into an Orbitrap Fusion Lumos mass spectrometer via a nano-ESI emitter. ETD was performed with fluoranthene at a reaction time of 100 ms. All mass spectra were acquired in the Orbitrap and analyzed via Xcalibur software.

3.2.2. Trypsin Digestion and Preparation of S-Palmitoylated Peptides for LC/MS Experiments:

Lysozyme from chicken egg white was purchased from Sigma-Aldrich (St. Louis, MO, USA). Trypsin digestion was performed based on Thermo protocols with some modifications. Protein was dissolved in 100 mM Tris-buffer solution with 0.1% Waters RapiGest surfactant. The protein was reduced with 5mM tris(2-carboxyethyl)-phosphine hydrochloride (TCEP). This solution was heated at 70^{o}C for 1 hour and cooled down to ambient temperature. Reduced protein was incubated with Promega sequencing-grade modified trypsin at a ratio of 1:50 at 37^{o}C overnight. Samples were desalted with C-18 Zip-Tips from Millipore Sigma and dried in a SpeedVac. Digested samples were then chemically S-palmitoylated according to the procedure described above.

S-palmioylated sample was purified with a C8 spin column. The resulting sample was dried in a SpeedVac. The dried, purified sample was prepared in 5:25:70:0.1 IPA:ACN:H2O:FA with 0.1%

RapidGest. The sample was then heated to 60 °C for 30 minutes, cooled to ambient temperature and diluted to 50 ng/µL in 5:25:70:0.1 IPA:ACN:H2O:FA with 0.1% RapidGest before LC/MS/MS experiments. The autosampler was heated to 37°C to prevent precipitation of S-palmitoylated peptides.

3.2.3. Supercharging Tee Setup with C8 Reverse Phase Nano-Column

All experiments were performed on an Orbitrap Fusion Lumos tribrid mass spectrometer (Thermo Fisher) coupled with a Dionex UPLC system and equipped with ETD. MS^1 settings were: ESI voltage: 1650 V, vaporizer temperature: 100 °C, ion transfer tube temperature: 150 °C, sheath gas: 4, Aux gas: 1, sweep gas: 0, Orbitrap MS^1 resolution: 150k, scan range: 200-2000, max inject time: 150 ms, AGC target: $5x10^5$, RF lens: 35%, dynamic exclusion: 60 s, mass tolerance: 10 ppm. MS^2 settings were: detector: Orbitrap, 60k resolution, activation: HCD (15, 20, 25), scan rate: normal, max injection time: 35 ms, isolation window: 1.4 Da.

Proteolytic and chemically palmitoylated peptides were resuspended in 0.1% RapiGest with 5:25:70:0.1 IPA:ACN:H_2O:FA before loading and separation on a 75 µm×50 cm, 2 µm, 100 Å, C8

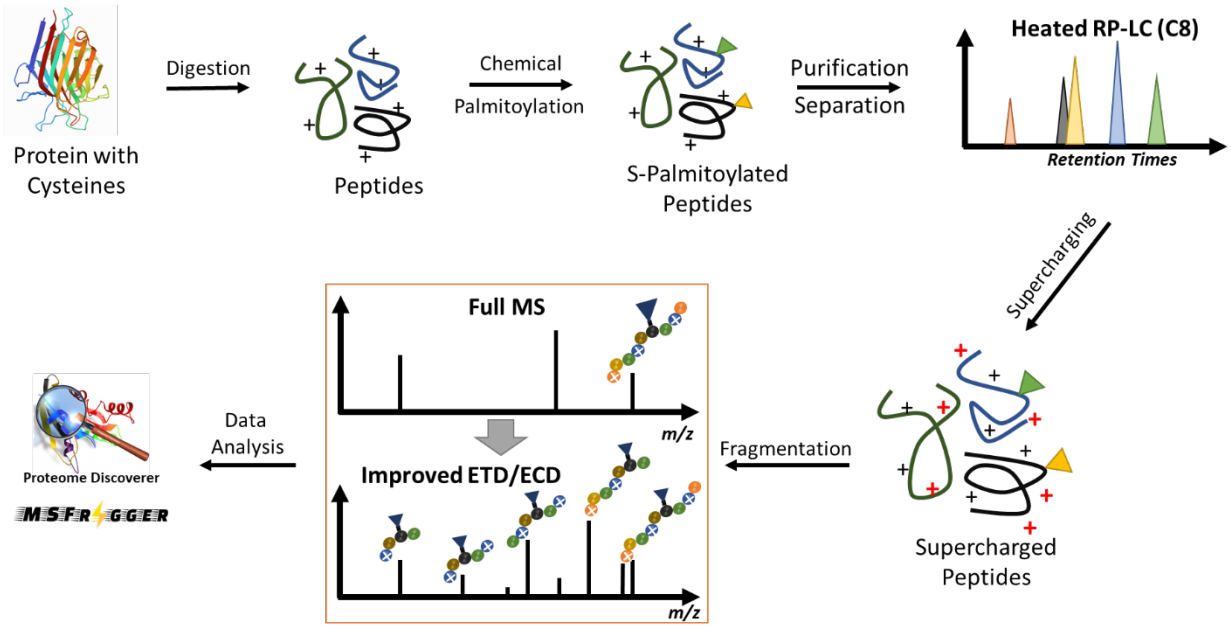

Figure 38. Supercharging workflow for S-palmitoylated samples.

column (Thermo Fisher) at a flow rate of 350 nL/min. The column was heated to 50 ^{O}C for all LC/MS experiments. Supercharging reagent was introduced through a post column Tee with an Agilent Infinity II HPLC system equipped with a nanodapter to yield a flow rate of 50-70 nL/min. LC solvents were 0.1% FA in H_2O (A) and 80% ACN/20% H_2O/0.1% FA (B).

For lysozyme analysis, a 90 min gradient was held at 2% over 5 mins, held at 4% over 5 mins, held at 6% over 5 mins, then ramped from 8% to 50% solvent B over 40 mins, ramped up again to 98% solvent B over 20 mins, and held at 98% solvent B for 10 mins before returning to 2% solvent B for 5 mins. To achieve the 50-70 nL/min supercharging reagent flow rate, a microflow between 10-20 µL/min was reduced in a 1:100 ratio split with the nanodapter, composed of split tee and resistor capillary. The nanoflow was controlled with an Agilent electronic flow sensor and attenuator system. With a mixing ratio of 1:6, the output flow after fusion of the two liquid

streams was ~400 nL/min. The compositions of supercharging reagent and mobile phases were modified as follows: 1% m-NBA in 90% ACN/20% H2O/0.1 %FA. The instrument was operated in data-dependent mode.

The MS^1 scans (300mz-2000mz) were acquired in the Orbitrap (120K resolution and 4e5 AGC) followed by one of the following tandem activation methods: HCD, ETD, EThCD, or HCD product ion-triggered ETD (HCDptETD). The detection for MS^2 events with mass range between 150mz-2000mz occurred in the Orbitrap with 60K resolution and $4e^5$ AGC. Dynamic exclusion was enabled with an exclusion duration of 15s and both mass tolerances of low and high as 10 ppm. HCD was performed with stepped collisional activation energy at 20%, 25% and 30%. ETD was performed based on calibrated charge-dependent reaction times. EThcD was operated with ETD reaction time of 50ms with supplemental energy of 20% HCD activation. For HCD neutral loss ETD experiments. Subsequent ETD events occurred if one of the neutral losses were identified (i.e., 238.23 m/z and 271.21 m/z) within the top 20 peak intensities. ETD reactions for HCDnlETD was executed based on calibrated charge-dependent reaction times.

3.2.4. Data Analysis

All raw spectra were searched with Proteome Discoverer and MSFragger. The search parameters were as follows: (1) up to two missed cleavages; (2) dynamic modification: palmitoyl (238.23 Da) on cysteine and methionine residues; (3) variable modifications: oxidation (M), deamidation (N,Q); and (4) mass tolerance: 20 ppm for MS^1 scans and 20 ppm for MS^2 scans. The results were filtered with both strict FDR < 0.05 and relaxed FDR < 0.1. XCaliber 3.0 was used for manual data processing. To monitor and validate the presence of palmitoyl groups in HCD,

EThCD, and HCDpdETD experiments, all MS/MS spectra were manually examined for the signature neutral palmitate loss (i.e. 238.23 Da for full palmitate loss and 271.12 Da for partial palmitate loss).

3.3. Results and Discussion

3.3.1. Supercharging of Synthetic, Chemically Palmitoylated Peptides. Three synthetic peptide standards (with different numbers of palmitoylation sites, previously introduced by Costello and co-workers) were chemically palmitoylated and used as model peptides to evaluate the supercharging nanoLC/MS/MS workflow. ESI mass spectra of the peptide PDFRIAFQELLCLR are shown in Figure 3.3 with (Fig. 3.3., bottom) and without (*Fig. 3.3., top*) palmitoylation. As expected, the average charge state (CS) was significantly shifted from 2.46 to 2.10 upon addition of palmitate. In particular, the 3+ charge state, required for effective ETD, shows significantly reduced abundance for the palmitoylated peptide. In the previous work with these synthetic peptides, Lin et al. performed their ETD experiments with triply charged precursor ions for all three peptides to show extensive sequence coverage with improved PTM

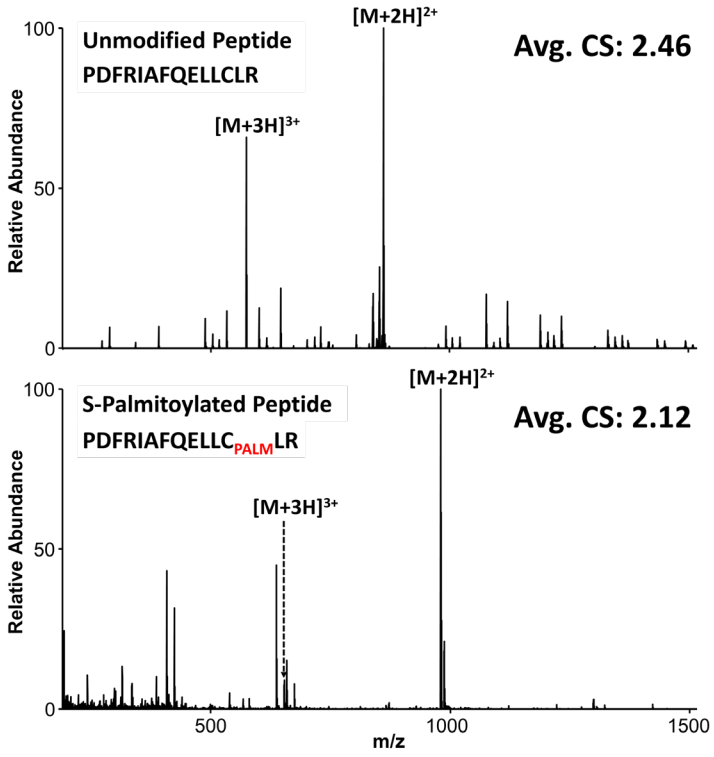

Figure 39. ESI mass spectra of (Top) unmodified PDFRIAFQELLCLR peptide and (Bottom) chemically S-palmitoylated peptide.

retention compared with ECD and CID.[26] However, it appears that a significant amount of peptide signal is unavailable for such analysis.

Upon addition of supercharging reagent, the average charge state of the palmitoylated peptides was significantly increases. For the peptide PDFRIAFQELLC$_{PALM}$LR, almost exclusively doubly protonated ions were generated (86%) in the absence of supercharging reagent (Figure 3.4., top) whereas addition of either sulfolane (*Figure 3.4., middle*) or m-NBA (*Figure 3.3., bottom*) allowed observation of relatively abundant 3^+ ions, with m-NBA generating the highest abundance of this higher charge state (*Fig. 3.4, bottom*). m-NBA-based supercharging shifted the average charge state from 2.12 to 2.93 whereas addition of sulfolane shifted the average charge state from 2.12 to 2.63.

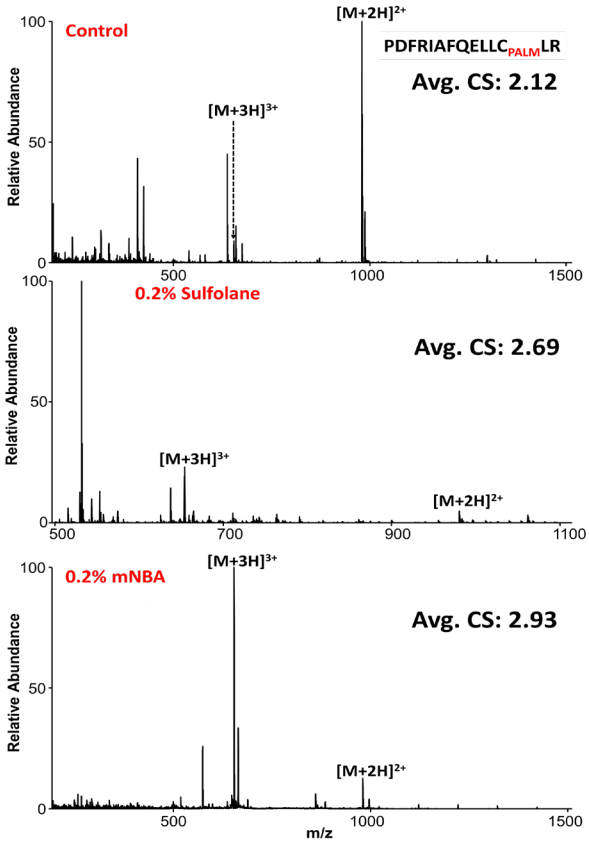

Figure 40. ESI mass spectra of the palmitoylated peptide, PDFRIAFQELLC$_{PALM}$LR in the absence of supercharging (top), and following supercharging with sulfolane (middle) and m-NBA (bottom).

3.3.2. ETD of Supercharged Synthetic, Chemically Palmitoylated Peptides. ETD of the doubly protonated charge state, which was dominantly observed in the absence of supercharging, of the peptide PDFRIAFQELLC$_{PALM}$LR only yielded three product ions, c^{13+}, $z^{12+\bullet}$ and $z^{13+\bullet}$ (*Figure 3.5., top*). By contrast, ETD of the triply protonated charge state, observed in abundance following m-

NBA-based supercharging showed extensive backbone fragmentation, including a variety of *c* and *z*-type ions with no accompanying palmitate loss (*Figure 3.5., bottom*).

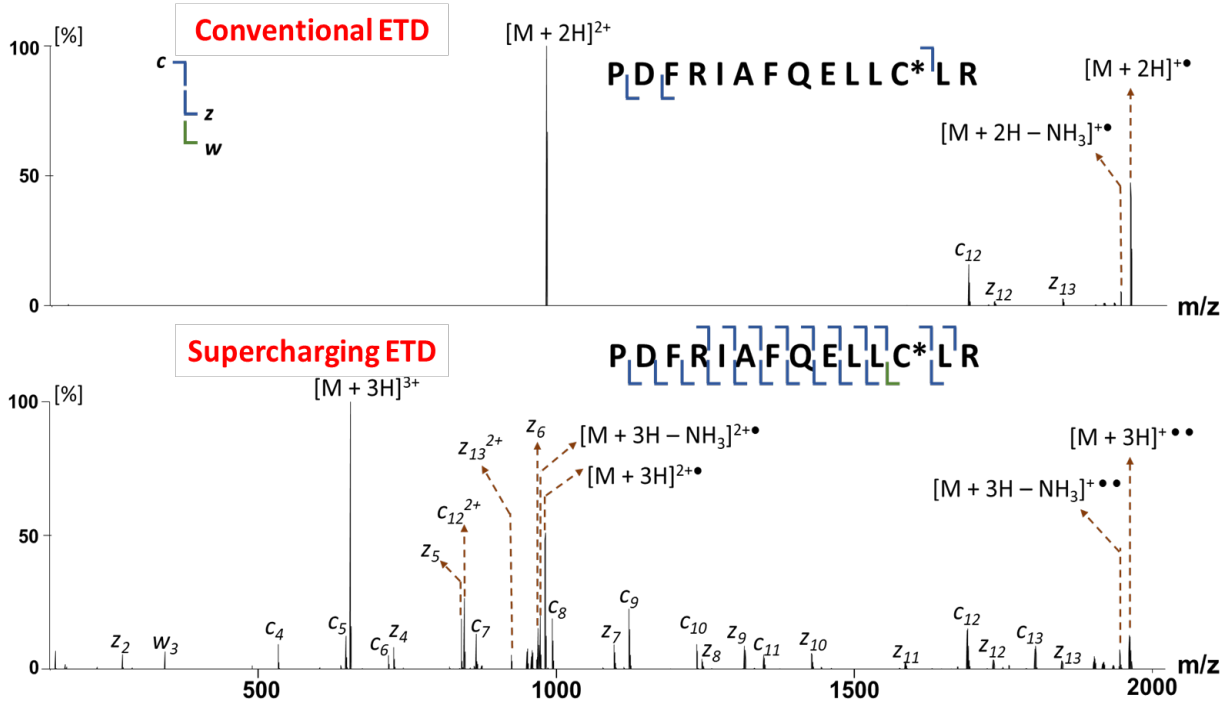

Figure 41. ETD of doubly- (top) and triply-protonated (bottom) S-palmitoylated PDFRIAFQELLCLR. Abundant 3+ precursor ions were only observed upon supercharging.

Supercharging was also effective for the doubly palmitoylated peptide $MGC_{Palm}VQC_{Palm}KDKEA$, which showed an average charge state of 2.00 in the absence of supercharging reagent (*Figure 3.6, Top*). For this peptide, both m-NBA and sulfolane were effective with an average charge state of 2.38 observed with sulfolane (*Fig. 3.6., Middle*) and 2.67 with m-NBA (*Fig. 3.6., Bottom*). ETD of the 2^+ ion yielded only 3 backbone fragments whereas the 3^+ ion generated extensive fragmentation (data not shown). For another peptide, $ARAW_{PALM}C_{PALM}QVAQKF$, only doubly protonated ions were generated in the absence of supercharging reagent whereas addition of either m-NBA or sulfolane allowed the observation of 3^+ ions, with sulfolane generating the highest abundance of this higher charge state. Chemical palmitoylation of this peptide also

palmitolyated the tryptophan residue.[35] Similar to the other peptides, ETD of the doubly charged precursor ions resulted in few *c*- and *z*-type ions whereas ETD of triply charged precursor ions generated significantly more abundant *c*- and *z*-type ion series as well as a few *a*-type ions. Again, no palmitate loss was observed. While both m-NBA and sulfolane were effective for increasing the average charge state of the examined S-palmitoylated peptides, addition of sulfolane significantly increased chemical noise. Thus, m-NBA was chosen for most of the subsequent LC/MS/MS experiments.

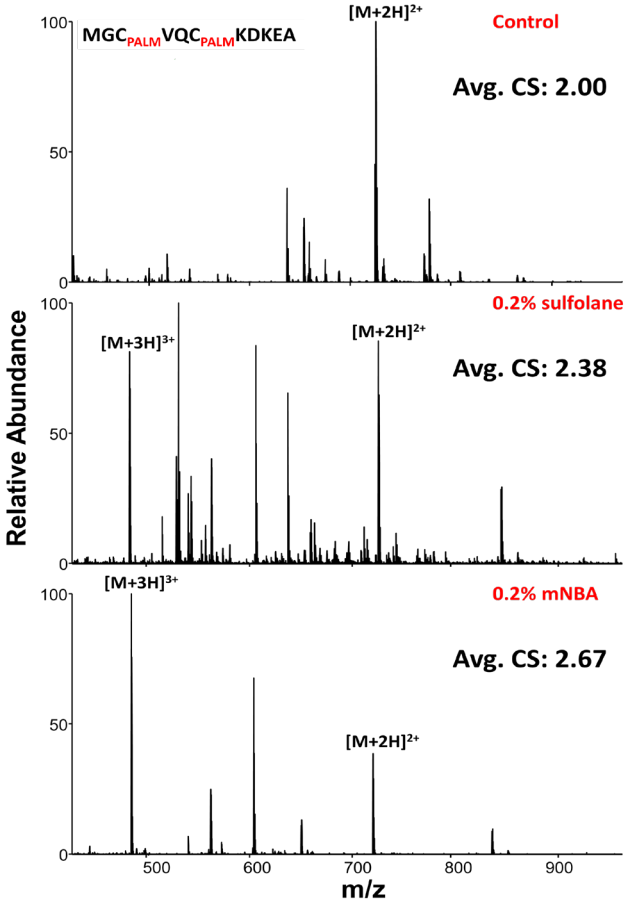

Figure 42. ESI mass spectra of the doubly S-palmitoylated peptide, MGC$_{Palm}$VQC$_{Palm}$KDKEA in the absence of supercharging (top), and following supercharging with sulfolane (middle) and m-NBA (bottom).

As a comparison to supercharging, we explored supplemental infrared activation approaches for the doubly protonated palmitoylated peptides. Interestingly, while AI-ETD (*Figure 3.7, top right*) did not result in palmitate loss, it was not effective in increasing sequence coverage of the model S-palmitoylated peptide, PDFRIAFQELLCLR. Only one additional fragment ion, $z_{11}^{+\bullet}$, was observed compared with conventional ETD (*Figure 3.7, top left*). On the other hand, ETirD in an MS^3 implementation (ETD MS^2 followed byIR irradiation of the isolated charged reduced species) generated complete sequence coverage without palmitate loss (*Fig. 3.7, bottom left*). However, this MS^3

implementation is not ideal because it lowers throughput in LC-MS/MS experiments. A summary of these three MS/MS approaches is shown in Figure 3.7, bottom right).

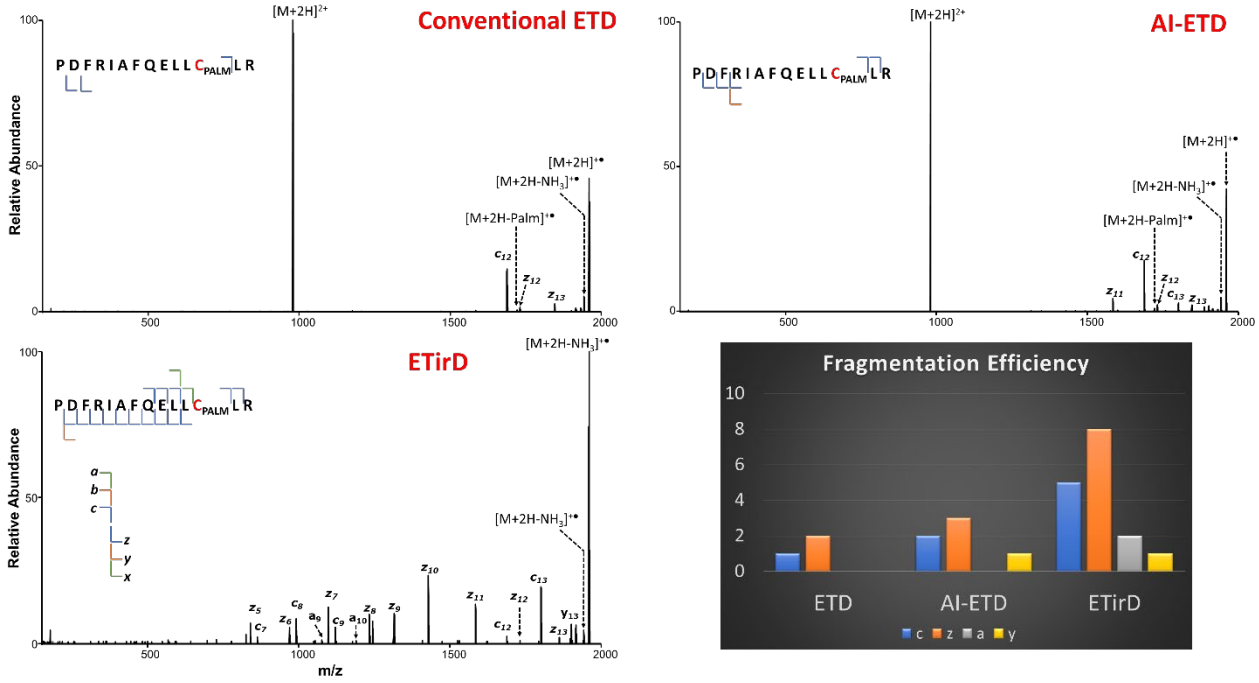

Figure 43. Supplemental IR activation methods for improved ETD of doubly charged S-palmitoylated peptides. Conventional ETD (Top, left) Activated Ion ETD (Top, right) and ETD followed by MS^3 IR Activation (Bottom, left). Summary of observed fragment ions (Bottom, right).

3.3.3. Sample Preparation for C8 Separation of Palmitoylated Peptides. After protein digestion, the presence of reagents such as alkylators, reductants, denaturants, surfactants, and buffer salts in the resulting peptide samples can lead to column contamination, ion suppression, and/or fouling of the MS ion source. Here, we employed online sample desalting with a C8 trap column connected to the 10-port valve associated with our nLC setup. After sample injection, 2% B, 4% B, and 6% B were used to (1) concentrate the palmitoylated peptides, and (2) divert salts and other low molecular weight materials to avoid contamination of the analytical column and mass spectrometer.

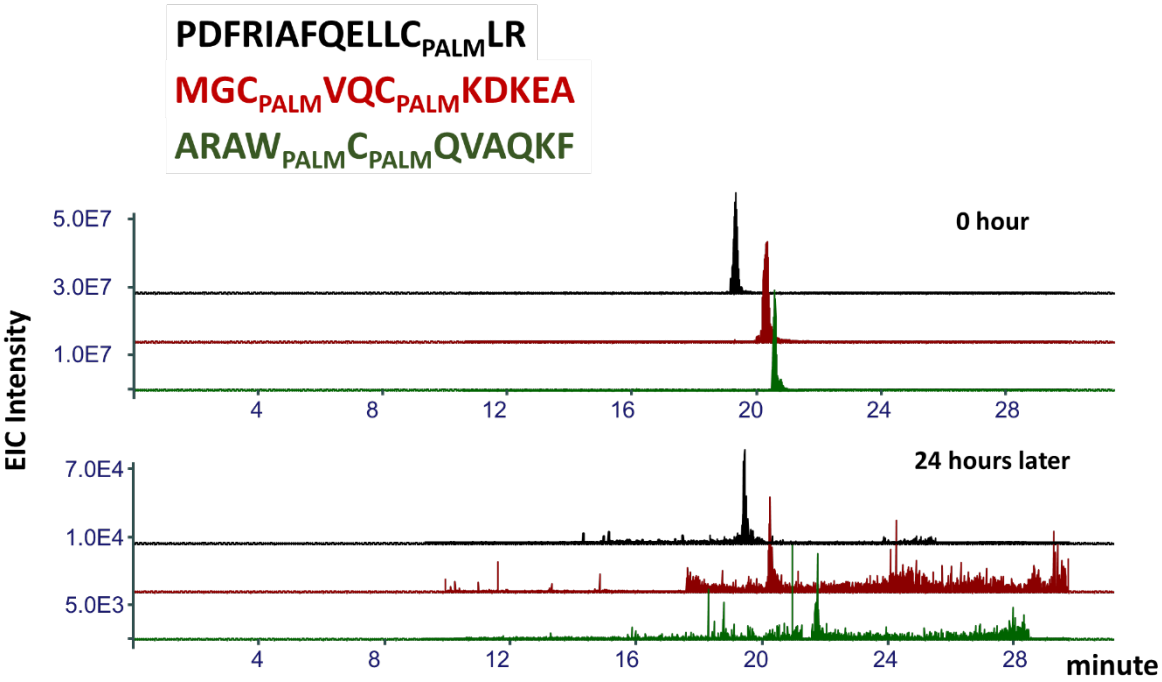

Figure 44. C8 separation of S-palmitoylated peptides from a freshly prepared sample (top) and a sample sitting in the autosampler for 24 hours (bottom).

To mitigate aggregation and/or precipitation of insoluble acetylated peptides, samples were diluted into mixed organic-phase buffers containing 5%:25%:0.1% IPA:ACN:RapiGest before sample injection and inline desalting. Another added benefit of inline desalting is that simultaneous removal of surfactant can be achieved with 0.1% FA at pH 3. To evaluate the sample

solubility over time, LC/MS/MS of freshly prepared sample (*Figure 3.8, top*) was compared with LC/MS/MS of a sample that had been sitting in the autosampler for 24 h (Figure 3.8. bottom). The analytical C8 nano-column was heated to 50^{o}C. As can be seen in Fig. 3.8, sample precipitation after 24 hours resulted in limited detection of the doubly palmitoylated peptides, MGC$_{PALM}$VQC$_{PALM}$KDKEA and ARAW$_{PALM}$C$_{PALM}$QVAQKF (*Fig. 3.8, bottom*). To minimize aggregation and precipitation, the autosampler was also heated to 37 ^{o}C. However, these data show the importance of freshly prepared samples for optimal detection of S-palmitoylated peptides.

3.3.4. LC-ETD MS/MS of Supercharged Lipidated Peptides. With the optimized sample preparation and LC method for lipidated peptides, we added supercharging to examine the utility of ETD MS/MS for such analytes. A farnesylated and O-methylated peptide from neuroblastoma Ras viral oncogene homolog (N-Ras), an important therapeutic component348,349 with a palmitoylation site near the C-terminal farnesylated cysteine350,351 was spiked into a palmitoylated lysozyme tryptic digest to a concentration of 15 ng/µL. Supercharging was performed with both m-NBA and sulfolane via the nanoflow post-column Tee described in Chapter 2. For the N-Ras peptide, sulfolane again did not have a significant effect on the average charge state, showing a moderate increase from 1.59 in the absence of supercharging reagent (*Figure 3.9., Top Left*) to 1.91, with doubly protonated ions dominating (95%) and remaining signal consisting of singly protonated ion, i.e., charge states incompatible with efficient ETD (*Figure 3. 9, Middle Left*). By contrast, m-NBA showed a higher degree of supercharging with the average charge state increase to 2.31, including detection of triply protonated ions at reasonable signal abundance (*Figure 3.9, Bottom Left).*

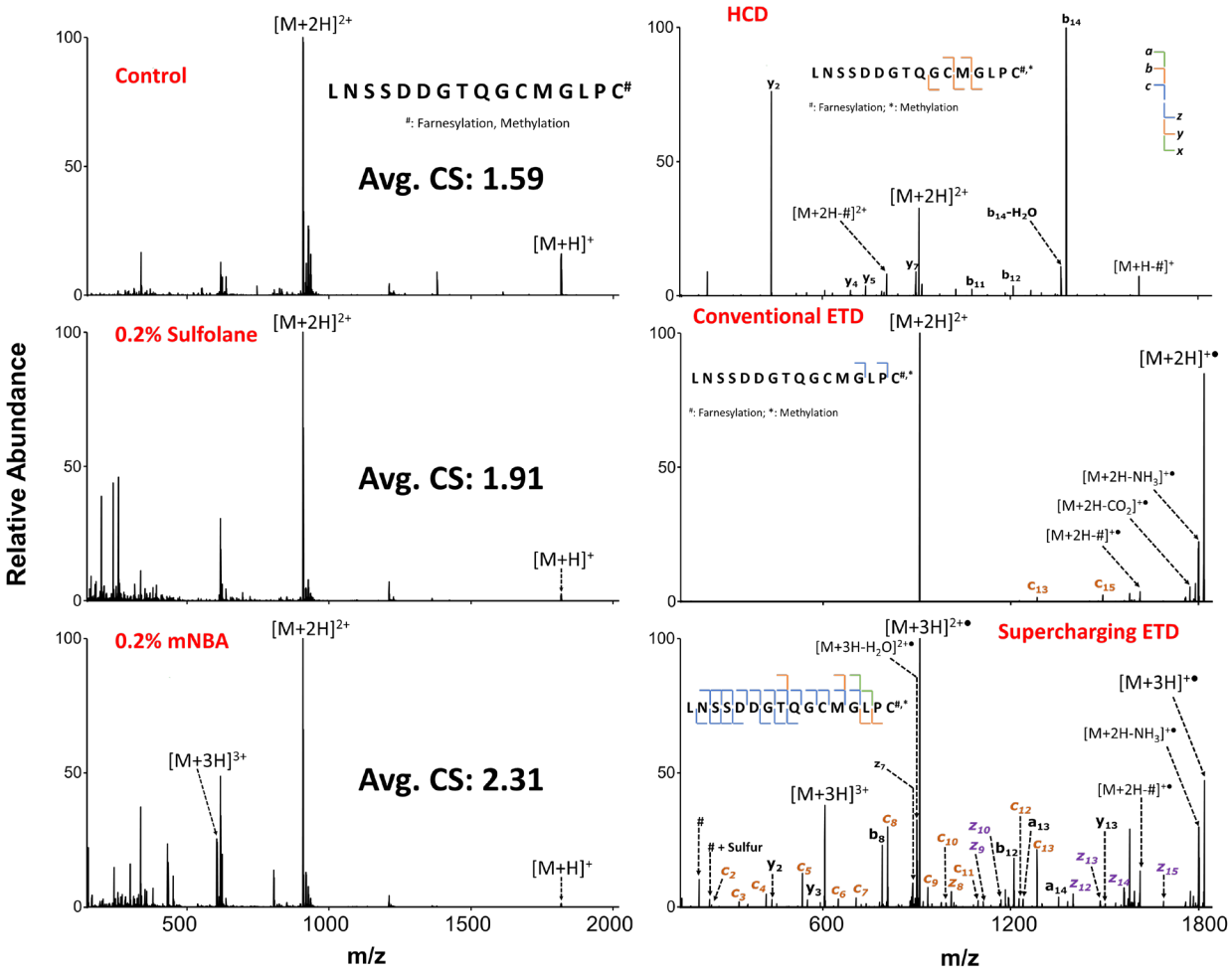

Figure 45. LC/MS/MS of an N-Ras peptide with and without supercharging. MS^1 spectra without supercharging (Top, Left) and following post-column addition of sulfolane (Middle, Left) and m-NBA (Bottom, Left). HCD (Top, Right) and ETD (Middle, Right) MS^2 spectra of the dominant doubly protonated charge state as well as ETD of the triply protonated charge state, only observed in the presence of m-NBA (Bottom, Left).

In the absence of supercharging reagent, the doubly protonated N-Ras peptide was selected for fragmentation in LC/MS/MS experiments. HCD of this doubly protonated peptide, LNSSDDGTQGCMGLPC#*, (# = farnesylation and * = C-terminal O-methylation), generated few backbone fragments including some farnesyl loss (*Figure 3.9, Top Right*). ETD showed even less backbone fragmentation but with a lower degree of farnesyl loss: only two backbone fragments,

[1] *: methylation on cysteine

c_{13}^{+} and c_{15}^{+}, were generated (Figure 3.9, Middle Right). By contrast, ETD of the triply protonated species generated via m-NBA supercharging showed high sequence coverage for the N-Ras peptide (*Figure 3.9, Bottom Right*).

We also explored LC-EThcD MS/MS both with and without supercharging. For the N-Ras peptide, EThcD of the doubly protonated precursor ion at 15% HCD did not show effective fragmentation (*Figure 3.10, a*). Higher HDC energy (20%) did not improve the sequence coverage but instead increased loss of the farnesyl modification (*Figure 3.10, b*). By contrast, EThcD of the triply protonated peptide observed following supercharging showed extensive sequence coverage with a higher degree of farnesyl retention (*Figure 3.10, c*). Thus, supercharging also benefitted EThcD experiments for this peptide.

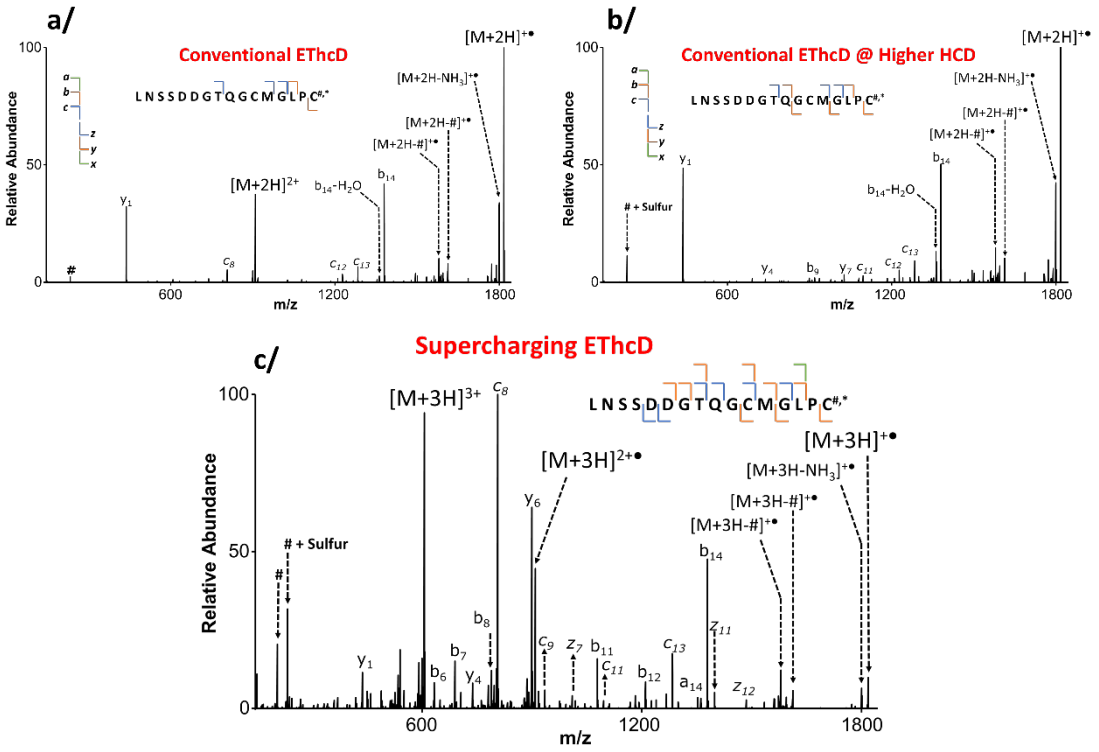

Figure 46. LC-EThcD MS/MS of an N-Ras peptide without (a, b) and with (c) m-NBA-based supercharging. Two different HCD voltages were used in the absence of supercharging: 15 HCD units (a) and 20 HCD units (b).

3.3.5. Neutral-loss Triggered ETD MS/MS of Supercharged Lipidated Peptides. To increase throughput in LC-ETD MS/MS experiments, we implemented a neutral-loss triggered acquisition method.[36] In this approach, a CID or HCD scan is first performed and, only if a defined neutral loss is observed, ETD data acquisition is triggered for the corresponding peptide (HCDnltETD). To adapt this strategy towards S-palmitoylated peptides a neutral palmitate losses of 238.23 and 273.12 Da were entered into the ETD-triggering data acquisition script. This workflow was evaluated with a chemically palmitoylated lysozyme tryptic digest spiked with the N-Ras peptide. Chicken lysozyme contains 8 cysteine residues, distriuted over 9 peptides following tryptic digestion with each peptide containing 1-3 cysteine sulfhydryl groups for chemical palmitoylation (*Table 3.1*). The resultingS-palmitoylated peptides were separated with the C-8 nano-LC column at 50 ^{o}C and subjected to HCDnltETD. Data analysis was performed with Thermo Proteome Discoverer and MSFragger. However, only 9 out of the 14 peptides palmitoylated peptides were identified (*Table 3. 1*). One interesting observation is that most of the undetected S-acetylated peptides contain three palmitoyl groups, i.e., a plausible explanation for the failure to detect these peptides is their insoluble nature, even with 0.1% RapiGest. Another possible explanation is that triply palmitoylated peptides were too strongly retainedon the C8 column Further work is needed to determine the root cause of incomplete detection of S-acetylated peptides from lysozyme. However, triple palmitoylation may not be a commonly occuring analytical challenge in proteomic samples.

S-Acetylated Peptide Sequence	**HCD**	**ETD**	**EThcD**	**Supercharge ETD**	**Supercharge HCDnlETD**
Lysozyme, Chicken Egg White					
(R)C$_{PALM}$ELAAAMK(R)	PD	PD, MSF	PD	PD, MSF	PD, MSF
(R)WWC$_{PALM}$NDGR(T)	PD		MSF	MSF	MSF
(R)WW$_{PALM}$C$_{PALM}$NDGR(T)			MSF	PD, MSF	PD, MSF

(R)W$_{PALM}$W$_{PALM}$C$_{PALM}$NDGR(T)					
(R)GYSLGNWVC$_{PALM}$AAK(F)	MSF			PD, MSF	PD, MSF
(R)GYSLGNW$_{PALM}$VC$_{PALM}$AAK(F)				MSF	PD, MSF
(R)NLC$_{PALM}$NIPCSALLSSDITASVNCAK(K)			MSF	MSF	MSF
(R)NLCNIPC$_{PALM}$SALLSSDITASVNCAK(K)				PD, MSF	MSF
(R)NLCNIPCSALLSSDITASVNC$_{PALM}$AK(K)				MSF	PD, MSF
(R)NLC$_{PALM}$NIPC$_{PALM}$SALLSSDITASVNCAK(K)					
(R)NLC$_{PALM}$NIPCSALLSSDITASVNC$_{PALM}$AK(K)				MSF	MSF
(R)NLCNIPC$_{PALM}$SALLSSDITASVNC$_{PALM}$AK(K)					
(R)NLC$_{PALM}$NIPC$_{PALM}$SALLSSDITASVNC$_{PALM}$AK(K)					
Synthetic N-Ras Peptide					
LNSSDDGTQGCMGLPC$^{\#,*}$			PD, MSF	PD, MSF	PD, MSF
*Methylation. #Farnesylation. Palm: S-Palmitoylation. PD: SequestHT Node on Proteome Discoverer. MSF: MSFragger.					

3.4. Conclusion

In this work, we further addressed issues with sample processing, separation, and LC/MS/MS analysis of lipidated peptides. We utilized TCEP and RapiGest to minimize sample loss, heated C8 nanoflow chromatography, and post-column nano T-junction supercharging for improved analysis in ETD-based experiments. Overall, with these modifications, we were able to directly detect S-palmitoylated peptides as well as an N-Ras highly hydrophobic peptide.

3.5. References

(1) El-Husseini, A. E. D.; Schnell, E.; Dakoji, S.; Sweeney, N.; Zhou, Q.; Prange, O.; Gauthier-Campbell, C.; Aguilera-Moreno, A.; Nicoll, R. A.; Bredt, D. S. Synaptic Strength Regulated by Palmitate Cycling on PSD-95. *Cell* **2002**, *108* (6), 849–863. https://doi.org/10.1016/S0092-8674(02)00683-9.

(2) Busconi, L.; Michel, T. Endothelial Nitric Oxide Synthase. N-Terminal Myristoylation Determines Subcellular Localization. *Journal of Biological Chemistry* **1993**, *268* (12), 8410–8413. https://doi.org/10.1016/S0021-9258(18)52889-1.

(3) Remsberg, J. R.; Suciu, R. M.; Zambetti, N. A.; Hanigan, T. W.; Firestone, A. J.; Inguva, A.; Long, A.; Ngo, N.; Lum, K. M.; Henry, C. L.; Richardson, S. K.; Predovic, M.; Huang, B.; Dix, M. M.; Howell, A. R.; Niphakis, M. J.; Shannon, K.; Cravatt, B. F. ABHD17 Regulation of Plasma Membrane Palmitoylation and N-Ras-Dependent Cancer Growth. *Nature Chemical Biology 2021 17:8* **2021**, *17* (8), 856–864. https://doi.org/10.1038/s41589-021-00785-8.

(4) Burgoyne, J. R.; Haeussler, D. J.; Kumar, V.; Ji, Y.; Pimental, D. R.; Zee, R. S.; Costello, C. E.; Lin, C.; McComb, M. E.; Cohen, R. A.; Bachschmid, M. M. Oxidation of HRas Cysteine Thiols by Metabolic Stress Prevents Palmitoylation in Vivo and Contributes to Endothelial Cell Apoptosis. *The FASEB Journal* **2012**, *26* (2), 832–841. https://doi.org/10.1096/FJ.11-189415.

(5) Lynch, S. J.; Snitkin, H.; Gumper, I.; Philips, M. R.; Sabatini, D.; Pellicer, A. The Differential Palmitoylation States of N-Ras and H-Ras Determine Their Distinct Golgi Subcompartment Localizations. *Journal of Cellular Physiology* **2015**, *230* (3), 610–619. https://doi.org/10.1002/JCP.24779.

(6) Lin, D. T. S.; Davis, N. G.; Conibear, E. Targeting the Ras Palmitoylation/Depalmitoylation Cycle in Cancer. *Biochemical Society Transactions* **2017**, *45* (4), 913–921. https://doi.org/10.1042/BST20160303.

(7) Gesehenes, R. J.; Miller, J. J. Protein Modifications | Protein Palmitoylation. *Encyclopedia of Biological Chemistry: Third Edition* **2021**, *3*, 182–185. https://doi.org/10.1016/B978-0-12-819460-7.00145-6.

(8) Xiang, S.; Bai, W.; Bepler, G.; Zhang, X. Activation of Ras by Post-Translational Modifications. *Conquering RAS: From Biology to Cancer Therapy* **2017**, 97–118. https://doi.org/10.1016/B978-0-12-803505-4.00006-0.

(9) Guan, X.; Fierke, C. A. Understanding Protein Palmitoylation: Biological Significance and Enzymology. *Sci China Chem* **2011**, *54* (12), 1888. https://doi.org/10.1007/S11426-011-4428-2.

(10) Tak, I. ur R.; Ali, F.; Dar, J. S.; Magray, A. R.; Ganai, B. A.; Chishti, M. Z. Posttranslational Modifications of Proteins and Their Role in Biological Processes and Associated Diseases. *Molecular Nutrition: Vitamins* **2019**, 1–35. https://doi.org/10.1016/B978-0-12-811913-6.00001-1.

(11) Dekker, F. J.; Rocks, O.; Vartak, N.; Menninger, S.; Hedberg, C.; Balamurugan, R.; Wetzel, S.; Renner, S.; Gerauer, M.; Schölermann, B.; Rusch, M.; Kramer, J. W.; Rauh, D.; Coates, G. W.; Brunsveld, L.; Bastiaens, P. I. H.; Waldmann, H. Small-Molecule Inhibition of APT1 Affects Ras Localization and Signaling. *Nature Chemical Biology 2010 6:6* **2010**, *6* (6), 449–456. https://doi.org/10.1038/nchembio.362.

(12) Wan, J.; Roth, A. F.; Bailey, A. O.; Davis, N. G. Palmitoylated Proteins: Purification and Identification. *Nature Protocols* **2007**, *2* (7), 1573–1584. https://doi.org/10.1038/NPROT.2007.225.

(13) Roth, A. F.; Wan, J.; Bailey, A. O.; Sun, B.; Kuchar, J. A.; Green, W. N.; Phinney, B. S.; Yates, J. R.; Davis, N. G. Global Analysis of Protein Palmitoylation in Yeast. *Cell* **2006**, *125* (5), 1003–1013. https://doi.org/10.1016/J.CELL.2006.03.042.

(14) Zhang, M. M.; Tsou, L. K.; Charron, G.; Raghavan, A. S.; Hang, H. C. Tandem Fluorescence Imaging of Dynamic S-Acylation and Protein Turnover. *Proc Natl Acad Sci U S A* **2010**, *107* (19), 8627–8632. https://doi.org/10.1073/PNAS.0912306107/-/DCSUPPLEMENTAL.

(15) Hang, H. C.; Linder, M. E. Exploring Protein Lipidation with Chemical Biology. *Chemical Reviews* **2011**, *111* (10), 6341–6358. https://doi.org/10.1021/CR2001977.

(16) Kathayat, R. S.; Elvira, P. D.; Dickinson, B. C. A Fluorescent Probe for Cysteine Depalmitoylation Reveals Dynamic APT Signaling. *Nat Chem Biol* **2017**, *13* (2), 150–152. https://doi.org/10.1038/NCHEMBIO.2262.

(17) Raghavan, A. S.; Hang, H. C. Seeing Small Molecules in Action with Bioorthogonal Chemistry. *Drug Discovery Today* **2009**, *14* (3–4), 178–184. https://doi.org/10.1016/J.DRUDIS.2008.09.014.

(18) Wang, Q.; Chan, T. R.; Hilgraf, R.; Fokin, V. v.; Sharpless, K. B.; Finn, M. G. Bioconjugation by Copper(I)-Catalyzed Azide-Alkyne [3 + 2] Cycloaddition. *J Am Chem Soc* **2003**, *125* (11), 3192–3193. https://doi.org/10.1021/JA021381E/SUPPL_FILE/JA021381E_S.PDF.

(19) Martin, B. R.; Wang, C.; Adibekian, A.; Tully, S. E.; Cravatt, B. F. Global Profiling of Dynamic Protein Palmitoylation. *Nature Methods 2011 9:1* **2011**, *9* (1), 84–89. https://doi.org/10.1038/nmeth.1769.

(20) Martin, B. R.; Cravatt, B. F. Large-Scale Profiling of Protein Palmitoylation in Mammalian Cells. *Nature Methods 2009 6:2* **2009**, *6* (2), 135–138. https://doi.org/10.1038/nmeth.1293.

(21) Collins, M. O.; Woodley, K. T.; Choudhary, J. S. Global, Site-Specific Analysis of Neuronal Protein S-Acylation. *Scientific Reports 2017 7:1* **2017**, *7* (1), 1–14. https://doi.org/10.1038/s41598-017-04580-1.

(22) Forrester, M. T.; Hess, D. T.; Thompson, J. W.; Hultman, R.; Moseley, M. A.; Stamler, J. S.; Casey, P. J. Site-Specific Analysis of Protein S-Acylation by Resin-Assisted Capture. *J Lipid Res* **2011**, *52* (2), 393–398. https://doi.org/10.1194/JLR.D011106.

(23) Mcclure, M. L.; Wen, H.; Fortenberry, J.; Hong, J. S.; Sorscher, E. J. S-Palmitoylation Regulates Biogenesis of Core Glycosylated Wild-Type and F508del CFTR in a Post-ER Compartment. *Biochemical Journal* **2014**, *459* (2), 417–425. https://doi.org/10.1042/BJ20131037.

(24) Tu, Y.; Wang, J.; Ross, E. M. Inhibition of Brain G(z) GAP and Other RGS Proteins by Palmitoylation of G Protein α Subunits. *Science (1979)* **1997**, *278* (5340), 1132–1135. https://doi.org/10.1126/SCIENCE.278.5340.1132/ASSET/D747EE6C-4250-422C-9A75-921E6F7D45D6/ASSETS/GRAPHIC/SE467595602A.JPEG.

(25) Xue, L.; Gollapalli, D. R.; Maiti, P.; Jahng, W. J.; Rando, R. R. A Palmitoylation Switch Mechanism in the Regulation of the Visual Cycle. *Cell* **2004**, *117* (6), 761–771. https://doi.org/10.1016/J.CELL.2004.05.016.

(26) Ji, Y.; Leymarie, N.; Haeussler, D. J.; Bachschmid, M. M.; Costello, C. E.; Lin, C. Direct Detection of S-Palmitoylation by Mass Spectrometry. *Analytical Chemistry* **2013**, *85* (24), 11952–11959. https://doi.org/10.1021/AC402850S/SUPPL_FILE/AC402850S_SI_001.PDF.

(27) Good, D. M.; Wirtala, M.; McAlister, G. C.; Coon, J. J. Performance Characteristics of Electron Transfer Dissociation Mass Spectrometry. *Mol Cell Proteomics* **2007**, *6* (11), 1942–1951. https://doi.org/10.1074/MCP.M700073-MCP200.

(28) Frese, C. K.; Altelaar, A. F. M.; van den Toorn, H.; Nolting, D.; Griep-Raming, J.; Heck, A. J. R.; Mohammed, S. Toward Full Peptide Sequence Coverage by Dual Fragmentation Combining Electron-Transfer and Higher-Energy Collision Dissociation Tandem Mass Spectrometry. *Analytical Chemistry* **2012**, *84* (22), 9668–9673. https://doi.org/10.1021/AC3025366/SUPPL_FILE/AC3025366_SI_001.PDF.

(29) Riley, N. M.; Hebert, A. S.; Dürnberger, G.; Stanek, F.; Mechtler, K.; Westphall, M. S.; Coon, J. J. Phosphoproteomics with Activated Ion Electron Transfer Dissociation. *Analytical Chemistry* **2017**, *89* (12), 6367–6376. https://doi.org/10.1021/ACS.ANALCHEM.7B00212/SUPPL_FILE/AC7B00212_SI_001.PDF.

(30) Kjeldsen, F.; Giessing, M. B. A.; Ingrell, R. C.; Jensen, N. O. Peptide Sequencing and Characterization of Post-Translational Modifications by Enhanced Ion-Charging and Liquid Chromatography Electron-Transfer Dissociation Tandem Mass Spectrometry. *Analytical Chemistry* **2007**, *79* (24), 9243–9252. https://doi.org/10.1021/AC701700G.

(31) Wang, Q.; Hakansson, K. The Presence of b Ions in Electron Capture/Transfer Dissociation of Supercharged Peptides. In *In 66th ASMS Conference on Mass Spectrometry and Allied Topics*; San Diego, 2018.

(32) Dekker, F. J.; Rocks, O.; Vartak, N.; Menninger, S.; Hedberg, C.; Balamurugan, R.; Wetzel, S.; Renner, S.; Gerauer, M.; Schölermann, B.; Rusch, M.; Kramer, J. W.; Rauh, D.; Coates, G. W.; Brunsveld, L.; Bastiaens, P. I. H.; Waldmann, H. Small-Molecule Inhibition of APT1 Affects Ras Localization and Signaling. *Nature Chemical Biology 2010 6:6* **2010**, *6* (6), 449–456. https://doi.org/10.1038/nchembio.362.

(33) Martin, B. R.; Lambert, N. A. Activated G Protein Gαs Samples Multiple Endomembrane Compartments. *The Journal of Biological Chemistry* **2016**, *291* (39), 20295. https://doi.org/10.1074/JBC.M116.729731.

(34) Drisdel, R. C.; Green, W. N. Labeling and Quantifying Sites of Protein Palmitoylation. *Biotechniques* **2004**, *36* (2), 276–285. https://doi.org/10.2144/04362RR02/ASSET/IMAGES/LARGE/FIGURE4.JPEG.

(35) Bar-Sagi, D. A Ras by Any Other Name. *Molecular and Cellular Biology* **2001**, *21* (5), 1441–1443. https://doi.org/10.1128/MCB.21.5.1441-1443.2001/ASSET/9C8A235D-D123-4048-B728-C5AB0683FF70/ASSETS/GRAPHIC/MB0511874001.JPEG.

(36) Creese, A. J.; Grant, M. M.; Chapple, I. L. C.; Cooper, H. J. On-Line Liquid Chromatography Neutral Loss-Triggered Electron Transfer Dissociation Mass Spectrometry for the Targeted Analysis of Citrullinated Peptides. *Analytical Methods* **2011**, *3* (2), 259–266. https://doi.org/10.1039/C0AY00414F.

Chapter 4. Collision Induced Unfolding-Electron Capture Dissociation (CIU-ECD) for Improved Analysis of PTM-containing Peptides

4.1. Introduction

Posttranslational modification (PTM) is a later but important step in protein biosynthesis. PTMs are responsible for many major biological processes and PTM-disordered associated diseases (e.g., cancer)[1]. In fact, different PTMs would play specific functions such as phosphorylation in regulating protein function and transmitting signals throughout the cell[2,3], glycosylation in immune system[4] and cell adhesion[5,6], and palmitoylation in membrane-associated function and trafficking[7–10]. Thus, it is critical to timely and accurately distinguish the PTM types and sites on proteins to develop better therapeutic treatments. However, labile nature of these PTMs poses challenges to study them. For instance, acid lability of the phosphopeptide, glycan lability from glycopeptides, and labile thioester linkage from S-Palmitoylation makes them difficult to study with vibrational activation methods (i.e., CID/HCD, IRMPD, and UVPD)[11–16]. Electron Capture Dissociation (ECD)/ electron transfer dissociation (ETD) can retain labile[17–20]. Thus, ECD/ETD is an ideal alternative for labile PTM analysis of phosphor-[21–24], glyco-[19,25,26], and palmitoylated peptides[11,22,27]. However, these electron-based techniques have reduced performance at higher m/z (>1000 m/z)[28,29]. In contrast to unmodified

counterparts, PTM-carrying peptides would promote unique and diverse gas-phase peptide structures[30].

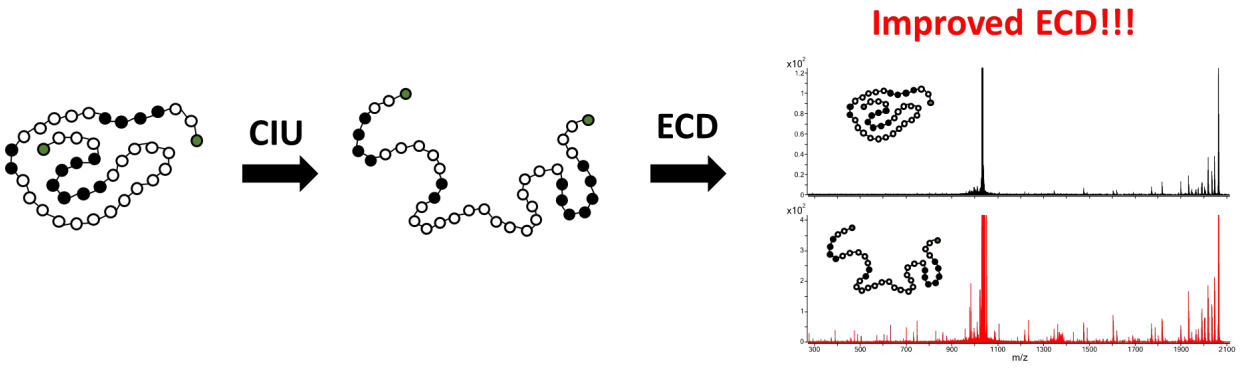

Figure 4.1. Collisional induced unfolding for improved ECD

Cooper and coworkers have shown that phosphorylation has a detrimental influence on the ECD of doubly protonated peptides due to salt bridge structure between negatively charged phosphate group and protonated amino acid residues[31]. To achieve improved sequence coverage for ECD, hot ECD was used. The presence of phospho-group altered the peptide confirmation leading observation of fragmentation at only peptide terminal ends. To break these noncovalent interactions with large enough Coulombic repulsion, an alternative approach supercharging was utilized to generate highly protonated precursor ions[32]. Coon and coworkers have shown that infrared activation ETD (AI-ETD) of phosphopeptide provided extensive sequence coverage but with numerous phosphate neutral losses. For glycopeptide, Marshall and coworkers have shown that ECD alone was not effective enough to fragment glycopeptide from Lectin Erythrina glycoprotein, VETISFSFSEFEPGNDN$_{Hex(3)HexNac(2)dHexPent}$LTLQGAALITQSGVLQLTK[24]. The inefficient fragmentation observed in ECD is presumably due to the compact gas phase structure of glycopeptide resulting from the intramolecular interaction between glycan and peptide portion.

A multistage MS^3 experiment of ECD followed by IR laser irradiation of same glycopeptide would result in extensive backbone dissociation into c- and z-type fragment ions.

Collisional induced unfolding has been utilized to probe subtle changes in protein structure, stability, or composition via gas-phase activation[33–38]. In a typical CIU workflow, an isolate ion would be activated with neutral background gas to rise its internal energy for unfolding to happen. During the unfolding event, IM was employed to obtain structural transition from compact to elongated states. Then, preprocessed of data happened with CIU-Suite2 for visualization of CIU fingerprint[39,40]. This process is well-known for protein analysis. However, there was no previous reports of using CIU-ECD for peptide unfold in combination with ECD. In this chapter, I utilized CIU in conjunction with ECD to exploit on peptide unfolding for improved ECD (*Fig. 4.1*).

4.2. Experimental

4.2.1. Preparation of S-Palmitoylated Peptides:

Synthetic peptides, PDFRIAFQELLCLR and MGCVQCPKDKEA, were purchased from GenScript. Thioacylation reactions were performed by dissolving synthetic peptides in 100% TFA[41]. Palmitoyl chloride was added and allowed to react for 10 min under ambient conditions. The product mixture was dried under nitrogen and purified by HPLC. Purification of the products was performed on an Agilent Infinity II HPLC system using Thermo Scientific™ Hypersil GOLD™ C4 HPLC Column (C4, 5 µm, 250Å, 2.1 mm i.d. × 150 mm). Mobile phase A consisted of 95:5 water/ACN with 0.1% TFA, and mobile phase B consisted of 90:5:5 ACN/IPA/water with 0.1% TFA. A linear gradient of 30−100% B (singly palmitoylated peptides) or 40−100% B (doubly

palmitoylated peptides) over 20 min was employed with a flow rate of 0.3 mL/min. The aliquots of palmitoylated peptides were kept inside 80^{o}C until MS analysis.

4.2.2. Preparation of Glycopeptides:

Glycoprotein, Erythrina cristagalli lectin purchased from Sigma-Aldrich (St. Louis, MO, USA), were digested with trypsin to obtain N-glycosylated peptides. Trypsin digestion procedure was performed based on Thermo protocols with modifications. Briefly, glycoproteins were reduced by 5mM Tris(2-carboxyethyl)-phosphine hydrochloride (TCEP) in 50 mM ammonium bicarbonate (NH_4HCO_3) buffer with pH 8.5 at 37^{0}C for 1 hour. Alkylation was followed with 20 mM iodoacetamide from Sigma-Aldrich (St. Louis, MO, USA) at room temperature for another hour. Proteins were then incubated with Promega sequencing-grade modified trypsin in ratio of 1:50 at 37^{o}C overnight. Samples were desalted with C-18 Zip-Tip from Millipore Sigma. The desalted digests were dried in SpeedVac. After C18 desalting, peptides were dissolved in 85%:0.1% ACN:FA solution for further HILIC enrichment. Glycopeptides were then enriched with HILIC NuTip (GlySci, Columbia, MD). The enriched peptides were dried with SpeedVac again and kept at 80^{o}C until MS analysis.

4.2.3. Preparation of Phosphopeptide and Antimicrobial Peptide:

Bovine β-casein phosphopeptide with at least 95% purity was purchased from AnaSpec. Melittin was purchase with at least 95% purity were purchased from GenScript. Various electrospray solvents (50 mM ammonium acetate, 50%:50%:0.1% methanol:water:formic acid, 50%:50%:0.1% acetonitrile:water:formic acid, 100% isopropanol, 100% methanol, and 100% acetonitrile) were used for direct infusion into an Agilent 6560 mass spectrometer, modified for CIU and equipped with an e-MSion ExD cell. The sample concentration was prepared between 2

µM to 5 µM to be sprayed effectively with the dual jet stream AJS source. CIU was performed with nitrogen buffer gas. The CIU voltage was increased from 0 V to 280 V in 5 V increments, then 2 V increments to 300 V to prevent arcing. All mass spectra were acquired in IM-QTOF mode and analyzed with Agilent IM-MS Browser. CIU fingerprint was generated with CIU-Suite2 developed by Ruotolo and coworkers[40]. From chapter 2, we have shown that only one fragment can be resulted from ETD of the same peptide and supercharging is required for improved ETD.

4.2.4. Molecular dynamics (MD) simulation:

β-casein phosphopeptide structure was built with custom CHARMM script. Phosphoserine force field was built with CHARMM36 Additive Force Field. This force field did not contain neutral phosphate group, so only single deprotonated group was chosen for the phospho-group for the simulation. To obtain the doubly protonated group, the positive charges were added lysine, N-terminus and one highlighted glutamine on the following sequence FQsEEQ**Q**QTEDELQDK. The complete structure was then energy-minimized to remove steric clashes during the MD simulation. A custom script for replica exchange MD was utilized to sample all the conformational landscape to experimentally search for compact and elongated structures. A total of 20 replica was chosen for the REMD simulation. The simulation temperature was between 500K and 800K. The simulation duration was 100 nanoseconds. The total of 100,000 structures were generated from REMD simulation. IMPACT (Ion Mobility Projection Approximation Calculation Tool) software package was employed to obtain the theoretical CCS for all the generated structures[42]. Simulated structures were filtered to within ±2.5% of the experimentally derived CCS for compact and unfolded states. The K-clustering method was employed to the filtered structures. ECD

results were also used to confirm the appropriate structure from CIU-ECD experiments. PyMol was used for visualization and generation of compact and unfolded peptide structures.

4.3. Results and Discussion

4.3.1. CIU-ECD of S-Palmitoylated Peptide:

From drift time ion mobility (IM) analysis, we found the peptides substance P, melittin, tyrosine phosphopeptide, β-casein phosphopeptide, and tryptic peptides from coral tree lectin, to have diverse gas-phase conformations following nano-ESI from ammonium acetate. Palmitoylation is a relatively large, uncharged modification, typically increasing the mass-to-charge ratio of palmitoylated vs. unmodified peptides. Both ECD and ETD have shown reduced performance at high m/z ratios for such peptides. While polar modifications such as phosphorylation and glycosylation are likely to participate in intramolecular hydrogen bonding, such interactions are unlikely in the context of palmitoylation. Surprisingly, IM experiments showed that a doubly protonated palmitoylated peptide, PDFRIAFQELLC$_{Palm}$LR, has a rather compact gas-phase structure, possessing a CCS that is significantly (~10%) increased upon CIU via a single gas-phase structure transition observed over the accelerating voltage range probed here (*Fig. 4.2, left panel*). Interestingly, the resulting increased CCS is similar to the size recorded for the triply protonated peptide. On the other hand, the doubly palmitoylated peptide, MGC$_{Palm}$VQC$_{Palm}$KDKEA, did not show a major shift in gas-phase cross section upon CIU.

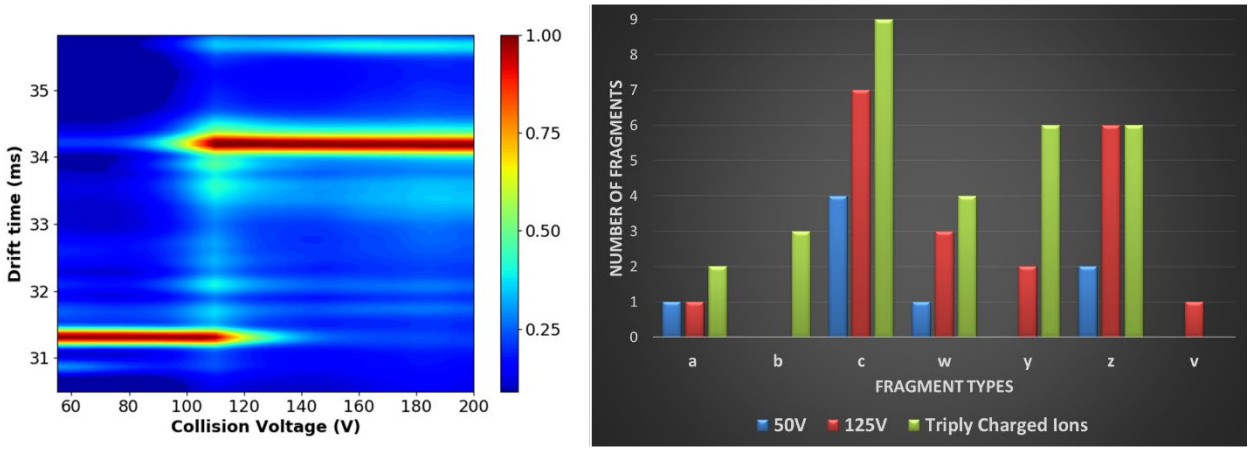

Figure 4.2. CIU of a doubly protonated S-palmitoylated model peptide (left) and the effects of peptide unfolding on ECD fragmentation as well as a comparison to ECD of the triply protonated peptide (right).

ECD of a typical doubly protonated precursor, PDFRIAFQELLC$_{Palm}$LR, yielded little fragmentation—mostly from the terminal end of the peptide (*Fig. 4.3, top*). On the other hand, CIU-ECD of the same precursor ions at 125V yielded extensive backbone fragmentation for c- and z- type ions for the same S-Palmitoylated peptide (*Fig. 4.3, bottom*). One noteworthy observation was that most of the new fragments were resulted from interior fragmentation of that peptides. Surprisingly, there was a little neutral loss of the palmitate group than initially expected. CIU was expected to produce numerous neutral losses from slow-heating activation, but CIU-ECD at 125V was more gentle than other hybrid techniques such AI-ECD, AI-ETD, or EThcD. Another interesting finding was that the charge-reduced species was significantly reduced indicating the CIU disrupted the intramolecular interaction to allow the separation of product ions from ECnoD (*Fig. 4.3*). The right graph of *fig. 4.2* shows the fragments generated from ECD of doubly ions at 50V, CIU-ECD of doubly ions at 125V, and ECD of triply charged ions at 50V. Upon activation of doubly protonated ions, we can observe similar fragmentation pattern between doubly and triply protonated precursors—as expected because CIU allowed doubly charged precursor to have similar CCS value of triply charged precursor.

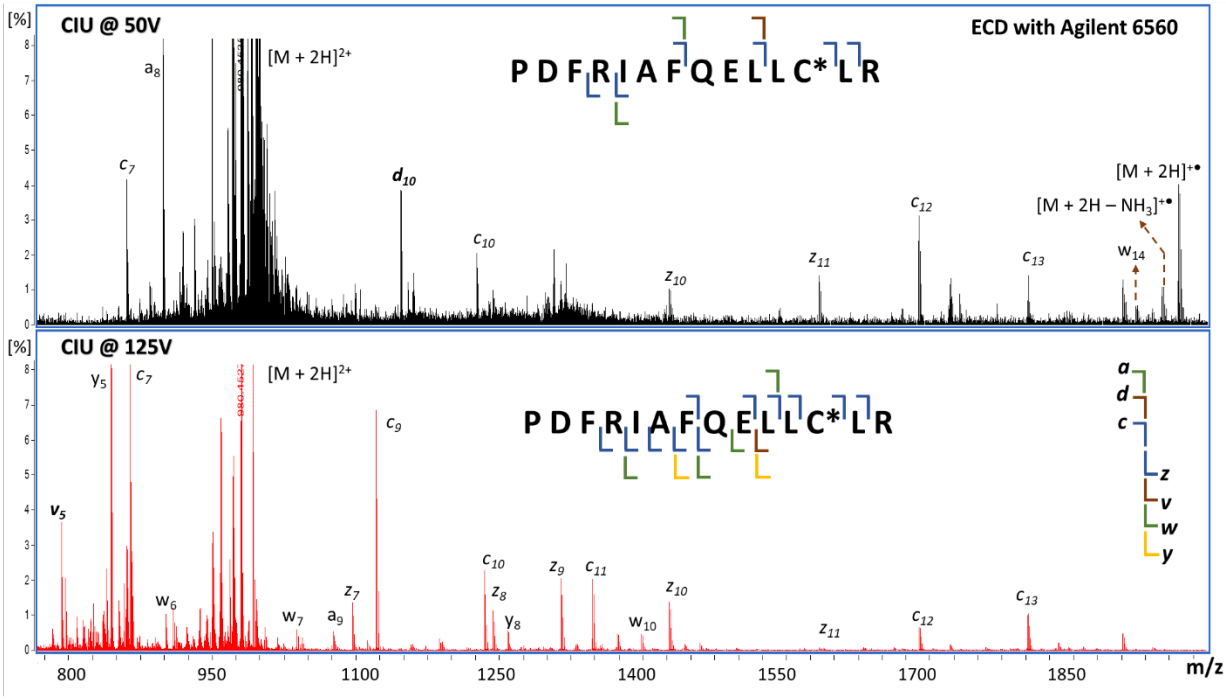

Figure 4.3. ECD of S-Palmitoylated peptide, PDFRIAFQELLCLR, with (top) no CIU and (bottom) at 125V CIU.

4.3.2. CIU-ECD of N-Glycosylated and Phosphorylated Peptides:

The triply protonated glycopeptide, SKPAQGYGYLGIF**N**$_{Hex3HexNac2dHexPent}$NSK, undergoes CIU to produce an unfolded structure at 180V that is ~17% larger than its ground state structure at 50V via multiple intermediate CIU transitions (*Fig. 4.4a*). While ECD of compact state produced fragmentation of peptide portion away from glycosylation sites preventing annotation of glyco-site (*Fig. 4.4, top*), ECD of the extended conformer resulted in additional c/z ions from cleavages near the glycosylation site, c_{14}^{+} and $z_5^{\bullet}$ (*Fig. 4.4, bottom*). Our hypothesis for such behavior is due to the intramolecular interaction between the glycan and peptide portions. Also, as expected from our previous observation from S-Palmitoylation, charged reduced species was significantly reduced due to the structural changes of precursor ions to diminish the ECnoD phenomenon (*Fig.*

4.5). The intermediate transition at ~125V was not probed (*Fig. 4.4a*), but ECD was expected to generate a unique fragmentation compared to the non-CIU and CIU at 180V.

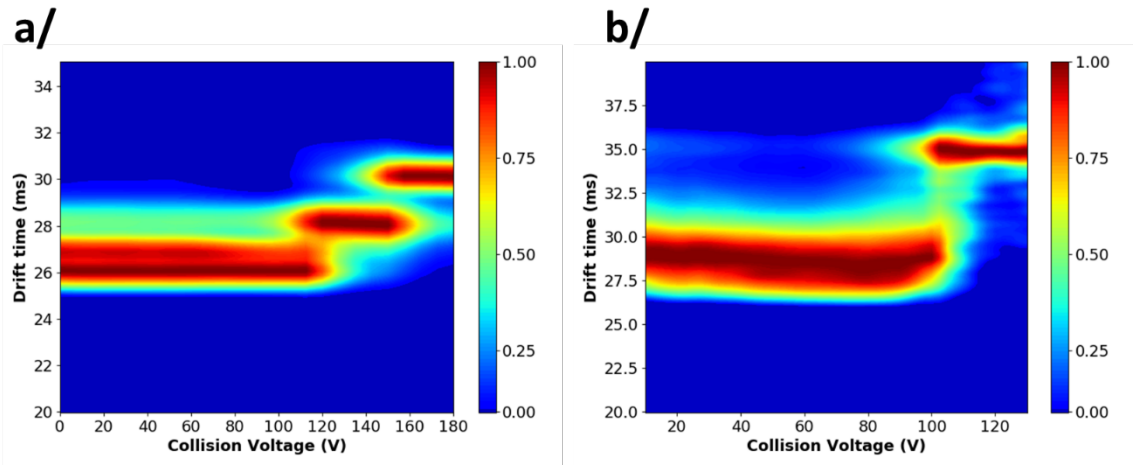

Figure 4.4. CIU of (a) Lectin Glycosylated peptide, SKPAQGYGYLGIFN$_{Hex(3)HexNac(2)dHexPent}$NSK (b) β-Casein Phosphorylated peptide, FQsEEQQQTEDELQDK.

Another interesting remark is that CIU-ECD of glycopeptide would not only produce extensive peptide backbone fragmentation but also generate glycosidic cleavages on the glycan portion similar to EThcD or AI-ETD[17,43]. This fragmentation scheme from CIU-ECD would enable us to obtain complete information of both glycan and peptide in one single spectrum. In addition to that information, with IM information, we could observe the structural transition for our peptide of interest. Since glycopeptide is hard-to-ionized and often has low charge state, CIU-ECD is vital for the analysis of low charge density glycopeptides to provide the highest amount of structural information needed for site-specific annotation.

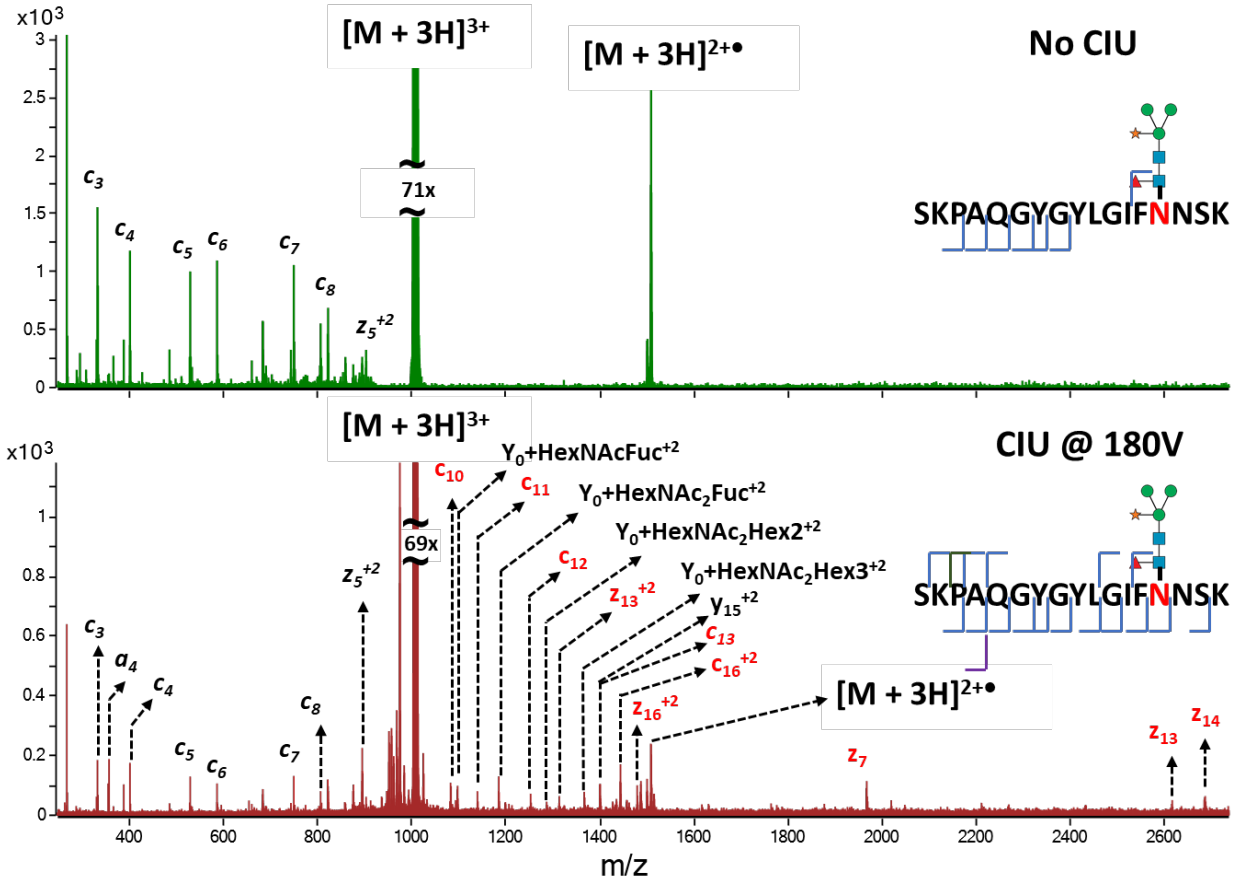

Figure 4.5. ECD of glycosylated peptide, SKPAQGYGYGLGIFN$_{Hex3HexNac2dHexPent}$NSK, with (top) no CIU and (bottom) 180V CIU.

The doubly protonated β-casein phosphopeptide, FQsEEQQQTEDELQDK, which we previously found to undergo minimum fragmentation under FT-ICR ECD conditions, undergoes a ~29% increase in collision cross-section upon CIU (*Fig. 4.4b*). For the resulting elongated peptide form, having a CIU50 of 103.5 V, ECD sequence coverage was greatly enhanced (~82%), including a variety of c and z-type ions across the entire phosphopeptide as compared with ECD of the pre-activated conformer that only yielded fragmentation close to the peptide termini (~20%), similar to FT-ICR ECD (*Fig. 4.6, top*). As evidence in previous studies with ECD/ETD, noncovalent interactions between the basic side chains and phosphoserine were impeding the separation of

any ECD/ETD fragments that had just formed[31,44]. By unfolding the phosphopeptide, electrons have more access to the entire peptide backbone for fragmentation without the effect of ECnoD or ETnoD. One interesting observation for CIU-ECD of phosphorylated peptides is that the drift time distribution at lower drift time (i.e. lower CCS measurement) tends to span across numerous drift times representing the structural diversity of compact state. This structural heterogeneity could possibly be stemmed from salt-bridges and hydrogen bonds. Further investigation to understand this effect could be done with molecular dynamics simulation.

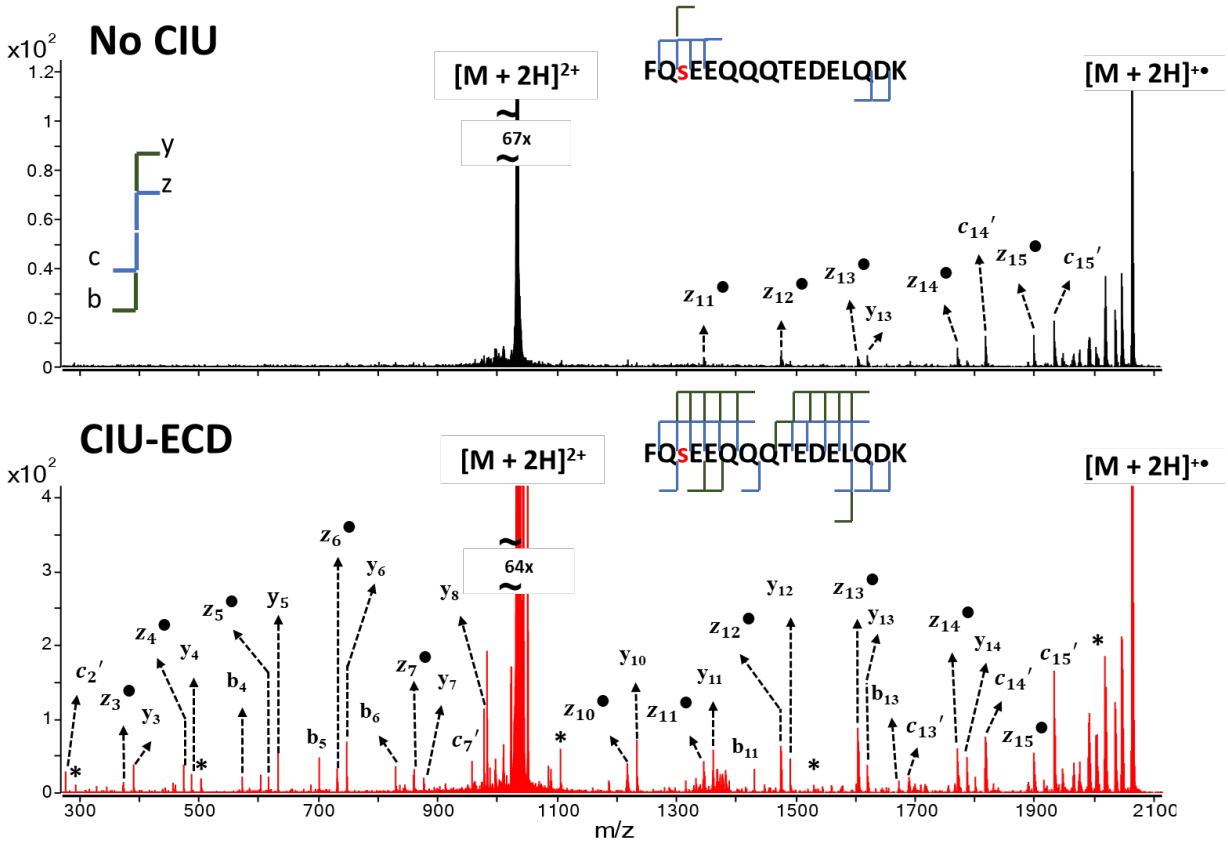

Figure 4.6 ECD of Phosphorylated peptide ,FQsEEQQQTEDELQDK, with (top) no CIU and (bottom) 125V with CIU.

4.3.3. CIU-ECD of an unmodified polypeptide:

To further evaluate the applicability of this method for non-modified peptide, a large antimicrobial peptide around 2.8 kDa "melittin" was used. We found that CIU of triply protonated ions yielded two new conformations (one started at 100V and another one started at around 250V) with larger cross sections than prior to CIU (*Fig. 4.7, left*). For the conformation at higher drift time, more structural diversity could be observed. For the largest CCS, having a CIU50 of 250 V, ECD fragmentation efficiency was greatly enhanced, yielding a variety of c-, z-, a-, b-, y-, and w-type ions (*Fig. 4.8, top*). Overall, the combination of CIU and ECD allows improved ECD fragment ion generation for larger, lower charge state precursor ions.

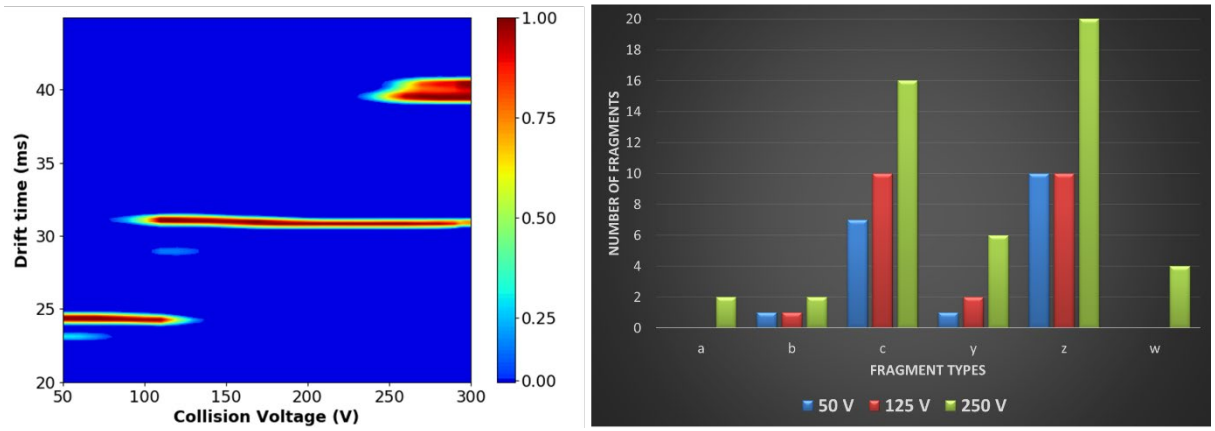

Figure 4.7. CIU of triply protonated melittin (left) and the effects of peptide unfolding on ECD fragmentation (right).

As the collisional voltage increase, CIU-ECD of melittin peptide shows an increase in CID like fragment (i.e., b/y fragment ions) as well as side chain losses like w-type ions (*Fig. 4.7, right*). Melittin from honeybee venom was chosen as a model system for CIU-ECD for its well-known helical secondary structure[45,46]. It has been shown that ECD would provide periodic sequence distribution of product ion abundances with ECD for alpha helical structure of melittin[47]. In our case, there was no observation of periodic distribution of ECD fragments (*Fig. 4.8*). The explanation for such observation could be the denaturation of secondary structure with spraying solution. To better evaluate the effect of structural changes, melittin should be sprayed in an appropriate solvent to obtain its native secondary structure. Overall, the combination of CIU and ECD lends insights into the relationship between ECD performance

and peptide structure, and allows improved ECD fragment ion production for larger, lower charge state precursor ions, especially for PTM-carrying peptides.

4.3.4. Molecular dynamics simulation of a phosphorylated peptide:

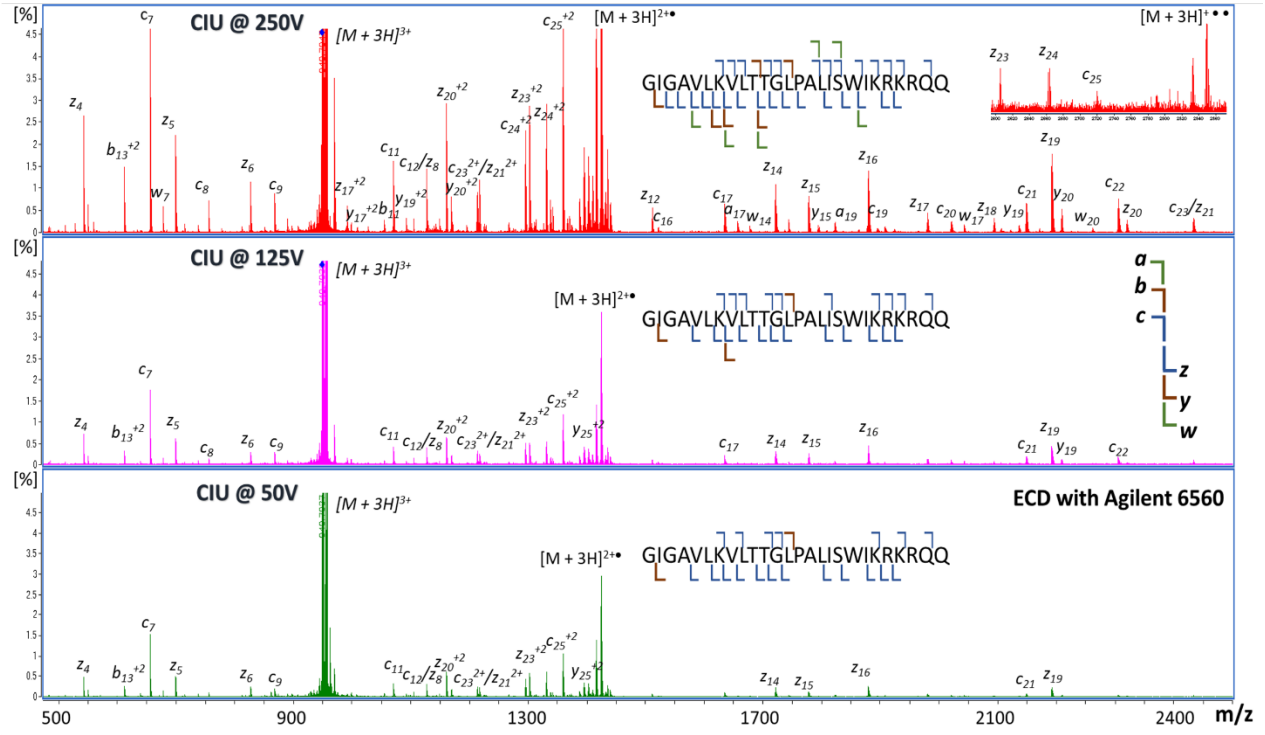

Figure 4.8. ECD of triply protonated melittin ions in a folded state at a CIU voltage of 50 V (bottom), partially unfolded state at a CIU voltage of 125 V (middle), and an unfolded state at a CIU voltage of 250 V (top).

After REMD simulation of phosphorylated of β-casein peptide, there were a total 100,000 of theoretical structure generated. Theoretical CCS measurements were obtained with the help of IMPACT software package. Experimental CCS of compact and unfolded states were utilized to filter theoretical CCSs. After filtering, there were approximately 500 structures for the compact states and 50 structures for elongated states. Clustering analysis was done for the compact structures to generate unique clusters for each compact states. There were 8 total clustering groups obtained after clustering analysis for the compact state corresponding to the lower drift time feature (*Fig. 4.9*).

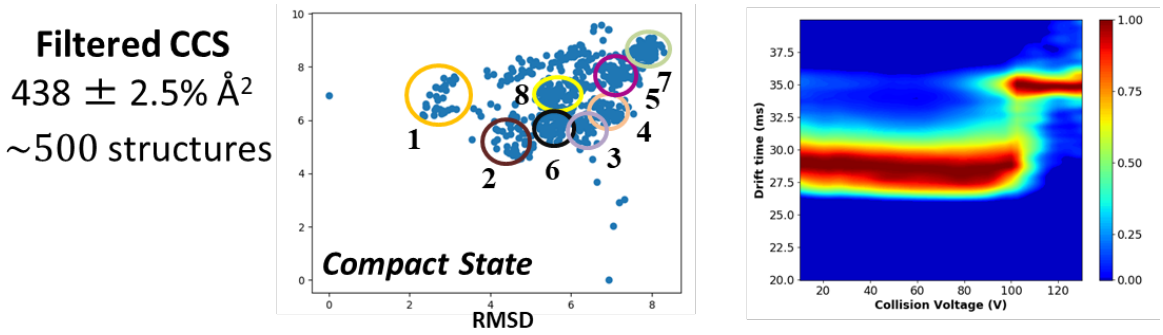

Figure 4.9 Clustering analysis for compact states.

Below are the representative structures for each cluster (*Fig. 4.10*). Overall, for these clusters, the general theme has the folded structure forming from the interaction between the protonated residues with negatively charge phosphate group. The highly expanded feature from CIU fingerprint for the compact states is represented with 8 different clusters from REMD. The folded structure explains the reason for inefficient ECD in interior of the peptide yet efficient for the external peptide termini. After undergoing clustering analysis, only one meaningful cluster was generated with the filtering of 2.5% standard deviation (*Fig. 4.11a*). The representative structures of unfolded state generated from clustering analysis are shown (*Fig. 4.11b*). Even though the

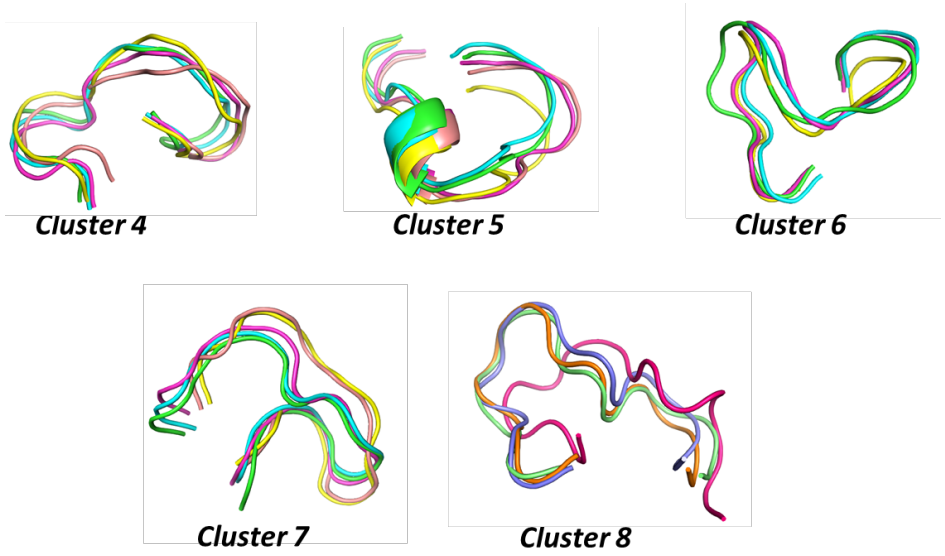

Figure 4.10 Representative structures from compact states with REMD.

peptide was unfolded, only one terminal end was fully unfolded, and the other terminal end was still compact due to the salt bridge formation between the protonated residue and phosphor-group (*Fig. 4.11c*). The unfolded structure did not fully explain the extensive backbone fragmentation of the phosphopeptide. From this structure, ECD should only for half of the peptide backbone and should not work on the other half.

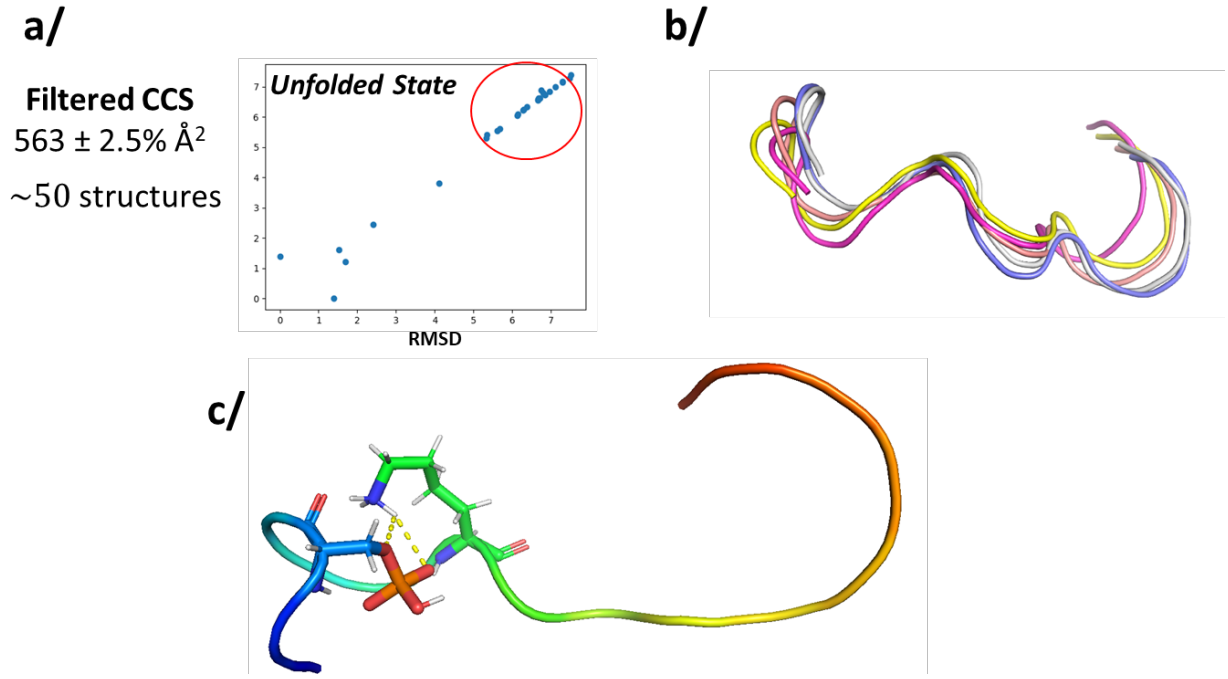

Figure 4.11. Clustering analysis for unfolded state. (a) CCS filtering (b) Representative structure of unfolded states (c) Zoom-In view of the salt bridge formation on the phosphopeptide.

4.4. Conclusion

A doubly protonated, S-palmitoylated peptide was effectively unfolded at a CIU voltage around 125 V without significant collision-based fragmentation. ECD of this unfolded, doubly protonated peptide yields high quality data with extensive backbone fragmentation and no significant palmitate loss. By contrast, ECD of the triply protonated peptide does result in PTM loss. CIU-ECD of glycosylated and phosphorylated shows significant improvement on ECD efficiency as well as provides direct measurement of transitional changes of folded to unfolded

states. The direct measurements enabled us to perform more detailed analysis with REMD. From REMD of phosphorylated peptides, theoretical structures for folded peptides were obtained for folded states showing the structural diversity forming with salt-bridges. For the unfolded states, theoretical structure did not efficiently explain the extensive peptide backbone fragmentation. This may be the result of having the additional positive charge placement on the interior of the peptide and the singly deprotonated phosphate group interaction. A new force field with neutral phosphate group should be used to properly explain the unfolding phenomena. A larger unmodified peptide was effectively unfolded at higher CIU voltage (i.e., 250 V) with no collision-based fragmentation. Upon ECD, unfolded melittin shows extensive backbone fragmentation, including a variety of c-, z-, a-, b-, and w- type ions.

4.5. References

(1) Walsh, Christopher. Posttranslational Modification of Proteins : Expanding Nature's Inventory. **2006**, 490.

(2) Cohen, P. The Origins of Protein Phosphorylation. *Nature Cell Biology 2002 4:5* **2002**, *4* (5), E127–E130. https://doi.org/10.1038/ncb0502-e127.

(3) Rubin, C. S.; Rosen, O. M. PROTEIN PHOSPHORYLATION. **1975**.

(4) Marth, J. D.; Grewal, P. K. Mammalian Glycosylation in Immunity. *Nature Reviews Immunology 2008 8:11* **2008**, *8* (11), 874–887. https://doi.org/10.1038/nri2417.

(5) LIS, H.; SHARON, N. Protein Glycosylation. *European Journal of Biochemistry* **1993**, *218* (1), 1–27. https://doi.org/10.1111/J.1432-1033.1993.TB18347.X.

(6) Hart, G. W. Glycosylation. *Current Opinion in Cell Biology* **1992**, *4* (6), 1017–1023. https://doi.org/10.1016/0955-0674(92)90134-X.

(7) Peng, T.; Thinon, E.; Hang, H. C. Proteomic Analysis of Fatty-Acylated Proteins. *Current Opinion in Chemical Biology* **2016**, *30*, 77–86. https://doi.org/10.1016/J.CBPA.2015.11.008.

(8) Zhou, B.; An, M.; Freeman, M. R.; Yang, W. Technologies and Challenges in Proteomic Analysis of Protein S-Acylation. *Journal of proteomics & bioinformatics* **2014**, *7* (9), 256. https://doi.org/10.4172/JPB.1000327.

(9) Guan, X.; Fierke, C. A. Understanding Protein Palmitoylation: Biological Significance and Enzymology. *Science China. Chemistry* **2011**, *54* (12), 1888. https://doi.org/10.1007/S11426-011-4428-2.

(10) Schmidt, M. F.; Bracha, M.; Schlesinger, M. J. Evidence for Covalent Attachment of Fatty Acids to Sindbis Virus Glycoproteins. *Proceedings of the National Academy of Sciences* **1979**, *76* (4), 1687–1691. https://doi.org/10.1073/PNAS.76.4.1687.

(11) Ji, Y.; Leymarie, N.; Haeussler, D. J.; Bachschmid, M. M.; Costello, C. E.; Lin, C. Direct Detection of S-Palmitoylation by Mass Spectrometry. *Analytical Chemistry* **2013**, *85* (24), 11952–11959. https://doi.org/10.1021/AC402850S/SUPPL_FILE/AC402850S_SI_001.PDF.

(12) Boersema, P. J.; Mohammed, S.; Heck, A. J. R. Phosphopeptide Fragmentation and Analysis by Mass Spectrometry. *Journal of Mass Spectrometry* **2009**, *44* (6), 861–878. https://doi.org/10.1002/JMS.1599.

(13) Boersema, P. J.; Mohammed, S.; Heck, A. J. R. Phosphopeptide Fragmentation and Analysis by Mass Spectrometry. *Journal of Mass Spectrometry* **2009**, *44* (6), 861–878. https://doi.org/10.1002/JMS.1599.

(14) An, H. J.; Froehlich, J. W.; Lebrilla, C. B. Determination of Glycosylation Sites and Site-Specific Heterogeneity in Glycoproteins. *Current Opinion in Chemical Biology* **2009**, *13* (4), 421–426. https://doi.org/10.1016/J.CBPA.2009.07.022.

(15) Dalpathado, D. S.; Desaire, H. Glycopeptide Analysis by Mass Spectrometry. *Analyst* **2008**, *133* (6), 731–738. https://doi.org/10.1039/B713816D.

(16) Ko, B. J.; Brodbelt, J. S. Comparison of Glycopeptide Fragmentation by Collision Induced Dissociation and Ultraviolet Photodissociation. *International Journal of Mass Spectrometry* **2015**, *377* (1), 385–392. https://doi.org/10.1016/J.IJMS.2014.07.032.

(17) Riley, N. M.; Hebert, A. S.; Westphall, M. S.; Coon, J. J. Capturing Site-Specific Heterogeneity with Large-Scale N-Glycoproteome Analysis. *Nature Communications 2019 10:1* **2019**, *10* (1), 1–13. https://doi.org/10.1038/s41467-019-09222-w.

(18) Perdivara, I.; Petrovich, R.; Alliquant, B.; Deterding, L. J.; Tomer, K. B.; Przybylski, M. Elucidation of O-Glycosylation Structures of the β-Amyloid Precursor Protein by Liquid Chromatography-Mass Spectrometry Using Electron Transfer Dissociation and Collision Induced Dissociation. *Journal of Proteome Research* **2009**, *8* (2), 631–642. https://doi.org/10.1021/PR800758G/SUPPL_FILE/PR800758G_SI_001.PDF.

(19) Håkansson, K.; Cooper, H. J.; Emmett, M. R.; Costello, C. E.; Marshall, A. G.; Nilsson, C. L. Electron Capture Dissociation and Infrared Multiphoton Dissociation MS/MS of an N-Glycosylated Tryptic Peptide To Yield Complementary Sequence Information. *Analytical Chemistry* **2001**, *73* (18), 4530–4536. https://doi.org/10.1021/AC0103470.

(20) Sweet, S. M. M.; Cooper, H. J. Electron Capture Dissociation in the Analysis of Protein Phosphorylation. *https://doi.org/10.1586/14789450.4.2.149* **2014**, *4* (2), 149–159. https://doi.org/10.1586/14789450.4.2.149.

(21) Molina, H.; Horn, D. M.; Tang, N.; Mathivanan, S.; Pandey, A. Global Proteomic Profiling of Phosphopeptides Using Electron Transfer Dissociation Tandem Mass Spectrometry. *Proceedings of the National Academy of Sciences* **2007**, *104* (7), 2199–2204. https://doi.org/10.1073/PNAS.0611217104.

(22) Shi, S. D. H.; Hemling, M. E.; Carr, S. A.; Horn, D. M.; Lindh, I.; McLafferty, F. W. Phosphopeptide/Phosphoprotein Mapping by Electron Capture Dissociation Mass Spectrometry. *Analytical Chemistry* **2000**, *73* (1), 19–22. https://doi.org/10.1021/AC000703Z.

(23) Sweet, S. M. M.; Bailey, C. M.; Cunningham, D. L.; Heath, J. K.; Cooper, H. J. Large Scale Localization of Protein Phosphorylation by Use of Electron Capture Dissociation Mass Spectrometry. *Molecular and Cellular Proteomics* **2009**, *8* (5), 904–912. https://doi.org/10.1074/MCP.M800451-MCP200/ATTACHMENT/B499D0AF-F82C-4023-A0E2-A14C98DDECF3/MMC1.ZIP.

(24) Håkansson, K.; Chalmers, M. J.; Quinn, J. P.; McFarland, M. A.; Hendrickson, C. L.; Marshall, A. G. Combined Electron Capture and Infrared Multiphoton Dissociation for Multistage MS/MS in a Fourier Transform Ion Cyclotron Resonance Mass Spectrometer. *Analytical Chemistry* **2003**, *75* (13), 3256–3262. https://doi.org/10.1021/AC030015Q.

(25) Mechref, Y. Use of CID/ETD Mass Spectrometry to Analyze Glycopeptides. *Current Protocols in Protein Science* **2012**, *1* (SUPPL.68), 1–11. https://doi.org/10.1002/0471140864.ps1211s68.

(26) Alley, W. R.; Mechref, Y.; Novotny, M. v. Characterization of Glycopeptides by Combining Collision-Induced Dissociation and Electron-Transfer Dissociation Mass Spectrometry Data. *Rapid Communications in Mass Spectrometry* **2009**, *23* (1), 161–170. https://doi.org/10.1002/RCM.3850.

(27) Hogan, J. M.; Pitteri, S. J.; Chrisman, P. A.; McLuckey, S. A. Complementary Structural Information from a Tryptic N-Linked Glycopeptide via Electron Transfer Ion/Ion Reactions and Collision-Induced Dissociation. *Journal of Proteome Research* **2005**, *4* (2), 628–632. https://doi.org/10.1021/pr049770q.

(28) Good, D. M.; Wirtala, M.; McAlister, G. C.; Coon, J. J. Performance Characteristics of Electron Transfer Dissociation Mass Spectrometry. *Molecular & cellular proteomics : MCP* **2007**, *6* (11), 1942–1951. https://doi.org/10.1074/MCP.M700073-MCP200.

(29) Kalli, A.; Håkansson, K. Comparison of the Electron Capture Dissociation Fragmentation Behavior of Doubly and Triply Protonated Peptides from Trypsin, Glu-C, and Chymotrypsin Digestion. *Journal of Proteome Research* **2008**, *7* (7), 2834–2844. https://doi.org/10.1021/PR800038Y/SUPPL_FILE/PR800038Y-FILE001.PDF.

(30) Kim, D.; Pai, P.-J.; Creese, A. J.; Jones, A. W.; Russell, D. H.; Cooper, H. J. Probing the Electron Capture Dissociation Mass Spectrometry of Phosphopeptides with Traveling Wave Ion Mobility Spectrometry and Molecular Dynamics Simulations. *Journal of The American Society for Mass Spectrometry 2015 26:6* **2015**, *26* (6), 1004–1013. https://doi.org/10.1007/S13361-015-1094-1.

(31) Creese, A. J.; Cooper, H. J. The Effect of Phosphorylation on the Electron Capture Dissociation of Peptide Ions. *Journal of the American Society for Mass Spectrometry* **2008**, *19* (9), 1263–1274. https://doi.org/10.1016/J.JASMS.2008.05.015.

(32) Biemann, K.; Martin, S. A.; Aebersold, R.; Mann, M.; Hunt, D. F.; Yates, J. R.; Shabanowitz, J.; Winston, S.; Hauer, C. R.; Fenn, J. B.; Meng, C. K.; Wong, S. F.; Whitehouse, C. M.; Olsen, J. v; Ong, S. E. Peptide Sequencing and Characterization of Post-Translational Modifications by Enhanced Ion-Charging and Liquid Chromatography Electron-Transfer Dissociation Tandem Mass Spectrometry. *Analytical Chemistry* **2007**, *79* (24), 9243–9252. https://doi.org/10.1021/AC701700G.

(33) Haler, J. R. N.; Massonnet, P.; Far, J.; de la Rosa, V. R.; Lecomte, P.; Hoogenboom, R.; Jérôme, C.; de Pauw, E. Gas-Phase Dynamics of Collision Induced Unfolding, Collision Induced Dissociation, and Electron Transfer Dissociation-Activated Polymer Ions. *Journal of the American Society for Mass Spectrometry* **2019**, *30* (4), 563–572. https://doi.org/10.1007/s13361-018-2115-7.

(34) Tian, Y.; Ruotolo, B. T. Collision Induced Unfolding Detects Subtle Differences in Intact Antibody Glycoforms and Associated Fragments. *International Journal of Mass Spectrometry* **2018**, *425*, 1–9.

(35) Tian, Y.; Ruotolo, B. T. Collision Induced Unfolding Detects Subtle Differences in Intact Antibody Glycoforms and Associated Fragments. *International Journal of Mass Spectrometry* **2018**, *425*, 1–9. https://doi.org/10.1016/j.ijms.2017.12.005.

(36) Dixit, S. M.; Polasky, D. A.; Ruotolo, B. T. Collision Induced Unfolding of Isolated Proteins in the Gas Phase: Past, Present, and Future. *Current Opinion in Chemical Biology* **2018**, *42*, 93–100. https://doi.org/10.1016/J.CBPA.2017.11.010.

(37) Dixit, S. M.; Polasky, D. A.; Ruotolo, B. T. Collision Induced Unfolding of Isolated Proteins in the Gas Phase: Past, Present, and Future. *Current Opinion in Chemical Biology*. Elsevier Ltd February 1, 2018, pp 93–100. https://doi.org/10.1016/j.cbpa.2017.11.010.

(38) Gadkari, V. v.; Ramírez, C. R.; Vallejo, D. D.; Kurulugama, R. T.; Fjeldsted, J. C.; Ruotolo, B. T. Enhanced Collision Induced Unfolding and Electron Capture Dissociation of Native-like Protein Ions. *Analytical Chemistry* **2020**, *92* (23), 15489–15496. https://doi.org/10.1021/ACS.ANALCHEM.0C03372.

(39) Eschweiler, J. D.; Rabuck-Gibbons, J. N.; Tian, Y.; Ruotolo, B. T. CIUSuite: A Quantitative Analysis Package for Collision Induced Unfolding Measurements of Gas-Phase Protein Ions. *Anal. Chem* **2015**, *87*, 57. https://doi.org/10.1021/acs.analchem.5b03292.

(40) Polasky, D. A.; Dixit, S. M.; Fantin, S. M.; Ruotolo, B. T. CIUSuite 2: Next-Generation Software for the Analysis of Gas-Phase Protein Unfolding Data. *Analytical Chemistry* **2019**, *91* (4), 3147–3155. https://doi.org/10.1021/ACS.ANALCHEM.8B05762/SUPPL_FILE/AC8B05762_SI_001.PDF.

(41) YOUSEFI-SALAKDEH, E.; JOHANSSON, J.; STRÖMBERG, R. A Method for S- and O-Palmitoylation of Peptides: Synthesis of Pulmonary Surfactant Protein-C Models. *Biochemical Journal* **1999**, *343* (3), 557–562. https://doi.org/10.1042/BJ3430557.

(42) Marklund, E. G.; Degiacomi, M. T.; Robinson, C. v.; Baldwin, A. J.; Benesch, J. L. P. Collision Cross Sections for Structural Proteomics. *Structure* **2015**, *23* (4), 791–799. https://doi.org/10.1016/J.STR.2015.02.010.

(43) Yu, Q.; Wang, B.; Chen, Z.; Urabe, G.; Glover, M. S.; Shi, X.; Guo, L. W.; Kent, K. C.; Li, L. Electron-Transfer/Higher-Energy Collision Dissociation (EThcD)-Enabled Intact Glycopeptide/Glycoproteome Characterization. *Journal of the American Society for Mass Spectrometry* **2017**, *28* (9), 1751. https://doi.org/10.1007/S13361-017-1701-4.

(44) Riley, N. M.; Hebert, A. S.; Dürnberger, G.; Stanek, F.; Mechtler, K.; Westphall, M. S.; Coon, J. J. Phosphoproteomics with Activated Ion Electron Transfer Dissociation. *Analytical Chemistry*

2017, *89* (12), 6367–6376. https://doi.org/10.1021/ACS.ANALCHEM.7B00212/SUPPL_FILE/AC7B00212_SI_001.PDF.

(45) Straus, R. N.; Jockusch, R. A. Hydrogen-Deuterium Exchange and Electron Capture Dissociation to Interrogate the Conformation of Gaseous Melittin Ions. *Journal of the American Society for Mass Spectrometry* **2019**, *30* (5), 864–875. https://doi.org/10.1007/S13361-019-02150-5.

(46) Yu, S.; Jang, H. Y.; Oh, H. bin. Electron Capture Dissociation Mass Spectrometry for Gaseous Protonated Melittin Ions and Its Single Amino Acid Substituted Variants. *Mass Spectrometry Letters* **2019**, *10* (4), 117–122. https://doi.org/10.5478/MSL.2019.10.4.117.

(47) Hamidane, H.; He, H.; Tsybin, O. Y.; Emmett, M. R.; Hendrickson, C. L.; Marshall, A. G.; Tsybin, Y. O. Periodic Sequence Distribution of Product Ion Abundances in Electron Capture Dissociation of Amphipathic Peptides and Proteins. *Journal of the American Society for Mass Spectrometry* **2009**, *20* (6), 1182–1192. https://doi.org/10.1016/J.JASMS.2009.02.015/SUPPL_FILE/JS8B03496_SI_001.DOC.

Chapter 5. Collision Induced Unfolding-Electron Capture Dissociation (CIU-ECD) for Improved Middle-Down Analysis of Monoclonal Antibodies

5.1. Introduction

mAbs have become increasingly popular as a biotherapeutic treatment. However, there are no standard and reliable workflows for mAbs to achieve an automated, high throughput, fast, and information-rich analytical method. In this chapter, we utilized CIU-ECD to observed structural transition upon unfolding and its effects on ECD patterns. CIU-ECD has demonstrated to significantly increase the sequence coverage of mAb glycosylated Fc domain fragment. We further developed an automated system for online digestion of mAb and ultimately couple CIU-ECD to such system.

In recent years, monoclonal antibodies (mAbs) derived from the immunoglobulin G (IgG) have been demonstrated as an effective clinical choice for the treatment of human diseases, including cancer and COVID-19[1–4]. There are currently over 40 mAbs and their derivatives authorized for clinical treatments. With an ever-increasing number of new mAb-based therapeutic pipelines and eminent endings of many current approved mAb-based patents, biosimilars have become an increasingly attractive alternative[5–9]. mAbs are multichain glycoproteins with a total molecular weight of ~150 kDa, including two light chains (Lc) of ~25 kDa and 2 heavy chains (Hc) of ~50 kDa—all linked together by 16 disulfide bonds. Therapeutic mAbs are heavily modified with

glycosylation, sulfation, Met oxidation, pyroGlu, Lys clipping, and deamidation[10–12]. Post-translational modifications (PTMs) significantly contribute to antibody biological functions, including antigen binding, half-life[13], and effector functions[14]. PTMs are an essential component in the development of therapeutic mAbs[15] and perhaps making of better diagnostic tools[16,17]. For instance, due to glycan profiling, we have discovered that influenza vaccination stimulates changes in glycosylation pattern of IgG1 Fc sub-domain[17], and COVID-19 infection may alter levels of IgG1 fucosylation[16]. As the levels of complexity from mAb analysis expands, the analytical challenges have risen considerably and thus there is an urgent need for accurate and consistent analysis of mAbs.

Recent innovations in MS instrumentation, MS/MS methods, separation technologies, and data analysis software have allowed us to gain a great wealth of novel insights into antibody repertoires with much more detailed and accurate proteoform descriptions[18–23]. Even with such technological advancements, a lack of standard workflow and consistent benchmarking methods for antibody proteomics would limit our understanding for complete characterization of protein therapeutics in terms of composition (e.g., amino acid sequence, lysine clipping or truncation), glycosylation and disulfide bond patterns, higher order structures and their dynamics (just to name a few). This ultimately hinders the development of vaccines, therapeutic antibodies, and diagnostics. Thus, there is an urgent need for novel workflows and technologies to mitigate such setbacks. The traditional sequencing protocol, bottom-up proteomics, demands extensive sample preparation and may introduce artifacts during the process[24,25]. Top-down and middle-down proteomics have demonstrated a promising potential to significantly streamline therapeutic antibody discovery. ECD, ETD, UVPD, and HCD/CID have successfully been

implemented in both top-down and middle-down MS manners for the analysis of monoclonal antibodies[21,26–31]. However, top-down MS only provides up to 30% sequence coverage[32]. Activated methods (e.g., EThcD, AI-ETD or AI-ECD) can be used to increase the sequence coverage[33–36], yet the difficulty of the top-down spectra is exponentially increased with complex samples, including mAbs[21,26–28]. Middle-level MS (middle-up or middle-down) which sequences large protein subunit from restricted proteolysis of mAbs (i.e., this would reduce the complexity of the sample for a more specific analysis) represents a sensible compromise between bottom-up and top-down MS (*Fig. 5.1*)[28].

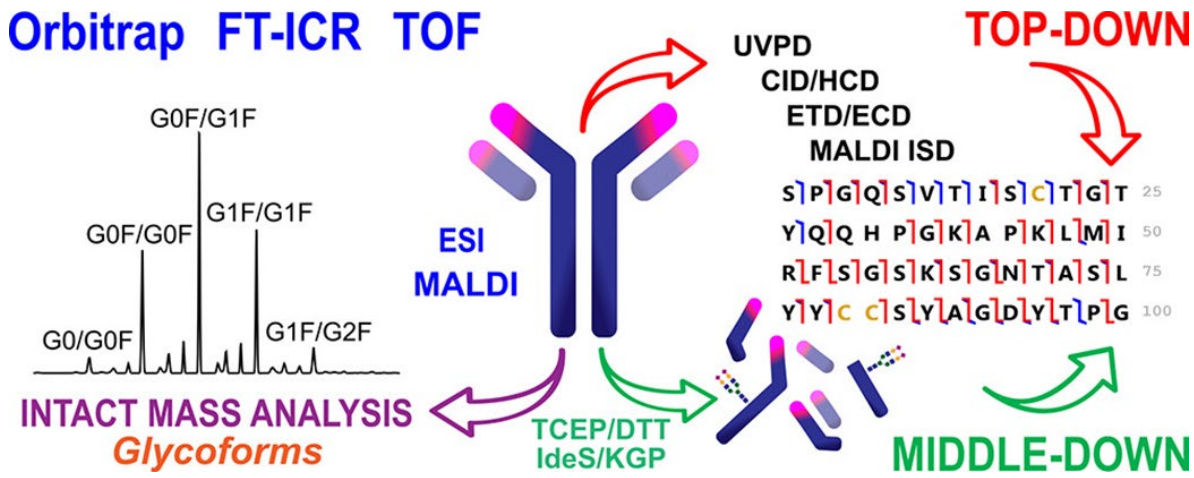

Figure 5.1. Modes of Analysis for Therapeutic mAbs (left panel) Intact mass analysis (right panel, top) top-down analysis (right panel, down) middle-down analysis.[28]

Fornelli et al. utilized ETD in middle-down fashion to examine therapeutic mAbs in denatured, including Adalimumab, Bevacizumab and Trastuzumab, with ≥50% sequence coverage[37]. Antibodies are digested at one specific site below the hinge region using the immunoglobulin G-degrading enzyme of Streptococcus pyogenes (IdeS or FabRICATOR) protease to yield Fc/2 and F(ab´)2 fragments[38]. This digestion is fast (~30 min) and complete (i.e., only one cleavage site and no mis-cleavage) with no optimization necessary[39,40]. With middle-down MS, they were able to

detect and localize oxidation sites on mAb fragments. In this work, they have demonstrated that middle-down method as a fast and reliable alternative with double the sequence coverage compared to the traditional top-down approach. Additionally, middle-down MS requires minimal sample preparation and, as a result, reduces the introduction of artifacts compared to bottom-up MS. To further increase the sequence coverage for middle-down analysis, Kelleher and coworkers have utilized EThcD to generate up to 70% of complete sequence information[21]. However, MS^2-derived information along often yields insufficient information for detailed structural analysis of complex biomolecules like mAbs.

Lately, ion mobility MS has been widely deployed for structural characterization of mAbs. The utility of IM-MS can add another dimension of measurements for both light and heavy antibody chains[41]. However, there is only limited information that one can obtain from IM-derived information. A tandem technique would be beneficial for a more complete information on the biomolecule of interest. CIU has extensively been used for biotherapeutics study to probe subtle differences in biomolecule structure, stability, and composition[42–44]. CIU in combination with ECD (CIU-ECD) would provide not only structural transition of the subdomain unfolding but also the specific unfolding region of subdomain. In chapter, we have shown that CIU-ECD can improve sequence coverage for S-Palmitoylated, N-glycosylated, and phosphorylated peptides. Here, we also extend this approach to glycosylated Fc subdomain of therapeutic mAbs in middle-down implementations.

To cope with popular demand for fast and high throughput analysis with minimal human errors from the biopharmaceutical industry, there is a pronounced requirement for fast method and automatic process for analysis of these biologics. In particular, middle-level analysis has

gained its popularity as an attractive choice for automated protocol recently and thus an automated middle-down workflow is highly desired. Papain[45–47], pepsin[48,49], and Lys-C[50] have been employed extensively in middle-down level analysis. However, there has not yet been reports for online digestion with such enzymes for automated middle-level 2D-LC-MS analysis of biologics and biologics-derived samples. In the second part of this work, we attempted to develop an automated online digestion/separation setup for the middle-level analysis of mAbs and simultaneously coupled CIU-ECD into such system.

5.2. Experimental

5.2.1. CIU-ECD of model glycoproteins:

Ribonuclease A and B were purchased from SigmaAlrich. For direct nESI experiment, these proteins were buffered exchanged three times with pure water. Then, samples were diluted into 50:50:0.1 methanol:water:formic acid, 50:50:0.1 acetonitrile:water:formic acid, and 100mM ammonium acetate. For supercharging experiments, 0.1% m-NBA was added to the spraying solution.

5.2.2. CIU-ECD of Fc fragments from Papain and IdeS Digest:

IgG1 mAbs were purchased from different vendors (Sigma, Waters, and NIST mAbs). Before digestion, sample was buffered-exchanged with 100 mM ammonium acetate at pH 7.5 to remove storage formulation chemicals. For optimal papain digestion, sample was prepared at ≥ 2 mg/mL. The immobilized papain beads were washed three time with 20mM cysteine-HCl and 10mM EDTA in 10 mM Tris-buffer to remove the storage solution. The beads were then equilibrated with 20mM cysteine-HCl and 10mM EDTA in 10 mM Tris-buffer. Mouse and human IgG1 were

incubated with immobilized papain (37^{o}C, 0.5-5 hr time points, 1:80 enzyme:protein ratio) to generate glycosylated Fc fragments. Fc fragments were purified by protein A spin columns (Thermo). For IdeS digestion, there was no optimization required. Fabricator was digest based on the public Genovis protocol. Briefly, mAbs was buffered exchanged with 150mM ammonium acetate. Then, clean sample incubated enzyme in ratio 1:40 at 37oC. The pH was kept at 7.5 for the entire digestion of 30 minutes.

Samples were diluted into methanol:water:formic acid and 150mM ammonium acetate, 2-7 µM, and directly infused into an Agilent 6560 IM-Q-ToF, modified for high-energy CIU and equipped with an e-MSion ExD cell. CIU voltage was increased from 10 to 500 V in 5 V increments in ultrapure grade SF_6 gas at 1.5 psi pressure. For optimization of papain digestion, nESI spraying was achieved on a Thermo Scientific Q Exactive UHMR Hybrid Quadrupole-Orbitrap mass spectrometer. Full scan data were acquired at resolving power 6250 at m/z 400 in the m/z range 400−20 000. Mass spectra presented are averaged ∼100-150 scans. The automatic gain control (AGC) mode was automatic. Ion transfer optics and voltage gradients throughout instrument were tuned specifically to prevent ion activation. Data were analyzed with Xcaliber software, Viewer software from e-MSion, and FreeStyle software.

5.2.3. Online-Digestion with Pepsin Immobilized Column:

The configuration of the LC-MS system is shown in Figure 3 and instrument parameters are shown in Tables 1. Waters Enzymate Protein Pepsin Column was coupled directly to the UV detector of the LC system and ran at a flow rate of 50 µl/min at 4^{o}C in 0.1% FA at pH 3. Following digestion, sample was then introduced into the SEC column for separation at flow rate of 200 µl/min at 30^{o}C via switching valve position.

LC Setup		MS Setup	
Pump	Agilent 1290 Infinity Series	**Instrument**	Agilent 6560C IM-QTOF
Columns	Waters Enzymate Protein Pepsin Column (300Å, 5 µm, 2.1 mm X 30 mm, 4°C) Agilent AdvanceBio SEC (4.6 × 50 mm, 1.9 µm, 200 Å)	**Mass range**	300-5000 m/z
Valve	Agilent 1200 Series 6-port valves	**ESI source voltage**	4 kV
Mobile phase	Digestion: 0.1% FA Separation: 150mM ammonium acetate	**Nebulizer gas pressure**	22 psi
Detector	Diode array detector	**Drying gas flow rate**	6 L/min
		Drying gas temperature	150^{o}C

Table 5.1 LC and MS Setups for Online Digestion

50 µg NIST mAb was injected into pepsin column for digestion and was then collected in 100µL loop in 5 minutes. After digestion, sample loop direction was changed to SEC column under isocratic condition (150 mM ammonium acetate at pH 7.5) for 20 minutes with UV absorptions at 235nm and 250 nm wavelengths. To avoid damaging the SEC column due to pressure differential, the flow rate was ramped at 0.1 mL/min (*Fig. 5.2*).

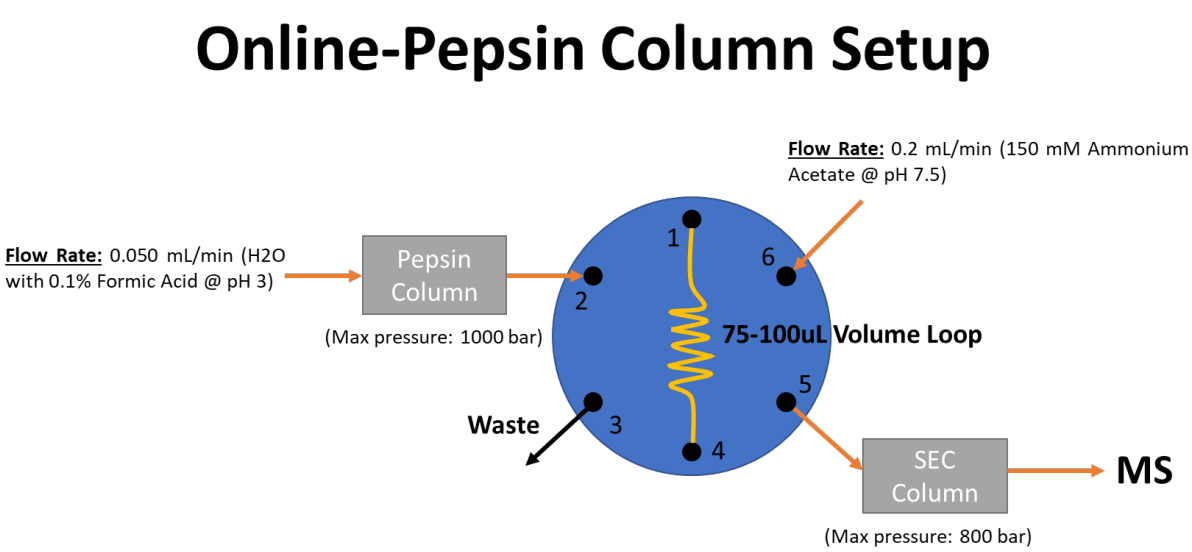

Figure 5.2. Valve Setup for Online Digestion of mAbs for Middle-Down Analysis

5.3. Results and Discussion

5.3.1. CIU-ECD for model proteins, Ribonuclease A and Ribonuclease B (glycoprotein):

Upon nESI, Ribonuclease A (RiboA) produced 3 different charge states. CIU was performed one two charge states, 8+ and 7+ (*Fig. 5.3*). As expected, CIU fingerprint of 7+ ions required higher unfolding transition at ~170V compared to 8+ ions with ~150V. Since 6+ did not have enough signal intensities for later experiment, CIU-ECD. We did not consider fingerprint for 6+ ions.

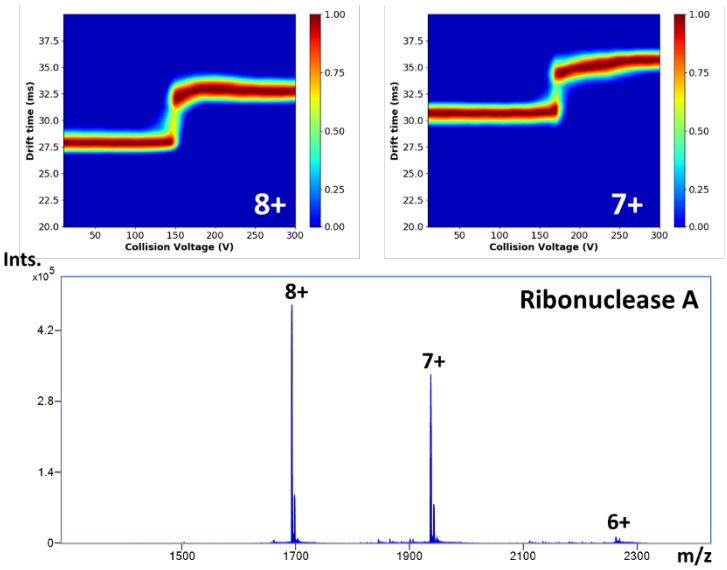

Figure 5.3. CIU of Ribonuclease A

With the addition of glycan portions on Ribonuclease B (RiboB), 8+ charge state was significantly reduced and there was more presence of 6+ ions. Overall, the 8+ of glycosylated RiboB had similar unfolding voltage at ~150V (*Fig. 5.4*). Surprisingly, 7+ charge state had lower CIU voltage at ~160V. That is somewhat contradictory to the traditional belief that glycosylation would increase the stability of the protein. For 6+ charge state, a third feature appeared between 160V to 190V CIU voltage. This can be explained that the increased stability of lower charge state ions to have more structural transition upon CIU.

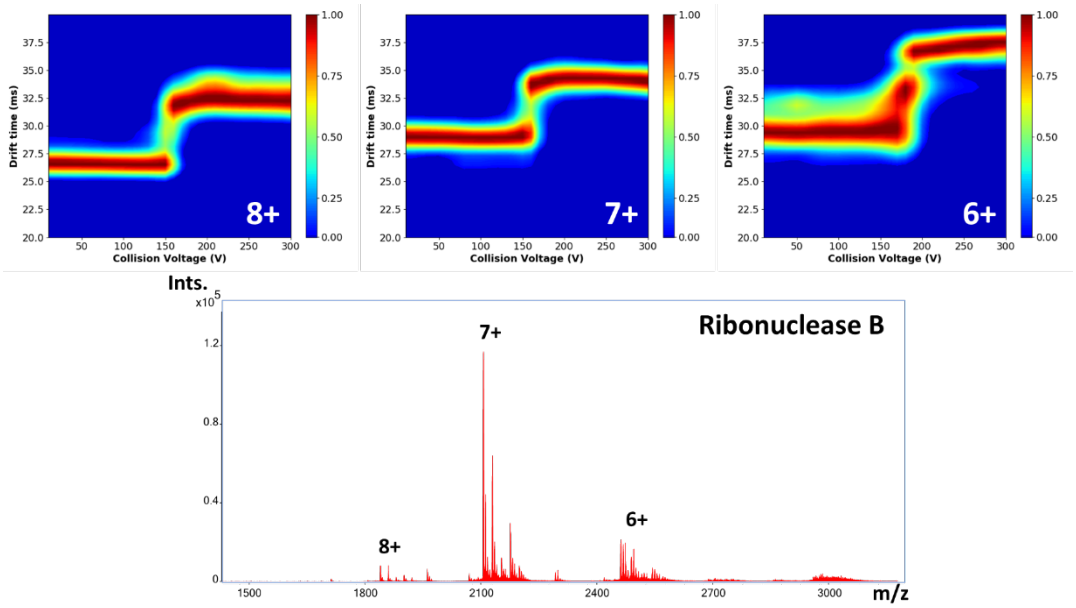

Figure 5.4. CIU of Ribonuclease B

ECD of RiboB for all charge states showed reduced performance without CIU yielding ~7% sequence coverage. Most fragments were resulted from cleavage from either terminus. This glycoprotein is heavily disulfide, so that would be one of the reasons for such low coverage, percentage number. When ECD was combined with CIU at 200V, the sequence coverage was significantly increased to ≥ 20% sequence coverage. Beside the fragments from both termini, we also observed fragments from interior part of the protein. Overall, we can see the utility of tandem approach CIU-ECD for improved sequence coverage and simultaneously structural information (*Fig. 5.5*).

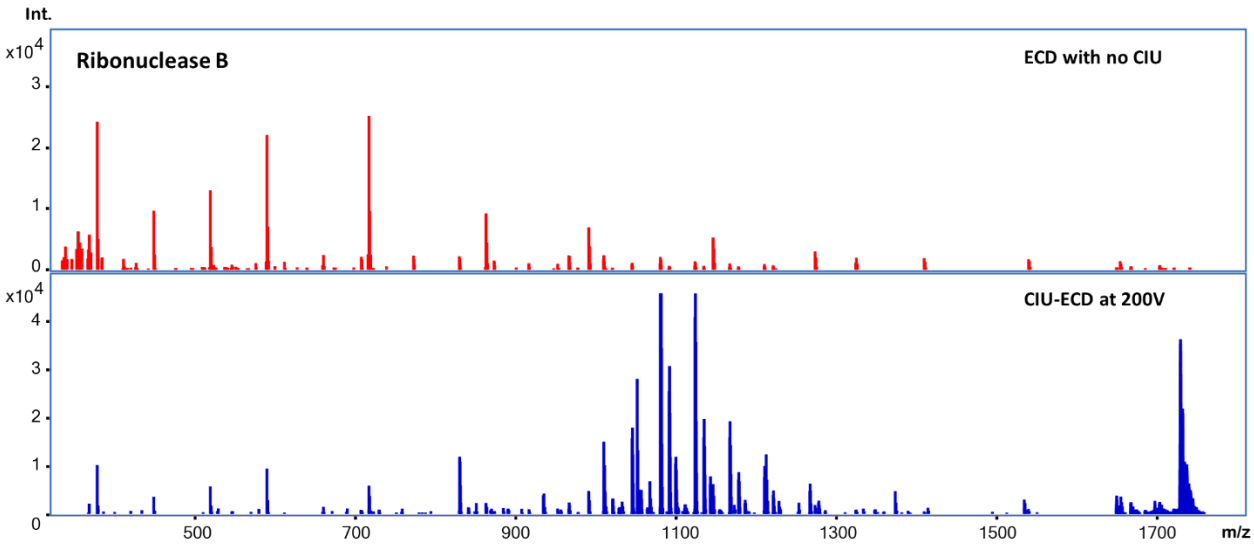

Figure 5.5. ECD of Ribonulcease B (top) without CIU (bottom) with CIU at 200V

5.3.2. Middle-Down Digestion Optimization with Papain and IdeS:

Middle-level digestion was performed with two enzymes in solution. The first enzyme papain that was used for this work would produce 2Fab and Fc fragments (*Fig. 5.6*). Initially, papain would produce heavily digest Fc fragment without extensive optimization. The expected Fc fragment should be around ~54 kDa without reduction.

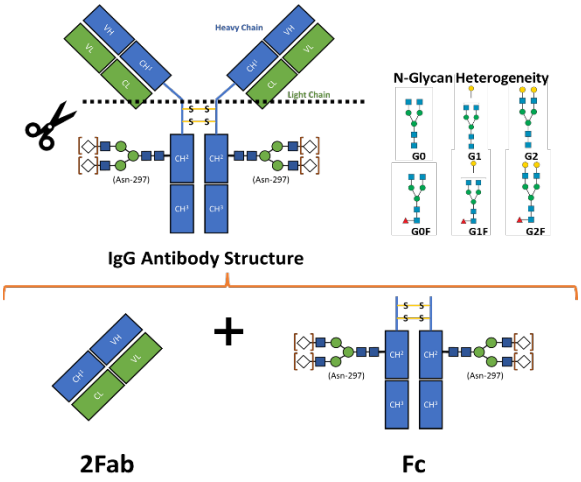

Figure 5.6. Antibody Digestion with Papain Enzyme

However, only partial Fc fragment (i.e., partial Fc/2 fragment) was generated with molecular weight around ~16 kDa. The possible explanations for such small fragment were the results of digestion in reducing conditions and the highly efficient papain enzyme. Further optimization was needed to produce the correct Fc fragment such as changing the pH, removing Cysteine-HCl after

enzyme activation, lower digestion temperature, reducing the digestion time, and increasing the enzyme to protein ratio for digestion.

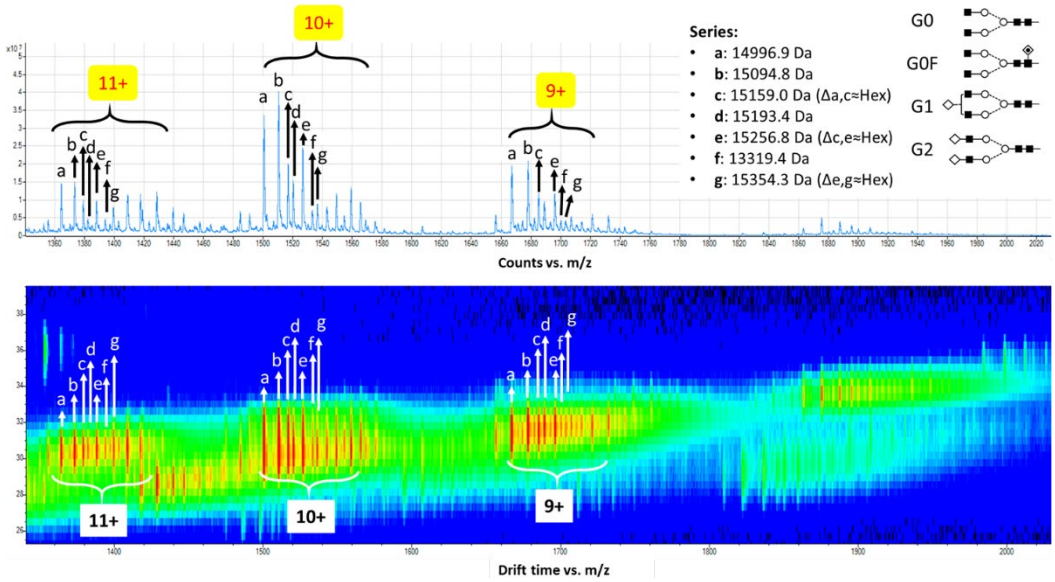

Figure 5.7. Initial results of papain digestion of mAb. (a) Mass spectrum of partial reduced Fc (b) IM-MS of Fc with different glycoforms.

IM-MS experiment shows different glycoforms for mouse Fc/2 fragment (~16k Da) including: G0, G0F, G1, and G2 (with G1 as the most dominant glycoform) (*Fig. 5.7*). Upon CIU of G1 glycoform of mouse Fc/2 between 300 and 400 V, glycosylated fragment produced two additional states. At 400 V, a significant increase in ECD fragment ions corresponding to peaks between 550-800 m/z and 1000-1300 m/z. However, annotation was challenging due to mouse IgG1's resistance to papain digestion.

To confirm of glycosylation sites on the partially digested Fc, deglycosylation procedure was performed to remove the glycoforms. With PNGaseF enzyme, partial Fc was deglycosylated (*Fig. 5.8*). As observed in the deglycosylated spectrum, there were no

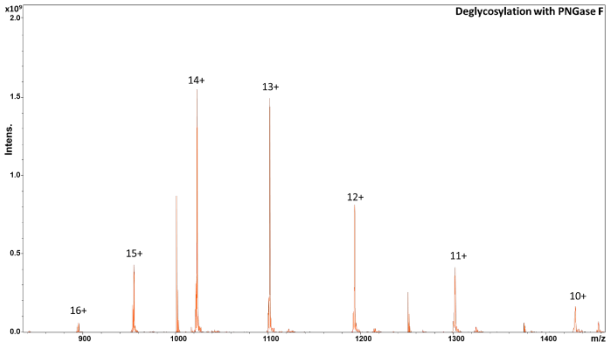

Figure 5.8. De-glycosylation of over-digested Fc fragment with PNGase F.

glycosylation patterns for partial Fc fragment. This confirmed our generated fragments as a partial portion of reduced Fc.

For papain optimization in *Fig. 5.9*, optimal enzyme ratio was first determined. With 1:20 ratio, most mAbs were extensively digested. Thus, only Fab was detected. For 1:40 ratio, dominantly Fab was detected. That might be due the over-digestion of Fc fragment leading low intensity for Fc. For 1:100 ratio, it was determined as the best ratio due the largest number of full Fc fragment generated. For 1:200 ratio, Fc abundance was reduced by ≥50%.

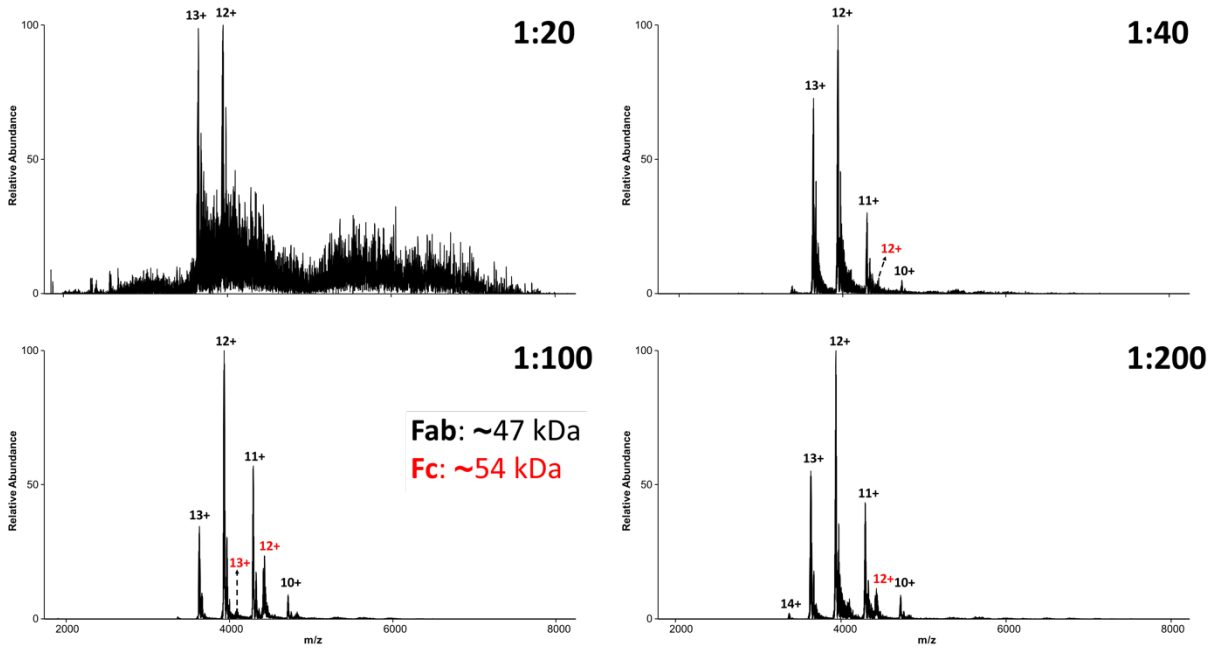

Figure 5.9. Enzyme to mAb Ratio Optimization for Sufficient Fc Generation.

Additionally, digestion buffer was varied between Tris-buffer and sodium phosphate buffer at pH 8.5 and 7.0 respectively. The optimal digestion time was determined with different time points (30 mins, 40 mins, 1 hour, and 4 hours). For sodium phosphate buffer, optimal digestion occurred before 1 hour. If being digested over 1 hour time point, Fc was over-digested leading lower Fc signal intensity. Digestion times needed to be controlled well to generate same Fc fragment, but the result was not reproducible. For Tris-buffer, digestion efficiency was greatly

reduced leading to a longer time for digestion. This is an ideal buffer because papain cleavage efficiency could be controlled this week. For this digestion, both Fab and Fc were observed (*Fig. 10, right panel*). However, Fc generation was much better controlled in Tris-buffer digestion than sodium phosphate buffer. At 4-hour time point, Fc intermediate with ~90 kDa molecular weight was produced considerably (*Fig. 5.10*). An interesting observation about using Tris-Buffers was that the appearance of Fc Intermediate. This was not observed with the digestion in sodium phosphate buffer. We believe that this intermediate was the result of well-controlled slower digestion process[51,52] in Tris-Buffer.

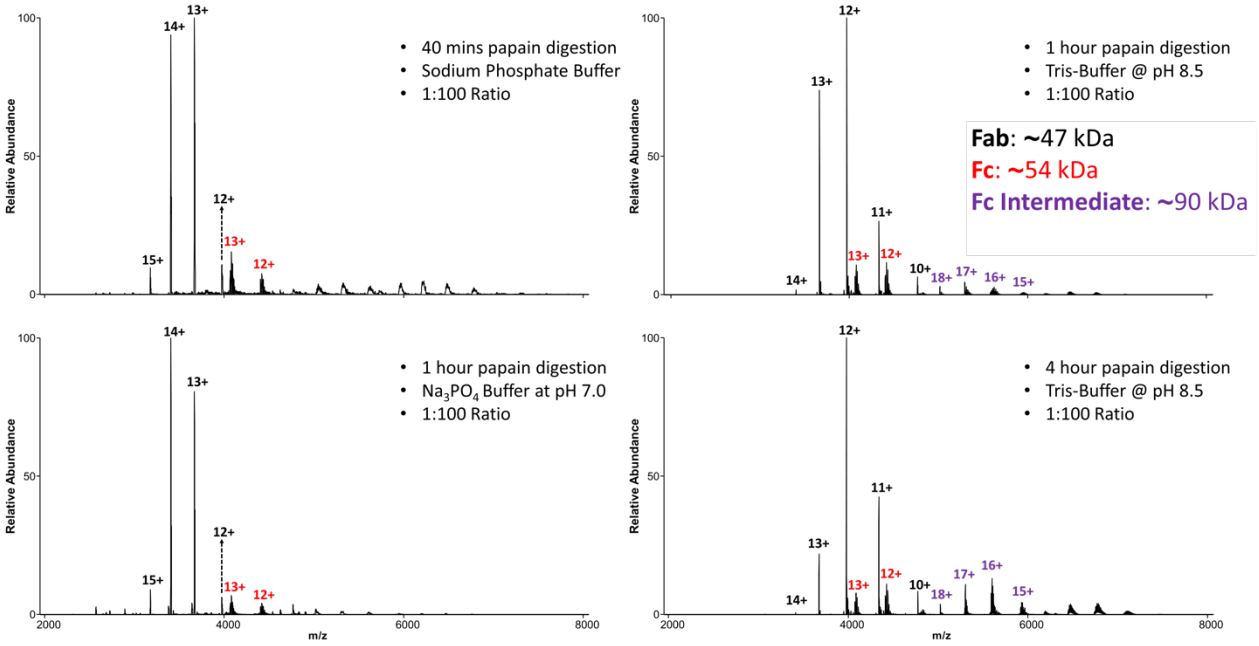

Figure 5.10. Buffer Optimization for Proper Fc Fragment Generation.

With the correct parameters determined, we were able to achieve the properly digested papain fragments. From the optimized pH, buffer, and enzyme ratio, we were able to obtain the full Fab and Fc domain fragments (*Fig. 5.10, right*). Tris-buffer was determined the optimal buffer

for papain digestion since Fc fragment generation from papain could be better controlled within this buffer at pH 8.5 in 10mM EDTA and 20mM Cysteine-HCl.

An alternative enzyme IdeS (or Fabricator) was chosen due to its ease of use and minimal optimization, human IgG1 from NIST mAbs was chosen for proteolytic digest to produce full Fc/2 fragments (~25k Da) and F(ab')2 (~97k Da) (*Fig. 5.11*). To better analyze the middle-level digestion in a systematic and high-accurate manner, Q-Exactive UHMR was used for its great sensitivity, resolution, and mass accuracy for larger protein complexes[53].

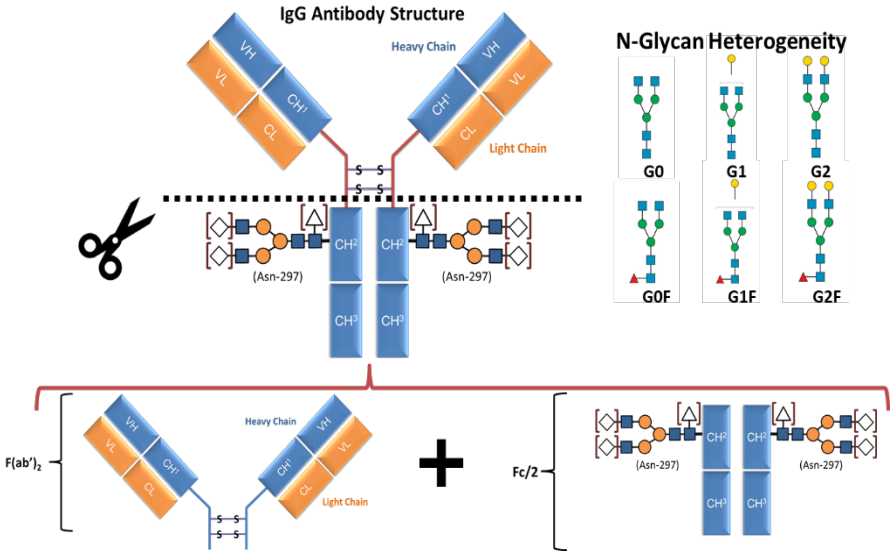

Figure 5.11. Antibody Digestion with IdeS Enzyme (Fabricator).

With the immunoglobulin G-degrading enzyme of Streptococcus pyogenes (IdeS), we were able to obtain the full F(ab')2 and Fc fragments in only 30 mins (*Fig. 12, top*). For the glycosylated portion, it was expected to contain only two of the Fc/2. However, Fc/2 dimer were not separated due to the weak intramolecular interactions. The presence of Fc/2 monomer fragment could only be obtained from 3-hour digestion (*Fig. 5.12, bottom*). This could be explained from the prolonged digestion led to degradation of weakly bound Fc/2 dimers. Unlike papain, there was no over-digestion problem with IdeS enzyme.

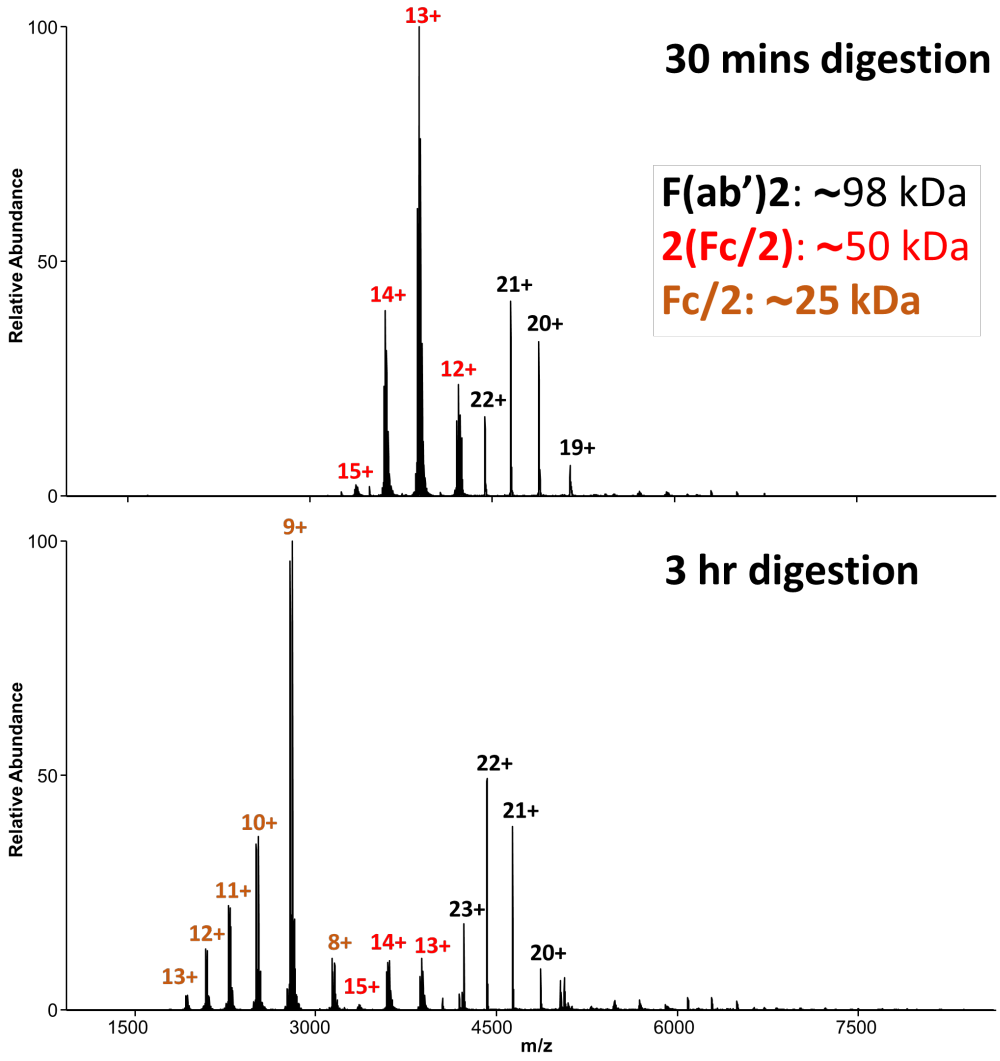

Figure 5.12. Digestion optimization of IdeS Digest with NIST mAbs

5.3.3. CIU-ECD for Fc fragment from therapeutic antibodies (NIST mAb)

For human IgG1 Fc fragment, CIU of the 14+ charge state produced four total features between 200 and 500 V. For the 15+ and 16+ charge states, the CIU fingerprints recorded showed a reduced number of features when compared with lower charge states (*Fig. 5.13, bottom panel*). Overall, human IgG1 Fc fragment unfolded at lower voltages with additional features compared

with mouse IgG1. For F(ab')2 fragment, CIU fingerprint of 13+ and 14+ showed three main features between 100V and 500V. However, additional feature was observed with 15+ and 16+. The increase charge density could be the possible explanation for an additional feature (*Fig. 5.13, top panel*).

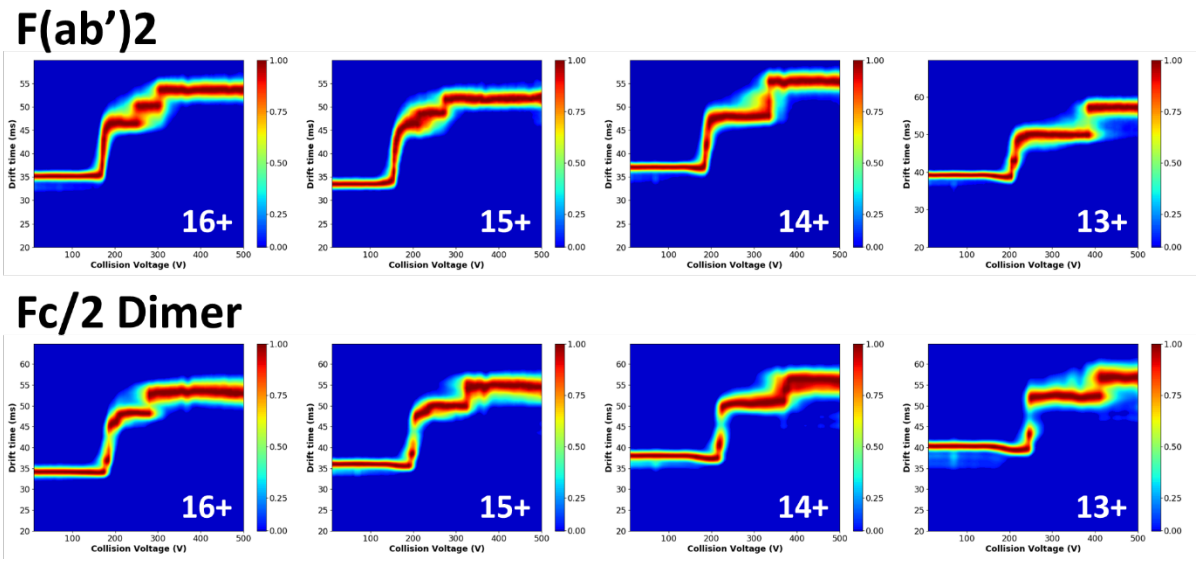

Figure 5.13. CIU of (top) F(ab')2 and (bottom) Dimer Fc/2.

Without CIU, ECD produced only fragment near the end of both termini with sequence coverage of 14%. Localization of N-Glycan was not possible prior CIU. With CIU at 225V, ECD of Fc/2 dimers were significantly more efficient, ≥ 30% sequence coverage (*Fig. 5.14*). There were more fragmentation happening in the interior of glycosylated antibody fragments. Identification and localization of N-Glycan was possible upon CIU. The increase in ECD fragmentation could be explained by the unfolding of the protein to allow more capturing are for electrons. The lower sequence coverage compared with other ECD experiments were due to the sulfide bonds resulted from non-reducing conditions. Around 30% of peaks were un-annotated due to no matching fragments. One possible explanation for unidentified peaks were the internal fragment

ions[54–57]. Internal fragments have earned a significant attention to identify un-annotated peaks as top-down and middle-down proteomics become widely popular. Terminal fragment ions have been mainstream beliefs, but recent works showed that internal fragments do happen for UVPD and HCD but to smaller extent than terminal fragments[54]. HCD which can undergo secondary fragmentation with large enough initial input energy is more likely to create internal fragments than ECD/ETD or UVPD[54]. CIU has similar nature like HCD, but at much lower extent. As a result of vibration activation, CIU-ECD would be likely to produce more internal fragment compared to ECD alone.

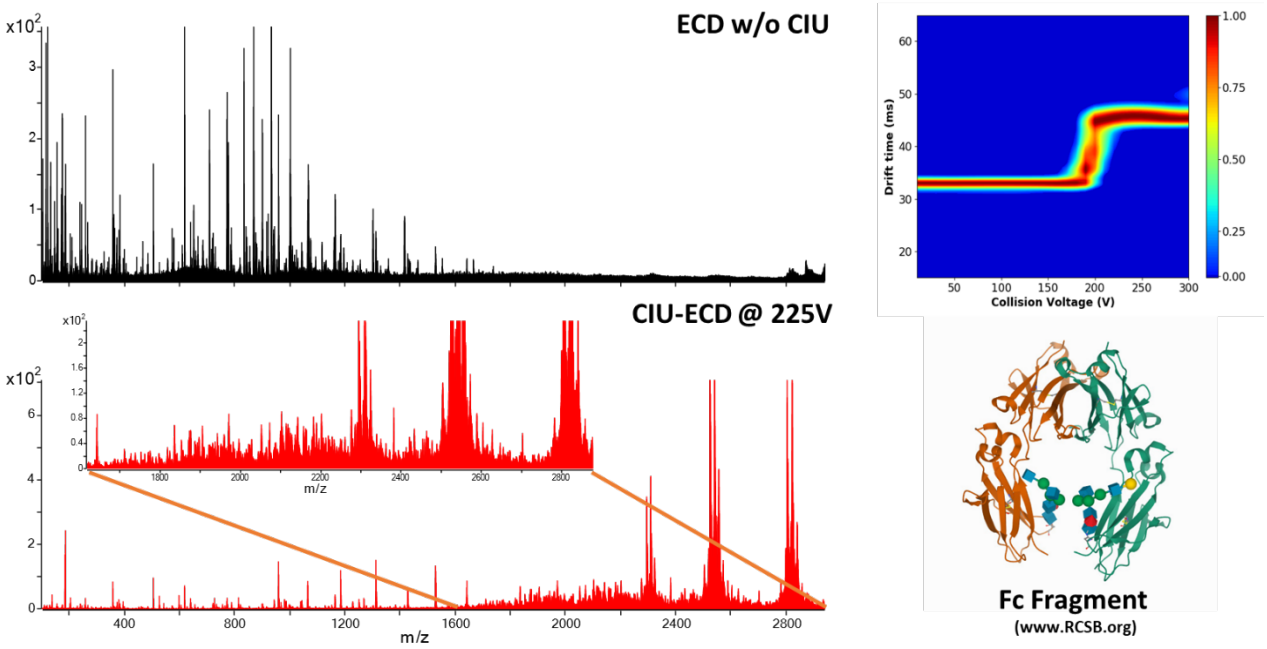

Figure 5.14. ECD of Fc/2 Dimers (top) without CIU (bottom) with CIU at 225V

5.3.4. Supercharging coupled with CIU-ECD

In our laboratory, humidity was the main factor for the usage of nESI. Especially, during summer months, the increase in humidity created ionization issues with sample spraying. To fix that issue, we incorporated supercharging to nESI to help with ionization efficiency. Surprising

discovery was made with when combining supercharging with CIU. We discovered that supercharging has a stabilizing effect on higher CIU voltages. As you can see, 7+ and 8+ started to fragment at above 400V. However, the addition of m-NBA onto ammonium acetate and ACN allowed the ions to be less activated at higher CIU voltages leading to less fragmentation. Interestingly, supercharging has a dramatic effect on stabilization for denaturing solvents. As observed, all charge states were fragmented at higher CIU voltages for sample sprayed with ACN. However, addition of m-NBA stabilized the ions leading to less fragments (*Fig. 5.15*).

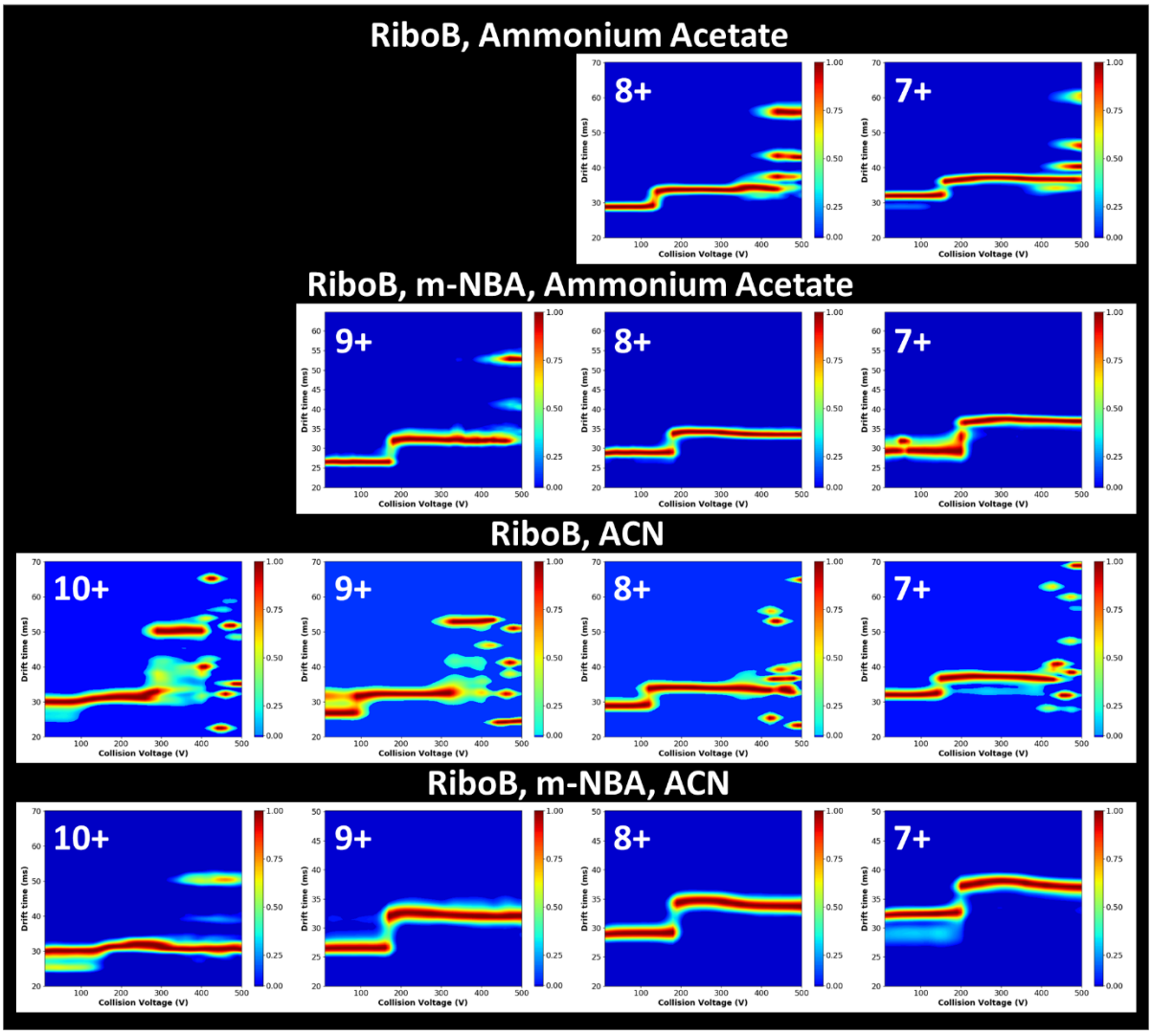

Figure 5.15 CIU incorporated supercharging.

5.3.5. Middle-down Online-Digestion for Improved CIU-ECD workflow:

To optimize the digestion setup for 6-port valve, we allowed the sample to go through the peptide column first. We observed a small degree of separation with just online digestion. We hypothesized that there were some interactions between samples and immobilized pepsin for such separation to happen (*Fig. 5.16, top*). The digested sample was then stored in the loop. When being stored in the loop, the initial separation disappeared due to diffusion. The 6-port valve was then switched, so sample was transferred from loop to SEC column. Different pepsin-derived fragments were separated efficiently with SEC column based on their sizes.

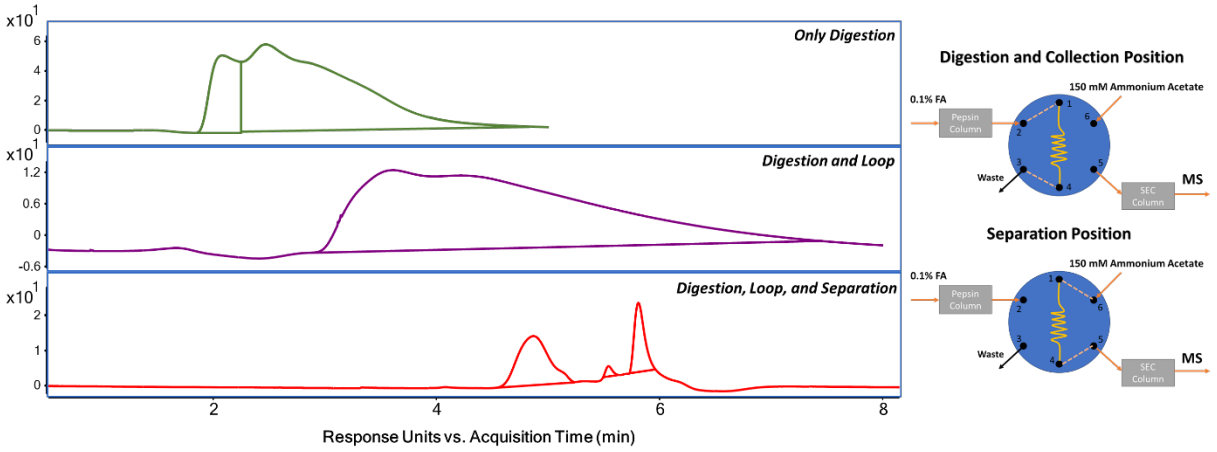

Figure 5.16. Online Digestion Setup and Optimization.

With MS information, the second peak was determined to be Fab. There was no observation of Fc as expected. Based on literature, Fc fragments would be truncated with pepsin proteolytic mechanism[49,58]. Surprisingly, for pepsin digestion in solution, F(ab')2 would be expected[48,58]. However, only Fab was produced. We believed that F(ab')2 was over-digested to create Fab. For reaction time determination, we could not observe any fragment until having a reaction ≥1.5 min (*Fig. 5.17, top panel*). The presence of Fab could only be seen for online digestion of ≥3 mins. The inconsistency between our generated data and literature was expected

because pepsin digestion would require a lot of optimizations of the setup. This however showed promising results for the combination of on-line digestion with CIU-ECD. Online digestion in conjunction with CIU-ECD would allow rapid, high throughput, and human-error-free analysis of mAbs.

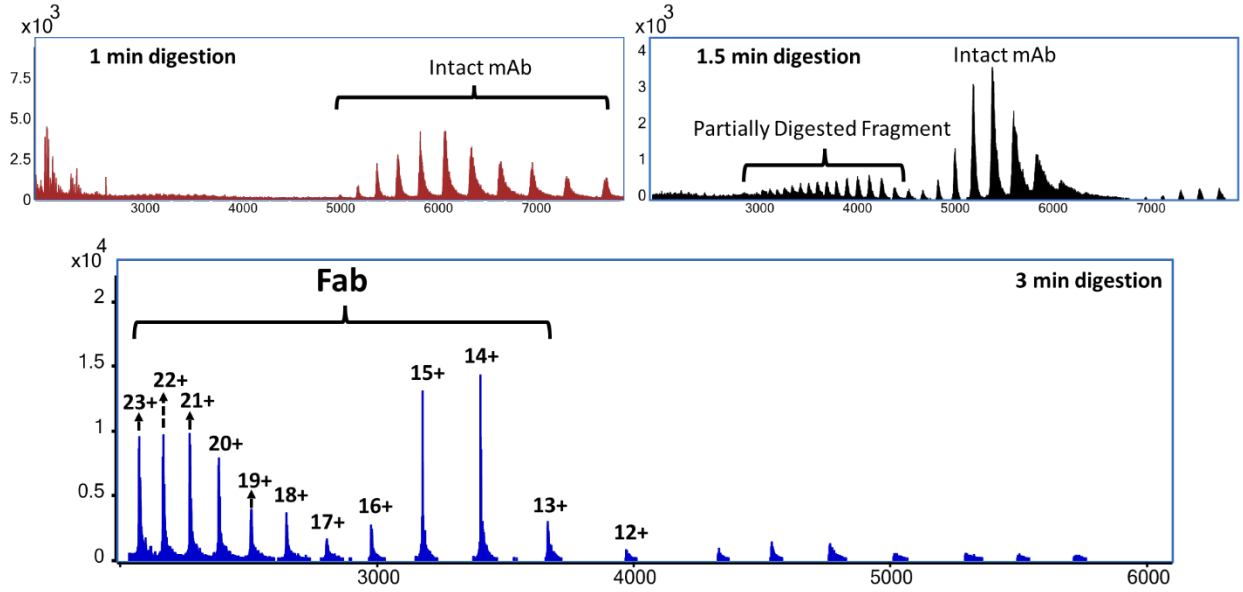

Figure 5.17. Online Pepsin Digestion Optimization with Different Times

5.4. Conclusion

We were able to incorporate CIU-ECD to middle-level analysis for improved ECD sequence coverage as well as better determination of PTM sites. Interestingly, supercharging can be incorporated into CIU workflow to stabilize proteins and protein complexes in higher CIU regions. This would not only allow us to study very labile molecules as well as observed more structural transition with a more stable protein or protein complex. We were also able to develop a workflow for automated middle-level analysis of a mAb. This is based on a 2D-LC setup where the mAb is digested in the first LC dimension and its fragments were separated and analyzed in the second LC dimension. This is highly applicable for routine analysis of mAbs because this would require rapid analysis, high throughput, and minimal sample handling to prevent errors. Pepsin-

derived column may not be an ideal choice since it would not produce fragment with PTMs. A different column for future work is recommended such as immobilized Fabricator column.

5.5. References

(1) Marovich, M.; Mascola, J. R.; Cohen, M. S. Monoclonal Antibodies for Prevention and Treatment of COVID-19. *JAMA* **2020**, *324* (2), 131–132. https://doi.org/10.1001/JAMA.2020.10245.

(2) Taylor, P. C.; Adams, A. C.; Hufford, M. M.; de la Torre, I.; Winthrop, K.; Gottlieb, R. L. Neutralizing Monoclonal Antibodies for Treatment of COVID-19. *Nature Reviews Immunology 2021 21:6* **2021**, *21* (6), 382–393. https://doi.org/10.1038/s41577-021-00542-x.

(3) Berger, M. D.; Lenz, H. J. The Safety of Monoclonal Antibodies for Treatment of Colorectal Cancer. *http://dx.doi.org/10.1517/14740338.2016.1167186* **2016**, *15* (6), 799–808. https://doi.org/10.1517/14740338.2016.1167186.

(4) Drewe, E.; Powell, R. Clinically Useful Monoclonal Antibodies in Treatment. *Journal of Clinical Pathology* **2002**, *5*, 81–85.

(5) Cai, H. H. Therapeutic Monoclonal Antibodies Approved by FDA in 2020. *Clinical Research in Immunology* **2021**, *4* (1).

(6) Ledford, H. "Biosimilar" Drugs Poised to Penetrate Market. *Nature* **2010**, *468* (7320), 18–19. https://doi.org/10.1038/468018A.

(7) Genazzani, A. A.; Biggio, G.; Caputi, A. P.; del Tacca, M.; Drago, F.; Fantozzi, R.; Canonico, P. L. Biosimilar Drugs: Concerns and Opportunities. *BioDrugs* **2007**, *21* (6), 351–356. https://doi.org/10.2165/00063030-200721060-00003/FIGURES/TAB1.

(8) Mulcahy, A. W.; Predmore, Z.; Mattke, S. Perspective Expert Insights on a Timely Policy Issue The Cost Savings Potential of Biosimilar Drugs in the United States.

(9) Kumar, R.; Singh, J. Biosimilar Drugs: Current Status. *International Journal of Applied and Basic Medical Research* **2014**, *4* (2), 63. https://doi.org/10.4103/2229-516X.136774.

(10) Gao, Y.; Huang, X.; Zhu, Y.; Lv, Z. A Brief Review of Monoclonal Antibody Technology and Its Representative Applications in Immunoassays. *https://doi.org/10.1080/15321819.2018.1515775* **2018**, *39* (4), 351–364. https://doi.org/10.1080/15321819.2018.1515775.

(11) Chiu, M. L.; Goulet, D. R.; Teplyakov, A.; Gilliland, G. L. Antibody Structure and Function: The Basis for Engineering Therapeutics. *Antibodies 2019, Vol. 8, Page 55* **2019**, *8* (4), 55. https://doi.org/10.3390/ANTIB8040055.

(12) Wang, W.; Singh, S.; Zeng, D. L.; King, K.; Nema, S. Antibody Structure, Instability, and Formulation. *Journal of Pharmaceutical Sciences* **2007**, *96* (1), 1–26. https://doi.org/10.1002/JPS.20727.

(13) Pyzik, M.; Sand, K. M. K.; Hubbard, J. J.; Andersen, J. T.; Sandlie, I.; Blumberg, R. S. The Neonatal Fc Receptor (FcRn): A Misnomer? *Frontiers in Immunology* **2019**, *10* (JULY), 1540. https://doi.org/10.3389/FIMMU.2019.01540/BIBTEX.

(14) Hmiel, L. K.; Brorson, K. A.; Boyne, M. T. Post-Translational Structural Modifications of Immunoglobulin G and Their Effect on Biological Activity. *Analytical and Bioanalytical Chemistry* **2015**, *407* (1), 79–94. https://doi.org/10.1007/S00216-014-8108-X/TABLES/2.

(15) Carter, P. J.; Lazar, G. A. Next Generation Antibody Drugs: Pursuit of the “High-Hanging Fruit.” *Nature Reviews Drug Discovery 2017 17:3* **2017**, *17* (3), 197–223. https://doi.org/10.1038/nrd.2017.227.

(16) Larsen, M. D.; de Graaf, E. L.; Sonneveld, M. E.; Plomp, H. R.; Nouta, J.; Hoepel, W.; Chen, H. J.; Linty, F.; Visser, R.; Brinkhaus, M.; Šuštić, T.; de Taeye, S. W.; Bentlage, A. E. H.; Toivonen, S.; Koeleman, C. A. M.; Sainio, S.; Kootstra, N. A.; Brouwer, P. J. M.; Geyer, C. E.; Derksen, N. I. L.; Wolbink, G.; de Winther, M.; Sanders, R. W.; van Gils, M. J.; de Bruin, S.; Vlaar, A. P. J.; Rispens, T.; den Dunnen, J.; Zaaijer, H. L.; Wuhrer, M.; van der Schoot, C. E.; Vidarsson, G. Afucosylated IgG Characterizes Enveloped Viral Responses and Correlates with COVID-19 Severity. *Science* **2021**, *371* (6532). https://doi.org/10.1126/SCIENCE.ABC8378/SUPPL_FILE/PAPV3.PDF.

(17) Selman, M. H. J.; de Jong, S. E.; Soonawala, D.; Kroon, F. P.; Adegnika, A. A.; Deelder, A. M.; Hokke, C. H.; Yazdanbakhsh, M.; Wuhrer, M. Changes in Antigen-Specific IgG1 Fc N-Glycosylation upon Influenza and Tetanus Vaccination. *Molecular and Cellular Proteomics* **2012**, *11* (4), 1–10. https://doi.org/10.1074/MCP.M111.014563/ATTACHMENT/2F8E9F9C-11A3-48B8-83DA-442AA6A5DF86/MMC1.PDF.

(18) Bailey, A. O.; Han, G.; Phung, W.; Gazis, P.; Sutton, J.; Josephs, J. L.; Sandoval, W. Charge Variant Native Mass Spectrometry Benefits Mass Precision and Dynamic Range of Monoclonal Antibody Intact Mass Analysis. *mAbs* **2018**, *10* (8), 1214–1225. https://doi.org/10.1080/19420862.2018.1521131/SUPPL_FILE/KMAB_A_1521131_SM0987.ZIP.

(19) Rosati, S.; Yang, Y.; Barendregt, A.; Heck, A. J. R. Detailed Mass Analysis of Structural Heterogeneity in Monoclonal Antibodies Using Native Mass Spectrometry. *Nature Protocols 2014 9:4* **2014**, *9* (4), 967–976. https://doi.org/10.1038/nprot.2014.057.

(20) Beck, A.; Terral, G.; Debaene, F.; Wagner-Rousset, E.; Marcoux, J.; Janin-Bussat, M. C.; Colas, O.; Dorsselaer, A. van; Cianférani, S. Cutting-Edge Mass Spectrometry Methods for the Multi-Level Structural Characterization of Antibody-Drug Conjugates. *http://dx.doi.org/10.1586/14789450.2016.1132167* **2016**, *13* (2), 157–183. https://doi.org/10.1586/14789450.2016.1132167.

(21) Fornelli, L.; Srzentić, K.; Huguet, R.; Mullen, C.; Sharma, S.; Zabrouskov, V.; Fellers, R. T.; Durbin, K. R.; Compton, P. D.; Kelleher, N. L. Accurate Sequence Analysis of a Monoclonal Antibody by Top-Down and Middle-Down Orbitrap Mass Spectrometry Applying Multiple Ion Activation Techniques. *Analytical Chemistry* **2018**, *90* (14), 8421–8429. https://doi.org/10.1021/ACS.ANALCHEM.8B00984/SUPPL_FILE/AC8B00984_SI_001.PDF.

(22) Zhang, H.; Cui, W.; Gross, M. L. Mass Spectrometry for the Biophysical Characterization of Therapeutic Monoclonal Antibodies. *FEBS Letters* **2014**, *588* (2), 308–317. https://doi.org/10.1016/J.FEBSLET.2013.11.027.

(23) Snapkov, I.; Chernigovskaya, M.; Sinitcyn, P.; Lê Quý, K.; Nyman, T. A.; Greiff, V. Progress and Challenges in Mass Spectrometry-Based Analysis of Antibody Repertoires. *Trends in Biotechnology* **2021**, *0* (0). https://doi.org/10.1016/J.TIBTECH.2021.08.006/ATTACHMENT/0A478BC2-69CA-4356-B15C-577B5A6FF1DD/MMC1.PDF.

(24) Krokhin, O. v.; Antonovici, M.; Ens, W.; Wilkins, J. A.; Standing, K. G. Deamidation of -Asn-Gly- Sequences during Sample Preparation for Proteomics: Consequences for MALDI and HPLC-MALDI Analysis. *Analytical Chemistry* **2006**, *78* (18), 6645–6650. https://doi.org/10.1021/AC061017O.

(25) Ren, D.; Pipes, G. D.; Liu, D.; Shih, L. Y.; Nichols, A. C.; Treuheit, M. J.; Brems, D. N.; Bondarenko, P. v. An Improved Trypsin Digestion Method Minimizes Digestion-Induced Modifications on Proteins. *Analytical Biochemistry* **2009**, *392* (1), 12–21. https://doi.org/10.1016/J.AB.2009.05.018.

(26) Lodge, J. M.; Schauer, K. L.; Brademan, D. R.; Riley, N. M.; Shishkova, E.; Westphall, M. S.; Coon, J. J. Top-Down Characterization of an Intact Monoclonal Antibody Using Activated Ion Electron Transfer Dissociation. *Analytical Chemistry* **2020**, *92* (15), 10246–10251. https://doi.org/10.1021/ACS.ANALCHEM.0C00705/SUPPL_FILE/AC0C00705_SI_001.PDF.

(27) Shaw, J. B.; Liu, W.; Vasil'ev, Y. v.; Bracken, C. C.; Malhan, N.; Guthals, A.; Beckman, J. S.; Voinov, V. G. Direct Determination of Antibody Chain Pairing by Top-down and Middle-down Mass Spectrometry Using Electron Capture Dissociation and Ultraviolet Photodissociation. *Analytical Chemistry* **2020**, *92* (1), 766–773. https://doi.org/10.1021/ACS.ANALCHEM.9B03129/SUPPL_FILE/AC9B03129_SI_001.PDF.

(28) Interlaboratory Study for Characterizing Monoclonal Antibodies by Top-Down and Middle-Down Mass Spectrometry Graphical Abstract HHS Public Access. https://doi.org/10.1021/jasms.0c00036.

(29) Fornelli, L.; Ayoub, D.; Aizikov, K.; Beck, A.; Tsybin, Y. O. Middle-down Analysis of Monoclonal Antibodies with Electron Transfer Dissociation Orbitrap Fourier Transform Mass Spectrometry. *Analytical Chemistry* **2014**, *86* (6), 3005–3012. https://doi.org/10.1021/AC4036857/SUPPL_FILE/AC4036857_SI_001.PDF.

(30) Santos, I. C.; Brodbelt, J. S. Structural Characterization of Carbonic Anhydrase-Arylsulfonamide Complexes Using Ultraviolet Photodissociation Mass Spectrometry. *Journal of the American*

Society for Mass Spectrometry **2021**, *32* (6), 1370–1379. https://doi.org/10.1021/JASMS.1C00004/SUPPL_FILE/JS1C00004_SI_001.PDF.

(31) Brodbelt, J. S.; Morrison, L. J.; Santos, I. Ultraviolet Photodissociation Mass Spectrometry for Analysis of Biological Molecules. *Chemical Reviews* **2019**, *120* (7), 3328–3380. https://doi.org/10.1021/ACS.CHEMREV.9B00440.

(32) Fornelli, L.; Ayoub, D.; Aizikov, K.; Liu, X.; Damoc, E.; Pevzner, P. A.; Makarov, A.; Beck, A.; Tsybin, Y. O. Top-down Analysis of Immunoglobulin G Isotypes 1 and 2 with Electron Transfer Dissociation on a High-Field Orbitrap Mass Spectrometer. *Journal of Proteomics* **2017**, *159*, 67–76. https://doi.org/10.1016/J.JPROT.2017.02.013.

(33) Rush, M. J. P.; Riley, N. M.; Westphall, M. S.; Coon, J. J. Top-Down Characterization of Proteins with Intact Disulfide Bonds Using Activated-Ion Electron Transfer Dissociation. *Analytical Chemistry* **2018**, *90* (15), 8946–8953. https://doi.org/10.1021/ACS.ANALCHEM.8B01113/SUPPL_FILE/AC8B01113_SI_001.PDF.

(34) Riley, N. M.; Hebert, A. S.; Dürnberger, G.; Stanek, F.; Mechtler, K.; Westphall, M. S.; Coon, J. J. Phosphoproteomics with Activated Ion Electron Transfer Dissociation. *Analytical Chemistry* **2017**, *89* (12), 6367–6376. https://doi.org/10.1021/ACS.ANALCHEM.7B00212/SUPPL_FILE/AC7B00212_SI_001.PDF.

(35) Riley, N. M.; Westphall, M. S.; Coon, J. J. Activated Ion Electron Transfer Dissociation for Improved Fragmentation of Intact Proteins. *Analytical Chemistry* **2015**, *87* (14), 7109–7116. https://doi.org/10.1021/ACS.ANALCHEM.5B00881.

(36) Shi, S. D. H.; Hemling, M. E.; Carr, S. A.; Horn, D. M.; Lindh, I.; McLafferty, F. W. Phosphopeptide/Phosphoprotein Mapping by Electron Capture Dissociation Mass Spectrometry. *Analytical Chemistry* **2000**, *73* (1), 19–22. https://doi.org/10.1021/AC000703Z.

(37) Fornelli, L.; Ayoub, D.; Aizikov, K.; Beck, A.; Tsybin, Y. O. Middle-down Analysis of Monoclonal Antibodies with Electron Transfer Dissociation Orbitrap Fourier Transform Mass Spectrometry. *Analytical Chemistry* **2014**, *86* (6), 3005–3012. https://doi.org/10.1021/AC4036857/SUPPL_FILE/AC4036857_SI_001.PDF.

(38) von Pawel-Rammingen, U.; Johansson, B. P.; Björck, L. IdeS, a Novel Streptococcal Cysteine Proteinase with Unique Specificity for Immunoglobulin G. *The EMBO journal* **2002**, *21* (7), 1607–1615. https://doi.org/10.1093/EMBOJ/21.7.1607.

(39) Carillo, S.; Jakes, C.; Zaborowska, I.; Bones, J. IdeS-Cleaved MAb Subunit Analysis with LC-HRAM-MS: A Quick and Accurate Comparison of Biosimilar and Originator Biotherapeutics.

(40) Fredriksson, S.; Kullman, M.; Olsson, F.; Ab, G. FabRICATOR ®-Perfect F(Ab′) 2 Fragments in Minutes.

(41) Melani, R. D.; Srzentić, K.; Gerbasi, V. R.; McGee, J. P.; Huguet, R.; Fornelli, L.; Kelleher, N. L. Direct Measurement of Light and Heavy Antibody Chains Using Ion Mobility and Middle-down Mass Spectrometry. *mAbs* **2019**, *11* (8), 1351–1357. https://doi.org/10.1080/19420862.2019.1668226/FORMAT/EPUB.

(42) Ferguson, C. N.; Gucinski-Ruth, A. C. Evaluation of Ion Mobility-Mass Spectrometry for Comparative Analysis of Monoclonal Antibodies. *Journal of the American Society for Mass Spectrometry* **2016**, *27* (5), 822–833. https://doi.org/10.1007/S13361-016-1369-1/SUPPL_FILE/JS8B05281_SI_001.DOC.

(43) Pisupati, K.; Tian, Y.; Okbazghi, S.; Benet, A.; Ackermann, R.; Ford, M.; Saveliev, S.; Hosfield, C. M.; Urh, M.; Carlson, E.; Becker, C.; Tolbert, T. J.; Schwendeman, S. P.; Ruotolo, B. T.; Schwendeman, A. A Multidimensional Analytical Comparison of Remicade and the Biosimilar Remsima. *Analytical Chemistry* **2017**, *89* (9), 4838–4846. https://doi.org/10.1021/ACS.ANALCHEM.6B04436/SUPPL_FILE/AC6B04436_SI_001.PDF.

(44) Botzanowski, T.; Erb, S.; Hernandez-Alba, O.; Ehkirch, A.; Colas, O.; Wagner-Rousset, E.; Rabuka, D.; Beck, A.; Drake, P. M.; Cianférani, S. Insights from Native Mass Spectrometry Approaches for Top- and Middle- Level Characterization of Site-Specific Antibody-Drug Conjugates. *mAbs* **2017**, *9* (5), 801–811. https://doi.org/10.1080/19420862.2017.1316914/SUPPL_FILE/KMAB_A_1316914_SM4831.DOCX.

(45) Newkirk, M. M.; Edmundson, A.; Wistar, R.; Klapper, D. G.; Capra, J. D. A New Protocol to Digest Human IgM with Papain That Results in Homogeneous Fab Preparations That Can Be Routinely Crystallized. *https://home.liebertpub.com/hyb* **2009**, *6* (5), 453–460. https://doi.org/10.1089/HYB.1987.6.453.

(46) Andrew, S. M.; Titus, J. A. Fragmentation of Immunoglobulin G. *Current Protocols in Immunology* **1997**, *21* (1), 2.8.1-2.8.10. https://doi.org/10.1002/0471142735.IM0208S21.

(47) Adamczyk, M.; Gebler, J. C.; Wu, J. Papain Digestion of Different Mouse IgG Subclasses as Studied by Electrospray Mass Spectrometry. *Journal of Immunological Methods* **2000**, *237* (1–2), 95–104. https://doi.org/10.1016/S0022-1759(00)00135-6.

(48) Jones, R. G. A.; Landon, J. Enhanced Pepsin Digestion: A Novel Process for Purifying Antibody F(Ab')2 Fragments in High Yield from Serum. *Journal of Immunological Methods* **2002**, *263* (1–2), 57–74. https://doi.org/10.1016/S0022-1759(02)00031-5.

(49) Gauci, P. J.; Alderton, M. R. Pepsin Digestion of Antibodies to Produce Functional Antigen-Binding Fragments (Fab): A Scientific Fantasy? **2001**.

(50) Gadgil, H. S.; Bondarenko, P. v.; Pipes, G. D.; Dillon, T. M.; Banks, D.; Abel, J.; Kleemann, G. R.; Treuheit, M. J. Identification of Cysteinylation of a Free Cysteine in the Fab Region of a Recombinant Monoclonal IgG1 Antibody Using Lys-C Limited Proteolysis Coupled with LC/MS Analysis. *Analytical biochemistry* **2006**, *355* (2), 165–174. https://doi.org/10.1016/J.AB.2006.05.037.

(51) Nardella, F. A.; Teller, D. C. Fc Intermediate (Fci), a Papain-Generated Fragment of Human IgG, Intermediate in Charge, Molecular Weight and Cleavage between the Fc and Fc' Fragments of IgG. *Molecular immunology* **1985**, *22* (6), 705–713. https://doi.org/10.1016/0161-5890(85)90101-4.

(52) Mihaesco, C.; Seligmann, M. PAPAIN DIGESTION FRAGMENTS OF HUMAN IGM GLOBULINS. *The Journal of Experimental Medicine* **1968**, *127* (3), 431. https://doi.org/10.1084/JEM.127.3.431.

(53) Griffiths, R. L.; Konijnenberg, A.; Viner, R.; Cooper, H. J. Direct Mass Spectrometry Analysis of Protein Complexes and Intact Proteins up to >70 KDa from Tissue. *Analytical Chemistry* **2019**, *91* (11), 6962–6966. https://doi.org/10.1021/ACS.ANALCHEM.9B00971/SUPPL_FILE/AC9B00971_SI_001.PDF.

(54) Lyon, Y. A.; Riggs, D.; Fornelli, L.; Compton, P. D.; Julian, R. R. The Ups and Downs of Repeated Cleavage and Internal Fragment Production in Top-Down Proteomics. *Journal of the American Society for Mass Spectrometry* **2018**, *29* (1), 150–157. https://doi.org/10.1007/S13361-017-1823-8/SUPPL_FILE/JS8B05668_SI_001.DOCX.

(55) Rolfs, Z.; Smith, L. M. Internal Fragment Ions Disambiguate and Increase Identifications in Top-Down Proteomics. *Journal of Proteome Research* **2021**, *20* (12), 5412–5418. https://doi.org/10.1021/ACS.JPROTEOME.1C00599/SUPPL_FILE/PR1C00599_SI_001.PDF.

(56) Lantz, C.; Zenaidee, M. A.; Wei, B.; Hemminger, Z.; Ogorzalek Loo, R. R.; Loo, J. A. ClipsMS: An Algorithm for Analyzing Internal Fragments Resulting from Top-Down Mass Spectrometry. *Journal of Proteome Research* **2021**, *20* (4), 1928–1935. https://doi.org/10.1021/ACS.JPROTEOME.0C00952/SUPPL_FILE/PR0C00952_SI_001.PDF.

(57) Schmitt, N. D.; Berger, J. M.; Conway, J. B.; Agar, J. N. Increasing Top-Down Mass Spectrometry Sequence Coverage by an Order of Magnitude through Optimized Internal Fragment Generation and Assignment. *Analytical Chemistry* **2021**, *93* (16), 6355–6362. https://doi.org/10.1021/ACS.ANALCHEM.0C04670/SUPPL_FILE/AC0C04670_SI_001.PDF.

(58) Jones, R. G. A.; Landon, J. Enhanced Pepsin Digestion: A Novel Process for Purifying Antibody F(Ab')2 Fragments in High Yield from Serum. *Journal of Immunological Methods* **2002**, *263* (1–2), 57–74. https://doi.org/10.1016/S0022-1759(02)00031-5.

Chapter 6. Negative Ion Electron Capture Dissociation (niECD) for Ganglioside Analysis

6.1. Introduction

Gangliosides are heterogeneous biomolecules composed of a sialic acid-containing glycan headgroup attached to a ceramide lipid tail. Gangliosides are abundant in the nervous system and involved in, e.g., cell-cell recognition, adhesion, and signal transduction. Due to their acidity, gangliosides show preferred ionization in negative ion mode. However, conventional collision-induced dissociation (CID) mainly cleaves glycosidic bonds and thus provides limited sugar, including sialic acid, linkage information. Conversely, electron-based tandem mass spectrometry, i.e., electron detachment dissociation, can enhance cross-ring cleavage but shows low efficiency and complex fragmentation pathways. Here, we apply negative ion electron capture dissociation (niECD) towards ganglioside structural analysis and show that niECD efficiency is sensitive to the number of sialic acid moieties, ganglioside isomeric state, and lipid tail length.

Gangliosides constitute to a special class of glycolipids, containing an oligosaccharide head and fatty acid tail[1]. The role of gangliosides is ubiquitous in biochemical systems and plays many vital functions on cell-cell signaling, cell surface binding, and membrane signal transductor[2–7]. Abnormality in gangliosides can lead to cancer or neurological diseases such as Alzheimer's disease, Parkinson's disease, and Huntington's disease[8–13]. Thus, there is a growing interest in ganglioside profiling in cellular lipids. However, structural complexity of gangliosides has been

the main obstacle for lipid profiling and lipidomics. The structural heterogeneity of gangliosides can be branching from both the glycan head (i.e., type of carbohydrates, number of saccharides, and acidic/labile nature) and the lipid tail (i.e., saturation and length)[1,14]. Additionally, amphipathic nature presents analytical challenges for the separation[15–18] as well as the acidic nature contributes to the low ionization efficiency in positive ion mode. Gangliosides often bear one or more N-acyl neuraminic acid moieties on the head group, which is highly labile and often lost during ionization[19,20]. Due to those factors, mass spectral analysis of gangliosides has always presented as a particularly difficult task.

The initial work on gangliosides were done with conventional vibrational-based activation method. However, structural elucidation of gangliosides with CID requires MS^2 spectra in both negative and positive modes. While positive-mode CID only reveals information about the ceramide portion, negative-mode CID mainly generated glycosidic cleavages on glycan head group[21]. Another shortcoming of CID/HCD is the lack of diagnostic fragment generation for isomer differentiation. Thus, those techniques cannot be utilized to obtain structurally specific features of ganglioside epimers.

To mitigate the deficiency of traditional collision-based methods, ECD, EDD and IRMPD were employed to evaluate the ganglioside[22]. IRMPD similar to CID/HCD produced mostly glycosidic cleavage but no information about the lipid tail. On the other hand, EDD provided extensive fragmentation of negative ions, but suffer low efficiency. ECD generated comparable information with EDD in positive-ion mode. ETD followed by CID has been applied to sodiated gangliosides to show extensive information about the lipid tail portion[23]. However, acidic nature of ganglioside

(i.e., more readily ionized to form deprotonated species for negative mode study) has impeded the widespread of electron-based activation techniques, which mostly operate in positive mode.

Due to its highly acidic nature, ganglioside is best suited to be study in negative mode. Ultraviolet photon dissociation (UVPD) showed promising potential for producing a wide varies of cross ring and glycosidic cleavages[21]. However, implementation of UV laser is not straightforward and often costly. Negative ion electron capture dissociation (niECD) which was developed in our laboratory has gained its recognition as a versatile ion for the analysis of acidic peptides (sulfated peptide), glycans, and nucleic acids[24,25]. Here, we extend niECD towards ganglioside structural analysis. As shown in later, niECD results in the production of diagnostic cross-ring cleavages fragment ions. These fragments enhance the ability for isomer differentiation of glycan moieties that have proven to be problematic for other methods.

6.2. Experimental

GM1 (ovine brain, Galβ1,3GalNAcβ1,4(NeuAcα2,3)Galβ1,4Glcβ1,1'Ceramide), GD1a (porcine brain, Neu5Acα2,3Galβ1,3GalNAcβ1,4(Neu5Acα2,3)Galβ1,4Glcβ1,1'Ceramide), GD1b (porcine brain, Galβ1,3GalNAcβ1,4(Neu5Acα2,8Neu5Acα2,3)Galβ1,4Glcβ1,1'Ceramide) and GM3 (bovine milk, Neu5Acα2,3Galβ1,4Glcβ1,1'Ceramide) were purchased from AvantiLipids. LC/MS grade water, acetonitrile (ACN), isopropanol (IPA), and triethyl amine (TEA) were from Fisher Scientific. All standards were prepared at 0.01 mg/mL in 40:10:50 ACN:IPA:H_2O containing 0.1% TEA and infused into an ESI source in negative ion mode (flowrate 125-150 µL/hour, 3.2-3.5 kV ESI voltage, 1.5 L/min drying gas flow rate at 70^oC). All niECD MS/MS experiments (3.5-6.5 eV electrons, 1-2 s irradiation) were performed on a Bruker 7T SolariX Q-FT-ICR mass spectrometer with 100 scans

averaging. Product ion annotations were achieved using GlycoWorkbench. Electron induced dissociation (EID) was performed at higher electron energy (18-19.5 eV) for comparison.

6.3. Results and Discussion

For monosialogangliosides, niECD outperformed both CID and EID. For GM1, niECD yielded extensive cross-ring fragmentation compared with relatively few glycosidic fragments from CID and EID (*Fig. 6.*). With EID, mostly sialic acid cleavage was observed (*Fig. 6.2, middle*). The presence of niECD was confirmed with the diagnostic ions from

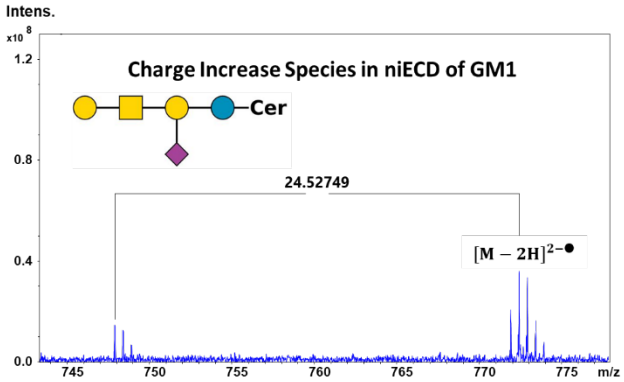

Figure 6.1 Isotopic pattern of charge-increase species.

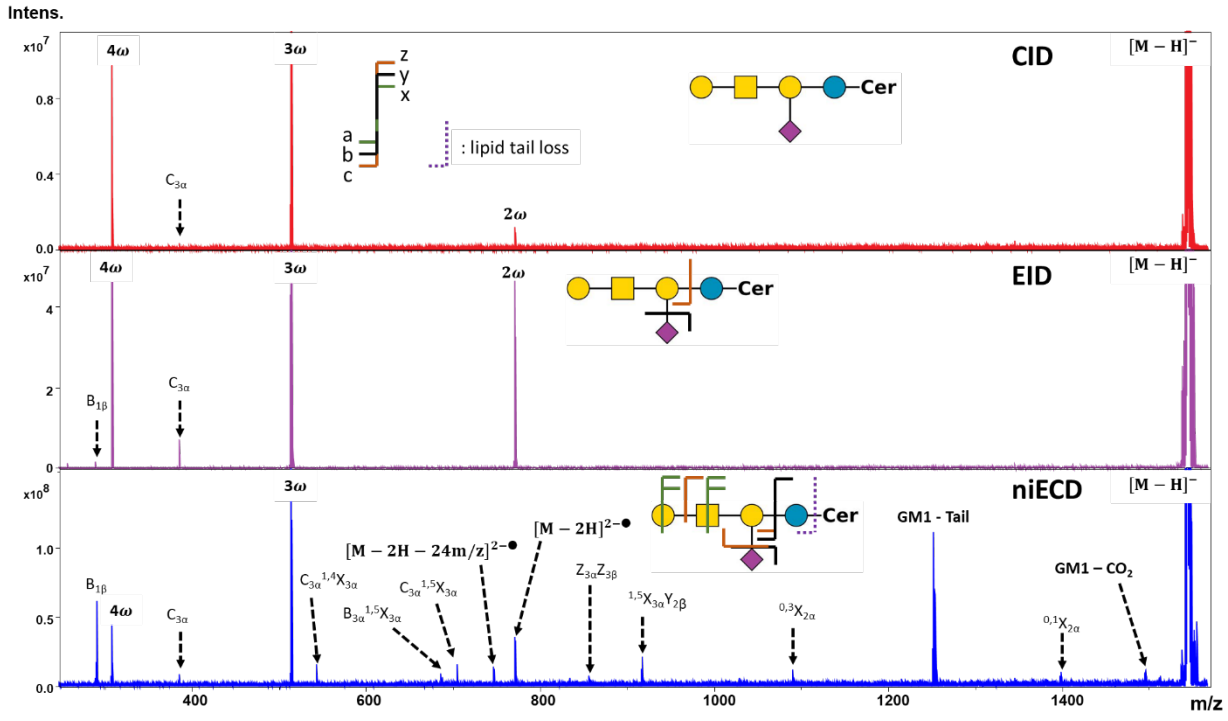

Figure 6.2. Negative mode tandem MS of GM1 (Top) CID (Middle) EID (Bottom) niECD

hydrogen radical injection of charged increased species (*Fig. 6.1*). Beside other cross link and glycosidic cleavage, there was also neutral CO_2 losses from niECD process.

For GM3, which has a smaller headgroup (2 saccharides less than GM1), niECD performance was reduced. For this ganglioside, both niECD and EID generated more extensive fragmentation than CID (*Fig. 6.3*). In niECD of GM3, abundant hydrogen radical ejection from the charge-increased species was observed upon electron capture, thus preventing further radical rearrangement to yield structurally informative fragmentation (*Fig. 6.3, bottom*). This reduced niECD efficiency may be due to either a higher charge density upon electron capture for the smaller ganglioside, or the ability of the larger ganglioside to form gas-phase structures favorable for electron capture, including zwitterionic and/or salt-bridged structures.

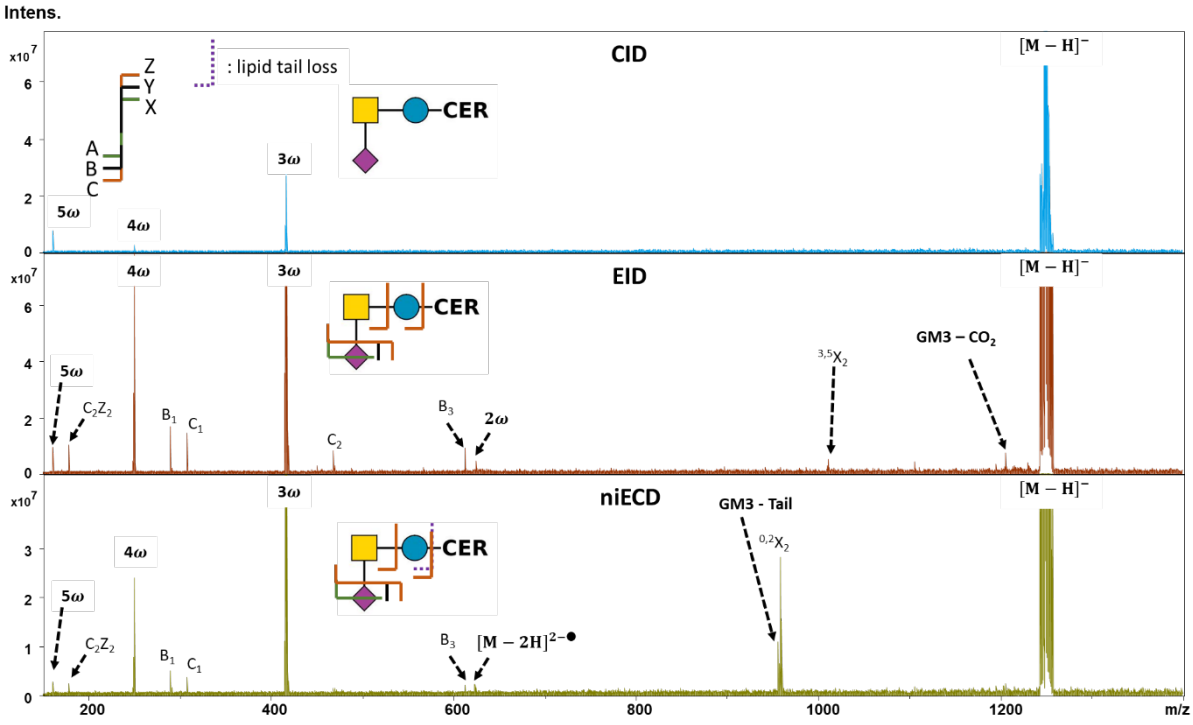

Figure 6.3. Negative mode tandem MS of GM3 (Top) CID (Middle) EID (Bottom) niECD

In one of our previous mechanistic studies, we have shown that hydrogen radical migration plays a significant role in niECD fragmentation pattern of glycosaminoglycans. For GM3, we

mainly observed the formation ejection of hydrogen radical instead of participating in the niECD process (*Fig. 6.4*). Thus, this explains the reason for such low fragmentation efficiency. As previously mentioned, the increase in hydrogen radical ejection is due the structural change.

Structural effects in ganglioside niECD were further explored with the disialogangliosides GD1a and GD1b. These isomeric species contain the same number of sialic acid residues, but their linkage is different: while GD1a has a single sialic acid on each galactose residue, GD1b has two sialic acids on the galactose residue adjacent to the terminal glucose. For GD1a niECD outperformed EID and CID (*Fig. 6.5*), similar to GM1. However, most observed fragments resulted from glycosidic cleavages. Also, for GD1a with a longer ceramide tail (2 carbon units longer), niECD was further enhanced.

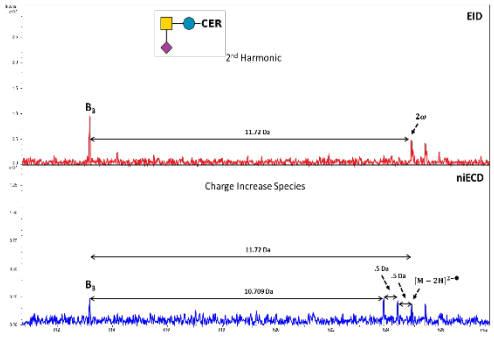

Figure 6.4 Isotopic pattern of charge increase species.

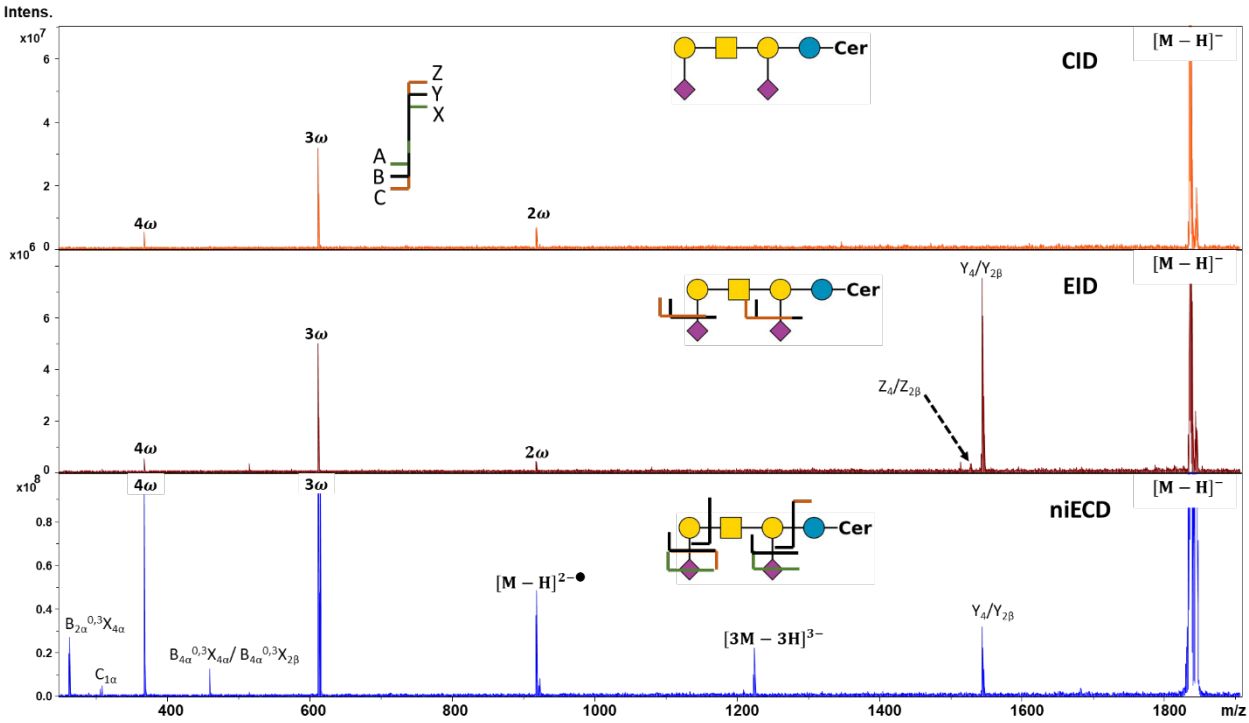

Figure 6.5. Negative mode tandem MS of GD1a (Top) CID (Middle) EID (Bottom) niECD

For GD1b, with sialic acids in closer proximity, niECD was even more effective showing extensive fragmentation with numerous cross-ring fragments throughout the entire structure (*Fig. 6.6*). niECD produced not only glycosidic cleavages for complete glycan characterization but also diagnostic fragment for structural differentiation between GD1a and GD1b isomers. For GD1b, niECD results in the production of C-C and C-N bond cleavage at sphingosine and fatty acid groups, which can be used for lipid tail characterization. These preliminary data further demonstrate the versatility of niECD for the structural analysis of complex, heterogeneous biomolecules as well as the major influence of ion structure on niECD.

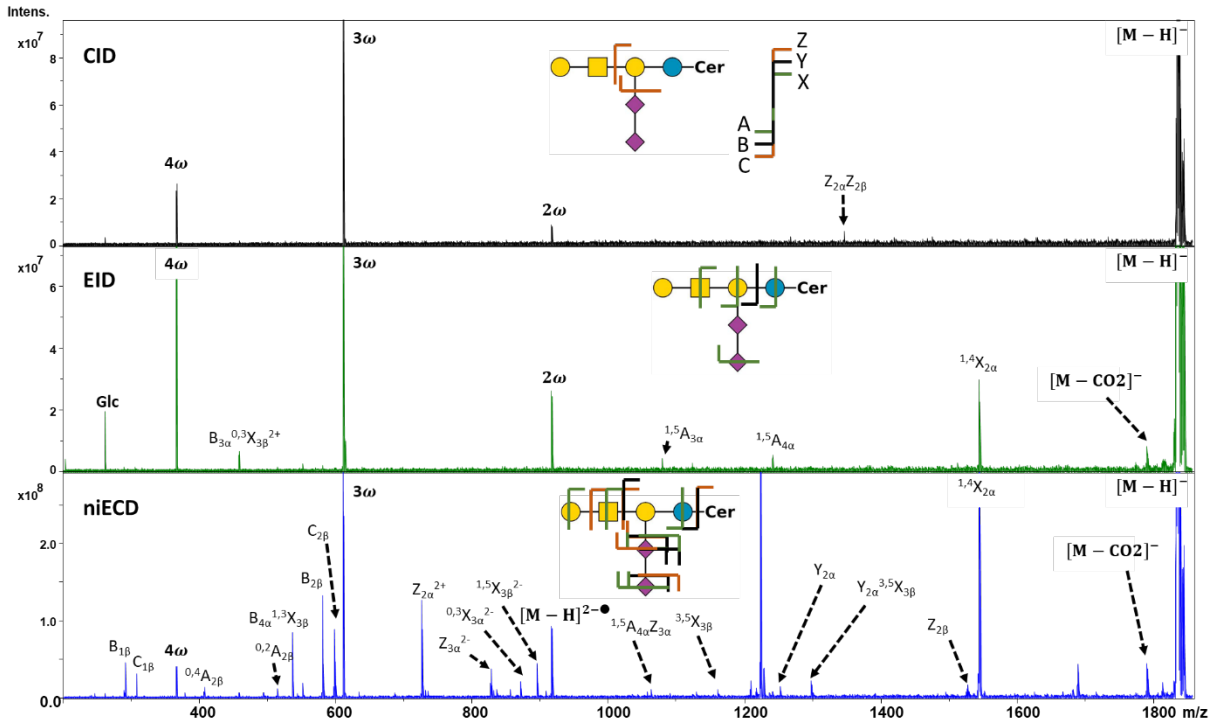

Figure 6.6. Negative mode tandem MS of GD1a (Top) CID (Middle) EID (Bottom) niECD.

6.4. Conclusion

In this work, a numerous of negative mode MS/MS techniques have been evaluated for analysis of ganglioside. niECD has proven its utility for acidic ganglioside structural analysis

compared to CID and EID. From our reports, it was demonstrated that niECD efficiency is sensitive to the number of sialic acid moieties, ganglioside isomeric state, and lipid tail length. Additionally, niECD is well suited for acidic and labile biomolecules such as gangliosides (i.e., more likely to produce deprotonated species). Unlike traditional CID/HCD, niECD produces not only glycosidic cleavages but also cross-ring cleaves for ganglioside analysis. The rich fragmentation patterns of niECD would enhance identification and differentiation of isobaric ganglioside structures in brand and eliminate the dependence on low-efficient positive-mode activation approaches like ECD/ETD.

6.5. References

(1) Kolter, T. Ganglioside Biochemistry. *Article ID* **2012**, *2012*, 36. https://doi.org/10.5402/2012/506160.

(2) Davidsson, P.; Wallin, A.; Fredman, P.; Gottfries, C. G.; Karlsson, I.; Månsson, J. E.; Svennerholm, L.; Blennow, K. Gangliosides in Cerebrospinal Fluid in "Probable Alzheimer's Disease." *Archives of neurology* **1991**, *48* (10), 1032–1035. https://doi.org/10.1001/ARCHNEUR.1991.00530220048018.

(3) Desplats, P. A.; Denny, C. A.; Kass, K. E.; Gilmartin, T.; Head, S. R.; Sutcliffe, J. G.; Seyfried, T. N.; Thomas, E. A. Glycolipid and Ganglioside Metabolism Imbalances In Huntington's Disease. *Neurobiology of disease* **2007**, *27* (3), 265. https://doi.org/10.1016/J.NBD.2007.05.003.

(4) Sipione, S.; Monyror, J.; Galleguillos, D.; Steinberg, N.; Kadam, V. Gangliosides in the Brain: Physiology, Pathophysiology and Therapeutic Applications. *Frontiers in Neuroscience* **2020**, *14*, 1004. https://doi.org/10.3389/FNINS.2020.572965/BIBTEX.

(5) Sipione, S.; Monyror, J.; Galleguillos, D.; Steinberg, N.; Kadam, V. Gangliosides in the Brain: Physiology, Pathophysiology and Therapeutic Applications. *Frontiers in Neuroscience* **2020**, *14*, 1004. https://doi.org/10.3389/FNINS.2020.572965/BIBTEX.

(6) Maglione, V.; Marchi, P.; di Pardo, A.; Lingrell, S.; Horkey, M.; Tidmarsh, E.; Sipione, S. Impaired Ganglioside Metabolism in Huntington's Disease and Neuroprotective Role of GM1. *Journal of Neuroscience* **2010**, *30* (11), 4072–4080. https://doi.org/10.1523/JNEUROSCI.6348-09.2010.

(7) Wu, G.; Lu, Z. H.; Kulkarni, N.; Ledeen, R. W. Deficiency of Ganglioside GM1 Correlates with Parkinson's Disease in Mice and Humans. *Journal of neuroscience research* **2012**, *90* (10), 1997–2008. https://doi.org/10.1002/JNR.23090.

(8) van Echten-Deckert, G.; Walter, J. Sphingolipids: Critical Players in Alzheimer's Disease. *Progress in Lipid Research* **2012**, *51* (4), 378–393. https://doi.org/10.1016/J.PLIPRES.2012.07.001.

(9) el Khadem, Hassan. Carbohydrate Chemistry : Monosaccharides and Their Oligomers. **1988**, 267.

(10) Posse de Chaves, E.; Sipione, S. Sphingolipids and Gangliosides of the Nervous System in Membrane Function and Dysfunction. *FEBS Letters* **2010**, *584* (9), 1748–1759. https://doi.org/10.1016/J.FEBSLET.2009.12.010.

(11) Merrill, A. H.; Stokes, T. H.; Momin, A.; Park, H.; Portz, B. J.; Kelly, S.; Wang, E.; Cameron Sullards, M.; Dongmei Wang, M.; Jr, A. H.; Stokes, T. H.; Momin, A.; Park, H.; Portz, B. J.; Kelly, S.; Wang, E.; Sullards, M. C.; Dongmei Wang, M.; Lipid, J. Sphingolipidomics: A Valuable Tool for Understanding the Roles of Sphingolipids in Biology and Disease. *Journal of Lipid Research* **2009**, *50* (SUPPL.), S97–S102. https://doi.org/10.1194/JLR.R800073-JLR200.

(12) Wang, J. R.; Zhang, H.; Yau, L. F.; Mi, J. N.; Lee, S.; Lee, K. C.; Hu, P.; Liu, L.; Jiang, Z. H. Improved Sphingolipidomic Approach Based on Ultra-High Performance Liquid Chromatography and

Multiple Mass Spectrometries with Application to Cellular Neurotoxicity. *Analytical Chemistry* **2014**, *86* (12), 5688–5696. https://doi.org/10.1021/AC5009964/SUPPL_FILE/AC5009964_SI_001.PDF.

(13) Nagai, Y. Functional Roles of Gangliosides in Bio-Signaling. *Behav. Brain Res.* **1995**, *66* (1–2), 99–104. https://doi.org/10.1016/0166-4328(94)00130-8.

(14) Hakomori, S. Structure, Organization, and Function of Glycosphingolipids in Membrane. *Curr. Opin. Hematol.* **2003**, *10* (1), 16–24. https://doi.org/10.1097/00062752-200301000-00004.

(15) Kadowaki, H.; Bremer, E. G.; Evans, J. E.; Jungalwala, F. B.; McCluer, R. H. Acetonitrile-Hydrochloric Acid Hydrolysis of Gangliosides for High Performance Liquid Chromatographic Analysis of Their Long Chain Bases. *Journal of Lipid Research* **1983**, *24* (10), 1389–1397. https://doi.org/10.1016/S0022-2275(20)37890-1.

(16) Gazzotti, G.; Sonnino, S.; Ghidoni, R. Normal-Phase High-Performance Liquid Chromatographic Separation of Non-Derivatized Ganglioside Mixtures. *Journal of Chromatography A* **1985**, *348* (C), 371–378. https://doi.org/10.1016/S0021-9673(01)92475-6.

(17) Busch, C. M.; Desai, A. v.; Moorthy, G. S.; Fox, E.; Balis, F. M. A Validated HPLC-MS/MS Method for Estimating the Concentration of the Ganglioside, GD2, in Human Plasma or Serum. *Journal of Chromatography B* **2018**, *1102–1103*, 60–65. https://doi.org/10.1016/J.JCHROMB.2018.10.010.

(18) Sonnino, S.; Ghidoni, R.; Gazzotti, G.; Kirschner, G.; Galli, G.; Tettamanti, G. High Performance Liquid Chromatography Preparation of the Molecular Species of GM1 and GD1a Gangliosides with Homogeneous Long Chain Base Composition. *Journal of Lipid Research* **1984**, *25* (6), 620–629. https://doi.org/10.1016/S0022-2275(20)37775-0.

(19) Powell, A. K.; Harvey, D. J. Stabilization of Sialic Acids in N-Linked Oligosaccharides and Gangliosides for Analysis by Positive Ion Matrix-Assisted Laser Desorptiod Ionization Mass Spectrometry. *RAPID COMMUNICATIONS IN MASS SPECTROMETRY* **1996**, *10*, 1027–1032. https://doi.org/10.1002/(SICI)1097-0231(19960715)10:9.

(20) O'connor, P. B.; Mirgorodskaya, E.; Costello, C. E. High Pressure Matrix-Assisted Laser Desorption/Ionization Fourier Transform Mass Spectrometry for Minimization of Ganglioside Fragmentation. **2002**.

(21) O'Brien, J. P.; Brodbelt, J. S. Structural Characterization of Gangliosides and Glycolipids via Ultraviolet Photodissociation Mass Spectrometry. *Analytical Chemistry* **2013**, *85* (21), 10399–10407. https://doi.org/10.1021/AC402379Y/SUPPL_FILE/AC402379Y_SI_001.PDF.

(22) McFarland, M. A.; Marshall, A. G.; Hendrickson, C. L.; Nilsson, C. L.; Fredman, P.; Månsson, J. E. Structural Characterization of the GM1 Ganglioside by Infrared Multiphoton Dissociation, Electron Capture Dissociation, and Electron Detachment Dissociation Electrospray Ionization FT-ICR MS/MS. *Journal of the American Society for Mass Spectrometry* **2005**, *16* (5), 752–762. https://doi.org/10.1016/J.JASMS.2005.02.001.

(23) Liang, X.; Liu, J.; LeBlanc, Y.; Covey, T.; Ptak, A. C.; Brenna, J. T.; McLuckey, S. A. Electron Transfer Dissociation of Doubly Sodiated Glycerophosphocholine Lipids. *Journal of the American Society for Mass Spectrometry* **2007**, *18* (10), 1783–1788. https://doi.org/10.1016/J.JASMS.2007.07.013.

(24) Hersberger, K. E.; Håkansson, K. Characterization of O-Sulfopeptides by Negative Ion Mode Tandem Mass Spectrometry: Superior Performance of Negative Ion Electron Capture Dissociation. *Analytical Chemistry* **2012**, *84* (15), 6370–6377. https://doi.org/10.1021/AC301536R/SUPPL_FILE/AC301536R_SI_001.PDF.

(25) Yoo, H. J.; Wang, N.; Zhuang, S.; Song, H.; Håkansson, K. Negative-Ion Electron Capture Dissociation: Radical-Driven Fragmentation of Charge-Increased Gaseous Peptide Anions. *Journal of the American Chemical Society* **2011**, *133* (42), 16790–16793. https://doi.org/10.1021/JA207736Y/SUPPL_FILE/JA207736Y_SI_001.PDF.

Chapter 7. Conclusions and Future Directions

7.1. Dissertation Summary

Radical-driven tandem MS involves the use of electron-ion reactions to effectively fragment the analyte of interest and is indispensable in the field of mass spectrometry. The work described in this dissertation centers around improved radical-driven tandem MS for enhance detection of labile post translation modifications.

In Chapter 2 and 3, we have demonstrated the use of supercharging for improved ETD of labile PTMs such as glycosylated and S-Palmitoylated peptides. For glycosylated sample, supercharging increased the ionization efficiency of the glycopeptides for enhanced detection as well as increased charged states. ETD of supercharged peptides resulted in extensive peptide backbone fragmentation whereas ETD of highly supercharged N- and O-glycopeptides also yielded glycan fragmentation, i.e., B and Y type ions, similar to EThcD or activated ion-ETD but with the added benefit of higher experimental throughput as ETD reaction times can be greatly shortened (from 150 ms for doubly/triply-charged ions to 25-45 ms for higher charge states). The number of ETD events following post-column supercharging increased ~50% compared with conventional nanoHPLC ETD MS/MS. Abundances of glycopeptide-specific oxonium fragment ions from HCD also increased in the presence of mNBA. Supercharging therefore also appears beneficial for targeted glycopeptide analysis, i.e., HCDpdETD. With supercharging, 40% more glycopeptides were detected from lectin and transferrin tryptic digests in HCDpdETD experiments compared with conventional HCD/CID, EThcD, and HCDpdETD without

supercharging. For S-Palmitoylated sample, supercharging was incorporated in the neutral loss triggered approach to increase the throughput with HCD and generate high quality of MS^2 spectra of PTM-carry peptides. Supercharging is also beneficial for EThcD, which produced higher quality MS^2 data with supercharged peptides. To have successful annotation and identification of S-Palmitoylated, we discovered that RapidGest in low organic composition is need to main the solubility of the S-Palmitoylated peptides for LC/MS analysis.

In Chapter 4, we have demonstrated the utility of CIU in tandem with ECD for improved analysis of glycosylated, S-Palmitoylated, and phosphorylated peptides. Upon CIU, the elongated conformer generated extensive sequence information with minimal labile PTM loss. With CIU-ECD, we were able to have the direct measurements of structural changes of PTM-carrying peptides. Additionally, ECD provides another dimension of analysis for unfolded peptides. The doubly protonated β-casein phosphopeptide, FQsEEQQQTEDELQDK, which we previously found to undergo minimum fragmentation under FT-ICR ECD conditions, undergoes a ~29% increase in collision cross-section upon CIU. For the resulting elongated peptide form, having a CIU_{50} of 103.5 V, ECD sequence coverage was greatly enhanced (~82%), including a variety of c and z-type ions across the entire phosphopeptide as compared with ECD of the pre-activated conformer that only yielded fragmentation close to the peptide termini (~20%), similar to FT-ICR ECD. With REMD, we were able to simulate the folded and unfolded state of β-casein peptide. The folded state shows structural diversity compared to unfolded state.

In Chapter 5, we extend the use of CIU-ECD to analysis of therapeutic mAbs at middle-level MS. Upon CIU, glycosylated Fc/2 dimer generated double amount of sequence coverage. During our optimization for papain proteolytic of NIST mAb, we discovered that a more controlled

digestion can be achieved within Tris-buffer. Within Tris-buffer, papain digestion generated Fc, Fab, and Fc intermediate compared to traditional recommended buffer, sodium phosphate. We also discovered that supercharging has a stabilizing effect on the glycoproteins for higher CIU activation. The same ions would produce additional features and less fragmentation in the presence of m-NBA. We were also able to develop an automated 2D-LC setup for online digestion of mAbs to generate Fab fragments. This setup eliminates the error-prone manual digestion process and enabled a fast and high throughput approach for mAb analysis.

In Chapter 6, we were able to apply niECD to another class of biomolecules, gangliosides. In this work, we demonstrated that niECD efficiency is sensitive to the number of sialic acid moieties, ganglioside isomer state, and lipid tail length. In our report, niECD seems to be a more superior technique in negative mode compared to CID and EID. niECD not only provides sequence-rich information but also the ability to distinguish the isomeric gangliosides with diagnostic fragments.

7.2. Future Directions

7.2.1. Implementation of Post-Separation Supercharging for S-Palmitoylated Proteome:

Following our study reading supercharging of S-Palmitoylated peptides in positive mode in chapter 3, there are several interesting questions worth further investigation. We have shown the supercharging is effective for N-Ras peptide. However, this peptide was not in its biologically active state. To further evaluate this method, we would like to test on the biologically relevant N-Ras peptides with three modifications: S-Palmitoylation, farnesylation and methylation (*Fig. 7.1*). From our previous study, it was shown that this peptide could only be observed when mis-cleavage happened—leading to an additional charge from additional lysine. However, only S-Palmitoylation was detected in this peptide with

our previous study. We hypothesize that an additionally PTM (i.e., farnesylation) reduced ionization efficiency and thus ultimately affected the detection of the mature N-Ras peptide. With supercharging, we can significantly enhance the ionization efficiency and allow the detection of mature N-Ras peptide with improved ETD efficiency.

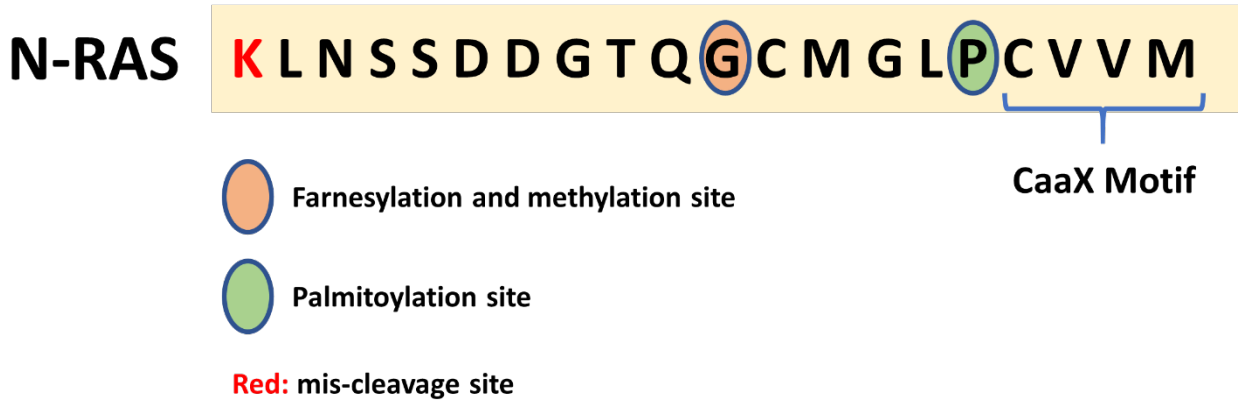

Figure 7.1 N-Ras is post-translationally farnesylated and methylated at the clipped C CaaX motif before being palmitoylated.

7.2.2. Investigation of the occurrence of B- and Y-type from N-Glycosylated and O-glycosylated ions of supercharged peptides:

ETD is a relatively soft method, and we were surprised to discover the EThcD-like fragments from ETD of supercharged glycosylated peptide. This proves to be beneficial since it provided us comprehensive characterization of glycopeptides without the usage of collision-based activation. Our work in chapter 2 sheds light on a minor mechanistic pathway of ETD fragmentation. One interesting observation is that different type of glycopeptides would require a different degree of supercharging. While N-glycopeptides need to extreme supercharging to produce EThcD-like fragments, a more labile O-glycopeptides only requires a smaller degree of supercharging to create a similar effect (*Fig. 7.2*). Further fundamental studies of this effect are valuable to better incorporate supercharging into MS workflows for improved

glycopeptide analysis and evaluate designs for MS experiments with minimal vibrational activation to reduce PTM loss.

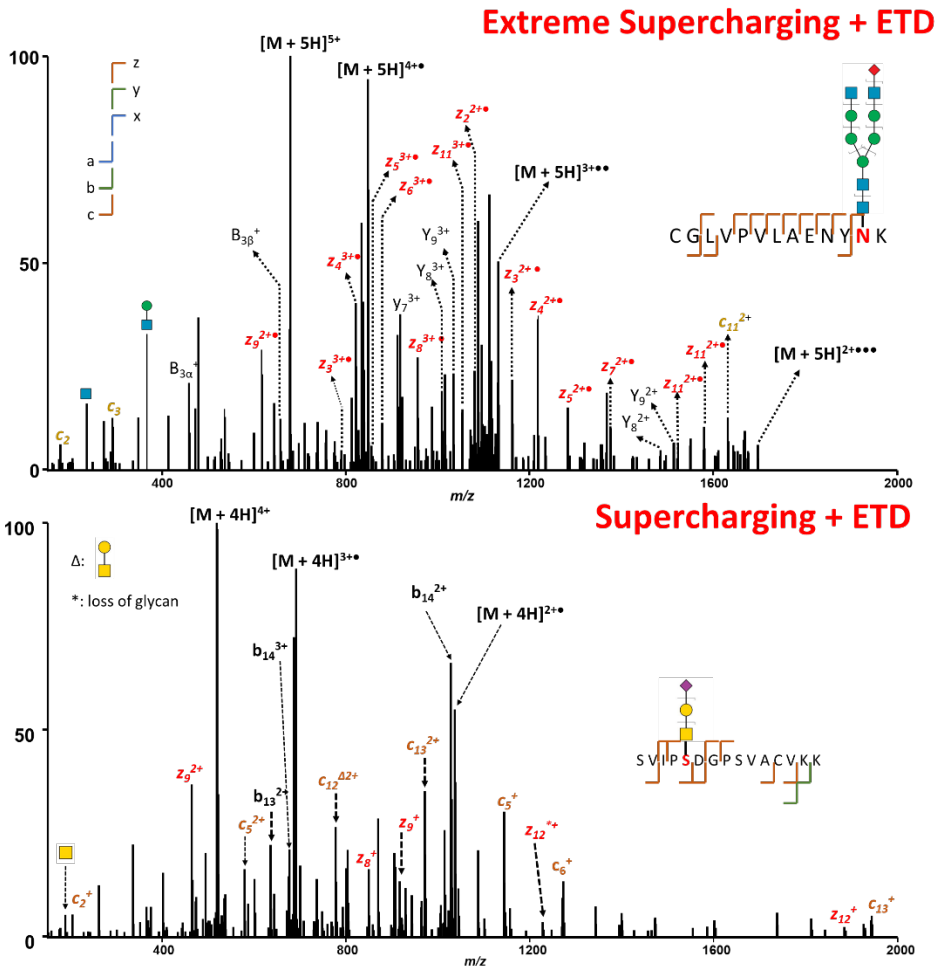

Figure 7.2 ETD of supercharged glycosylated peptides (Top) N-glycopeptide (Bottom) O-Glycopeptide

7.2.3. Implementation of CIU-ECD to automated online 2D-LC for middle-level digestion:

Preliminary data for middle-level digestion with immobilized pepsin column shows promising potential for the integration of CIU-ECD to the automated online 2D-LC system. However, pepsin only produced truncated fragments and extensive optimization is needed to produce same mAb fragments[1,2]. Therefore, more specific proteolytic enzyme is needed for consistent and reproducible results. Fabricator is the enzyme of choice due to ease of use and minimal

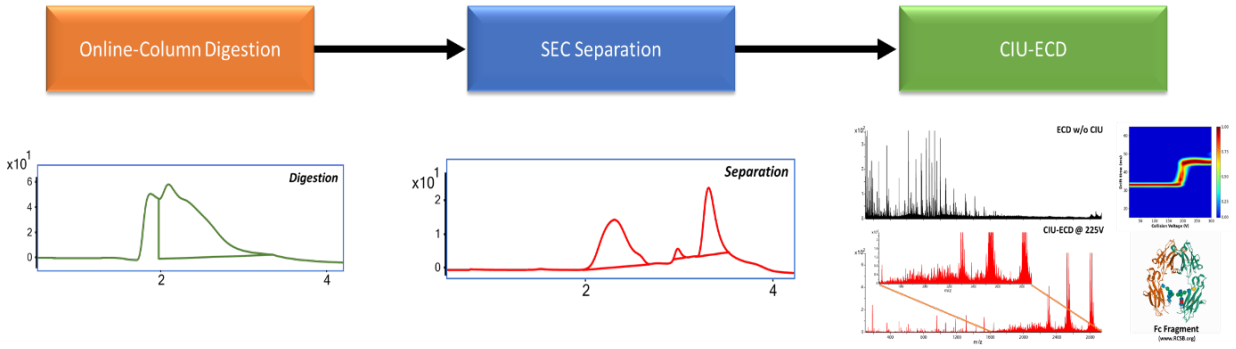

Figure 7.3. Automated Middle-Level Online Digestion Coupled to CIU-ECD.

optimization requirement[3–5]. With immobilized IdeS (Fabricator-HPLC) column, a more robust, reproducible, high throughput and error-free workflow for CIU-ECD can be achieved for analysis of mAbs and mAbs-derived samples (*Fig. 7.3*). This is also ideal for native studies since it requires less effort to analyze sample natively.

7.2.4. CIU-ECD as a tool for MD Studies at Middle-Level:

Our middle-level CIU-ECD demonstrated that CIU can unfold antibody domain for improved fragmentations. However, to further understand the unfolding process, MD simulation can be utilized. Recent study has shown that MD simulation can be used to study binding effect and thermal stability of antibody[6–9]. For this work, we want to combine the IM-derived information, ECD fragmentation, and MD to explore the thermal stability of mAbs domain fragments (i.e., Fab, Fc, F(ab')2, and F/2). This perhaps can provide novel insights into the correlation between solution-phase and gas-phase stability.

7.3. References:

(1) Pang, Y.; Wang, W. H.; Reid, G. E.; Hunt, D. F.; Bruening, M. L. Pepsin-Containing Membranes for Controlled Monoclonal Antibody Digestion Prior to Mass Spectrometry Analysis. *Analytical*

Chemistry **2015**, *87* (21), 10942–10949. https://doi.org/10.1021/ACS.ANALCHEM.5B02739/SUPPL_FILE/AC5B02739_SI_001.PDF.

(2) Inouye, K.; Ohnaka, S. Pepsin Digestion of a Mouse Monoclonal Antibody of IgG1 Class Formed F(Ab')2 Fragments in Which the Light Chains as Well as the Heavy Chains Were Truncated. *Journal of Biochemical and Biophysical Methods* **2001**, *48* (1), 23–32. https://doi.org/10.1016/S0165-022X(00)00141-X.

(3) Farsang, E.; Guillarme, D.; Veuthey, J. L.; Beck, A.; Lauber, M.; Schmudlach, A.; Fekete, S. Coupling Non-Denaturing Chromatography to Mass Spectrometry for the Characterization of Monoclonal Antibodies and Related Products. *Journal of Pharmaceutical and Biomedical Analysis* **2020**, *185*, 113207. https://doi.org/10.1016/J.JPBA.2020.113207.

(4) Wouters, B.; Currivan, S. A.; Abdulhussain, N.; Hankemeier, T.; Schoenmakers, P. J. Immobilized-Enzyme Reactors Integrated into Analytical Platforms: Recent Advances and Challenges. *TrAC Trends in Analytical Chemistry* **2021**, *144*, 116419. https://doi.org/10.1016/J.TRAC.2021.116419.

(5) Camperi, J.; Dai, L.; Guillarme, D.; Stella, C. Development of a 3D-LC/MS Workflow for Fast, Automated, and Effective Characterization of Glycosylation Patterns of Biotherapeutic Products. *Analytical Chemistry* **2020**, *92* (6), 4357–4363. https://doi.org/10.1021/ACS.ANALCHEM.9B05193/SUPPL_FILE/AC9B05193_SI_001.PDF.

(6) Bekker, G. J.; Ma, B.; Kamiya, N. Thermal Stability of Single-Domain Antibodies Estimated by Molecular Dynamics Simulations. *Protein Science* **2019**, *28* (2), 429–438. https://doi.org/10.1002/PRO.3546.

(7) Ning, L.; Li, Z.; Bai, Z.; Hou, S.; He, B.; Huang, J.; Zhou, P. Computational Design of Antiangiogenic Peptibody by Fusing Human IgG1 Fc Fragment and HRH Peptide: Structural Modeling, Energetic

Analysis, and Dynamics Simulation of Its Binding Potency to VEGF Receptor. *International Journal of Biological Sciences* **2018**, *14* (8), 930. https://doi.org/10.7150/IJBS.24582.

(8) Yamashita, T. Toward Rational Antibody Design: Recent Advancements in Molecular Dynamics Simulations. *International Immunology* **2018**, *30* (4), 133–140. https://doi.org/10.1093/INTIMM/DXX077.

(9) Lai, B.; Hasenhindl, C.; Obinger, C.; Oostenbrink, C. Molecular Dynamics Simulation of the Crystallizable Fragment of IgG1—Insights for the Design of Fcabs. *International Journal of Molecular Sciences 2014, Vol. 15, Pages 438-455* **2014**, *15* (1), 438–455. https://doi.org/10.3390/IJMS15010438.